

**Investigation of Weakly Interacting Chemical Systems Involving
Noble Gas Atom**

By

**Ayan Ghosh
(CHEM01201304007)**

Bhabha Atomic Research Centre, Mumbai

*A thesis submitted to the
Board of Studies in Chemical Sciences*

*In partial fulfillment of requirements
for the Degree of*

DOCTOR OF PHILOSOPHY

of

HOMI BHABHA NATIONAL INSTITUTE

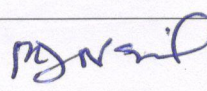
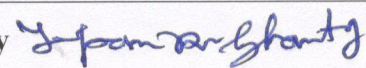
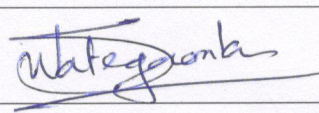
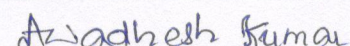
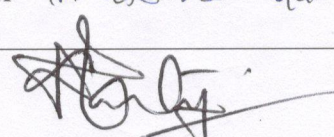


December, 2018

Homi Bhabha National Institute¹

Recommendations of the Viva Voce Committee

As members of the Viva Voce Committee, we certify that we have read the dissertation prepared by **Shri Ayan Ghosh** entitled “**Investigation of Weakly Interacting Chemical Systems Involving Noble Gas Atom**” and recommend that it may be accepted as fulfilling the thesis requirement for the award of Degree of Doctor of Philosophy.

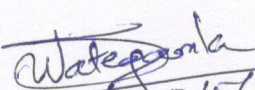
Chairman – Prof. P. D. Naik		Date: 3/5/19
Guide / Convener – Prof. T. K. Ghanty		Date: 3/5/19
Co-guide – Prof. S. Wategaonkar		Date: 3/5/2019
Examiner – Prof. G. Rajaraman		Date: 3/5/19
Member 1 – Prof. Awadhesh Kumar		Date: 03.5.2019
Member 2 – Prof. D. K. Maity		Date: 03/05/19
Member 3 – Prof. C. Majumder		Date:

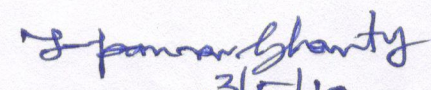
Final approval and acceptance of this thesis is contingent upon the candidate's submission of the final copies of the thesis to HBNI.

We hereby certify that we have read this thesis prepared under our direction and recommend that it may be accepted as fulfilling the thesis requirement.

Date: 3rd May, 2019

Place: HBNI,
Mumbai


3/5/2019
Signature
Co-guide


3/5/19
Signature
Guide

¹ This page is to be included only for final submission after successful completion of viva voce.

STATEMENT BY AUTHOR

This dissertation has been submitted in partial fulfillment of requirements for an advanced degree at Homi Bhabha National Institute (HBNI) and is deposited in the Library to be made available to borrowers under rules of the HBNI.

Brief quotations from this dissertation are allowable without special permission, provided that accurate acknowledgement of source is made. Requests for permission for extended quotation from or reproduction of this manuscript in whole or in part may be granted by the Competent Authority of HBNI when in his or her judgment the proposed use of the material is in the interests of scholarship. In all other instances, however, permission must be obtained from the author.

Ayan Ghosh.

Ayan Ghosh

DECLARATION

I, hereby declare that the investigation presented in the thesis has been carried out by me. The work is original and has not been submitted earlier as a whole or in part for a degree / diploma at this or any other Institution / University.

Ayan Ghosh.

Ayan Ghosh

List of Publications arising from the thesis

Journal

1. “Theoretical Prediction of Rare Gas Inserted Hydronium Ions: HRgOH_2^+ ”, **A. Ghosh**, D. Manna and T. K. Ghanty, *J. Chem. Phys.*, **2013**, *138*, 194308.
2. “Theoretical Prediction of Rare Gas Containing Hydride Cations: HRgBF^+ . (Rg = He, Ar, Kr, and Xe)”, A. Sirohiwal, D. Manna, **A. Ghosh**, T. Jayasekharan and T. K. Ghanty, *J. Phys. Chem. A*, **2013**, *117*, 10772–10782.
3. “Theoretical Prediction of XRgCO^+ Ions (X = F, Cl, and Rg = Ar, Kr, Xe)”, D. Manna, **A. Ghosh** and T. K. Ghanty, *J. Phys. Chem. A*, **2013**, *117*, 14282–14292.
4. “Theoretical Prediction of Noble Gas Inserted Thioformyl Cations: HNgCS^+ (Ng = He, Ne, Ar, Kr, and Xe)”, **A. Ghosh**, D. Manna and T. K. Ghanty, *J. Phys. Chem. A*, **2015**, *119*, 2233–2243.
5. “Prediction of a Neutral Noble Gas Compound in the Triplet State”, D. Manna, **A. Ghosh** and T. K. Ghanty, *Chem. –Eur. J.*, **2015**, *21*, 8290–8296.
6. “Noble-Gas-Inserted Fluoro(sulphido)boron (FNgBS, Ng = Ar, Kr, and Xe): A Theoretical Prediction”, **A. Ghosh**, S. Dey, D. Manna and T. K. Ghanty, *J. Phys. Chem. A*, **2015**, *119*, 5732–5741.
7. “Noble Gas Inserted Protonated Silicon Monoxide Cations: HNgOSi^+ (Ng = He, Ne, Ar, Kr, and Xe)”, P. Sekhar, **A. Ghosh**, D. Manna and T. K. Ghanty, *J. Phys. Chem. A*, **2015**, *119*, 11601–11613.
8. “Prediction of Neutral Noble Gas Insertion Compounds with Heavier Pnictides: FNgY (Ng = Kr and Xe; Y = As, Sb and Bi)”, **A. Ghosh**, D. Manna and T. K. Ghanty, *Phys. Chem. Chem. Phys.*, **2016**, *18*, 12289–12298.
9. “Unprecedented Enhancement of Noble Gas–Noble Metal Bonding in NgAu_3^+ (Ng = Ar, Kr, and Xe) Ion through Hydrogen Doping”, **A. Ghosh** and T. K. Ghanty, *J. Phys. Chem. A*, **2016**, *120*, 9998–10006.
10. “Noble Gas Encapsulated Endohedral Zintl Ions Ng@Pb_{12}^{2-} and Ng@Sn_{12}^{2-} (Ng = He, Ne, Ar, and Kr): A Theoretical Investigation”, P. Sekhar, **A. Ghosh**, M. Joshi and T. K. Ghanty, *J. Phys. Chem. C*, **2017**, *121*, 11932–11949.

11. "Theoretical Prediction of Noble Gas Inserted Halocarbenes: FN_gCX (N_g = Kr, and Xe; X = F, Cl, Br, and I)", P. Chopra, **A. Ghosh**, B. Roy and T. K. Ghanty, *Chem. Phys.*, **2017**, *494*, 20–30.

12. "Noble Gas Hydrides in the Triplet State: HN_gCCO⁺ (N_g = He, Ne, Ar, Kr, and Xe)", **A. Ghosh**, A. Gupta, R. Gupta and T. K. Ghanty, *Phys. Chem. Chem. Phys.*, **2018**, *20*, 20270–20279.

Conferences

1. "Super Strong" van der Waals Complexes between a Rare Gas Atom and Metal Halides", **A. Ghosh** and T. K. Ghanty, Current Trends in Theoretical Chemistry (CTTC-2013), Training School Hostel, Bhabha Atomic Research Centre, Anushakti Nagar, Mumbai, September 26-28, **2013**.

2. "van der Waals Clusters of Argon and Noble Metal: A Bonding Analysis", **A. Ghosh** and T. K. Ghanty, Trombay Symposium on Radiation & Photochemistry (TSRP-2016), Training School Hostel, Bhabha Atomic Research Centre, Anushakti Nagar, Mumbai, January 5-9, **2016**.

3. "van der Waals Complexes of Noble Gas Atom with Coinage Metal Clusters: Effect of Relativistic Interaction", **A. Ghosh**, A. Chandrasekar, M. Joshi, T. K. Ghanty, Trombay Symposium on Radiation & Photochemistry (TSRP-2018), D.A.E. Convention Centre, Bhabha Atomic Research Centre, Anushakti Nagar, Mumbai, January 3-7, **2018**.

Other Publications (not included in the Thesis)

1. "Atom- and Ion-Centered Icosahedral Subnanometer-Sized Clusters of Molecular Hydrogen", M. Joshi, **A. Ghosh** and T. K. Ghanty, *J. Phys. Chem. C*, **2017**, *121*, 15036–15048.

2. "Counter-Intuitive Stability in Actinide-Encapsulated Metalloid Clusters with Broken Aromaticity", M. Joshi, **A. Ghosh**, A. Chandrasekar and T. K. Ghanty, *J. Phys. Chem. C*, **2018**, *122*, 22469–22479.

Ayan Ghosh

Ayan Ghosh

Dedicated to

My Beloved Uncle

(Shri Utpal Ghosh)

(My Friend, Philosopher and Teacher)

ACKNOWLEDGEMENTS

First and foremost, I would like to take this opportunity to owe my deepest gratitude and indebtedness to my mentor and Ph.D. supervisor Dr. Tapan K. Ghanty for his precious inspiration, guidance, profound advice, constant stimulating encouragement, deep interest, good wishes and valuable suggestions during my entire research tenure. His versatile knowledge and his rational way of thinking on critical scientific problems have been of great importance for me on academic level. I am deeply indebted to Dr. Sanjay Wategaonkar for his invaluable guidance, critical comments, continuous encouragement, good wishes and valuable suggestions during the entire course of this study.

It is my great privilege to acknowledge Shri Rajendra K. Rajawat (AD, BTDG), and Dr. Prakash D. Naik (AD, CG) for motivating me and providing immense support for pursuing my Ph.D in the unique field of noble gas chemistry. It gives me immense pleasure to thank all other doctoral committee members Dr. Prakash D. Naik, Dr. Awadhesh Kumar, Dr. Dilip K. Maity and Dr. Chiranjib Majumder for their critical review and suggestions during the progress review and pre-synopsis viva voce. I wish to express my sincere thanks to all my co-workers (specifically Dr. Debashree Manna and Ms. Meenakshi Joshi) for their scientific help in the course of this study. I am very much thankful to all TCS and L&PTD members for sharing their excellent knowledge and scientific understanding with me. The supercomputing facility of Bhabha Atomic Research Centre is also gratefully acknowledged for providing the computational resources.

I would like to express my earnest gratitude to Dr. Subrata Chattopadhyay, Dr. Prabhat K. Singh and Mr. Pijush K. Mandal for their immense help, stimulating inspiration, continuous encouragements and moral support for pursuing my Ph.D. program. It is my immense pleasure to express sincere thanks to Mrs. Tuntun Ghanty for providing very strong moral support and advices which have been proven as extremely beneficial for the successful completion of my Ph.D. work. Finally, I would like to thank all my family members for their love, inspiration, encouragement, blessings and constant support to make my journey smoother.

Ayan Ghosh.

Ayan Ghosh

CONTENTS

	Page No.
SYNOPSIS	i-vii
LIST OF FIGURES	viii-ix
LIST OF TABLES	x-xii
CHAPTER 1 Introduction	1
1.1. A Brief Historical Aspects: Discovery of Noble Gas Elements	1
1.2. Natural Abundance and Occurrences	5
1.2.1. Atmospheric Composition	5
1.2.2. Composition in the Soil	6
1.2.3. Occurrence in the Groundwater	8
1.3. Physical and Chemical Properties	8
1.4. Applications of Noble Gases: Advantages and Disadvantages	11
1.5. The Promising Diverse Chemistries	15
1.5.1. 'Classical' Noble Gas Compound involving Conventional Chemical Bonds	16
1.5.2. 'Non-Classical' Noble Gas Compound involving Unusual Chemical Bonds	19
1.6. Scope of the Present Thesis	31
CHAPTER 2 Theoretical and Computational Methodologies	33
2.1. Introduction	33
2.2. Theoretical Methodologies	35
2.2.1. Wave Function Based Methods	41
2.2.2. Density Based Methods: Density Functional Theory	48
2.3. Basis Set	54
CHAPTER 3 Novel Class of Fascinating Noble Gas Insertion Compounds: Predictions from Theoretical Calculations	57
3.1. Introduction	57
3.2. Computational Details	62
3.3. Results and Discussions	65
3.3.1. A Comparative Accounts of Optimized Structural Parameters	65

	3.3.2. Thermodynamic and Kinetic Stability	
	3.3.3. Harmonic Vibrational Frequencies	73
	3.3.4. Charge Distribution Analysis	78
	3.3.5. Analysis of Topological Properties	81
		83
	3.4. Conclusions	89
CHAPTER 4	Neutral and Ionic Noble Gas Compound in the Triplet State	91
	4.1. Introduction	91
	4.2. Computational Details	94
	4.3. Results and Discussions	94
	4.3.1. Optimized Structural Parameters	94
	4.3.2. Analysis of Harmonic Vibrational Frequencies	98
	4.3.3. Energetics and Stability	100
	4.3.4. Analysis of Potential Energy Diagram	107
	4.3.5. Charge and Spin Distribution Analysis	109
	4.3.6. Atoms-in-molecule (AIM) Analysis	111
	4.4. Concluding Remarks	114
CHAPTER 5	Investigation of ‘Super-Strong’ Noble Metal–Noble Gas Bonding	115
	5.1. Introduction	115
	5.2. Computational Details	116
	5.3. Results and Discussions	117
	5.3.1. Structural Analysis of Hydrogen Doped NgAu ₃ ⁺ Ions	117
	5.3.2. Energetics and Stability	119
	5.3.3. Change in Vibrational Frequencies on Hydrogen Doping in NgAu ₃ ⁺ Ions	120
	5.3.4. Molecular Orbitals and HOMO–LUMO Energies	121
	5.3.5. Charge Distribution Analysis	123
	5.3.6. Analysis of Topological Properties of Hydrogen Doped NgAu ₃ ⁺ Ions	124
	5.3.7. Comparative Accounts of NgAu _{3–k} H _k ⁺ with NgAg _{3–k} H _k ⁺ and NgCu _{3–k} H _k ⁺ Ions	127
	5.4. Conclusion	127

CHAPTER 6	Electronic Structure and Stability of Noble Gas Encapsulated Endohedral Zintl Ions	129
6.1.	Introduction	129
6.2.	Computational Details	131
6.3.	Results and Discussions	133
6.3.1.	Electronic Structure Analysis	133
6.3.2.	Harmonic Vibrational Frequencies	136
6.3.3.	Energetics and Stabilities of Ng@Zintl Ions	137
6.3.4.	Molecular Orbital Ordering of Ng@Zintl Ions	138
6.3.5.	Density of States of Ng@Zintl Ions	140
6.3.6.	Natural Population Analysis (NPA) of Ng@Zintl Ions	141
6.3.7.	<i>Ab Initio</i> Molecular Dynamics Simulation of Ng@Zintl Ions	143
6.3.8.	Electron Density Analysis of Ng@Zintl Ions	147
6.3.9.	Effect of Counterion on the Structure and Properties of Ng@Pb ₁₂ ²⁻ and Ng@Sn ₁₂ ²⁻ Clusters	148
6.3.10.	Energy Decomposition Analysis	150
6.3.11.	Energy Barrier Calculation	152
6.4.	Concluding Remarks	153
CHAPTER 7	Summary and Outlook	155
	REFERENCES	160

SYNOPSIS

Investigation of weakly-bonded intermolecular complexes and chemically bonded molecular systems involving noble gas atoms under ambient conditions is of immense interest in various fields like astronomical science, environmental science and fundamental basic sciences. It is primarily due to various potential applications of noble gas atoms or their complexes and compounds in different industries. Additionally, trapping of noble gas atom into various novel materials has also become the subject of enormous interest due to their numerous potential applications in the field of medicinal biology, nuclear waste management, etc.

In recent years, extensive researches are going on to provide an in-depth insight into the nature of chemical bonds in weakly interacting chemical system involving highly inert noble gas atoms possessing astronomical as well as environmental significance. Being most stable and chemically unreactive element in the periodic table due to its completely filled *s* and *p* valence orbitals, it is extremely difficult to predict any noble gas containing chemical compounds leading to highly challenging activities to the researchers. In general, the extremely inert noble gas atom can form weak chemical bonding with some selective compounds leading to van der Waals (vdW) complexes. Apart from the ability of formation of vdW complexes, in recent times, it has been well established that noble gas atoms can also participate in the conventional chemical bonding with the other elements of the periodic table. In particular, the discovery of first argon based noble gas insertion compound, HArF,¹ with H–Ar covalent character, has revolutionized the field of noble gas chemistry and has attracted considerable attention among the researchers. Subsequently, various ionic and neutral insertion type compounds of noble gas atoms with environmentally important species, like HOX (X = F, Cl, and Br) and H₃O⁺, and species of astronomical significance, such as HCO⁺, HCS⁺, HN₂⁺, and so on, have been investigated theoretically and experimentally.

Moreover, one such noble gas insertion molecule, HXeOBr ,²⁻³ has been successfully prepared and characterized using IR spectroscopic technique, which was theoretically predicted by our group earlier. Of late, an argon containing noble gas molecular ion, $^{36}\text{ArH}^+$ has been detected in the Crab Nebula which was observed in space with Fourier Transform Spectrometer (FTS) of the Spectral and Photometric Imaging Receiver (SPIRE) using the Herschel Space Observatory.⁴ Therefore, in recent times, exceedingly demanding activities to predict noble gas containing chemical compounds with unusual chemical bonding has become a fast growing field of noble gas chemistry.⁵⁻⁶ Stimulated from the diversity and significance of the field of research, in this thesis, we have made an attempt to predict some novel ionic and neutral insertion compounds of the noble gas atoms with the molecules having environmental and astronomical importance. These compounds are found to be stable either in the singlet or in the triplet ground electronic state in their respective potential energy surfaces.

The noble gas–noble metal interaction is expected to be extremely unusual from the viewpoint of the inert nature of both the atoms which throw a great challenge to the scientists to form a chemical bond between noble gas and noble metal atoms. One such series of complexes, i.e., NgMF ,⁷ formed through the interaction of a noble gas (Ng = Ar, Kr, and Xe) atom and coinage metal fluoride, MF (M = Cu, Ag, and Au) has received considerable attention because of the presence of very strong Ng–M bond as compared to the conventional vdW complexes. In the present thesis, our main objective is to assess the performance of various exchange–correlation energy density functionals in predicting the properties of experimentally observed NgMF systems. Moreover, very recent experimental report on the noble gas–noble metal interaction in Ar-complexes of mixed Au–Ag trimers⁸ and gold – hydrogen analogy⁹ have motivated us to investigate the effect of hydrogen doping on the Ng–M (Ng = Ar, Kr, and Xe; M = Cu, Ag, and Au) bonding through various *ab initio* based techniques which is also included in the present thesis. A new arena of noble gas chemistry is

the endohedral encapsulation of noble gas atoms into the fullerene, dodecahedrane, BN-fullerenes, etc.¹⁰ by employing suitable experimental techniques supported by theoretical calculations. The present thesis also includes a study of noble gas encapsulated plumbaspherene and stannaspherene cage clusters, Ng@Pb₁₂²⁻ and Ng@Sn₁₂²⁻, through *ab initio* density functional theory based methods.

The whole thesis is organized in the following manner.

Chapter 1: This introductory chapter highlights the brief history of discovery of noble gas elements and its compounds including their unique physical and chemical properties promising diverse chemistries. This chapter also emphasizes the enormous importance of noble gas containing chemical compounds, such as noble gas insertion compounds, super strong van der Waals complexes and noble gas encapsulated clusters in the field of astronomical science, environmental science, basic fundamental science and potential application in medicinal biology and nuclear waste management. We have discussed the requirement of the knowledge of chemical intuition and understanding of nature of interaction between the constituent elements in order to choose the chemical system which can participate in conventional chemical bonding with the noble gas atom. This concept is also necessary to form complexes with exceptionally strong noble gas-noble metal bond and noble gas encapsulated molecular cage clusters. In addition, we have also provided some commonly used experimental techniques to prepare and characterize the above-mentioned noble gas containing chemical compounds.

Chapter 2: It is well known that theoretical modeling is an important tool to provide better understanding on the complexation or encapsulation behavior of any particular molecular system or cluster towards noble gas atom(s). Therefore, the significance of computational

methods have been outlined which provides some of the most valuable information that experiments cannot provide. This chapter includes a brief overview of the computational methodologies which have been used to investigate the chemical systems involving noble gas atom. This chapter emphasizes the essential description of quantum mechanics, including DFT followed by some post-Hartree–Fock-based correlated methods utilized for our calculations.

Chapter 3: In this chapter, we have systematically discussed the possibility of existence of few interesting noble gas compounds. These novel class of fascinating insertion compounds obtained through the insertion of a noble gas atom into the molecules of interstellar origin have been explored by various *ab initio* quantum chemical techniques. We have investigated the following new class of noble gas containing cationic and neutral species, *viz.*, HNgOH_2^+ , HNgBF^+ , XNgCO^+ , HNgCS^+ , HNgOSi^+ , FNgBS , and FNgCX (Ng = Noble Gas, X = Halides). Density functional theory (DFT), second-order Møller–Plesset perturbation theory (MP2), and coupled cluster theory (CCSD(T)) based techniques have been used to explore the structure, energetics, charge distribution, and harmonic vibrational frequencies of these compounds. By utilizing all the methods, the true minima and transition state geometries of the predicted species are obtained in their respective singlet potential energy surfaces. All the predicted species are found to be thermodynamically stable with respect to all possible 2-body and 3-body dissociation channels, except the dissociation path leading to the respective global minimum products. Nevertheless, all these compounds are found to be kinetically stable with finite barrier heights corresponding to their transition states, which are connected to their respective global minima products. The atoms-in-molecules (AIM) analysis strongly reveals that there exists conventional chemical bonding with the noble gas atom in all the predicted compounds. For convenience, this chapter has been divided into two subsections,

viz., “cationic noble gas insertion compounds” and “closed-shell neutral noble gas insertion compounds” with singlet ground electronic state.

Chapter 4: In the previous chapter, the noble gas insertion compounds with singlet ground electronic state have been reported using various quantum chemical techniques. In this chapter, we have discussed new class of noble gas compounds involving open-shell species. For the first time, in a bid to predict neutral noble gas chemical compounds in their triplet electronic state, we have carried out a systematic investigation of noble gas inserted pnictides, FNgY (Ng = Kr and Xe; Y = N, P, As, Sb and Bi) species by using *ab initio* molecular orbital calculations. Density functional theory and various post-Hartree–Fock-based correlated methods, including the multireference configuration interaction technique have been employed to elucidate the structure, energetics, charge distribution, and harmonic vibrational frequencies. Moreover, we further extended our calculation to explore a new series of noble gas hydrides in the triplet ground electronic state for the first time by employing similar methods. All the predicted species are found to be thermodynamically stable with respect to all possible 2-body and 3-body dissociation channels except the global minima products and kinetically stable with sufficient barrier heights corresponding to their transition states. Similar to the previous chapter, this chapter is also composed of two subsections, *viz.*, “open-shell neutral noble gas insertion compounds” and “cationic noble gas hydrides with triplet ground electronic state”.

Chapter 5: In one subsection of this chapter, we have explored the unprecedented enhancement of noble gas–noble metal bonding strength in NgM₃⁺ (Ng = Ar, Kr, and Xe; M = Cu, Ag, and Au) ions through hydrogen doping by employing various *ab initio* based techniques. Detail optimized structural parameters, energetics, vibrational frequency, charge

distribution values have been reported using DFT, MP2, and CCSD(T) based methods with different basis sets. It has been found that among all the $\text{NgM}_{3-k}\text{H}_k^+$ complexes ($k = 0-2$), the strongest Ng–M bonding has been observed in NgMH_2^+ complex, particularly, in case of ArAuH_2^+ complex. The concept of gold–hydrogen analogy makes it possible to evolve this pronounced effect of hydrogen doping in Au-trimers leading to the strongest Ng–Au bond in NgAuH_2^+ species. Very recent successful experimental identification of Ar-complexes of mixed noble metal clusters, $\text{Ar}_k\text{Au}_n\text{Ag}_m^+$ ($n + m = 3$; $k = 0-3$) clearly indicate that it is possible to experimentally realize the predicted species, NgMH_2^+ with suitable technique(s). In the other subsection of this chapter, we have also included one benchmark study to assess the performance of various exchange-correlation energy density functional systematically in predicting the bond length, bond energies and vibrational frequencies in the super strong van der Waals complexes NgMF ($\text{Ng} = \text{Ar}, \text{Kr}, \text{and Xe}$; $\text{M} = \text{Cu}, \text{Ag}$ and Au).

Chapter 6: The possibility of occurring noble gas encapsulated inorganic fullerene clusters have been discussed in this chapter. The theoretical existence and thermodynamic stability of noble gas encapsulated endohedral Zintl ions, Ng@M_{12}^{2-} ($\text{Ng} = \text{He}, \text{Ne}, \text{Ar}, \text{and Kr}$; $\text{M} = \text{Sn}$ and Pb), have been investigated through density functional theory while the kinetic stability of the clusters have been studied through *ab initio* molecular dynamics simulation. Detail optimized structural parameters, binding energies, vibrational frequencies, and charge distribution values are reported by employing DFT based methods for noble gas encapsulated plumbaspherene, $[\text{Ng@Pb}_{12}^{2-}]$ and stannaspherene, $[\text{Ng@Sn}_{12}^{2-}]$ cage clusters. It has been found that the Ng@M_{12}^{2-} clusters are kinetically stable and thermodynamically unstable whereas the K^+ salt of Ng@M_{12}^{2-} clusters are found to be both kinetically as well as thermodynamically stable. Therefore, our results would incite further studies into the

experimental methods through which these molecular carriers for noble gas atoms can be produced.

Chapter 7: This chapter includes some concluding remarks based on our present study. This gives a brief summary about the accomplishments as well as possible future directions to explore different aspects of selective complexation and cluster formation using a specific noble gas atom with several interesting molecular systems utilizing various fundamental chemical concepts.

References

1. Khriachtchev, L.; Pettersson, M.; Runeberg, N.; Lundell, J.; Räsänen, M. *Nature (London, U. K.)* **2000**, *406*, 874.
2. Jayasekharan, T.; Ghanty, T. K. *J. Chem. Phys.* **2006**, *124*, 164309.
3. Khriachtchev, L.; Tapio, S.; Domanskaya, A. V.; Räsänen, M.; Isokoski, K.; Lundell, J. *J. Chem. Phys.* **2011**, *134*, 124307.
4. Barlow, M. J.; Swinyard, B. M.; Owen, P. J.; Cernicharo, J.; Gomez, H. L.; Ivison, R. J.; Krause, O.; Lim, T. L.; Matsuura, M.; Miller, S. *et al.*, *Science* **2013**, *342*, 1343.
5. Grandinetti, F. *Noble Gas Chemistry: Structure, Bonding, and Gas-Phase Chemistry*. Wiley-VCH: Weinheim, Germany, 2018.
6. Grochala, W. *Chem. Soc. Rev.* **2007**, *36*, 1632.
7. Michaud, J. M.; Gerry, M. C. L. *J. Am. Chem. Soc.* **2006**, *128*, 7613.
8. Shayeghi, A.; Johnston, R. L.; Rayner, D. M.; Schäfer, R.; Fielicke, A. *Angew. Chem., Int. Ed.* **2015**, *54*, 10675.
9. Kiran, B.; Li, X.; Zhai, H.-J.; Cui, L.-F.; Wang, L.-S. *Angew. Chem., Int. Ed.* **2004**, *43*, 2125.
10. Saunders, M.; Vázquez, H. A. J.; Cross, R. J.; Poreda, R. J. *Science* **1993**, *259*, 1428.

List of Figures

Serial No.	Descriptions	Page No.
1.1	Composition of Atmospheric Air	6
2.1	Schematic representations of the flow chart of <i>ab initio</i> MO & DFT calculations	54
3.1	Optimized structures of the minimum energy (a) and transition state (b) of HNgOH ₂ ⁺ (Ng = He, Ar, Kr, Xe) ions. (H1 and H2 are symmetry equivalent atoms).	63
3.2	Optimized geometrical parameters in graphical format for the linear minima [(a), (c) and (e)] and planar bent transition states [(b), (d) and (f)] of FNgBS molecules (Ng = Ar, Kr, and Xe) where the bond lengths are in Å and bond angles are in degrees.	68
3.3	Minimum Energy Path for [HNgCS ⁺ → HCS ⁺ + Ng] Reaction (Ng = Xe, Kr, Ar, He).	76
3.4	Electron density (ρ) contour plots of (a) FArBS, (b) FArBO, (c) FKrBS, (d) FKrBO, (e) FXeBS and (f) FXeBO species at the respective molecular plane calculated at the B3LYP level.	87
3.5	Contour plots of Laplacian of electron density (∇ ² ρ) of (a) FArBS, (b) FArBO, (c) FKrBS, (d) FKrBO, (e) FXeBS and (f) FXeBO species at the respective molecular plane calculated at the B3LYP level.	88
4.1	Potential-energy profile at CCSD(T)/aug-cc-pVTZ level for (a) XeP, (b) XeP ⁺ and (c) FXeP, and (d) FXeP potential-energy profile at MRCI/aug-cc-pVTZ level.	108
5.1	Optimized geometrical parameters of planer NgAu ₃ ⁺ (a, b, c), NgAu ₂ H ⁺ (d, e, f) and NgAuH ₂ ⁺ (g, h, i) (Ng = Ar, Kr, Xe) where the bond lengths are in angstroms and bond angles are in degrees.	118
5.2	Degenerate molecular orbitals depicting the Ar–Au bonding in (a) ArAu ₃ ⁺ , Orbital energy = –18.86 eV; (b) ArAu ₂ H ⁺ , Orbital energy = –19.65 eV; and (c) ArAuH ₂ ⁺ Orbital energy = –20.90 eV.	121

Serial Nos.	Descriptions	Page Nos.
5.3	Plot of the Ar–Au bond energy vs the LUMO energy, calculated using ω B97X–D/DEF2 Method (Correlation Coefficient corresponding to linear least square fit, $R^2 = 0.988$).	122
6.1	Optimized structures of (a) plumbaspherene (Pb_{12}^{2-}), (b) noble gas encapsulated Pb_{12}^{2-} , Ng@Pb_{12}^{2-} , and (c) noble gas dimer encapsulated Pb_{12}^{2-} , $\text{Ng}_2\text{@Pb}_{12}^{2-}$ as obtained by B3LYP/DEF levels of theory.	133
6.2	(A) Orbital energies of (a) Pb_{12}^{2-} , (b) He@Pb_{12}^{2-} , (c) Ne@Pb_{12}^{2-} , (d) Ar@Pb_{12}^{2-} , and (e) Kr@Pb_{12}^{2-} ; (B) Orbital energies of (a) Sn_{12}^{2-} , (b) He@Sn_{12}^{2-} , (c) Ne@Sn_{12}^{2-} , (d) Ar@Sn_{12}^{2-} , and (e) Kr@Sn_{12}^{2-} .	139
6.3	The variation of density of states (DOS) as a function of orbital energies of noble gas encapsulated Pb clusters for (a) He@Pb_{12}^{2-} , (b) Ne@Pb_{12}^{2-} , (c) Ar@Pb_{12}^{2-} , (d) Kr@Pb_{12}^{2-} , (e) $\text{H}_2\text{@Pb}_{12}^{2-}$, and (f) $\text{He}_2\text{@Pb}_{12}^{2-}$.	140
6.4	The variation in Ng–Pb distances of noble gas encapsulated Pb clusters for (a) He@Pb_{12}^{2-} , (b) Ne@Pb_{12}^{2-} , (c) Ar@Pb_{12}^{2-} , and (d) Kr@Pb_{12}^{2-} with respect to time at different temperatures during the course of molecular dynamics simulations.	144
6.5	The variation in average Pb–Pb distances of noble gas encapsulated Pb clusters for (a) He@Pb_{12}^{2-} , (b) Ne@Pb_{12}^{2-} , (c) Ar@Pb_{12}^{2-} , (d) Kr@Pb_{12}^{2-} , (e) $\text{H}_2\text{@Pb}_{12}^{2-}$, (f) $\text{He}_2\text{@Pb}_{12}^{2-}$, and bare Pb cluster (g) Pb_{12}^{2-} with respect to time at different temperatures during the course of molecular dynamics simulation.	145
6.6	Optimized structures of (a) C_{5v} Ng@KPb_{12}^- , (b) C_{3v} Ng@KPb_{12}^- , (c) D_{5d} $\text{Ng@K}_2\text{Pb}_{12}$ and (d) D_{3d} $\text{Ng@K}_2\text{Pb}_{12}$ as obtained by B3LYP/DEF levels of theory.	149

List of Tables

Serial No.	Descriptions	Page No.
1.1	Atomic Number (N), Atomic Radius (R in Å), Melting Point (MP in K), Boiling Point (BP in K), Density (ρ in gL^{-1}), Ionization Energy (IE in eV), Electron Affinity (EA in eV), Electronegativity (χ in eV), Polarizability (α in Å ³) of the Noble Gases.	9
1.2	Covalent Radii (r_{cov} in Å) and van der Waals (r_{vdW} in Å) of the Noble Gases.	10
3.1	Optimized Geometrical Parameters for the Minima Structures of HNgX' (X' = BF, CO, CS, N ₂ , OH ₂ , and OSi) Species by CCSD(T)/AVTZ Level of Theory.	69
3.2	CCSD(T)/AVTZ Calculated Energies (kJ mol^{-1}) Corresponding to Different Dissociation Channels for HNgX' (X' = BF, CO, CS, N ₂ , OH ₂ , and OSi).	75
3.3	B3LYP Computed Mulliken Atomic Charges (a.u.) on H, Ng Atoms and HNg Fragments in the Minima of HNgX'+ (X' = BF, CO, CS, N ₂ , OH ₂ , and OSi) Species.	82
3.4	Bond Critical Point Properties [BCP Electron Density (ρ in $e a_0^{-3}$), Its Laplacian ($\nabla^2\rho$ in $e a_0^{-5}$), and the Local Energy Density (E_d in a.u.)] of HNgX'+ (Ng = He, Ne, Ar, Kr, and Xe; X' = BF, CS, OH ₂ , and OSi) Species Calculated Using the B3LYP Method.	85
4.1	CCSD(T) Computed F–Ng and Ng–Y Bond Length (in Å) Comparisons in ³ FNgY (Ng = Kr and Xe; Y = N, P, As, Sb and Bi) with respect to the Corresponding Covalent (R_{cov}) ^a and van der Waals Limit (R_{vdW}) ^b and Bare ⁴ NgY, ² NgY, ³ NgY ⁺ and ¹ NgY ⁺ species.	95
4.2	Energies (in kJ mol^{-1}) of the Various Dissociated Species Relative to the ³ HNgCCO ⁺ (Ng = He, Ne, Ar, Kr, and Xe) Ions, Calculated at CCSD(T)/AVTZ Level.	103

Serial Nos.	Descriptions	Page Nos.
4.3	Energies of the Singlet FNgY Species Relative to the Corresponding Triplet Species (ΔE_{ST} in kJ mol^{-1}) Using B3LYP and MP2 Methods with DEF2 Basis Set and CCSD(T) Method with AVTZ Basis Set.	105
4.4	Energies (in kJ mol^{-1}) of the Singlet HNgCCO ⁺ (Ng = He, Ne, Ar, Kr, and Xe) Species Relative to the Corresponding Triplet Species (ΔE_{ST}), Calculated using B3LYP, MP2 Methods with DEF2 and AVTZ Basis Sets and CCSD(T) Method with AVTZ Basis Set.	105
4.5	Bond Critical Point Properties [BCP Electron Density (ρ in $e a_0^{-3}$), It's Laplacian ($\nabla^2\rho$ in $e a_0^{-5}$), the Local Electron Density (E_d in a.u.) and the Ratio of Local Kinetic Energy Density and Electron Density (G/ρ in a.u.)] of ³ HNgCCO ⁺ (Ng = He, Ne, Ar, Kr, and Xe) Ions, Calculated using the MP2 Method with AVTZ Basis Set.	112
5.1	CCSD(T) Computed Bond Dissociation Energy (BE in kJ mol^{-1}) and MP2 Calculated Stretching Frequency (ν in cm^{-1}) and Force Constant (k in N m^{-1}) Values for Ng–Au Bond in NgAu ₃ ⁺ , NgAu ₂ H ⁺ and NgAuH ₂ ⁺ Species.	119
5.2	MP2/AVTZ Calculated Values of the NBO Charges in Au ₃ ⁺ , Au ₂ H ⁺ , AuH ₂ ⁺ , NgAu ₃ ⁺ , NgAu ₂ H ⁺ , and NgAuH ₂ ⁺ (Ng = Ar, Kr, and Xe) Species.	123
5.3	Various Topological Properties [Local Electron Energy Density (E_d in a.u.), the Electron Density (ρ in $e a_0^{-3}$), and Ratio of Local Electron Energy Density and Electron Density ($-E_d/\rho$ in au)] at the Local Energy Density Critical Points [(3, +1) HCP] for the Ng–Au Bond in NgAu ₃ ⁺ , NgAu ₂ H ⁺ , and NgAuH ₂ ⁺ (Ng = Ar, Kr, and Xe) Species As Obtained by Using the ω B97XD and MP2 Methods with the DEF2 Basis Set.	125

Serial Nos.	Descriptions	Page Nos.
5.4	Calculated Values (kJ mol^{-1}) of Energy Decomposition Analysis for NgAu_3^+ , NgAu_2H^+ , and NgAuH_2^+ ($\text{Ng} = \text{Ar}, \text{Kr}, \text{and Xe}$) Species as Obtained Using PBE-D3 Method with TZ2P Basis Set by Employing ADF Packages and Taking MP2 Optimized Geometry.	126
6.1	Optimized Ng–Pb/Ng–Sn Distances ($R_{(\text{Ng-Pb/Ng-Sn})}$, in \AA) ^a , Shortest Pb–Pb/Sn–Sn Distances ($R_{(\text{Pb-Pb/Sn-Sn})}$, in \AA), Dissociation Energies (BE, in kJ mol^{-1}), HOMO–LUMO Gap (ΔE_{Gap} , in eV) and NPA Charge at Noble Gas Atom (q_{Ng} in a.u.) of Ng@Pb_{12}^{2-} and Ng@Sn_{12}^{2-} ($\text{Ng} = \text{He}, \text{Ne}, \text{Ar}, \text{and Kr}$) Clusters Calculated at B3LYP/DEF Level.	134
6.2	Calculated Values of He–He/H–H Distances ($R_{(\text{He-He/H-H})}$, in \AA), Shortest Pb–Pb/Sn–Sn Distances ($R_{(\text{Pb-Pb/Sn-Sn})}$, in \AA), Dissociation Energies (BE, in kJ mol^{-1}), HOMO–LUMO Gap (ΔE_{Gap} , in eV) and NPA Charge at Encapsulated Atoms ($q_{\text{He}}/q_{\text{H}}$ in a.u.) of $\text{He}_2@Pb_{12}^{2-}$, $\text{H}_2@Pb_{12}^{2-}$ and $\text{H}_2@Sn_{12}^{2-}$ Clusters as Performed at B3LYP/DEF Level.	135

Chapter 1. Introduction

1.1. A Brief Historical Aspects: Discovery of Noble Gas Elements

One of the most fascinating, intriguing and overwhelming event in the history of science is the spectacular discovery of noble gases which reflects the awesome creativeness, strong chemical intuition, rigorous studies, and tremendous patience of the scientists implementing the concept of both fundamental and applied science together. Although all noble gases except radon (Rn) are natural constituents of atmospheric air with different percentages in volume ranging from 0.9% (Ar) to $9 \times 10^{-6}\%$ (Xe), it took till the end of the nineteenth century to characterize the unknown noble gas elements after the development of very sophisticated experimental tools. In 1785, British chemist and physicist Henry Cavendish,¹ in his 'Experiments on Air', found that a certain part of the 'phlogisticated air' of the atmosphere behaved differently from the rest (nitrogen and oxygen) comprising not more than (1/120) part of the whole. Nevertheless, he had actually isolated argon and other noble gases but he could offer no explanation about this residue due to the limitation of development of science.

In 1892, British physicist John William Strutt (known as Lord Rayleigh)² had observed that the atomic weight of nitrogen obtained from the chemical reaction of ammonia with oxygen was lower than that of the nitrogen recovered from common atmospheric air. After performing a large number of experiments, Rayleigh could confirm that the density of the atmospheric nitrogen was higher as compared to the density of chemically obtained nitrogen consistently irrespective of the preparation methods. He attributed this discrepancy to a light gas included in chemical compounds of nitrogen during its preparation. Inspired by the deep curiosity on the puzzling gas as obtained by Rayleigh, one Scottish chemist Sir William Ramsay started independent work aimed at to isolate the unknown baffling heavier

component of air with the permission of the former. In 1893, after the removal of oxygen and repeated elimination of nitrogen Ramsay had observed that the residual gas became progressively heavier suspecting a hitherto undiscovered heavy gas in the atmospheric air. In 1894, both Rayleigh and Ramsay³ had isolated the mysterious gas from the atmospheric air, separately, and asked Sir William Crooks⁴ to obtain the spectrum of the gas. The spectral lines thus obtained were found to be totally different in comparison to nitrogen. With this stunning findings, Rayleigh and Ramsay were able to announce that they had found a monoatomic, chemically ‘inactive’ gaseous element called ‘argon’ after the Greek word ἀργός (*argós* means ‘idle’ or ‘lazy’ or ‘inactive’) constituted approximately one percent of the atmosphere. However, the accomplishment was really astonishing with the discovery of first noble gas atom in the earth surface. After so many criticism and debate, their discovery were reinforced in 1895 and they could officially read to the Royal Society their long waited paper on “Argon, a new constituent of the atmosphere”.⁵

After the outstanding journey of discovering “Argon”, motivated by himself Ramsay tried to find out the chemical reactivity of it and searched out one article written by a scientist of Geological Survey of United States, Dr. Hillebrand, mentioning the mysterious occurrence of nitrogen gas in uranium minerals.⁶ According to Dr. Hillebrand, the mineral of uranium, cleveite produced nitrogen gas on heating with dilute sulphuric acid. Doubting the detection of the evolved gas from cleveite, Ramsay re-examined the spectrum of the gas with the help of Crooks⁷ and found that a bright yellow line was observed at 587.49 nm of wavelength which is absent in argon as well as sodium. Interestingly, this spectral line was exactly coincided with the D₃ line as observed in the solar atmosphere. In this context, it is very important to mention that aiming at to observe a total solar eclipse French astronomer Pierre Janssen and British astronomer Joseph Norman Lockyer⁸ obtained an unusual yellow line spectrum emitted from an object, never seen before, and discovered a new element

spectroscopically at the chromosphere of the Sun in the year 1868 and named it 'Helium' after the Greek God for the Sun, ἥλιος (*hēlios*) but its reactivity was unknown since no chemical analysis was possible at that time period. Ramsay identified the terrestrial helium and communicated⁹ just before the independent isolation of helium in the laboratory by Swedish chemist Abraham Langlet. Consequently, after an exhaustive study on helium,¹⁰ Ramsay enthusiastically found that a yellow spectral line at 587.5 nm of wavelength was obtained by Italian scientist Luigi Palmieri in the year 1882 from a lava-like product ejected by Vesuvius which had not been possible to characterize at that time.

Similar physical and chemical properties of helium and argon ensured their existence in one natural family. On the basis of their atomic weights (4 for He and 40 for Ar) pattern, Ramsay was convinced that there must exist more than one new element with similar properties. Stimulated from his own idea, he along with Mr. Travers kept on searching new element(s) carrying out a large number of experiments with the evolved gases obtained from the different treatments with the minerals and meteorites. Further discovery of the noble gases was not possible till the invention of the machine which liquefied the gas by Dr. Hampson in 1898. Upon evaporation of 760 cc liquid air, the residue remained 10 cc of liquid which on boiling after removal of oxygen and nitrogen produced 26 cc of a gas with estimated atomic weight 80. Unlike argon, some new lines had been found in the spectrum of the gas obtained by fractional distillation and a new noble gas element was discovered named as 'Krypton' following the Greek words κρυπτός (*kryptós* means 'hidden') on 9th June in 1898 after giving tremendous effort by Ramsay and Travers¹¹ for continuous 3 years.

Most interestingly, after few days of the discovery of krypton, dealing with lower boiling fraction of the previously collected gas samples Ramsay and Travers¹² declared on 16th June, 1898 that they found another new element with same characteristic features like argon having intermediate atomic weight in between helium and argon. The new element

which possessed brilliant colored spectrum containing many red, orange and yellow lines, named as 'Neon' after the Greek νέος (*néos* means 'new').

After couple of months on September 1898, very surprisingly, Ramsay and Travers¹³ separated another element from krypton through fractional distillation and declared this as a new element bearing same physico-chemical behaviour like argon. The boiling point of the new element was found to be higher as compared to that of the krypton. They proposed the name of the newly discovered element as 'Xenon' after the Greek word ξένος (*ksénos* means 'stranger').

The emission of gas from a radioactive material, radium, was detected by German physicist Friedrich Ernst Dorn through his own developed apparatus in the year 1898,¹⁴ while a similar emission was observed by British physicist Ernest Rutherford emanating from thorium in the year 1900. After a prolonged controversy, it had been found out that the discovery of radon credited to Dorn since he had detected the most stable ²²²Rn isotope ($t_{1/2}=3.823$ days), whereas Rutherford reported the less stable one ²²⁰Rn ($t_{1/2}=54.5$ s). Subsequently, both Rutherford and the British chemist Frederick Soddy¹⁵ investigated and confirmed that the gas emanating from thorium and radium were identical and possess same chemical activity like argon series. Rutherford, first proposed the name as 'radium emanation' which was changed to 'Niton' by Ramsay in 1915 which in turn transformed to 'Radon' in 1923 by the International Committee of Chemical Elements¹⁶. In this context, it is very imperative to mention that Ramsay was fully involved for the detection and characterization of the element radon in collaboration with Frederick Soddy, John Norman Collie and Robert Whytlaw Gray. Specifically, Ramsay contributed in analyzing the emission spectrum of radon in 1904,¹⁷ and in determining the density of it in 1910,¹⁸ confirming its highest density among all the gases in the argon family.

Considering the independent role of the ‘non-inert pair’ of British scientists, in 1904, Lord Rayleigh was awarded the Nobel Prize in Physics¹⁹ “for his investigations of the densities of the most important gases and for his discovery of argon in connection with these studies” while the Nobel Prize in Chemistry²⁰ went to Sir William Ramsay “in recognition of his services in the discovery of inert gaseous elements in air, and his determination of their place in the periodic system”. During the award giving ceremony, the president of the Royal Swedish Academy of Sciences, Johan Erik Cederblom mentioned in his speech, “the discovery of an entirely new group of elements, of which no single representative had been known with any certainty, is something utterly unique in the history of chemistry, being intrinsically an advance in science of peculiar significance”.²⁰

1.2. Natural Abundance and Occurrences

1.2.1. Atmospheric Composition

It is worthwhile to mention that all the noble gases are present in the Earth’s atmosphere, except helium and radon.²¹ The highest constituent of the Earth’s atmosphere is nitrogen making up about 78% whereas oxygen makes 21% constituting together 99% of the air above the Earth’s surface. Argon possesses third rank with 0.93% of the total atmospheric air. The remaining 0.07% is made up with water vapor, carbon dioxide, ozone (O₃), and traces of the other noble gases. These noble gases are present in trace quantities which can best be described in terms of parts per million (ppm). The concentrations of helium, neon, krypton, and xenon in the atmosphere are 5, 18, 1, and 0.09 ppm, respectively, as depicted in Figure 1.1.²² Therefore, the commercial source of argon, neon, krypton and xenon is the atmospheric air from which they are obtained by liquefaction and fractional distillation. Most of the commercially viable helium is produced from certain natural gas wells.

It is well known that the abundances of the noble gases decrease as their atomic numbers increase, which makes helium as the second highest most abundant element in the universe after hydrogen. Surprisingly, helium is only the third most abundant noble gas in the atmosphere on Earth's surface due to the small mass of the atom for which the primordial²³ helium cannot be retained by the Earth's gravitational field. The source of the major portion of helium in the universe was the Big Bang nucleo-synthesis, while the amount of helium is steadily increasing in the interstellar medium due to the fusion of hydrogen.²⁴

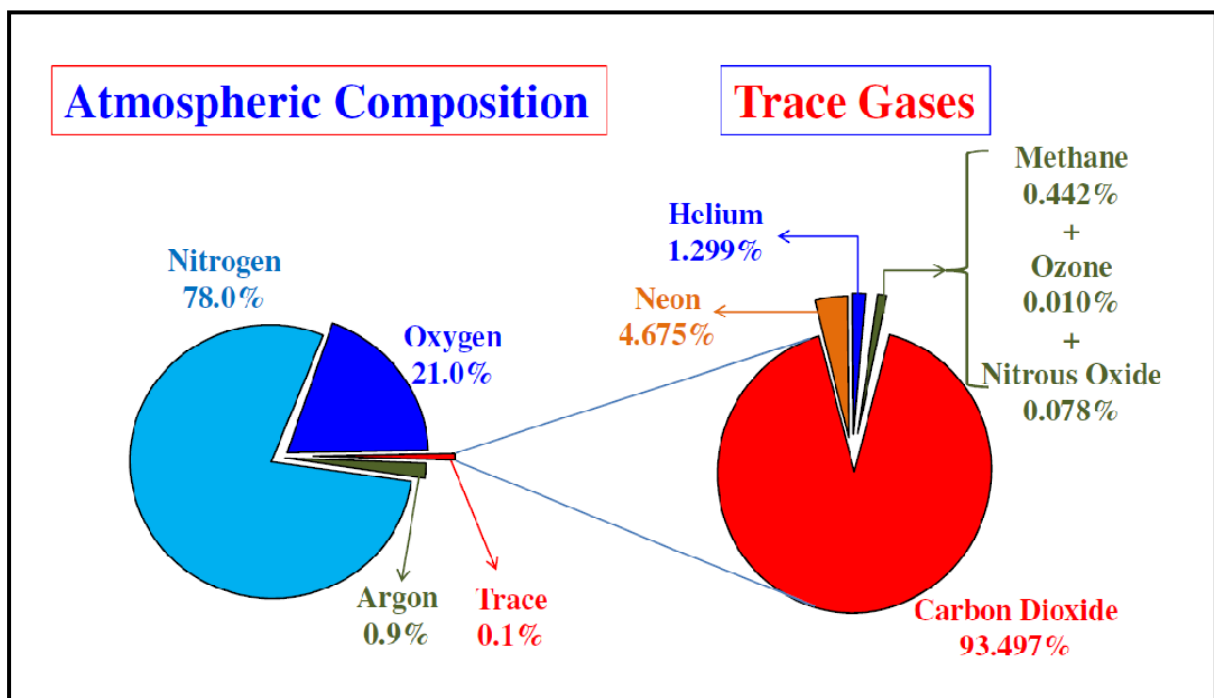


Figure 1.1. Composition of Atmospheric Air

1.2.2. Composition in the Soil

Although the major source of the noble gases is the atmospheric air, all the noble gases were discovered from the minerals and meteorites on the Earth's crust. It is believed that all these noble gases were released into the atmosphere very long ago as a by-product of the decay of the radioactive materials in the Earth's surface. The radiogenic noble gases are primarily produced by radioactive decay processes²⁵ and nucleogenic reactions.²⁶

One of the most important sources of helium (^4He) on Earth is the alpha decay of radioactive nuclides such as uranium (^{238}U and ^{235}U) and thorium (^{232}Th) found in the continental crust leading to the accumulation in the natural gas.²⁷ On the other hand, the abundance of argon is increased as a result of the beta decay of potassium (^{40}K) to produce argon (^{40}Ar). Although only 11% radiogenic decay of ^{40}K produces ^{40}Ar by electron capture, ^{40}Ar dominates among all the isotopes of argon with isotopic abundance of 99.6% in the Earth's atmosphere.²⁸ A very minor quantity of krypton is produced through the radiogenic decay processes. However, xenon has an exceptionally low abundance in the atmosphere. The xenon gas is only trapped from the Earth's crust since most of the isotopes of xenon are the fission product of the radioactive nuclides like ^{238}U and ^{244}Pu in minerals. The most significant fission product is ^{136}Xe which is accompanied by the lesser amounts of other isotopes of xenon.²⁹ The occurrence of radon in the aerial atmosphere is virtually negligible. The only source of it is the fission process of the heavier radio nuclides. Radon usually is isolated as a product of the radioactive decay of radium compounds found in the lithosphere. The nuclei of radium atoms spontaneously disintegrate by emitting energy and particles, *viz.*, helium nuclei (alpha particles) and radon nuclides.

In this context, it is important to mention that nucleogenic reactions²⁶ are also responsible for the formation of noble gases in the atmosphere. The alpha particles and neutrons generated from the decay of uranium and thorium nuclides can bombard lighter elements producing noble gases through nuclear reactions. Particularly, the production of neon in the Earth's crust is entirely due to nucleogenic routes. Different isotopes of neon had been successfully produced by bombarding alpha particles on silicates and fluorite ore. Alternatively, bombardment of neutron on ferro-magnesium rocks leads to the formation of various isotopes of neon. On the other hand, ^3He isotope is also produced through the neutron

bombardment on the ${}^6\text{Li}$ isotopes which is an incompatible element present in high concentration in granite rocks.³⁰

1.2.3. Occurrence in the Groundwater

Depending on the solubility in water, the atmospheric noble gases are dissolved in water and subsequently migrate into basin aquifers transported by groundwater.³¹ All the noble gases are observed in terrestrial deep-sea sedimentary rocks as obtained from eastern equatorial Pacific.³² The solubility of the noble gases in any fluid has also been studied with the knowledge of fractional composition of the noble gases in the atmosphere, solubility of noble gases in water, and the extent of degassing in ground water.³³ The production of ${}^{36}\text{Ar}$ in the crust is smaller as compared to the amount of atmosphere-derived ${}^{36}\text{Ar}$ that is actually released from the dissolved groundwater.³⁴ Very recently, Sturchio *et al.* have found one million year old groundwater in the Sahara as revealed by krypton dating (${}^{81}\text{Kr}$).³⁵ The natural abundances of the noble gas isotopes found in one litre of groundwater are 8500, 1200 atoms of ${}^{39}\text{Ar}$ and ${}^{81}\text{Kr}$ isotopes, respectively.

1.3. Physical and Chemical Properties

Physical Properties

The noble gases are colorless, odorless, tasteless, and non-flammable in nature. In general, the monoatomic noble gases behave like ideal gases under some typical conditions, but most of the times they disobey the ideal gas law. Considering the deviation from the ideal behavior, it was assumed that there exist intermolecular interactions between the noble gas atoms. Based on experimental results of argon, in 1924, John Edward Lennard-Jones deduced a potential from the first principle to understand the intermolecular forces playing between the noble gas atoms which is famous as ‘Lennard-Jones Potential’.³⁶ Due to this weak

intermolecular interaction, some noble gases have higher atomic weights than the naturally occurring solid elements. Some important physical parameters³⁷ of the noble gas atoms have been listed in Table 1.1.

Table 1.1. Atomic Number (N), Atomic Radius (R in Å), Melting Point (MP in K), Boiling Point (BP in K), Density (ρ in gL^{-1}), Ionization Energy (IE in eV), Electron Affinity (EA in eV), Electronegativity (χ in eV), Polarizability (α in \AA^3) of the Noble Gases.

Element	N ^a	R ^a	MP ^a	BP ^a	ρ ^a	IE ^b	EA ^c	χ ^c	α ^d
He	2	0.31	0.95 ^e	4.4	0.179	24.587	-2.70	11.12	0.2050
Ne	10	0.38	24.7	27.3	0.900	21.565	-4.88	8.41	0.3956
Ar	18	0.71	83.6	87.4	1.782	15.760	-3.14	6.31	1.6411
Kr	36	0.88	115.8	121.5	3.708	14.000	-2.41	5.86	2.4844
Xe	54	1.08	161.7	166.6	5.851	12.130	-1.76	5.34	4.0440
Rn	86	1.20	202.2	211.5	9.970	10.749	-1.27	5.23	5.3000

^aReference 38; ^bReference 39; ^cReference 40; ^dReference 41; ^eAt 25 bar.

Down the group in the periodic table, the atomic radius increases with the increase in the number of electron leading to increase in size of the atoms. Consequently, some physical properties, *viz.*, ionization potential³⁹ and electronegativity⁴⁰ of the atom decreases on going from helium to radon because the valence electrons are loosely held with the nucleus in the larger noble gases due to larger atomic radius.^{41,42} Therefore, among all the noble gases helium has highest ionization potential while radon has the least value. It is worthwhile to mention that noble gases have the largest ionization potential among all the elements in each period in the periodic table. On the other hand, the electron affinity⁴⁰ value increases from neon to radon except helium due to the absence of *p* orbital. In this context, it is of immense interest to know the covalent (r_{cov}) and van der Waals (r_{vdw}) radii of the noble gas atoms (reported in Table 1.2) which are essential for analyzing the nature of chemical bonds formed between the noble gas and other elements.

Table 1.2. Covalent Radii (r_{cov} in Å) and van der Waals (r_{vdw} in Å) of the Noble Gases.

Element	r_{cov}^a			r_{vdw}			
	Single	Double	Triple	Bondi ^b	Pyykkö ^c	VogAlv ^d	RahHofAsh ^e
He	0.46			1.40		1.43	1.34
Ne	0.67	0.96		1.54	1.55	1.58	1.56
Ar	0.96	1.07	0.96	1.88	1.88	1.94	1.97
Kr	1.17	1.21	1.08	2.02	2.00	2.07	2.12
Xe	1.31	1.35	1.22	2.16	2.18	2.28	2.32
Rn	1.42	1.45	1.33		2.24	2.40	2.43

^aReference 43; ^bReference 44; ^cReference 45; ^dReference 46; ^eReference 47.

The macroscopic physical properties of the noble gases are primarily dominated by the weak van der Waals forces acting between the atoms. Going down the group from helium to radon, the attractive force increases with the increase in size of the atoms which in turn increase the polarizability resulting into an enhancement of melting point, boiling point, enthalpy of vaporization, and solubility. One unique feature of helium is its exceptionally lower melting and boiling points compared to any known substance exhibiting its superfluidity. In order to make solid helium, one has to apply a huge pressure of 2500 kPa at a temperature of 0.95 K (-272.2°C).⁴⁸ One more important physical parameter is density, which is increased with the increase in atomic weight of the noble gas atoms while going down the group from helium to radon.

Chemical Properties

In general, the chemical properties of an atom exclusively depend on the number of electrons in the outermost occupied orbital known as valence shell. In 1916, both W. Kossel⁴⁹ and G. N. Lewis⁵⁰ reported and highlighted the electronic configuration of noble-gas atom which was found to be the most stable electronic configuration among all the elements exists in nature. According to them, there was always a tendency of all the elements to get the stable

neighbouring noble gas electronic configuration by gaining or losing electron(s). Since all the atoms had inherent affinity to obtain the electron arrangements of the nearest noble gas atoms, therefore the chemical inertness of the noble gases was self evident.

The valence electronic configuration of all the noble gas atoms are ns^2np^6 (i.e., 8 electrons) except $1s^2$ for He atom with two valence electrons. All the noble gases have closed shell structures with full valence eight electrons usually represented by the group term 'octet', except helium having two electrons in the outermost shell possesses 'duet' with closed shell electronic arrangement. Since noble gas atoms are extremely stable due to full valence electron shell, therefore, they do not have a tendency to form chemical bond with the other elements by gaining or losing any electron(s).⁵¹ This fact clearly indicates the inert nature of the noble gas atoms. Considering the most stable electronic configuration among all the elements of the periodic table, Mendeleev labelled the noble gas atoms as 'Group 0' and placed them in the periodic table in a separate group since the valency of the noble gas atoms is zero. In this context, it is important to emphasize that being the most stable electronic arrangement 'noble gas notation'⁵² is widely used to represent any electronic configuration of any other element in the periodic table. For example, the electronic configuration of sulphur atom is $1s^22s^22p^63s^23p^4$, which can be written in terms of 'noble gas notation' as $[\text{Ne}] 3s^23p^4$.

1.4. Applications of Noble Gases: Advantages and Disadvantages

Advantages

Being a lighter element after hydrogen, helium, of course, is widely used in balloons for both in large airships and for the balloons to bring joy and fun among children. Irrespective of the expensiveness, helium is used instead of hydrogen for providing buoyancy to airships due to high inflammability of hydrogen. By utilizing its buoyancy effects, helium is also used as breathing gas for going down beneath the surface of the ocean due to its less solubility in the

human blood as compared to nitrogen. The most promising applications of helium are mainly related to its extraordinarily low freezing point. Liquid helium (~4 K) has played a significant role in the low-temperature science known as cryogenics providing wide range of applications, *viz.*, used to cool superconducting magnets needed for nuclear magnetic resonance (NMR) imaging.⁵³ Very close to absolute zero *i.e.*, mili-kelvin of temperature can also be achieved by supersonic expansion of liquid helium. It is worthwhile to mention that helium is also used as filling gas in nuclear fuel rods for nuclear reactors.⁵⁴ Helium is vastly used as a buffer gas in CO₂ laser which is very powerful laser till today for application in military grade weapon. In He-Ne laser, helium gas is used in the cavity as the core gas.

Inspired by the discovery of neon by Ramsay, in 1910 French chemist Georges Claude conducted experiments that led to the development of the neon light which produced an eye-catching bright red glow when charged with electricity. Eventually Claude was able to create letters and pictures producing a variety of colors across the spectrum by mixing other gases with neon. In 1928, the first color television was produced by using neon, helium and mercury tubes to generate red, blue and green color, respectively, in the receiver. In this regard, it is also important to mention that the neon gas is used in copper vapor laser and He-Ne laser.

Upon subject to extremely high temperatures, the volcanic rocks release argon, specifically ⁴⁰Ar, formed by the radioactive decay of ⁴⁰K. One of the most fascinating uses of argon is the ⁴⁰Ar-dating which is widely used by geologists and palaeontologists. Estimating the amount of released ⁴⁰Ar, palaeontologists have been able to determine the age of volcanic layers above and below fossil and artefact remains in east Africa. For the trapping of reactive intermediates, solid argon has been used as an inert matrix at very low temperatures.⁵⁵ In order to shield the welding arcs and the surrounding base metal from the atmosphere during welding and cutting, the most commonly used gases are both helium and argon. They are also

used in other metallurgical processes, *viz.*, in the production of silicon for the semiconductor industry. Moreover, argon ion laser is extremely useful in the field of scientific research and in various other fields.

According to Loosli and Oeschger, ^{81}Kr ($t_{1/2} = 2.29 \times 10^5$ yr) is produced in the upper atmosphere by cosmic-ray induced spallation and neutron activation of stable Kr isotopes.⁵⁶ Employing laser-based atom-counting method, the measurements of $^{81}\text{Kr}/\text{Kr}$ in deep groundwater from the Nubian Aquifer (Egypt) reveal a recurrent Atlantic moisture source during Pleistocene pluvial periods. These results clearly indicate that the ^{81}Kr dating method for old groundwater is found to be robust and such measurements could be applicable for a wide range of hydrologic problems.³⁵ Krypton has an enormous number of specialized applications *viz.*, manufacturing high level of thermal efficient windows and high performance light bulbs, constructing laser mixing with fluorine, etc. On the other hand, krypton is in competition with its sister element, xenon, in the development of fuel for space exploration. Although xenon provides better performance, krypton has become more useful as a fuel for space flight due to ten times less expensive than xenon.

In addition to its potential use as a space fuel, xenon has versatile applications in different fields, *viz.*, in arc lamps for motion-picture film projection and automobile headlamps, in high-pressure ultraviolet radiation lamps, in specialized flashbulbs, etc.⁵⁷ The movement of sands along a coastline can be traced with the use of one particular isotope of xenon. Moreover, xenon is used as an aesthetic medicine due to its high solubility in lipids and easy elimination from the body resulting faster recovery.⁵⁸ Furthermore, xenon possesses potential application in the field of neuroscience for diagnostic purpose to illuminate the X-ray images of the human brain. Noble gases which are found in the submarine glasses from mid-oceanic ridges and submarine pillow basalt glasses from Loihi reveal the early history of the Earth.⁵⁹ Surprisingly, of late, scientists have found noble gases in iddingsite from the

Lafayette meteorite which is the strong evidence of presence of liquid water on Mars in the last few hundred million years.⁶⁰ In this context, it is very important to mention that the noble gases are used in excimer lasers in combination with halogen based on short-lived electronically excited molecules, *viz.*, ArF, KrF, XeF, XeCl, etc. producing ultraviolet light with short wavelength. Excimer lasers have wide range of applications in the field of industries and medical sciences including laser surgery, laser angioplasty, laser eye surgery, etc.⁶¹

In spite of radiation hazards to the human life, radon has a plenty of applications in various fields, specifically, for detecting leaks, measuring flow rates, and inspecting metal welds. In addition, the concentration of radon in groundwater provides a potential application in seismography in predicting earthquakes which in turn helps to take preventive measures against this devastating natural disaster. In medical science, radon is widely used in radiotherapy.

Disadvantages

During the circulation of atmospheric air used as a coolant in the nuclear reactor, the isotope of argon (^{40}Ar) having natural abundance 99.6% converted to radioactive isotope (^{42}Ar , $t_{1/2} = 32.9$ yrs) emits β^- when air passes through the components of the reactor leading to an environmental pollution. On the other hand, the radioactive Kr and Xe nuclides which are produced as a by-product from the nuclear fission of the fuel in the nuclear reactor are released from the nuclear stack. These released gases contaminate the atmospheric air leading to environmental air pollution.

The radioactive decay of radium isotope in the lithosphere leads to the formation of radon which seeps into the buildings through cracks in their foundation accumulates in areas that are not well ventilated. A huge number of lung cancer deaths per annum in the United

States are due to the significant health hazard created by the radon isotope. According to United States Environmental Protection Agency (EPA), during the late 1980s and 1990s about ten million American homes that has been weather-sealed to improve the efficiency of heating and cooling systems, it is indeed potentially high risk due to the presence of harmful radon levels in soils containing high concentrations of uranium.

1.5. The Promising Diverse Chemistries

After the pioneering discovery of the inert gas atoms, Ramsay and co-workers had made a large number of attempts to chemically combine the inert gas atoms with the other elements of the periodic table. Unfortunately, they were unable to make chemical bonding with the inert gas atom even under vigorous reaction conditions and their tremendous efforts became unsuccessful. Looking at the extreme unreactiveness of the inert gas atoms, Hugo Erdmann (cf. Renouf Edward)⁶² first introduced the term ‘Noble Gas’. In general, noble gas elements were originally considered to be extremely stable and therefore chemically unreactive due to their completely filled *s* and *p* valence orbitals. This concept persisted until theoretical predictions of stable molecules with heavier noble gas atoms by Pauling in 1933.⁶³ According to Walter Kossel and Linus Pauling, highly reactive atoms such as fluorine might form compounds with the heaviest of the noble gas elements like xenon whose valence electrons are weakly bound as compared to lighter gases. Sometimes spectacular discovery made by a person, changes the concept of a scientific field forever. One such noble person is Prof. Neil Bartlett⁶⁴ whose experimental findings of xenon hexafluoroplatinate $\text{Xe}[\text{PtF}_6]$ in 1962 in his laboratory alone alter the fundamental perception of the “inertness” nature of noble gas elements. Nevertheless, the small ionization potential of xenon atom resembles to that of the oxygen molecule that led Bartlett to attempt oxidizing xenon using platinum hexafluoride, an oxidizing agent found to be strong enough to react with oxygen. He found that with the

combination of xenon the deep red platinum hexafluoride vapour turns into yellow solid of $\text{Xe}[\text{PtF}_6]$. With the discovery of $\text{Xe}[\text{PtF}_6]$, a new chemistry is born called ‘Noble Gas Chemistry’. Depending on the nature of chemical bonding exists between the noble gas atom and the other elements, the noble gas compounds can be classified into two major categories, *viz.*, ‘Classical’ and ‘Non-Classical’ possessing usual and unusual chemical bonding, respectively.⁶⁵

1.5.1. ‘Classical’ Noble Gas Compound involving Conventional Chemical Bonds

Noble Gas Halides, Oxides, Oxo-halides and their Salts

After the pioneering discovery of first noble gas compound, $\text{Xe}[\text{PtF}_6]$, by Bartlett, scientists all over the world were very keen to explore the field of noble gas chemistry by synthesizing various kinds of noble gas compounds. Inspired by his work, in the same year 1962, Claassen and co-workers had synthesized xenon tetrafluoride (XeF_4)⁶⁶ whereas, xenon difluoride (XeF_2) was prepared and characterized by two groups of scientists⁶⁷ simultaneously. Since the chemical bonds existing between noble gas and other atoms are very delicate due to various electron transfer processes, low-temperature experimental techniques only provide the suitable conditions for the preparation of noble gas containing chemical compounds.⁶⁸ Consequently, cryogenic matrix isolation techniques had been employed to synthesize a large number of novel noble gas compounds, *viz.*, noble gas halides like KrF_2 ,⁶⁹ KrF_4 ,⁷⁰ XeF_2 ,⁶⁷ XeF_6 ,⁷¹ XeF_8 ⁷¹ and noble gas mixed halides, XeClF .⁷² In this context, it is very important to mention that xenon fluorides⁷³ and krypton fluorides⁷⁴ had also been prepared by using ionizing radiation in the form of γ rays or electron beams by MacKenzie and co-workers. Later, the same group had successfully synthesized xenon fluorides *viz.*, XeF_2 , XeF_4 , XeF_6 and krypton difluoride, KrF_2 upon proton bombardment on the gas mixtures of xenon or krypton and fluorines.⁷⁵ It is well known that the xenon fluorides are thermodynamically

stable compounds whereas the xenon chlorides and xenon bromides are not stable. Nelson and Pimentel had successfully prepared and characterized XeCl_2 at low temperature by using infrared spectroscopic technique.⁷⁶ In contrast, XeBr_2 were obtained by some special method⁷⁷ due to the unstable nature of the compound.

Ab initio density functional theory (DFT) based methods have been employed to optimize the structures of XeF_n ($n = 2, 4$ and 6) molecules followed by vibrational frequency calculations.⁷⁸ In general, the most stable XeF_2 exists as soft molecular crystals and easily sublimates at room temperature. In XeF_2 , the observed Xe–F bond lengths are found to be 1.974 and 2.000 Å in the gas phase⁷⁷ and solid state,⁷⁹ respectively. Similarly, the experimentally detected Xe–F bond length values are 1.954 and 1.895 Å in the gaseous XeF_4 ⁸⁰ and XeF_6 ⁸¹, respectively. In the recent past, Liao and Zhang have systematically reported the nature of chemical bonding in the noble gas halides in the gaseous phase and solid state.⁸² It has been well established that the noble gas halides behaves like a Lewis base and can combine with strong Lewis acid by simple addition reaction. Scientists have found that XeF_6 reacts with BF_3 , AsF_5 and SbF_5 at room temperature to form 1:1 addition compound existing as $[\text{XeF}_5^+][\text{BF}_4^-]$,⁸³ $[\text{XeF}_5^+][\text{AsF}_6^-]$ and $[\text{XeF}_5^+][\text{SbF}_6^-]$,⁸⁴ respectively. Similarly, XeF_6 forms salt with some transition metal pentafluorides that can be represented as $[\text{XeF}_5^+][\text{MF}_6^-]$ ($M = \text{Ru, Rh, Os, Ir, Pt, Pd}$ and Au).⁸⁵ Like XeF_6 , XeF_2 is also a potential candidate for the salt formation with several halides. XeF_2 combines with AsF_6 and SbF_6 in 1:1 and 1:2 ratio producing $[\text{Xe}_2\text{F}_3^+][\text{AsF}_6^-]$ ⁸⁶ and $[\text{XeF}^+][\text{Sb}_2\text{F}_{11}^-]$ ⁸⁷ salts, respectively. Like XeF^+ salt, it has also been made possible to isolate the $[\text{XeCl}^+][\text{Sb}_2\text{F}_{11}^-]$ ⁸⁸ salts having Xe–Cl bond. Since XeF_4 is a poor fluoride ion donor, it forms complexes only with the strongest Lewis acid, SbF_5 , leading to salt formation with the formulation of $[\text{XeF}_3^+][\text{SbF}_5^-]$ and $[\text{XeF}_3^+][\text{Sb}_2\text{F}_{11}^-]$.⁸⁹ Nevertheless, krypton difluoride also participated in the preparation of

salts while combining with Lewis acid resulting to the formation of $[\text{KrF}^+][\text{MF}_6^-]$ ($\text{M} = \text{As}$, Sb and Pt), $[\text{Kr}_2\text{F}_3^+][\text{MF}_6^-]$ ($\text{M} = \text{As}$ and Sb) and $[\text{KrF}^+][\text{Sb}_2\text{F}_{11}^-]$.⁹⁰ In this context, it is important to emphasize that there exists two type of Ng–F bonds with very different bond lengths in the case of ionic $[\text{A–F}] \cdots [\text{NgF}^+]$ salts, where A represents a strong Lewis acid like AsF_5 , SbF_5 , etc.⁹¹ In $[\text{XeF}^+][\text{Sb}_2\text{F}_{11}^-]$ salt, the closest Xe–F distances have been found to be 1.888 and 2.343 Å which implies that there exists more covalent character in between Xe and F atoms in the XeF^+ cation than that in the gaseous XeF_2 molecule.⁹²

Stimulated from the similar ionization potential of xenon and oxygen, researchers were devoted towards the finding of chemical bonding existing between the xenon and oxygen atom. In that episode, it had been experimentally observed that the partial hydrolysis of XeF_6 in either static or dynamic system lead to the formation of XeOF_4 ⁹³ and XeO_2F_2 ⁹⁴ while the complete hydrolysis of XeF_6 or XeOF_4 resulted highly explosive XeO_3 .⁹⁵ In that context, xenon tetroxide (XeO_4)⁹⁶ which was first prepared in the form of yellow solid at low temperature and characterized by Selig *et al.* was found to be dangerous by its explosive nature. On the contrary, sodium or barium salts of xenon oxides are found to be highly stable and obtained as insoluble sodium perxenate (Na_4XeO_6), potassium perxenate (K_4XeO_6), barium perxenate (Ba_2XeO_6), etc.⁹⁷ Very recently, Beckers and co-workers have investigated the molecular structures and vibrational spectra of XeOF_4 molecule through joint experimental-computational study.⁹⁸ Similar to the XeF_4 , being weak Lewis base the noble gas oxofluorides are also poor donor of fluoride ion. Therefore, XeOF_4 and XeO_2F_2 can only form adduct with strongest Lewis base, SbF_5 leading to the formation of the salts. For example, XeOF_4 reacts with SbF_5 in 1:1 and 1:2 ratio with the formation of $[\text{XeOF}_3^+][\text{SbF}_6^-]$, $[\text{XeOF}_3^+][\text{Sb}_2\text{F}_{11}^-]$ salts while the XeO_2F_2 only forms 1:2 adduct, $[\text{XeO}_2\text{F}^+][\text{Sb}_2\text{F}_{11}^-]$.⁹⁹

1.5.2. 'Non-Classical' Noble Gas Compound involving Unusual Chemical Bonds

Typical Ng–N and Ng–C Containing Compounds

Motivated by the most overwhelming discovery of Ng–F and Ng–O chemical bonds, researchers were very enthusiastic to explore the nature of chemical bonding exists between the noble gas atoms with the other elements. In 1974, LeBlond and DesMarteau¹⁰⁰ first discovered $[\text{FXe}^+][\text{N}(\text{SO}_2\text{F})_2^-]$ complexes containing Xe–N bond while its crystalline structure was reported by Sawyer *et al.* in 1982.¹⁰¹ This finding paved the way for the discovery of several Ng–N containing chemical compounds for the next two to three decades, for examples, $\text{Xe}^{\text{II}}[\text{N}(\text{SO}_2\text{F})_2^-]_2$,¹⁰² $\text{Xe}[\text{N}(\text{SO}_2\text{R})_2^-](2,6\text{-F}_2\text{C}_6\text{H}_3^-)$ where R = F, CF_3 ,¹⁰³ and $[\text{F}_3\text{SN-XeF}][\text{AsF}_6^-]$.¹⁰⁴ All the Xe–N compounds are found to be thermally stable whereas the Kr–N containing compounds are stable only below -60°C .¹⁰⁵

Analogous to Ng–N bond, it was also very difficult to obtain genuine Ng–C containing compounds. Taking this challenge, two groups of scientists, *viz.*, Naumann *et al.*¹⁰⁶ and Frohn *et al.*¹⁰⁷ independently prepared $[(\text{F}_5\text{C}_6)\text{Xe}^+][\text{B}(\text{C}_6\text{H}_5)_3\text{F}^-]$ and $[(\text{F}_5\text{C}_6)\text{Xe}^+][\text{B}(\text{C}_6\text{H}_5)_3\text{F}_3^-]$ as colorless solids having Xe–C bond. Following the above synthesis, $[(\text{F}_5\text{C}_6)\text{XeF}]$ combined with Lewis acid AsF_5 leading to the formation of the salt $[(\text{F}_5\text{C}_6)\text{Xe}^+][\text{AsF}_6^-]$ which has very high melting point (102°C).¹⁰⁸ Due to its significant stability, a new field has been emerged commonly known as 'Organoxenon Chemistry' where the fluoroarsenate salt is considered as an important reagent. Subsequently, a large number of organoxenon compounds have been synthesized, *viz.*, $[\{(\text{F}_5\text{C}_6)\text{Xe}\}_2\text{F}^+][\text{AsF}_6^-]$,¹⁰⁹ $[(\text{F}_5\text{C}_6)\text{XeF}_2^+][\text{BF}_4^-]$,¹¹⁰ etc. Similarly, the novel crystalline salt, $[\{(\text{F}_5\text{C}_6)\text{Xe}\}_2\text{Cl}^+][\text{AsF}_6^-]$ ¹¹¹ which was also prepared from $[(\text{F}_5\text{C}_6)\text{XeCl}]$ as an adduct with AsF_5 , was found to be reasonably stable at an ambient temperature. It is worthwhile to mention that the Xe–Cl bond in this compound is found to be more stable as compared to that in the XeCl_2 molecule.

Noble Gas–Metal (Ng–M) Bonding

Till 1983, it was believed that noble gas can bind only with the non-metals due to its similar gaseous nature. It was really a remarkable discovery of first Ng–M containing compound, $\text{XeM}(\text{CO})_5$ ($\text{M} = \text{Cr}, \text{Mo}$ and W) in liquid xenon or in liquid krypton doped with xenon by Simpson *et al.*¹¹² and Wells and co-workers¹¹³ in 1983. In this case, electron-rich Xe atom behaves like a Lewis base towards an electron scarce metal centre acting as a ligand in coordination complexes. In 1996 with the advent of supercritical fluid, Sun *et al.*¹¹⁴ had developed a new technique where supercritical fluids of Ar, Kr and Xe can provide a generous route to investigate the interaction of weakly coordinating ligand (noble gas) in solution phase. In these compounds, five CO π acceptors withdraw a large amount of electron density from the metal leading to an electron deficient metal centre which in turn compels Xe to donate electron to the metal center. In this episode, Thompson and Andrews had succeed to make Ng–M bond by synthesizing NgBeO ($\text{Ng} = \text{Ar}, \text{Kr}$ and Xe) species,¹¹⁵ where Ng atom forced to donate the electron to the empty *sp* hybridised orbital of coordinatively unsaturated Be^{II} cation and thereby Ng atom behaves like a Lewis base. Although NgBeO was first prepared in 1994, it was predicted earlier by Frenking *et al.* in 1988.¹¹⁶ In this context, Pyykkö and his co-workers¹¹⁷ have reported that there exist weaker dispersive interactions between the lighter noble gas atoms and BeO molecule. Very recently, Grandinetti *et al.*¹¹⁸ have investigated the bonding strength of Ng–M in NgBeS analogue theoretically which was experimentally prepared by Wang and Wang after one decade.¹¹⁹ Of late, it has been established that the metal oxide-noble gas complexes are detected in cold matrices which provides an ideal condition for synthesizing Ne–BeCO_3 ,¹²⁰ $\text{Ne–Be}_2\text{O}_2\text{–Ne}$ ¹²¹, and Ne–BeSO_2 .¹²² It has also been established that the noble gas can form chemical bond with actinide elements. One of the most interesting noble gas-actinide complex is trans-

[U(C)(O)Ng₄] (Ng = Ar, Kr and Xe), trans-[UO₂Ng₄] (Ng = Ne and Ar), etc. where Ng acts as a ligand to the metal centre having low coordination number.¹²³ The first detection of the complexes formed by noble gas atoms with CUO and other uranium compounds originates a new unprecedented noble gas-actinide chemistry. Evidence for the formation of mixed noble clusters [CUO(Ar)_{4-n}(Xe)_n] and [CUO(Ar)_{4-n}(Kr)_n] (n = 1, 2, 3, 4), have also been reported by Andrews and co-workers.¹²⁴

The bonding between noble gas and noble metal is unusual since both are extremely reluctant to form chemical bonding due to their inert nature. Schröder *et al.* first experimentally identified chemical compounds involving noble gas and noble metal, XeAu⁺ and XeAuXe⁺, by mass spectrometry in 1998,¹²⁵ although they were first conceived by Pyykkö, who predicted the stability of the species theoretically in 1995.¹²⁶ According to Buckingham and co-workers,¹²⁷ the origin of the noble metal–noble gas bonding is the long-range polarization and dispersion effect, and no significant covalent character persists therein as proposed by Pyykkö. At the outset of the millennium, one of the most unpredictable discoveries is the marriage between the noble gas and noble metals since both are extremely reluctant to form any complexes with the other elements. In 2000, Seidel and Seppelt¹²⁸ had successfully isolated the first complex [AuXe₄][Sb₂F₁₁]₂ containing noble gas–noble metal bond which is found to be thermally stable. The AuXe₄²⁺ salt consists of four Xe atoms acting as Lewis bases coordinate the divalent gold central metal ion in more or less square planer arrangement. Following this remarkable findings, a large number of Au–Xe complexes with variable oxidation states of gold, *viz.*, cis- and trans- [AuXe₂](Sb₂F₁₁)₂, [(AuXe)₂F](SbF₆)₃, [AuFXe₂](Sb₂F₁₁)(SbF₆), [(F₃As)AuXe](Sb₂F₁₁), etc.¹²⁹ have been synthesized in super acidic conditions. Analogous to gold, another heavy metal, mercury, also forms chemical bond with noble gas atom in the [HgXe](Sb₂F₁₁)(SbF₆) salt which were prepared and characterized by suitable experimental technique.¹³⁰ In this context, it should be

mentioned that it is possible to isolate some of the cationic noble gas–metal complexes, F_3Si-Xe^+ , F_3Ge-Xe^+ , in the gas phase as reported by Grandinetti and co-workers.¹³¹

The accidental finding of pure rotational spectra of $ArAuCl$ and $KrCuCl$ with the cavity pulsed-jet FTMW spectrometer by Gerry *et al.*¹³² open the gate of a new arena in the chemical sciences. Subsequently, a series of compounds containing Ng–M bond (Ng = Ar, Kr, and Xe; M = Au, Ag, and Cu), *viz.*, $NgMX$ (X = F, Cl, and Br) have been investigated both experimentally as well as theoretically.¹³³ In all these compounds, the noble-gas–noble-metal bondings are partially covalent in nature and strong interactions are playing between closed-shell fragments, *viz.*, noble gas and noble metal halides. *Ab initio* density functional theory have been employed to investigate the geometries and bond energies of the $He-MX$, $Ne-MX$, and $Ar-MX$ (M = Cu, Ag, Au; X = F, Cl) complexes by Wright *et al.*¹³⁴ In the recent past, $NeAuF$ has also been detected through matrix isolation technique supported by quantum chemical calculations.¹³⁵ Of late, Chattaraj and co-workers have compared noble gas binding ability of metal cyanides versus metal halides (Metal = Cu, Ag, Au) using *ab initio* molecular orbital theory based techniques.¹³⁶

The secondary basicity of F^- is drastically reduced due to the low lying lone pair of electrons of fluoride ion in XeF_2 molecule. Therefore, a strong Lewis acid is required for substantial interaction with a weak base. In the presence of strong Lewis acid, AsF_5 , AgF becomes $Ag(AsF_6)$ where the Ag^+ metal ion center is virtually ‘naked’. XeF_2 , acting as a ligand, easily forms adduct with $Ag(AsF_6)$ forming a colorless solid, $Ag(XeF_2)_2(AsF_6)$,¹³⁷ where the metal center is eight fold coordinated by four F atoms from XeF_2 and the other four F atoms from AsF_6^- . Motivated from the Bartlett’s discovery of $Ag(XeF_2)_2(AsF_6)$ in 1991, next one decade Žemva and co-workers have systematically investigated a numerous adducts formed between XeF_2 and various salts comprised of a range of XeF_2 molecules, *viz.*, three in $M(XeF_2)_3(AsF_6)_2$ (M = Pb, Sr),¹³⁸ $Ln(XeF_2)_3(AsF_6)_3$, $Ln(XeF_2)_3(BiF_6)_3$ (Ln =

Lanthanides),¹³⁹ four in $\text{Ba}(\text{XeF}_2)_4(\text{AsF}_6)_2$,¹⁴⁰ five in $\text{Cd}(\text{XeF}_2)_5(\text{SbF}_6)_2$, etc.¹³⁸ Although XeF_4 is a very poor Lewis base, it is also acting like a ligand in $\text{Mg}(\text{XeF}_4)(\text{AsF}_6)_2$ which has been successfully isolated.

Noble Gas Insertion Compounds

The first neutral argon compound, HArF ,¹⁴¹ was prepared experimentally at cryogenic conditions and was characterized using low temperature matrix isolation infrared spectroscopic technique by Khriachtchev *et al.*. The successful identification of the HArF molecule, associated with H–Ar covalent bonding, has revolutionized the field of ‘noble gas chemistry’. Since then, noble gas chemistry has become an enthralling field of research for both theoreticians and experimentalists and has experienced a renaissance during the past two decades,¹⁴²⁻¹⁶⁵ and today it is one of the frontier areas of research in chemical sciences¹⁶⁶⁻¹⁶⁸ involving both theory and experiment. Subsequently, an extensive amount of work has been carried out to provide an in-depth insight into the nature of chemical bonds and to enhance the general understanding about metastable molecules involving noble-gas atom. A wide range of different compounds containing various noble gas atoms have been theoretically anticipated and prepared. Here it is imperative to note that quantum chemical methods play an important role in predicting new noble gas compounds and also in interpreting their physicochemical properties.

The outstanding breakthrough by Räsänen and co-workers,¹⁴¹ with the discovery of first covalently bonded argon compound, HArF led to an entirely new direction of research in ‘noble gas chemistry’. Subsequently, a unique category of novel noble gas hydrides of the type HNgY ($\text{Ng} = \text{Ar}, \text{Kr}, \text{and Xe}$; $\text{Y} = \text{electronegative element or group}$) has received considerable attention among researchers and broaden the scope of the field of noble gas chemistry.^{141-144,160} Various ionic or neutral insertion molecules of noble-gas atoms with

environmentally important species, such as HOX^{156} ($\text{X} = \text{Cl}, \text{Br}, \text{F}$) and species of astronomical significance, like HCO^+ ,¹⁵⁷ HN_2^+ ,¹⁵⁸ and so on, have been theoretically investigated using various computational methods. Since hydrogen and helium are the two most abundant elements in nature, HeH^+ species is considered to be an important ion in astrochemistry, which was first detected¹⁶⁹ in mass spectrometry in 1925. In this context, it is essential to emphasize that the noble gas-containing compounds had not hitherto been detected in space before the detection of noble gas hydride cations ($^{36}\text{ArH}^+$) in the Crab Nebula by Barlow and co-workers.¹⁶⁶ The binding energies of these novel metastable molecular species are found to be between the vdW complexes and pure covalent compound. In general, noble gas inserted compounds including the hydrides are found to be stable only at very low temperature. Very recently, kinetic stability aspect of noble gas hydrides has been investigated in great detail in different molecular environments and conditions.¹⁷⁰

One of the most interesting aspects in all these compounds is the nature of the bond formed by the noble gas atom, which is mostly covalent and is somewhat in contrast to the conventional chemical intuition. First density functional study on centrosymmetric $(\text{Ng}_2\text{H})^+$ ions was presented by Jan Lundell.¹⁷¹ Subsequently, both the centrosymmetric $(\text{Ng}_2\text{H})^+$ and non-centrosymmetric $(\text{NgHNg}')^+$ cations have been prepared experimentally through electron bombardment matrix isolation technique and also characterized using Fourier transform infrared (FTIR) spectroscopy.¹⁷² Later on, detailed theoretical works have also been published on these cations.¹⁷³

Moreover, the environmental effect on the vibrational properties of HNgCl molecules embedded in other noble gas (Ng') matrices have also been investigated experimentally very recently by Khriachtchev and co-workers.¹⁶⁵ They have also analyzed the matrix effects theoretically using a number of quantum chemical methods. The insertion of Ng atoms in HCN molecule results in metastable HNgCN ($\text{Ng} = \text{Kr}, \text{Xe}$) species that have been

investigated both theoretically and experimentally by Pettersson *et al.*¹⁷⁴ Insertions of Ng atoms in its isoelectronic counterpart, HCO^+ , have also been investigated theoretically by our group in the recent past.¹⁵⁷ Furthermore, theoretical prediction of such molecules using quantum chemical calculations has proven to be useful in determining their stability and hence synthesizing these compounds experimentally. Of late, one of the noble-gas insertion molecules, HXeOBr , has been successfully prepared and characterized using IR spectroscopic technique by Khriachtchev *et al.*,¹⁶¹ which was theoretically predicted by our group earlier.¹⁵⁶

Studies with organo-xenon derivatives involving a Xe–C bond have significantly increased in the past decade and extensive research have been done on synthesising such molecules.^{108,175} Thus, several compounds containing Xe–C bond, such as HXeCN ,¹⁷⁴ HXeCCH ,¹⁷⁶ HXeCCXeH ,¹⁷⁶ HXeCCF ,¹⁷⁷ HXeC_3N ,¹⁷⁸ and HXeC_4H ¹⁷⁹ have been identified in the solid phase under a cryogenic environment. Moreover, a gate to organo-krypton chemistry has been opened with the discovery of HKrCCH by Khriachtchev *et al.*¹⁸⁰ Subsequently more compounds possessing Kr–C bonds have been prepared and characterized through matrix isolation technique followed by *ab initio* calculations.^{177,181} Additionally, stability of noble gas hydrocarbons has been studied in an organic liquid-like environment by using *ab initio* molecular dynamics simulations and it has been emphasized that the noble gas compounds may remain stable up to 150 K, which is well above the cryogenic temperature.¹⁷⁶

Following the remarkable discovery of HArF ,¹⁴¹ a large number of neutral and ionic noble gas containing chemical species have been discovered in subsequent years.¹⁴²⁻¹⁶⁸ Plenty of ionic and neutral noble gas inserted chemical compounds have been predicted theoretically with various computational techniques through insertion of a noble gas atom into ions/molecules having environmental or astronomical impacts. Of late, a new class of noble gas inserted compounds having the general formula ‘ XNgY ’, where X and Y are two separate

electronegative fragments, such as ClXeCN and BrXeCN¹⁸² have emerged, which are associated with a Ng–C bond as well. Very recently, FXeCN, FXeNC and FKrCN have been prepared and characterized by Khriachtchev and co-workers by UV photolysis of FCN in the Xe and Kr matrices and subsequent thermal annealing.¹⁸³ In this context it may be noted that a few ion–molecule complexes involving xenon were also investigated using mass spectrometric techniques and theoretical calculations while studying the gas phase reactions of XeF⁺ with acetonitrile and methanol.¹⁸⁴

Apart from the noble gas hydrides, our group has predicted the noble gas inserted noble metal fluorides (AuNgF) and hydroxides (AuNgOH) exploiting the gold–hydrogen analogy.¹⁵⁵ In order to understand the chemical bonding between the noble gas atom with group IIIB elements such as B and Al atoms, the stability of the noble gas inserted BF₃ and AlF₃ molecules have been investigated through *ab initio* molecular orbital based methods by our group earlier.¹⁸⁵ Earlier our group has also explored the possibility of existence of noble gas containing molecules by inserting Ng atom in between F and M (M = Be and Mg) atoms in HMF and FMF molecules leading to the formation of metastable HMNgF and FMNgF compounds, respectively, by employing *ab initio* quantum chemical techniques.¹⁸⁶

During the last two decades, noble gas chemistry entered a new era after the astonishing discovery of HArF. In this episode, one of the most fascinating findings of the scientists is the exceptional behavior of NgO species as a Lewis acid. In addition to the insertion type of compounds, Grochala and co-workers have investigated noble gas oxide molecule inside a dipolar cavity consisting of alkali metal fluoride molecules.¹⁸⁷ Apart from this work, W. –P. Hu and co-workers have demonstrated that the stability of F[–](NgO)_n anions is due to the charge-induced Ng–O bond formation. They have also found that the charge separation along the Ng–O bond decreases with the increase in size (n become larger) of the system leading to fully charged fluorine atom.¹⁸⁸

Various other Noble Gas Compounds

Confinement has become an important methodology in the field of ‘noble gas chemistry’.^{189–201} Endohedrally confined noble gas atoms in fullerene cages, $\text{Ng}_n@C_{60}$ and $\text{Ng}_n@C_{70}$, have been investigated theoretically and experimentally.^{189,190,202–206} Noble gas atoms have been successfully incorporated into the fullerene cages by employing techniques like ion bombardment,²⁰⁷ high temperature/high pressure methods, and “molecular surgery”.²⁰⁸ Studies on $\text{He}@C_{60}$ and $\text{Ne}@C_{60}$ by Saunders and co-workers have proposed a “window” mechanism, which involves reversible breaking of one or more bonds of the cage resulting in the incorporation of ^3He and Ne atoms on heating fullerenes in their presence, even though some controversies still exist.¹⁸⁹ The presence of encapsulated noble gas atoms in fullerenes has been detected by observing chemical shifts in the helium NMR spectrum of He-labeled C_{70} species,^{192,202} mass spectrometric evidence of ^{129}Xe NMR spectrum,¹⁹⁰ and by probing the internal magnetic fields inside fullerenes through the analysis of downfield ^3He chemical shifts.²⁰⁵ This experimental evidence instigates the preparation of other stable endohedral clusters in a similar fashion. $\text{Ng}@C_{60}$ complexes have also been reported to possess a high activation barrier of 90 kcal mol^{-1} with respect to dissociation.²⁰⁹ It was found that noble gas atoms can be successfully inserted into cavities even smaller than that of C_{60} such as $C_{10}H_{10}$, $C_{20}H_{20}$, and $\text{Mo}_6C_{18}F_6$.^{210–213} Cross and coworkers²¹¹ have incorporated helium atom into a smaller cage dodecahedrane, $C_{20}H_{20}$, even though theoretical studies revealed that $\text{He}@C_{20}H_{20}$ is less stable by $33.8 \text{ kcal mol}^{-1}$ with respect to isolated $C_{20}H_{20}$ and He atom. The correlation between the stability of endohedral clusters and the ionization potential of the encapsulated atoms has been established by Moran *et al.* by introducing a variety of guest atoms inside C_4H_4 , C_8H_8 , C_8H_{14} , $C_{10}H_{16}$, $C_{12}H_{12}$, and $C_{16}H_{16}$.²¹⁴ Recently, Chattaraj and co-workers have studied confinement-induced binding of noble gas atoms within magic BN-fullerenes like $B_{12}N_{12}$ and $B_{16}N_{16}$ ¹⁹³ and BN doped carbon nanotubes.²¹⁵

Moreover, Chakraborty and co-workers found a slightly higher reactivity of noble gas atoms as well as some other guests (C_2H_2 , C_2H_4 , C_2H_6 , CO_2 , CO , H_2 , NO_2 , and NO) in their confined state inside the octa acid cavitand.²¹⁶

Although most of the noble gas encapsulated cages have been found to be thermodynamically unstable, they exist due to their high kinetic stability. Several bonds involving cage atoms must be broken to knock out the Ng atom from any Ng@cage composite system, which results in this high kinetic stability. In addition to the noble gas encapsulation into various cages, movement of small molecules inside a fullerene have also been investigated experimentally in the recent past.^{217–220} H_2 , HD, and D_2 encapsulated C_{60} clusters have been studied experimentally by Ge *et al.* by using infrared spectroscopy.^{221–223} Dynamics of hydrogen molecules trapped inside anisotropic fullerene cages has also been investigated experimentally by using the inelastic neutron scattering method.²²⁴

Ab initio studies on confinement of noble gas dimers (Ng_2) in C_{60} ²²⁵ and other cages reveal that Ng–Ng bond distances in $Ng_2@C_{60}$ are shorter than those in the corresponding free noble gas dimers. Krapp and Frenking¹⁹⁶ reported the existence of a real Xe–Xe chemical bond in fullerenes, while a weak van der Waals interaction has been shown to exist between the lighter analogues, He and Ne. Cerpa *et al.*¹⁹⁷ have identified that a shorter He–He interaction does not always imply the existence of a chemical bond. Furthermore, *ab initio* molecular dynamics studies on $Ng_n@B_{12}N_{12}$ and $Ng_n@B_{16}N_{16}$ showed that the He–He dimer undergoes translation, rotation, and vibration inside the cavity.¹⁹³ These theoretical investigations on the confinement of noble gas atoms reveal how Ng atoms with completely filled valence orbitals behave when they are forced to confine themselves within a host at its equilibrium geometry. This kind of study attracted considerable attention from researchers because noble gas atoms are widely used in gas storage, gas filtration,^{226–228} etc. Apart from *ab initio* studies, London-type new formulations have been derived to describe the dispersion

interaction in endohedral systems such as A@B, where the interaction energy is expressed in terms of the properties of the monomers, and applied on several atom/molecule encapsulated C₆₀ systems including Ng@C₆₀ systems.^{229,230}

One of the major issues in nuclear fuel reprocessing and several accidental scenarios is to manage radioactive xenon and krypton. Due to the extreme inert nature of noble gases, it is very difficult to trap the radioactive noble gases in suitable matrix by van der Waals interactions using simple physisorption process. It is well known that the metal-organic frameworks (MOFs) are extensively used to absorb and separate various gases including noble gases due to its high intake capacity, better selectivity and tunable chemical properties. Theoretical modelling is necessary to select the suitable MOFs required for radioactive noble gas adsorption/separation. The binding strength at different adsorption sites are favored by van der Waals interactions between the noble gas atoms with MOFs network. In recent times, Thallapally and co-workers have exhaustively studied the adsorption of Ng atom with a large number of MOF systems, viz., Sb-MOF-2,²³¹ Ni/DOBDC,^{232,233} Sb-MOF-1,²³⁴ FMOFCu,²³⁵ M-MOF-74,²³⁶ etc. It has been well established that the successful deposition of Ag nanoparticles in porous MOF-74Ni (or Ni/DOBDC) significantly enhances the noble gas adsorption process in Ag@MOF-74Ni.²³⁷ Very recently, our group has reported that the creation of active centers in the lattice by doping hetero atom in graphene considerably increase the adsorption of fission gases Xe and Kr on pristine and doped graphene.²³⁸

One of the most surprising chemistry of noble gas atoms is the ability to form clusters among themselves. The clusters, Ng_n (n = 2–1000), are mostly of neutral or cationic species with homo or hetero nuclear systems. These clusters are held together by dispersive forces and predominantly detected in the gas phase within the cavities of cage compounds. Very recently, Wales *et al.*²³⁹ have predicted the probable geometries of the clusters Ng₃₋₁₇ by employing the Lennard-Jones potential. Effect of ionization strongly affects the structures of

the clusters. Nevertheless, the cationic dimer (Xe_2^+) and tetramer (Xe_4^+) had been detected in the bulk phase²⁴⁰, whereas the $[\text{Xe}_2^+][\text{Sb}_2\text{F}_{11}^-]$ salt was characterized by X-ray crystallographic techniques.²⁴¹ Therefore, Xe_n^+ makes a bridge between the gas phase and condensed phase chemistry. Although Xe_4^+ is not isolated in the crystalline form, Seidel *et al.*²⁴¹ have identified the cluster by spectroscopic methods. Detail structural analysis of the Xe_n^+ ($n = 2-25$) clusters has been carried out by Gascón *et al.*²⁴² in the light of photoabsorption experiments supported by theoretical calculations.

In general, the HOMO – LUMO energy gap has been found in the range of 8 to 12 eV in inert gas solids with filled valance band. Therefore, a very high pressure should be applied to omit the energy gap between the valence and conduction band for transition to the metallic state. In 1965, this concept of high pressure driven narrowed energy gap leading to the thermal excitation of valence electron to the conduction band of xenon was first conceived by Keeler *et al.*²⁴³ Subsequently, scientists had explained theoretically that xenon can be converted to metallic state on compression due to the transition of electrons from the filled $5p$ valence band to the vacant $5d$ –like conduction band.²⁴⁴ In 1979, this comes into reality after the manufacturing of diamond-anvil cell where an ultra-high pressure (130-150 GPa) has been applied on solid xenon at very low temperature (32 K) to attain the insulator (fcc) to metal (hcp) transion.²⁴⁵ The achievement opens the gate of a new field in noble gas chemistry under high pressure. Subsequently, a large number of the metallic alloys of xenon have been prepared successfully with variable stoichiometries, *e.g.*, XeAu_2 , XePt , CsXeAu_3 , BeTeXe , PbTeXe , etc.²⁴⁶ In 2007, Grochala has predicted that xenon can form novel metallic amalgam (HgXe) with mercury at 75 GPa much below the pressure required for synthesizing metallic xenon. He has also theoretically studied the effect of very high pressure on binary fluorides of xenon, *viz.*, XeF_2 , XeF_4 and XeF_6 . Both XeF_2 and XeF_6 undergo decomposition at elevated pressure whereas XeF_4 withstands the excessive high pressure.⁶⁵ Theoretical calculations

suggests the possibility of existence of XeM (M = Fe, Ni, Mg) alloys in the Earth's inner core due to pressure-activated generation of negatively charged metal centers.²⁴⁷ Very recently, first stable compound of helium, Na₂He, has been synthesized under very high pressure by Dong *et al.*²⁴⁸

1.6. Scope of the Present Thesis

Of late, the scientific curiosity to unravel the nature of interaction between the noble gas atom and the other elements has become the frontier area of research. In the current years, there is a surge to explore the chemistry of noble gas atoms by predicting a large number of novel noble gas compounds by *ab initio* quantum chemical techniques and subsequently creation of suitable experimental condition(s) to facilitate their formation. Inspired by the fast growing field of noble gas chemistry, we have investigated weakly interacting chemical systems containing noble gas atoms by employing *ab initio* molecular orbital methods. Our aim is to contribute towards science by exploring the reactivity of the 'inert' noble gas atoms through prediction of new novel class of noble gas compounds.

In this thesis, we have predicted few novel class of fascinating insertion compounds obtained through the insertion of a noble gas atom into the molecules of interstellar origin by various *ab initio* quantum chemical techniques. We have investigated the following most interesting noble gas containing closed-shell cationic and neutral species, *viz.*, HNgOH₂⁺, HNgBF⁺, XNgCO⁺, HNgCS⁺, HNgOSi⁺, FNgBS, and FNgCX (Ng = Noble Gas, X = Halides) with singlet ground electronic state. Subsequently, for the first time we have also predicted noble gas chemical compounds with triplet ground electronic state in neutral noble gas inserted pnictides, ³FNgY (Ng = Kr and Xe; Y = N, P, As, Sb and Bi) species as well as cationic noble gas hydrides, ³HNgCCO⁺, by using *ab initio* molecular orbital calculations. Density functional theory and various post-Hartree–Fock-based correlated methods have

been employed to explore the structure, energetics, charge distribution, and harmonic vibrational frequencies for the minima and transition state geometries of these compounds.

It is well known that the noble gas–noble metal interaction is expected to be extremely unusual from the viewpoint of the inert nature of both the noble gas and noble metal atoms. Therefore, it is of great challenge to the scientists to investigate a chemical bond that exists between a noble gas and noble metal by combining these two very unreactive atoms. Accepting this challenge, we have explored the unprecedented enhancement of noble gas–noble metal bonding strength in NgM_3^+ (Ng = Ar, Kr, and Xe; M = Cu, Ag, and Au) ions through hydrogen doping by employing various *ab initio* based techniques. All the calculations have been carried out by employing DFT, MP2, and CCSD(T) based methods. It has been found that among all the $\text{NgM}_{3-k}\text{H}_k^+$ complexes ($k = 0-2$), the strongest Ng–M bonding has been observed in NgMH_2^+ complex, particularly, in case of ArAuH_2^+ complex. The concept of gold–hydrogen analogy makes it possible to evolve this pronounced effect of hydrogen doping in Au-trimers leading to the strongest Ng–Au bond in NgAuH_2^+ species.

Although the confinement of noble gas atom(s) inside the fullerene cages have been studied in past decades, but the endohedral entrapment of noble gas atom inside the inorganic fullerene has not been revealed so far. In order to conceive the new field on entrapment of noble gas atom, we have also investigated the theoretical existence and thermodynamic stability of noble gas encapsulated endohedral Zintl ions, Ng@M_{12}^{2-} (Ng = He, Ne, Ar, and Kr; M = Sn and Pb), through density functional theory while the kinetic stability of the clusters have been studied through *ab initio* molecular dynamics simulation. DFT computed optimized structural parameters, binding energies, vibrational frequencies, and charge distribution values clearly indicate that $[\text{Ng@Pb}_{12}^{2-}]$ and $[\text{Ng@Sn}_{12}^{2-}]$ cage clusters are kinetically stable and thermodynamically unstable whereas the K^+ salt of Ng@M_{12}^{2-} clusters are found to be both kinetically as well as thermodynamically stable.

Chapter 2. Theoretical and Computational Methodologies

2.1. Introduction

Theoretical chemistry is an exhilarating, fascinating and contemporary broad field in chemistry. It has become the subject of enormous interest on all branches of chemistry due to its potential diverse applications in chemical sciences, physical sciences, medical sciences, biological sciences, computational materials sciences, chemical engineering, nuclear sciences, etc. Consequently, it stands astride as the interfaces between chemistry, physics, materials science and biology, and has been used to solve the chemical system related problems by applying mathematical and computational techniques. In a nutshell, theoretical chemistry seeks to provide most plausible explanations to physical and chemical observations by developing novel concepts or carrying out computations with the help of the available theoretical modeling or simulation techniques. It is not only used to explain the experimental findings but also used as a scientific tool to predict new novel class of solid, liquid and gaseous compounds of our interest having numerous applications in various fields. The most popular computational techniques are *abinitio*, density functional theory (DFT), semi-empirical and molecular mechanics. Defining these terminologies are of immensely helpful in understanding the utilization of computational techniques for chemistry:

Abinitio: (Latin word means “from the beginning”) It is a group of methods used to calculate the molecular structures based on the first principle with fundamental physical constants. Although it uses true Hamiltonian, it does not mean ‘100% correct’ since it takes the approximation in wave function Ψ as an antisymmetrized product of one-electron spin orbitals and uses finite (*i.e.*, incomplete) basis set.

Density Functional Theory (DFT): In contrast to ‘*ab initio*’, DFT attempts to calculate the electron density instead of molecular wave function. Subsequently, it calculates the electronic energy of the system as a functional of the electron density.

Semi-Empirical Methods: These quantum mechanical methods use approximations of taking Hamiltonian adjusted to fit the experimental data to provide the input into the mathematical models.

Molecular Mechanics: Unlike all other methods, it is not a quantum mechanical method since the calculations do not involve the molecular Hamiltonian operator or wave function. On contrary, it treats the molecule as a collection of atoms and the molecular energy is expressed in terms of force constants corresponding to the bond stretching and bending modes of vibrations.

In fact, in recent times, the computational chemistry has been proven to be rationally versatile in obtaining meaningful insights into the functioning of various chemical systems and processes. Therefore, the theoretical modeling approach can only provide a better way to predict new noble gas containing chemical systems. However, there are also practical limitations in employing theory/computation for these systems of interest for prolonged time requirement due to the larger size of the molecule. Therefore, choice of accurate atomistic method is very much challenging as far as theoretical calculations are concerned. Among all the available theoretical methods, the DFT²⁴⁹ has become one of the most popular computational methods for any sized-molecular systems because of its computational cost effectiveness and reasonably good accuracy.

In the present thesis, we have employed various quantum mechanical methods, *viz.*, wave function based MP2 and CCSD(T) methods and also the DFT based methods. In principle, the molecular level calculations are carried out by using the localised Gaussian basis sets. Within the framework of DFT, we have used several hybrid exchange-correlation

energy functionals, such as, the Becke's three-parameter exchange functional and Lee-Yang-Parr correlation functional (B3LYP)²⁵⁰ and dispersion corrected omega separated form of Becke's 1997 hybrid functional with short-range HF exchange (ω B97X-D).²⁵¹ The individual computational methods used will be discussed in respective chapters under the subsection computational details. In the following sub-section, we will provide a brief outline of the theoretical basis for all the computational methods that have been used to investigate the chemical systems.

2.2. Theoretical Methodologies

In this section, we will review some of the fundamental aspects of electronic structure theory in terms of elementary quantum mechanics to get a glimpse on density functional theory. Here it may be noted that in quantum mechanics all the information obtained for a given system is contained the system's wave function, Ψ .

The Schrödinger Equation

To understand the structure, stability and property of the chemical species, it is very essential to assess the electronic properties of the systems since the chemistry of the systems are correlated with their electronic configuration exclusively. In this regard, determination of the exact energy of a system, the Schrödinger equation, introduced by the Austrian physicist Erwin Schrödinger in 1926 is considered as a breakthrough in the history of quantum mechanics. In quantum mechanics, the ground state properties of many particle systems are described by a partial differential equation called time-independent Schrödinger equation,

$$\hat{H} \Psi = E \Psi \quad (2.1)$$

For many body systems containing M nuclei and N electrons, the time independent Schrödinger equation becomes,

$$\hat{H} \psi_i(r_1, r_2, r_3, \dots, r_N, R_1, R_2, R_3, \dots, R_M) = E_i \psi_i(r_1, r_2, r_3, \dots, r_N, R_1, R_2, R_3, \dots, R_M) \quad (2.2)$$

where, \hat{H} is the Hamiltonian operator, ψ_i is the wave function which depends on both the electronic and nuclear coordinates and E_i is the eigen value of the i^{th} state. The Hamiltonian is a differential operator representing the total energy for this system can be written, in atomic units, as

$$\hat{H} = -\frac{1}{2} \sum_{i=1}^N \nabla_i^2 - \frac{1}{2} \sum_{A=1}^M \nabla_A^2 - \sum_{i=1}^N \sum_{A=1}^M \frac{Z_A}{r_{iA}} + \sum_{i=1}^N \sum_{j>1}^N \frac{1}{r_{ij}} + \sum_{A=1}^M \sum_{B>A}^M \frac{Z_A Z_B}{R_{AB}} \quad (2.3)$$

Here, the distance between the i^{th} electron and the A^{th} nucleus is $r_{iA} = |r_i - R_A|$, the distance between the i^{th} and j^{th} electron is $r_{ij} = |r_i - r_j|$, and the distance between the A^{th} nucleus and B^{th} nucleus is $R_{AB} = |R_A - R_B|$. In the above equation (2.3), the first two terms represent the kinetic energy operators for electrons and nuclei, respectively. Out of the last three terms, which represent the potential energy part of the Hamiltonian, the first term represents the attractive interaction between the electrons and nuclei and the last two terms correspond to the repulsive potentials due to electron-electron and nucleus-nucleus interactions, respectively.

The Laplacian operator ∇^2 can be defined as (in Cartesian coordinates):

$$\nabla^2 = \frac{\partial^2}{\partial x^2} + \frac{\partial^2}{\partial y^2} + \frac{\partial^2}{\partial z^2} \quad (2.4)$$

It is worthwhile to mention that all the equations given in this text appear in a very compact form and does not account for any fundamental physical constants. The fundamental physical constants, *viz.*, mass of an electron (m_e), the modulus of its charge ($|e|$), Planck's constant (h) divided by 2π (\hbar) and the permittivity of the vacuum ($4\pi\epsilon_0$), are all set to unity. Exact solution of the many body Schrödinger equation (2.2) associated with the full Hamiltonian (2.3) for any realistic system is a formidable task since it requires dealing with $3(N + M)$ degrees of freedom to obtain a desired solution. Therefore, in practice, it is not

computationally affordable due to the huge number of variables involved for any system. The difficulty arises due to the electrostatic interaction terms which couple the degrees of freedom of the particles among themselves and also with those of others. Hence, it is very much essential to impose certain reasonable approximations to simplify the complex equation. Fortunately, the Born-Oppenheimer approximation helps to decouple the nuclear and electronic degrees of freedom and we can solely focus our attention on the Schrödinger equation for the electrons.

Born-Oppenheimer Approximation

In 1927, Max Born and J. Robert Oppenheimer proposed an approximation which simplifies the Schrödinger equation is known as the Born-Oppenheimer approximation makes it possible to split the wavefunction into nuclear and electronic components.

$$\psi_{total}(r, R) = \psi_{electronic}(r; R) \times \psi_{nuclear}(R) \quad (2.5)$$

According to this approximation, the nuclei are much heavier as compared to the electrons. Due to their large mass difference, the electrons can be approximated as if they are moving in the field of fixed nuclei.²⁵² By using this approximation, one can drop the kinetic energy of nuclei from the Hamiltonian. In addition, the positions of the nuclei can be treated as fixed parameters and thus the nucleus-nucleus repulsive interaction term becomes constant for a fixed set of nuclei. Consequently, the complete Hamiltonian given in equation (2.3) is reduced to the electronic Hamiltonian as,

$$\hat{H}_{elec} = -\frac{1}{2} \sum_{i=1}^N \nabla_i^2 - \sum_{i=1}^N \sum_{A=1}^M \frac{Z_A}{r_{iA}} + \sum_{i=1}^N \sum_{j>1}^N \frac{1}{r_{ij}} = \hat{T} + \hat{V}_{Ne} + \hat{V}_{ee} \quad (2.6)$$

The above expression clearly indicates that the electronic wavefunction only depends on the electronic coordinates and does not explicitly depend on nuclear coordinates. Then, the electronic Schrödinger equation can be written as,

$$\hat{H}_{elec} \psi_{elec} = E_{elec} \psi_{elec} \quad (2.7)$$

However, it should be noted that total energy of the system is given by sum of electronic energy and nuclear energy which is again the combination of nuclear repulsion energy and the nuclear kinetic energy.

$$E_{total} = E_{elec} + E_{nucl} \quad (2.8)$$

Even after introducing the Born-Oppenheimer approximation, the solution of the many electron Schrödinger equation is still a difficult task due to the second term which couples the electronic coordinates preventing the reduction of a many electron problem to an effective single electron problem.

The Variational Principle

In principle, by solving the equation (2.7), one can get the eigenfunctions ψ_i which correspond to eigen values E_i of the Hamiltonian operator \hat{H} . All observable properties of the system can be determined by calculating the expectation values of the desired operators on the wave functions, once wave functions (ψ_i) are determined. However, the above equation hardly has any practical relevance. Apart from a few trivial exceptions, the Schrödinger equation cannot be solved exactly for many-electron atomic and molecular systems. One of the important approximations is the variational principle which provides a systematic approach to find out the ground state eigen function (ψ_0), the state which delivers the lowest energy E_0 as the operator \hat{H} is applied on it. The variational principle states that the expectation value (E) of the Hamiltonian operator (\hat{H}) using any trial wave function (ψ_{trial}) is always greater than or equal to the true ground state energy (E_0). This statement can be written by using the bracket notation as,

$$\frac{\langle \psi_{\text{trial}} | \hat{H} | \psi_{\text{trial}} \rangle}{\langle \psi_{\text{trial}} | \psi_{\text{trial}} \rangle} = E \geq E_0 = \langle \psi_0 | \hat{H} | \psi_0 \rangle \quad (2.9)$$

Although the variational principle gives us some clue seeking the ground state eigen function and eigen value of a particular system, it does not provide any information about the selection the trial wave function (ψ_{trial}). The difficulties in solving equation (2.7) are mainly due to the electron-electron repulsive interaction ($\frac{1}{r_{ij}}$) that includes all the quantum effects of the electrons. In spite of the intractable nature of these interactions, various approximate methods have been developed to solve Schrödinger-like equations. There are basically two types of approaches, *viz.*, electronic wave function based methods and density based methods. However, considering the fundamental role in many aspects of electronic structure theory the Slater determinant will be introduced first.

Slater Determinants

Being fermions, electrons obey the Pauli Exclusion Principle which requires that the wave function of electrons should be antisymmetric with respect to the interchange of the coordinates x of any two electrons,

$$\Phi(x_1, \dots, x_i, \dots, x_j, \dots, x_N) = -\Phi(x_1, \dots, x_j, \dots, x_i, \dots, x_N) \quad (2.10)$$

Slater determinants perfectly satisfy the antisymmetric condition through an appropriate linear combination of Hartree products of non-interacting electron wavefunctions. For example, in case of a two electron system if we put electron one in χ_i orbital and electron two in χ_j orbital, we will have,

$$\Phi_{12}(x_1, x_2) = \chi_i(x_1)\chi_j(x_2) \quad (2.11)$$

Conversely, if we put the electron one in χ_j orbital and electron two in χ_i orbital, we will have

$$\Phi_{21}(x_1, x_2) = \chi_i(x_2)\chi_j(x_1) \quad (2.12)$$

By taking linear combination of these two products,

$$\Phi(x_1, x_2) = 2^{-\frac{1}{2}} \left(\chi_i(x_1)\chi_j(x_2) - \chi_i(x_2)\chi_j(x_1) \right) \quad (2.13)$$

where, the factor $2^{-\frac{1}{2}}$ is known as ‘normalization factor’. It has been proved that the antisymmetry is guaranteed during interchange of the coordinates of electron one and electron two:

$$\Phi(x_1, x_2) = -\Phi(x_2, x_1) \quad (2.14)$$

Nevertheless, the antisymmetric wave function of equation (2.13) can be rewritten as a determinant,

$$\Phi(x_1, x_2) = 2^{-\frac{1}{2}} \begin{vmatrix} \chi_i(x_1) & \chi_j(x_1) \\ \chi_i(x_2) & \chi_j(x_2) \end{vmatrix} \quad (2.15)$$

popularly known as ‘Slater determinant’.²⁸ For an N-electron system, the Slater determinant looks like,

$$\Phi(x_1, x_2, \dots, x_N) = (N!)^{-\frac{1}{2}} \begin{vmatrix} \chi_i(x_1) & \chi_j(x_1) & \dots & \chi_k(x_1) \\ \chi_i(x_2) & \chi_j(x_2) & \dots & \chi_k(x_2) \\ \vdots & \vdots & \dots & \vdots \\ \chi_i(x_N) & \chi_j(x_N) & \dots & \chi_k(x_N) \end{vmatrix} \quad (2.16)$$

To be very specific the rows of the N-electron Slater determinant are labeled by electrons: first row (x_1), second row (x_2), ..., final row (x_N). On the other hand, the columns are labeled by spin orbitals: first column (χ_i), second (χ_j), ..., final column (χ_k). Interchanging the coordinates of two electrons equals to the interchange of two rows of the Slater determinant which will change its sign. Hence, the Slater determinant meets the fulfillment of antisymmetry. Moreover, having two electrons occupying the same spin orbital corresponds to having two columns of the determinant identical which leads to the determinant being zero.

2.2.1. Wave Function Based Methods

The Hartree-Fock Approximation

Due to the presence of electron-electron repulsion term, the solution of Schrödinger equation for a N-electron system is really a computationally formidable task. To overcome such difficulties, Hartree developed the so called self-consistent field (SCF) theory which was further improved with the incorporation of electron exchange term by Fock and Slater.²⁵³ Within the framework of *ab initio* approaches, the Hartree-Fock (HF) theory²⁵⁴ is the simplest wave function-based method which solves the electronic Schrödinger equation for a particular geometric arrangement of nuclei in a molecule. The electronic structure of a molecule is obtained as a result of HF calculation, usually expressed in terms of one-electron wave functions (Molecular orbitals (MOs)) and associated eigenvalues (orbital energies). The MO is basically a linear combination of atomic orbitals (LCAO) which is nothing but a atom-based functions known as basis functions. A set of basis function, commonly known as basis set which is necessary to represent a MO, is a vital input parameter for any quantum mechanical calculations. By introducing the set of known basis functions $\{\chi_\mu(\mathbf{r}) \mid \mu = 1, 2, 3, \dots, K\}$, the unknown molecular orbitals can be expressed as a linear combination of the basis functions as

$$\phi_i = \sum_{\mu=1}^K C_{\mu i} \chi_\mu \quad (2.17)$$

Now, the choice of basis functions should be done in such a way that they resemble familiar atomic orbitals (AOs), thereby making the results of HF-SCF calculations more accessible chemically. However, this result relies on the following approximations: the Born-Oppenheimer approximation, the independent electron approximation, the linear combination of atomic orbitals approximation. The expectation value of Hamiltonian operator applied on the Slater determinant will give us HF energy, E_{HF} .

$$E_{HF} = \langle \Phi | \hat{H} | \Phi \rangle = \sum_i^N (i | \hat{h} | i) + \frac{1}{2} \sum_i^N \sum_j^N (ii | jj) - (ij | ji) \quad (2.18)$$

where

$$(i | \hat{h} | i) = \int \chi_i^* \vec{x}_1 \left\{ -\frac{1}{2} \nabla^2 - \sum_A^M \frac{Z_A}{r_{1A}} \right\} \chi_i(\vec{x}_1) d\vec{x}_1 \quad (2.19)$$

defines the contribution due to the kinetic energy and the electron-nucleus attraction. The second term can be expressed as:

$$(ii | jj) = \int \int |\chi_i(\vec{x}_1)|^2 \frac{1}{r_{12}} |\chi_j(\vec{x}_2)|^2 d\vec{x}_1 d\vec{x}_2 \quad (2.20)$$

$$(ij | ji) = \int \int \chi_i(\vec{x}_1) \chi_j^*(\vec{x}_1) \frac{1}{r_{12}} \chi_j(\vec{x}_2) \chi_i^*(\vec{x}_2) d\vec{x}_1 d\vec{x}_2 \quad (2.21)$$

are the so-called ‘Coulomb’ and ‘Exchange’ integrals, respectively. Here, the variational principle is applied for minimizing the E_{HF} , a functional of spin orbitals, by choosing an orthonormal set of orbitals. The resulting Hartree-Fock equations can be written as:

$$\hat{f} \chi_i = \varepsilon_i \chi_i (i = 1, 2, 3, \dots, N) \quad (2.22)$$

In the above expression \hat{f} is the Fock operator and ε_i are the Lagrangian multipliers which possesses the physical representation as the orbital energies.

Correlation Energy

According to the variational principle, the energy obtained with the trial wave function (Ψ_{trial}), E_{HF} , are found to be larger than the exact ground state energy, E_0 . The difference between these two energies is termed as the correlation energy (E_{corr}).

$$E_{corr} = E_0 - E_{HF} \quad (2.23)$$

Electrons having parallel spins always have a tendency to stay well apart and hence they repel each other less. In essence, the effect of spin correlation allows the atom to shrink slightly, so the electron-nucleus interaction is improved when the spins are parallel.

Therefore, electron correlation²⁵⁵ is mainly caused by the instantaneous repulsion of the electrons having same spin, which is not covered by the effective HF potential, as electrostatic interaction is treated only in an average manner in the HF method. There may be two types of correlations, *viz.*, dynamic and static. The dynamic correlation is considered due to the movement of electrons and its effect is short range. It is to be noted that the dynamic correlation energy is related to $(\frac{1}{r_{12}})$ term in the Hamiltonian. On the other hand, the static correlation arises due to the fact that in certain circumstances the ground state Slater determinant is not a good approximation to the true ground state, because there may be other Slater determinants with comparable energies.

Post-Hartree-Fock methods

The basic aim of Post-Hartree-Fock methods in quantum chemistry is to improve the Hartree-Fock energy by taking into account the effect of electron correlation. These methods include configuration interaction (CI), Møller-Plesset perturbation theory, and coupled cluster. In case of CI methods, a linear combination of Slater determinants rather than one single Slater determinant in Hartree-Fock is used to approximate the wave function. The Møller-Plesset perturbation theory, as the name suggests, treats electron correlation in a perturbative way. In the coupled cluster method, the electron correlation is handled through use of a so-called cluster operator.

Perturbation Theory

In 1934, Møller and Plesset proposed a perturbation treatment on the unperturbed Hartree-Fock wave functions of atoms and molecules and this form of many body perturbation theory (MBPT) is called Møller-Plesset (MP) perturbation theory. The perturbation \hat{H}' is defined as the difference between the true molecular electronic Hamiltonian (\hat{H}) and unperturbed Hamiltonia (\hat{H}^0).

$$\hat{H}' = \hat{H} - \hat{H}^0 = \sum_l \sum_{m>l} \frac{1}{r_{lm}} - \sum_{m=1}^n \sum_{j=1}^n [\hat{j}_j(m) - \hat{k}_j(m)] \quad (2.24)$$

where, r_{lm} is the distance between the l^{th} electron and the m^{th} electron whereas $\hat{j}_j(m)$ and $\hat{k}_j(m)$ represents the Coulomb and Exchange operators, respectively. From the above expression it is clear that the perturbation is the true inter-electronic repulsions and the Hartree-Fock inter-electronic potential, which is considered as the average potential.

First order Møller-Plesset (MP) perturbation correction to the ground state energy is $E_0^{(1)}$ which is expressed as,

$$E_0^{(1)} = \langle \psi_0^{(0)} | \hat{H}' | \psi_0^{(0)} \rangle = \langle \Phi_0 | \hat{H}' | \Phi_0 \rangle \quad (2.25)$$

where superscript 0 signifies the zeroth-order (unperturbed) parameters while subscript 0 denotes the ground state. Therefore, we may write

$$E_0^{(0)} + E_0^{(1)} = \langle \psi_0^{(0)} | \hat{H}^0 | \psi_0^{(0)} \rangle + \langle \Phi_0 | \hat{H}' | \Phi_0 \rangle = \langle \Phi_0 | \hat{H}^0 + \hat{H}' | \Phi_0 \rangle = \langle \Phi_0 | \hat{H} | \Phi_0 \rangle \quad (2.26)$$

Since $\langle \Phi_0 | \hat{H} | \Phi_0 \rangle$ is defined as the variational integral for the Hartree-Fock wave function Φ_0 and hence it equals to the Hartree-Fock energy (E_{HF}) for the system.

$$E_{HF} = E_0^{(0)} + E_0^{(1)} \quad (2.27)$$

In order to improve the Hartree-Fock energy, one should include the second order energy correction $E_0^{(2)}$ which is as follows,

$$E_0^{(2)} = \sum_{s \neq 0} \frac{|\langle \psi_s^{(0)} | \hat{H}' | \Phi_0 \rangle|^2}{E_0^{(0)} - E_s^{(0)}} \quad (2.28)$$

Here, it may be noted that the unperturbed functions $\psi_s^{(0)}$ includes all possible Slater determinants formed from n different spin orbitals. Let us assumed that i, j, k, l, \dots denotes the occupied spin orbitals in the ground state Hartree-Fock wave function Φ_0 while a, b, c, d, \dots represents the unoccupied (virtual) spin orbitals. Each unperturbed wave function can be classified by the number virtual spin orbitals (excitation level). Now, the singly excited

determinant (Φ_i^a) can be formed from Φ_0 by replacement of i^{th} spin orbital (u_i) by virtual a^{th} spin orbital (u_a) while the doubly excited determinant (Φ_{ij}^{ab}) differs from Φ_0 by the replacement of u_i by u_a and u_j by u_b , and so on. By applying the Condon-Slater rules, it is possible to evaluate the expectation value ($E_0^{(2)}$) as follows,

$$E_0^{(2)} = \sum_{b=a+1}^{\infty} \sum_{a=n+1}^{\infty} \sum_{i=j+1}^n \sum_{j=1}^{n-1} \frac{|\langle ab | r_{12}^{-1} | ij \rangle - \langle ab | r_{12}^{-1} | ji \rangle|^2}{\varepsilon_i + \varepsilon_j - \varepsilon_a - \varepsilon_b} \quad (2.29)$$

where

$$\langle ab | r_{12}^{-1} | ij \rangle = \int \int u_a^*(1) u_b^*(2) r_{12}^{-1} u_i(1) u_j(2) d\tau_1 d\tau_2 \quad (2.30)$$

The above integrals over the spin orbitals can be readily evaluated in terms of the electron repulsion integrals. The inclusion of all the doubly substituted $\psi_s^{(0)}$'s lead to the summation over $a, b, i,$ and j in equation (2.29).

Now, incorporation of the second order correction in energy in Hartree-Fock energy (E_{HF}) gives rise to a more accurate result in molecular energy.

$$E_{HF} + E_0^{(2)} = E_0^{(0)} + E_0^{(1)} + E_0^{(2)} \quad (2.31)$$

Therefore, this molecular energy calculation is designated as the MP2²⁵⁶ or MBPT2, where, '2' indicates the inclusion of energy corrections up to second order.

Coupled Cluster Theory

In 1958, Coester and Kümmel introduced the coupled cluster (CC) method which deals with a system of interacting particles. The fundamental equation in coupled cluster theory is

$$\psi = e^{\hat{T}} \Phi_0 \quad (2.32)$$

where ψ is the exact non-relativistic ground state molecular electronic wave function, Φ_0 denotes the normalized ground state Hartree-Fock wave function and the operator $e^{\hat{T}}$ is defined by the Taylor series expansion as,

$$e^{\hat{T}} \equiv 1 + \hat{T} + \frac{\hat{T}^2}{2!} + \frac{\hat{T}^3}{3!} + \dots = \sum_{k=0}^{\infty} \frac{\hat{T}^k}{k!} \quad (2.33)$$

where, \hat{T} is the ‘Cluster’ operator which is defined as,

$$\hat{T} \equiv \hat{T}_1 + \hat{T}_2 + \dots + \hat{T}_n \quad (2.34)$$

where, n is the number of electrons in the molecule, \hat{T}_1 is the ‘one particle excitation operator’ and \hat{T}_2 is the ‘two particle excitation operator’ are expressed as,

$$\hat{T}_1 \Phi_0 \equiv \sum_{a=n+1}^{\infty} \sum_{i=1}^n t_i^a \Phi_i^a \quad (2.35)$$

$$\hat{T}_2 \Phi_0 \equiv \sum_{b=a+1}^{\infty} \sum_{a=n+1}^{\infty} \sum_{j=i+1}^n \sum_{i=1}^{n-1} t_{ij}^{ab} \Phi_{ij}^{ab} \quad (2.36)$$

where (Φ_i^a) is the singly excited Slater determinant can be formed from Φ_0 by replacement of i^{th} spin orbital (u_i) by virtual a^{th} spin orbital (u_a) and t_i^a is the numerical coefficient whose value depends on i and a . The operator \hat{T}_1 converts the Slater determinant Φ_0 ($\Phi_0 = |u_1 \dots u_n\rangle$) into a linear combination of all possible singly excited Slater determinants. Here, (Φ_{ij}^{ab}) is the doubly excited Slater determinant differs from Φ_0 by the replacement of u_i by u_a and u_j by u_b , and t_{ij}^{ab} is the numerical coefficient. Similar explanation holds for $\hat{T}_3, \dots, \hat{T}_n$.

Individual Slater determinants have been considered in coupled cluster (CC) methods. The main aim in coupled cluster theory based calculations is to find out the coefficients $t_i^a, t_{ij}^{ab}, t_{ijk}^{abc}, \dots$ for all i, j, k, \dots , and all a, b, c, \dots . Subsequently, the wave function ψ has been derived from the values of the coefficients. Two approximations have been accounted for the application of the coupled cluster (CC) methods, *viz.*, first one is the use of finite (incomplete) basis set to express the spin orbitals in the SCF wave function and the second one is the approximation of taking some of the operators from the whole cluster operator (\hat{T}), e.g., the approximation $\hat{T} \approx \hat{T}_2$ gives rise to

$$\psi_{CCD} = e^{\hat{T}_2} \Phi_0 \quad (2.37)$$

Incorporation of only \hat{T}_2 gives an approximate coupled cluster approach known as coupled cluster doubles (CCD) method. Considering the Taylor series expansion of $e^{\hat{T}_2}$ ($e^{\hat{T}_2} = 1 + \hat{T}_2 + \frac{1}{2}\hat{T}_2^2 + \dots$), one can certainly say that the wave function ψ_{CCD} contains the Slater determinants with double substitutions, quadruple substitutions, hextuple substitutions, and so on. Now, invoking the CCD approximation, $\hat{T} \approx \hat{T}_2$, we may write,

$$E_{CCD} = \langle \Phi_0 | \hat{H} | e^{\hat{T}_2} \Phi_0 \rangle \quad (2.38)$$

$$\langle \Phi_{ij}^{ab} | \hat{H} | e^{\hat{T}_2} \Phi_0 \rangle = \langle \Phi_0 | \hat{H} | e^{\hat{T}_2} \Phi_0 \rangle \langle \Phi_{ij}^{ab} | e^{\hat{T}_2} \Phi_0 \rangle \quad (2.39)$$

Since these equations are approximate, therefore, the exact energy has been replaced by the CCD energy (E_{CCD}) and the coefficients (t_{ij}^{ab}) are also approximate. The first integral of the right hand side of the above equation can be written as,

$$\langle \Phi_0 | \hat{H} | e^{\hat{T}_2} \Phi_0 \rangle = \langle \Phi_0 | \hat{H} | \left(1 + \hat{T}_2 + \frac{1}{2}\hat{T}_2^2 + \dots \right) \Phi_0 \rangle = E_{HF} + \langle \Phi_0 | \hat{H} | \hat{T}_2 \Phi_0 \rangle \quad (2.40)$$

where, E_{HF} represents the Hartree-Fock energy. By applying the Condon-Slater rule, the equation (2.39) takes the form,

$$\langle \Phi_{ij}^{ab} | \hat{H} | \left(1 + \hat{T}_2 + \frac{1}{2}\hat{T}_2^2 \right) \Phi_0 \rangle = E_{HF} + \langle \Phi_0 | \hat{H} | \hat{T}_2 \Phi_0 \rangle \langle \Phi_{ij}^{ab} | \hat{T}_2 \Phi_0 \rangle \quad (2.41)$$

where, $i = 1, \dots, n; j = i + 1, \dots, n; a = n + 1, \dots; b = a + 1, \dots$

$\hat{T}_2 \Phi_0$ and $\hat{T}_2^2 \Phi_0$ are the multiple sum involving $t_{ij}^{ab} \Phi_{ij}^{ab}$ and $t_{ij}^{ab} t_{kl}^{cd} \Phi_{ijkl}^{abcd}$. Since for each unknown amplitude, t_{ij}^{ab} , there is one equation, thus the number of equations is equal to the number of unknowns. The net result is a set of simultaneous nonlinear equations for the unknown amplitudes (t_{ij}^{ab}) which takes the form of

$$\sum_{s=1}^m a_{rs} x_s + \sum_{t=2}^m \sum_{s=1}^{t-1} b_{rst} x_s x_t + c_r = 0, \quad r = 1, 2, \dots, m; \quad (2.42)$$

where, x_1, x_2, \dots, x_m are the unknowns t_{ij}^{ab} , the quantities a_{rs} , b_{rst} and c_r are the constants that include orbital energies and electron repulsion integrals, and m is the number of the unknown amplitudes t_{ij}^{ab} .

To improve the CCD method, one has to incorporate the operator \hat{T}_1 which takes the form of $\hat{T} \equiv \hat{T}_1 + \hat{T}_2$ in $e^{\hat{T}}$ operator. This combination is described as the coupled cluster theory with single and double excitations known as CCSD method. Further improvement in the coupled-cluster theory can only be possible with the inclusion of single and double excitations and an estimate of connected triples (CCSD(T)).²⁵⁷

2.2.2. Density Based Methods: Density Functional Theory

Density functional theory (DFT) is an alternative way to study electronic structure of matter in which the ground state electron density of a system is considered as a basic variable instead of a many-body wave function. It is well known that the wave function does not have any physical significance; however, the square of the wave function is an observable quantity. The physical observable which is related to the square of the wave function is known as the electron density ($\rho(\vec{r})$) and can be defined as the probability of finding an electron in the volume element $d\vec{r}$. It is worthwhile to deal with electron density rather than a many-body electron wavefunction since the density is a function of three variables in contrast to the $3N$ variables of the wave function. The DFT based calculations with the approximate functionals provide a useful balance between accuracy and computational cost.

Mathematically, the electron probability density can be expressed as,

$$\rho(\vec{r}) = N \int \dots \int |\psi(\vec{x}_1, \vec{x}_2, \dots, \vec{x}_N)|^2 ds_1 d\vec{x}_2 \dots d\vec{x}_N \quad (2.43)$$

It is essential to mention that the electron density, $\rho(\vec{r})$, is a non-negative function of only the three spatial variables which vanishes at infinity and integrates to the total number of electrons:

$$\rho(\vec{r} \rightarrow \infty) = 0 \quad (2.44)$$

$$\int \rho(\vec{r}) d\vec{r}_1 = N \quad (2.45)$$

The Thomas-Fermi Model

The first density-based theory to deal with a many-electron system was introduced by Thomas and Fermi in 1927. In Thomas-Fermi theory,²⁵⁸ the kinetic energy of electrons are derived from the quantum statistical theory based on the uniform electron gas, but the interaction between electron-nucleus and electron-electron are treated classically. According to this model, the kinetic energy of the electrons is defined as,

$$T[\rho] = C_F \int \rho^{\frac{5}{3}}(\vec{r}) d\vec{r} \quad (2.46)$$

where,

$$C_F = \frac{3}{10} (3\pi^2)^{\frac{2}{3}} = 2.871 \quad (2.47)$$

In the above expression, the approximation is made that the kinetic energy of the electron depends exclusively on the electron density. Addition of electron-nucleus and electron-electron interaction into above equation (2.46), the total energy in terms of ρ is obtained,

$$E[\rho] = C_F \int \rho^{\frac{5}{3}}(\vec{r}) d\vec{r} - Z \int \frac{\rho(\vec{r})}{r} d\vec{r} + \frac{1}{2} \iint \frac{\rho(\vec{r}_1)\rho(\vec{r}_2)}{|\vec{r}_1 - \vec{r}_2|} d\vec{r}_1 d\vec{r}_2 \quad (2.48)$$

In the above equation, the second and third terms are the electron-nucleus and electron-electron interactions, respectively. The significance of this simple Thomas-Fermi model is not how well it performs in computing the ground state energy and density but more as an illustration that the energy can be determined purely using the electron density. The two major drawbacks are associated with the above expression. One of the shortcomings is the

expression of kinetic energy, which is a very crude approximation to the actual kinetic energy. The other disadvantage of it is the complete negligence of exchange and correlation effects.

The Hohenberg-Kohn Theorems

The publication of the landmark paper by Hohenberg and Kohn^{249a} in the year 1964 has given the birth of a new era in quantum chemistry which is most widely known as density functional theory. The theory is based upon the following two theorems.

Theorem 1: The ground-state energy from Schrödinger's equation is a unique functional of the electron density ($\rho(\vec{r})$), in other words a one to one mapping between the external potential and electron density has been established.

Theorem 2: The electron density that minimizes the energy of the overall functional ($E[\rho(\vec{r})]$) is the true electron density corresponding to the full solution of the Schrödinger equation *i.e.*, the ground state density can be found by using variational principle.

One of the most important outcomes of these theorems is that the ground-state electron density uniquely determines all the properties, including the energy and wave function, of the ground state. The energy of any atomic or molecular system can be defined as:

$$E = (F[\rho] + \int \rho(\vec{r})V_{Ne} d\vec{r}) \quad (2.49)$$

while the ground state energy of any atomic or molecular system can be expressed as:

$$E_0 = \min_{\rho \rightarrow N} (F[\rho] + \int \rho(\vec{r})V_{Ne} d\vec{r}) \quad (2.50)$$

where, the universal functional $F[\rho]$ contains contributions due to the kinetic energy, the classical Coulomb interaction and the non-classical terms as self interaction correction,

exchange and electron correlation effects. It is essential to note that it is independent of the number of particles as well as the external potential. Therefore, we have

$$F[\rho(\vec{r})] = T[\rho(\vec{r})] + J[\rho(\vec{r})] + E_{ncl}[\rho(\vec{r})] \quad (2.51)$$

Out of all the terms present in the above equation, only $J[\rho(\vec{r})]$, accounts for the classical Coulomb interaction explicitly. $E_{ncl}[\rho(\vec{r})]$ is the *non-classical* contribution to the electron-electron interaction containing all the effects of self-interaction correction, exchange and correlation. It is of no surprise that finding explicit expressions for the yet unknown functionals, *i.e.*, $T[\rho(\vec{r})]$ and $E_{ncl}[\rho(\vec{r})]$, represents the major challenge in density functional theory.

The Hohenberg-Kohn (HK) theorems are non-constructive due to the presence of the unknown universal functional. In particular, the kinetic energy functionals are problematic as $T[\rho(\vec{r})]$ is so large that even a small relative error gives large absolute errors to the total energy of the system. The development of approximate functionals that can reasonably model experimental data is still a topic of most fascinating research in the DFT. Therefore, almost all DFT calculations rely on the Kohn-Sham approximation, which avoids the exact kinetic energy functional. It is important to point out that different DFT methods differ in the way of representing exchange and correlation terms.

The Kohn-Sham Method

From the Hohenberg-Kohn theorem, we can get the ground-state energy by minimizing the energy functional (equation 2.49) by using a variational principle,

$$E = (F[\rho] + \int \rho(\vec{r})V_{Ne} d\vec{r}) \quad (2.49)$$

Although the Hohenberg-Kohn theorem provided a proof in principle that the total energy could be obtained from the ground state electron density, it was not yet known how to

obtain the $\rho(\mathbf{r})$ or $F[\rho]$. In 1965, Kohn and Sham published a pioneering paper, which transformed density-functional theory into a practical electronic structure theory.^{249b} Kohn and Sham recognized that the failure of Thomas-Fermi theory was primarily resulted from the bad description of the kinetic energy. To address this problem they decided to re-introduce the idea of one electron orbitals and approximate the kinetic energy of the system by incorporating the kinetic energy of non-interacting electrons. This lead to the central equation in Kohn-Sham DFT which is one-electron Schrödinger-like equation, expressed as:

$$\left(-\frac{1}{2}\nabla^2 + v(\vec{r}) + \int \frac{\rho(\vec{r}')}{|\vec{r} - \vec{r}'|} d\vec{r}' + v_{xc}(\vec{r}) \right) \phi_i = \varepsilon \phi_i \quad (2.52)$$

Here ϕ_i are the Kohn-Sham orbitals and the electron density is expressed by,

$$\rho(\vec{r}) = \sum_i^N |\phi_i|^2 \quad (2.53)$$

The terms on the left side of the equation (2.52) are the kinetic energy of the non-interacting reference system, the external potential, the Hartree potential, and the exchange-correlation potential, respectively. The ε is the energy of the Kohn-Sham orbital. Additionally, the exchange-correlation potential is given by,

$$v_{xc}(\vec{r}) = \frac{\delta E_{xc}[\rho]}{\delta \rho(\vec{r})} \quad (2.54)$$

and $E_{xc}[\rho]$ is the exchange-correlation functional while the effective potential (v_{eff}) can be defined as

$$v_{eff} = v(\vec{r}) + \int \frac{\rho(\vec{r}')}{|\vec{r} - \vec{r}'|} d\vec{r}' + v_{xc}(\vec{r}) \quad (2.55)$$

Therefore, the equation (2.52) can be rewritten in a more compact form,

$$\left(-\frac{1}{2}\nabla^2 + v_{eff} \right) \phi_i = \varepsilon \phi_i \quad (2.56)$$

From the above expression, it is clearly evident that this is a Hartree-Fock like single particle equation which needs to be solved iteratively. Finally, the total energy can be determined from the resulting density through

$$E = \sum_i^N \varepsilon_i - \frac{1}{2} \iint \frac{\rho(\vec{r})\rho(\vec{r}')}{|\vec{r} - \vec{r}'|} d\vec{r}d\vec{r}' + E_{xc}[\rho] - \int v_{xc}(\vec{r})\rho(\vec{r})d\vec{r} \quad (2.57)$$

Equations (2.53), (2.54), and (2.56) are distinguished as Kohn-Sham equations. The Kohn-Sham equation must be solved self-consistently since the v_{eff} depends on $\rho(\vec{r})$ through the equation (2.55). In general, this computational procedure begins with an initial guess of the electron density, construction of the v_{eff} from the equation (2.55), and subsequently gets the Kohn-Sham orbitals. Based on these orbitals, a new density is obtained from equation (2.53) and the process repeated until convergence is achieved. Finally, the total energy of the system will be calculated from equation (2.57) with the final electron density. If each term in the Kohn-Sham energy functional was known, we would be able to obtain the exact ground state density and the total energy. Unfortunately, there is one unknown term, the exchange-correlation (xc) functional (E_{xc}). E_{xc} includes the non-classical aspects of the electron-electron interaction along with the component of the kinetic energy of the real system, which is different from the fictitious non-interacting system. Since E_{xc} is not known exactly, it is necessary to approximate it. Therefore, since the birth of DFT, some sorts of approximations for E_{xc} have been used. By now there is an almost endless list of approximations²⁵⁹ with varying levels of complexity.

Solving the Kohn-Sham Equation

In practice, the Kohn-Sham equation is solved numerically by an iterative procedure so-called the self-consistent field (SCF) method. The steps involved in the SCF calculations and its corresponding flow chart are given below.

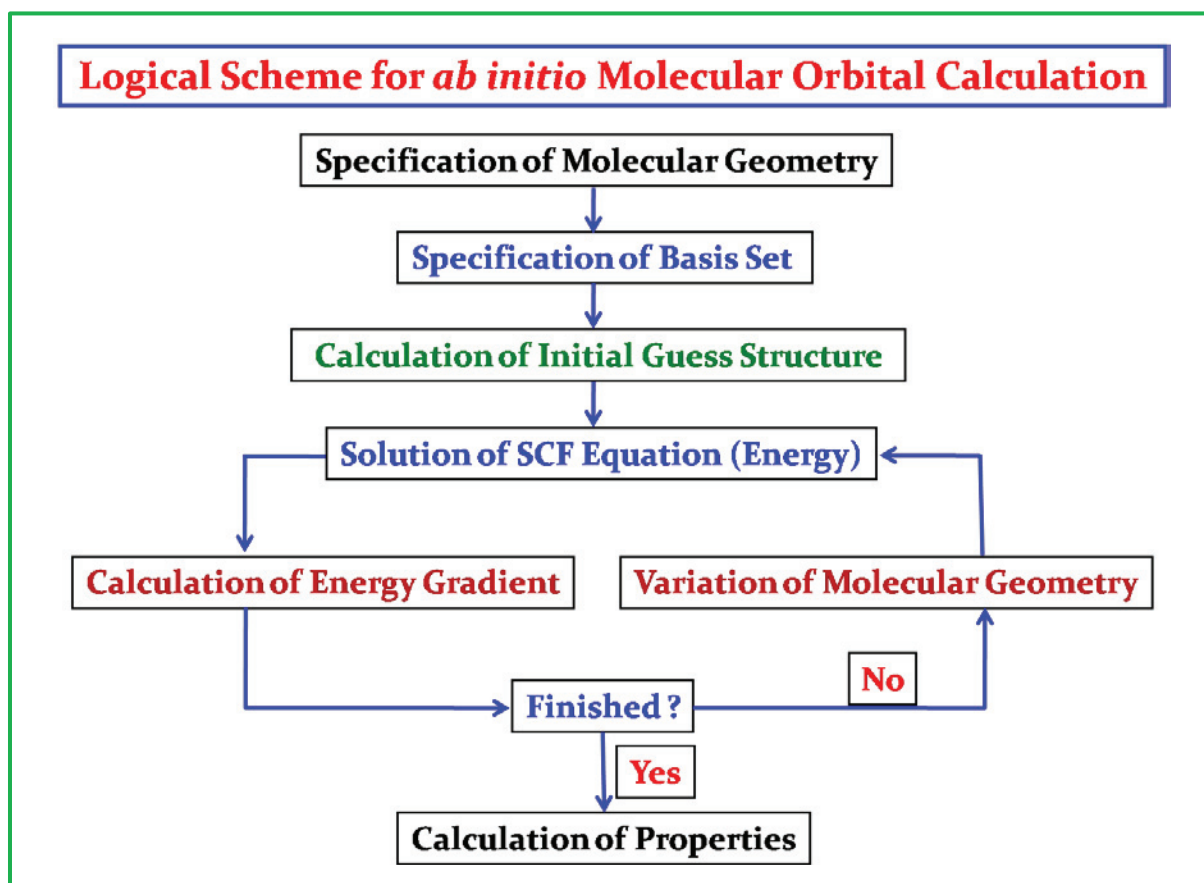


Figure 2.1. Schematic representations of the flow chart of *ab initio* MO & DFT calculations

2.3. Basis Set

Basis set is basically the set of mathematical functions used to construct any unknown arbitrary wavefunction. Molecular orbitals (MOs) are often expressed as a linear combination of atomic orbitals (LCAO) as,

$$\phi_i = \sum_{\mu=1}^K C_{\mu i} \chi_{\mu} \quad (2.17)$$

where, χ_{μ} indicates a predefined set of basis functions for the μ^{th} orbital and $C_{\mu i}$ represents expression coefficients. Although a complete basis set should contain infinite number of basis functions to accurately describe the wave function, in the practical scenario a finite number of basis functions is employed due to computational limitation. The error due to incomplete

basis set is known as basis set truncation error. The choice of the basis set is an important criteria to obtain a reasonably good computational results. Therefore, the basis set should be such that the associated truncation error is minimum, even though the number of basis function lies within the computational limit. The selection of basis function should also be such that the wave function is single valued, finite, continuous and quadratically integrable. The most popular basis sets for the electronic structure calculation includes

(i) Slater type orbital (STO)

(ii) Gaussian type orbital (GTO)

(iii) Plane wave basis set

We will discuss the first two basis sets due to relevance with our computational study.

Slater Type Orbital (STO)

The Slater Type Orbitals (STO) decay exponentially as a function of distance from the nucleus.²⁶⁰ The mathematical form of STO in polar coordinates is defined as,

$$X(r, \theta, \phi) = Nr^{n-1}e^{-\xi r}Y_{l,m}(\theta, \phi) \quad (2.58)$$

where (r, θ, ϕ) are the spherical coordinates, $Y_{l,m}$ stands for the conventional spherical harmonics, N is the normalization constant and ξ is known as the Slater orbital exponent. Due to the similarity of the mathematical form of STO with that of the hydrogenic orbital, STO becomes more attractive for electronic structure calculation. The shortcoming of the STO is the absence of radial node which can be introduced in the atomic orbitals as a linear combination of STOs. The most important feature of the STO is that it has a cusp at the nucleus, thus, electrons near the nucleus are well described by the STOs. Nevertheless non-availability of analytical solution of the general four center integral drastically limit the application of the STO basis sets in molecular systems of interest.

Gaussian Type Orbital (GTO)

In the year 1950, S. F. Boys proposed the Gaussian type functions for the atomic orbitals,²⁶¹ where the radial decay behaviour is changed to e^{ar^2} . The general functional form of a normalized Gaussian Type Orbital (GTO) in polar coordinate can be expressed as,

$$\psi_{\xi,h,l,m}(r, \theta, \phi) = Nr^{2n-2-l} e^{-\xi r^2} Y_{l,m}(\theta, \phi) \quad (2.59)$$

where, the exponent ξ controls the width of the GTO.

The main advantage of GTO basis set is that the analytical solution of the general four-index integral is available. Since, the product of two GTO centered at two different points results another GTO centered at a third point, many centred two electron integrals can be expressed into much simpler form. For a large molecular system, the electronic structure calculations become faster using GTO basis set. In spite of the computational feasibility certain limitations restrict the use of GTO as a basis function. One of the major problems is associated with the shape of the radial portion of the orbital. For example, as GTOs for S type functions are smooth and differentiable at $r = 0$ (nucleus), differing significantly from the real hydrogenic AOs which have a cusp. On the other hand, the radial decay of all hydrogenic orbital is quite slow (exponential in r), while the decay of GTOs, is too fast (exponential in r^2) leading to a drastic reduction in amplitude with the distance. Therefore, tail behaviour for GTOs is poorly described. To overcome these limitations, the basis sets have been constructed as a building block to approximate STO, which retain the best features STOs (appropriate radial shape). In this case, the basis functions are expressed as a linear combination of several GTOs to give as good a fit as possible to the Slater orbital. The basis function defined as a linear combination of Gaussians is known as a contracted Gaussian-type basis function (CGTF) while the individual Gaussians involved to construct the controlled basis function is known as Gaussian primitives.

Chapter 3. Novel Class of Fascinating Noble Gas Insertion Compounds: Predictions from Theoretical Calculations

3.1. Introduction

Stimulated from the renaissance discovery of HArF by Räsänen and co-workers,¹⁴¹ we have predicted interesting noble gas insertion compounds by using *ab initio* quantum chemical techniques. In this aspect, we have studied the noble gas inserted hydride cations having astronomical and astrophysical importance, *viz.*, hydride ions of boron (HNgBF⁺), thioformyl cations (HNgCS⁺), protonated silicone monoxide cations (HNgOSi⁺) and having biological significance, like, hydronium ions (HNgOH₂⁺). In various gas phase environments, especially in plasmas and terrestrial atmosphere, ionic complexes and clusters are important short-lived intermediates which are found to be the ideal systems for a detailed characterization of the intermolecular interaction involved in charged atomic or molecular systems. Apart from the noble gas insertion cations, we have also explored the possibility for the existence of neutral noble gas insertion compounds through *ab initio* quantum chemical methods. In this regard, we have predicted noble gas inserted fluoro(sulphido)boron (FNgBS) and noble gas inserted halocarbenes (FNgCX) where, X = halogens considering the strong environmental impacts of the precursor molecules, *viz.*, FBS and FCX, respectively. However, all these compounds possess closed-shell geometries and they have been found to be singlet in their respective potential energy surfaces. In this section, we will discuss these predicted chemical systems systematically.

Molecular complex of an atomic or molecular ion with a neutral molecule is of considerable importance because it shows various interesting chemistry either through proton transfer or electron transfer or molecular rearrangement. One of the simplest prototype

examples of such system is the hydronium ion (H_3O^+), which is formed through interaction of a proton with one water molecule. This hydronium ion plays an important role in various chemical and biological systems. In fact, molecular systems with an excess proton are of considerable recent interests and are investigated using various experimental and theoretical techniques.²⁶² Very recently, the production of van der Waals complexes of H_3O^+ with Ne, Ar, Kr, and Xe has been studied in supersonic jet expansion along with electron impact ionization, and vibrational energy levels are probed using IR photodissociation spectroscopy.²⁶³ The structures, physical, and chemical properties of the NgH_3O^+ complexes depend on the relative proton affinities of H_2O and Ng atom. If the attraction between proton and Ng atom is almost equivalent with that of H_2O , then the Ng–H interaction is expected to be more effective, leading to a short, strong, and rigid bond. The proton affinities of He, Ar, Kr, Xe, and H_2O are 178, 371, 425, 496, and 703 kJ mol^{-1} , respectively.²⁶⁴ In view of the importance of the hydronium ion and also recent experimental investigation on the van der Waals complex of H_3O^+ with noble gas atoms,²⁶³ we have been motivated to provide in-depth insight into the possible existence of HNgOH_2^+ insertion complexes.

The interaction of a boron (B) atom with a Ng atom is of interest due to the availability of empty $2p_y$ and $2p_z$ orbitals of boron. However, very few insertion-type molecules that contain both B and Ng atoms, for example, FNgBF_2 ,¹⁸⁵ FNgBO ,²⁶⁵ and FNgBN^- ,²⁶⁶ are predicted theoretically so far. In the recent past, a new class of B-containing molecular species HBX ($X = \text{F}, \text{Cl}, \text{Br}$) were prepared²⁶⁷ in a supersonic discharge jet source and characterized spectroscopically using the laser-induced fluorescence (LIF) technique. Further, the HBF^+ ion has also been produced in a glow discharge containing a mixture of both BF_3 and H_2 gas, and it was spectrally characterized using magnetic modulated IR laser spectroscopy.²⁶⁸ Interestingly, the HBF^+ ion is also isoelectronic with HCO^+ ,²⁶⁹ and N_2H^+ ions²⁷⁰ (14 electrons), which are important in atmospheric chemistry. The Ng inserted

molecular ions of HCO^{+157} and HN_2^{+158} were investigated theoretically by us recently. Considering the significance of HBF^+ ion, we have explored the feasibility of existence of another new series of noble gas hydrides, HNgBF^+ .

Thioformyl cation, HCS^+ , also known as thiomethylum, was first observed with mass spectroscopic methods in the interstellar medium by Thaddeus *et al.*²⁷¹ in 1981. They found four interstellar emission lines originating from HCS^+ due to the rotational transitions in the microwave region. This observation was subsequently confirmed by measuring the various rotational transitions due to the formation of HCS^+ in a glow discharge containing H_2S and CO gas mixture by Gudeman *et al.*²⁷² and Bogey *et al.*²⁷³ Botsch-wina and Sebald²⁷⁴ had reported the optimized structural parameters and spectroscopic properties of HCS^+ ion using *ab initio* molecular orbital theory to rationalize these experimental data.²⁷⁵ It is valence isoelectronic with the cations like HCO^+ , HOC^+ , HN_2^+ , *etc.*^{269,270} All these species including HCS^+ are found to be highly abundant in the interstellar medium and species of potential interest in astrochemistry and astrophysics. The vdW complexes between HCO^+ and noble gas have been investigated through spectroscopic techniques experimentally as well as theoretically.²⁷⁶ The isovalency of HCS^+ with HCO^+ and HN_2^+ , has motivated us to investigate another set of novel interesting ionic molecular species, HNgCS^+ .

The precursor molecule of our predicted ions, protonated silicon monoxide (SiOH^+),²⁷⁷ plays a significant role in ionospheric²⁷⁸ and interstellar chemistry.²⁷⁹ It was successfully generated by the hollow cathode discharge of $(\text{CH}_3)_3\text{SiOH}$ in a mixture of hydrogen and helium and also by the discharge of SiH_4 and N_2O in the same buffer gas.²⁸⁰ The release of silicon monoxide from SiOH^+ in interstellar gas clouds was suggested by Turner and Dalgarno.²⁸¹ The two isomers of protonated silicon monoxide, SiOH^+ and HSiO^+ ,²⁸² are important in processes like deposition of thin Si films, etching technology,²⁸³ and preparation of ultrapure semiconductor materials in the semiconductor industry.²⁸⁴ They

are also required for the modelling of bridging and terminal hydroxyls in zeolites²⁸⁵ and surface hydroxyls on amorphous silica.²⁸⁶ The study of the cluster growth and that of coexisting isomers of van der Waals complexes like $\text{SiOH}^+-\text{Ar}_n$ ($n = 1-10$) have been studied by Olkhov and co-workers²⁸⁷ using IR photodissociation spectroscopy and *ab initio* calculations. Very recently, Chattaraj and co-workers²⁸⁸ have investigated the stability of noble gas bound SiH_3^+ and SiX_3^+ clusters and also reported the existence of $\text{H}_3\text{SiNgNSi}$ and HSiNgNSi ($\text{Ng} = \text{Xe}$ and Rn)²⁸⁹ molecules with Si–Ng covalent bond and Ng–N ionic bond. The experimental detection of XeSiF_3^+ (Cipollini and Grandinetti¹³¹), ArSiF_3^+ and KrSiF_3^+ (Cunje and coworkers²⁹⁰) ions along with the theoretical investigation of noble gas inserted metastable compounds like FXeSiF (Lundell *et al.*¹⁷¹) and FArSiF_3 (Cohen *et al.*¹⁵¹) having noble gas–silicon interaction have encouraged us to investigate the presence of similar interaction in the noble gas inserted protonated silicon monoxide species, HNgOSi^+ . Studies related to these valence isoelectronic molecules, atmospheric importance of protonated silicon monoxide (analogous to HCO^+ and HOC^{+269} ions), and the existence of stable HNgCO^{+157} complexes have motivated us to investigate the change in stability of HOSi^+ and HSiO^{+282} on insertion of a noble gas atom.

In the year 2005, Hu and his group had theoretically predicted a series of noble gas insertion compound of the type of FNgBO^{265} ($\text{Ng} = \text{Ar}, \text{Kr}, \text{and Xe}$). Subsequently, FNgBN^{-266} species, which are isoelectronic with FNgBO molecules, have been reported by Grandinetti and co-workers. Very recently, FNgBNR ($\text{R} = \text{H}, \text{CH}_3, \text{CCH}, \text{CHCH}_2, \text{F}, \text{and OH}$) molecules have also been investigated.²⁹¹ Motivated from these theoretical findings and experimental study of FBS through microwave as well as photoelectron spectroscopic techniques,²⁹² we present here the theoretical investigation of a novel noble gas insertion molecules of the type FNgBS ($\text{Ng} = \text{Ar}, \text{Kr}, \text{and Xe}$). Here we are keen to understand the

nature of bonding present in the neutral molecule, FNgBS, and compare with the previously reported FNgBO²⁶⁵ species.

Carbenes have been an important subject of interest for experimentalists and theoreticians due to its significant difference in reactivity between low-lying singlet ($\sigma^2\pi^0$) and triplet ($\sigma^1\pi^1$) ground states, despite their energetic closeness.²⁹³ The simplest of these molecules, CH₂, shows greater stability in its triplet state,²⁹⁴ which is understood simply as a result of higher coulombic repulsion energy between the nonbonding electrons in the singlet state as compared to the triplet state. In CF₂, however, the singlet state is more stable due to stabilization of σ molecular orbital and/or destabilization of $2p-\pi$ atomic orbital on C atom where the molecule adopts sp^2 hybrid structure.²⁹⁵ The nature of interaction of such species is greatly determined by the relative stability of the singlet and triplet state.²⁹⁶ The carbene, 2,5-diazacyclopentadienylidene, for instance, is known to form an adduct with Xe when produced in matrix isolation. This species has been characterized spectroscopically and is found to have a significantly high electrophilic reactivity along with a singlet ground electronic state.²⁹⁷ Halogenated carbenes are very important reactive molecular species playing vital roles in large number of chemical reactions; *viz.*, these are the most possible photoproducts of halons and chlorofluorocarbons (CFCs) which have large ozone depletion potentials (ODPs) due to destruction of ozone layer in the stratosphere, and the halocarbenes are also very important intermediates in several organic synthesis as well as in the gas-phase combustion reactions.²⁹⁸ In fact, it has been estimated that the bromine containing halocarbons are 60 times more destructive to the ozone layer than the corresponding chlorine counterpart.²⁹⁹ The larger values of ODPs demand further investigation of the photoproducts of halons and CFCs, *i.e.*, halocarbenes. For this purpose, halocarbenes are the most significant specified species among all the carbenes in the frontier area of research.³⁰⁰ Considering the significance of the halocarbenes, we look into parent molecules of the type

FCX, where X = F, Cl, Br and I, forming FNgCX upon insertion of noble gas atom, Ng = Kr and Xe.

3.2. Computational Details

The electronic structures of all the ionic species, *viz.*, HNgOH₂⁺, HNgBF⁺, HNgCS⁺, HNgOSi⁺ and neutral species, *viz.*, FNgBS, FNgCX, have been optimized and relevant calculations have been performed through *ab initio* molecular orbital method using GAMESS³⁰¹ and MOLPRO 2012³⁰² program codes. Quantum computational methods such as second-order Møller–Plesset perturbation theory (MP2),²⁵⁶ density functional theory (DFT) along with the hybrid exchange correlation energy functional Becke 3-parameter exchange and Lee–Yang–Parr correlation (B3LYP),²⁵⁰ and coupled–cluster theory with the inclusion of single and double excitations and an estimate of connected triples (CCSD(T))²⁵⁷ have been employed to investigate the optimized geometrical structures of the predicted ions in their respective minima and transition states. The geometry optimizations have been performed at MP2, DFT, and CCSD(T) levels of theory based on analytical and numerical gradients for linear C_{∞v} and planar bent C_s symmetries, corresponding to the linear minima and planar transition states, respectively, for all the predicted ions except HNgOH₂⁺ and FNgCX. All HNgOH₂⁺ ions exhibit nonlinear planar structure (C_{2v} symmetry) at the minima except HHeOH₂⁺ which shows a slight deviation from the planar geometry while the corresponding transition states are found to be associated with nonlinear bent structures (C_s symmetry) (Figure 3.1). In case of FNgCX molecules, both minima and transitions state structures possess nonlinear bent structures with C_s symmetry. In this context, it is very important to mention that a good description of electron correlation could only be achieved by employing the coupled-cluster theory with CCSD(T) method at the expense of a longer computational

time. Therefore, the CCSD(T) calculated values are considered to be more accurate as compared to the corresponding B3LYP and MP2 results.

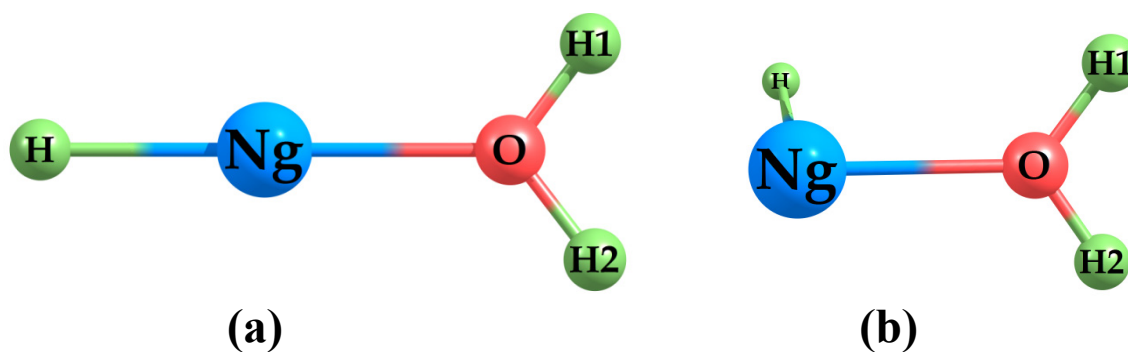


Figure 3.1. Optimized structures of the minimum energy (a) and transition state (b) of HNgOH_2^+ ($\text{Ng} = \text{He, Ar, Kr, Xe}$) ions. (H1 and H2 are symmetry equivalent atoms).

We have utilized the energy adjusted Stuttgart effective core potentials³⁰³ (ECPs) consisting of 28 and 46 core electrons for the Kr and Xe atom, respectively, and the corresponding valence only (6s6p1d1f)/[4s4p1d1f] basis sets. The standard split valence basis sets with polarization functions, *viz.*, 6-311++G(2d,2p) have been employed for all the remaining atoms for all the DFT and MP2 calculations. The basis sets aug-cc-pVTZ have been used for the later atoms in CCSD(T) method. It may be noted that similar combination of basis sets was previously used by Lignell *et al.*¹⁵⁹ while discussing the reliability of various theoretical methods, *viz.*, B3LYP, MP2, and CCSD(T), in the prediction of noble gas hydrides. In some cases, we have considered Kr and Xe atoms with 10 and 28 core electrons,³⁰⁴ respectively, by Stuttgart effective core potentials (ECP) along with aug-cc-pVTZ-PP basis sets whereas aug-cc-pVTZ³⁰⁵ basis sets have been utilized for the remaining atoms during B3LYP, MP2, and CCSD(T) calculations. This combination of basis sets has been denoted as AVTZ.

The stability of the predicted ionic species is determined by computing the energy differences between the predicted ions and the all possible 2-body and 3-body unimolecular

dissociation channels. Intrinsic reaction coordinate (IRC)³⁰⁶ analysis has been performed using second-order Gonzalez–Schlegel algorithms³⁰⁷ with a step size of 0.2 amu^{1/2} bohr to trace the minimum energy path connecting the metastable species with their global minimum products through the transition state. All the methods have been used to calculate the infrared harmonic vibrational frequencies numerically using finite difference approximation for all the predicted ions species (in their respective minima and transition states) to characterize the nature of the stationary point on the corresponding potential energy surface. During the analysis of the vibrational frequency, it is observed that the vibrational modes, especially the stretching vibrational modes, couple with each other strongly. Therefore, the Boatz and Gordon³⁰⁸ approach has been adopted to partition the normal coordinate frequencies into individual internal coordinates. The individual internal coordinate vibrational frequencies along with the force constant values of all the predicted ions have been calculated by using the MP2 and B3LYP methods.

In order to determine the nature of bonding that exists between the atoms or fragments in a neutral or ionic species, it is essential to know the partial atomic charges present on each atom constituting the molecule/ion. In this context, Mulliken population analysis has been employed to compute the partial atomic charges on the each atom of all the predicted ions by using MP2 and DFT methods. It is well-known that the Mulliken population analysis provides qualitative information about the electronic charge distribution within the chemical system. However, the basis set dependence of Mulliken charges is very commonly known in the literature. Accordingly, we have performed NBO (Natural Bond Orbital) analysis for obtaining the partial atomic charges in the predicted ions using DFT and MP2 methods with different basis sets in the MOLPRO program.

Atoms-in-molecules (AIM)³⁰⁹ approach has also been used to compute the topological properties of the predicted ions as well as to evaluate the nature of the bonding that exists

among the constituent atoms all the predicted ions using the MP2 and B3LYP methods by employing AIMPAC³⁰⁹ and Multiwfn programs.³¹⁰

3.3. Results and Discussions

3.3.1. A Comparative Accounts of Optimized Structural Parameters

In general, it has been observed that in many cases the experimentally determined parameters are closer with the CCSD(T) computed data rather than MP2 and DFT methods. Detail structural parameters of both the forms obtained by CCSD(T) method are discussed throughout the text unless otherwise mentioned (Table 3.1). Here it may be noted that the CCSD T1 diagnostics values for various minimum and transition state structures have been found to be below the limiting value of 0.02, indicating the adequacy of single reference based methods for the description of the present systems.

In this context, it may also be interesting to compare the H–Ng bond length values in HNgCS⁺ with reference to the HNgBF⁺, HNgCO⁺,¹⁵⁷ HNgN₂⁺,¹⁵⁸ HNgOSi⁺, HNgOH₂⁺, and HNgF³¹¹ systems. The computed H–Ng bond length values have been found to be 0.766–1.620 Å in HNgCS⁺, 0.764–1.610 Å in HNgCO⁺,¹⁵⁷ 0.765–1.607 Å in HNgN₂⁺,¹⁵⁸ 0.771–1.620 Å in HNgBF⁺, 0.751–1.615 Å in HNgOSi⁺ and 0.754–1.609 Å in HNgOH₂⁺ ions on going from He to Xe. On the other hand, the corresponding H–Ng bond lengths are from 0.824 to 1.680 Å in HNgF species and from 0.776 to 1.607 Å in bare H–Ng⁺ ions.^{171–173} Due to the close proximity of the H–Ng bond lengths in all the ions, it can be concluded that the H–Ng bonds are almost comparable in strength in all the HNgBF⁺, HNgCS⁺, HNgCO⁺, HNgN₂⁺, HNgOSi⁺ and HNgOH₂⁺ ions which in turn found to be stronger as compared to the same in HNgF and bare HNg⁺ ions. This observation leads to conclusion that there exists a strong bonding between the H and Ng atom in all the predicted ions. In this context, it is

important to mention that the $\text{NgHNg}^{+171-173}$ ions have been observed in noble gas matrices and investigated experimentally by mass spectrometric and matrix isolation techniques supported by theoretical calculations. The CCSD(T) computed H–Ng bond length values are 1.501, 1.662, and 1.845 Å for ArHAr^+ , KrHKr^+ , and XeHXe^+ species, respectively, which are larger than the corresponding bond length values in all the predicted ions. This results further confirm that there exists a strong interaction between the H and Ng atoms in all the predicted ions, rather than the same in $(\text{NgHNg})^+$ ions.

To find out the nature of interaction between the Ng and C atoms, it is necessary to compare the present system with HNgbF^+ , HNgcO^+ , and HNgN_2^+ ions. On going from He to Xe, the CCSD(T) computed bond length values are 2.240–3.090 Å for Ng–B bond in HNgbF^+ , 2.138–3.093 Å for Ng–N bond in HNgN_2^{+158} , 2.036–2.872 Å for Ng–C bond in HNgCS^+ and 2.221–3.124 Å for Ng–C bond in HNgcO^+ ions.¹⁵⁷ From the above results, it is clear that Ng–C bond lengths in HNgCS^+ ions are smaller than Ng–B in HNgbF^+ , Ng–N in HNgN_2^+ and Ng–C in HNgcO^+ bond lengths. Although atomic size decreases along the series B–C–N, the calculated shortest Ng–C bond distance in the present system suggests that the interaction between the Ng and C atom in HNgCS^+ ions is the strongest among all the Ng–X' interactions (X' = BF, CO, CS, and N₂) discussed above. The electronegativity of oxygen is higher than that of sulfur and the atomic size of oxygen is smaller than that of sulfur, which makes sulfur atom more polarizable than oxygen, leading to a shorter Ng–C bond in HNgCS^+ ions. The CCSD(T) optimized Ng–C bond length values are found to be 2.902, 2.838, 2.456, 2.420, and 2.571 Å along the He–Ne–Ar–Kr–Xe series, in bare NgCS^+ ions, which are shorter with respect to the respective bond lengths in HNgCS^+ ions, except for HHeCS^+ and HNeCS^+ . It may be due to the positive charge transfer from the CS fragment to the HNg moiety resulting into a short and strong H–Ng bond and a weak Ng–C bond.

Now, it is worthwhile to compare the Ng–O bond lengths in HNgOSi⁺ ions as compared to the same in NgOSi⁺ and HNgOH₂⁺ systems. The CCSD(T) computed Ng–O bond lengths are found to be 1.747–2.555 Å in HNgOSi⁺ and 1.841–2.714 Å in HNgOH₂⁺ ions along He–Ne–Ar–Kr–Xe series while the corresponding bond lengths have been calculated to be 3.739, 3.687, 2.682, 2.255, and 2.382 Å in HeOSi⁺, NeOSi⁺, ArOSi⁺, KrOSi⁺, and XeOSi⁺, respectively. In general, the shorter Ng–O bond lengths in HNgOSi⁺ ions as compared to the other ions clearly reveal a stronger Ng–O bond in the species. It has also been found that HNgOSi⁺ ions are more stable as compared to the isomeric HNgSiO⁺ species. Larger Ng–Si bond length values in HNgSiO⁺ ions as compared to NgSiH₃⁺²⁸⁸ and H₃SiNgNSi⁺²⁸⁹ species further reveal that these systems are less stable as compared to our predicted species, HNgOSi⁺.

Now, it is of immense interest to compare the F–Ng bond lengths in FNgBS with that in FNgBO molecules. Using the CCSD(T) method for calculation, we found that the F–Ng bond lengths are 1.989, 2.023, and 2.103 Å for FArBO, FKrBO, and FXeBO species, respectively, while the corresponding F–Ng bond lengths are 2.028, 2.054, and 2.127 Å along the Ar–Kr–Xe series in FNgBS molecules. There is a slight increase in F–Ng bond length values in going from FNgBO to FNgBS species. Increase in the F–Ng bond length values in both FNgBO and FNgBS species along the Ar–Kr–Xe series can be attributed to the increase in the size of the noble gas atom. The CCSD(T) computed Ng–B bond length values are 1.806, 1.954, and 2.160 Å in FArBS, FKrBS, and FXeBS species, respectively. The CCSD(T) calculated Ng–B bond lengths are 1.828, 1.966, and 2.169 Å along the series Ar–Kr–Xe, respectively, in FNgBO⁺²⁶⁵ species, and the corresponding values in FNgBN⁻²⁶⁶ are 1.820, 1.961, and 2.153 Å. From the above results, it is obvious that the Ng–B bond in FNgBS is almost the same (very slight smaller side) as compared with the Ng–B bonds present in the FNgBO and FNgBN⁻ systems. The calculated Ng–B bond lengths in FNgBS

are also found to be comparable to that in the FNgBNR systems (R = H, CH₃, CCH, CHCH₂, F, and OH) reported recently.²⁹¹

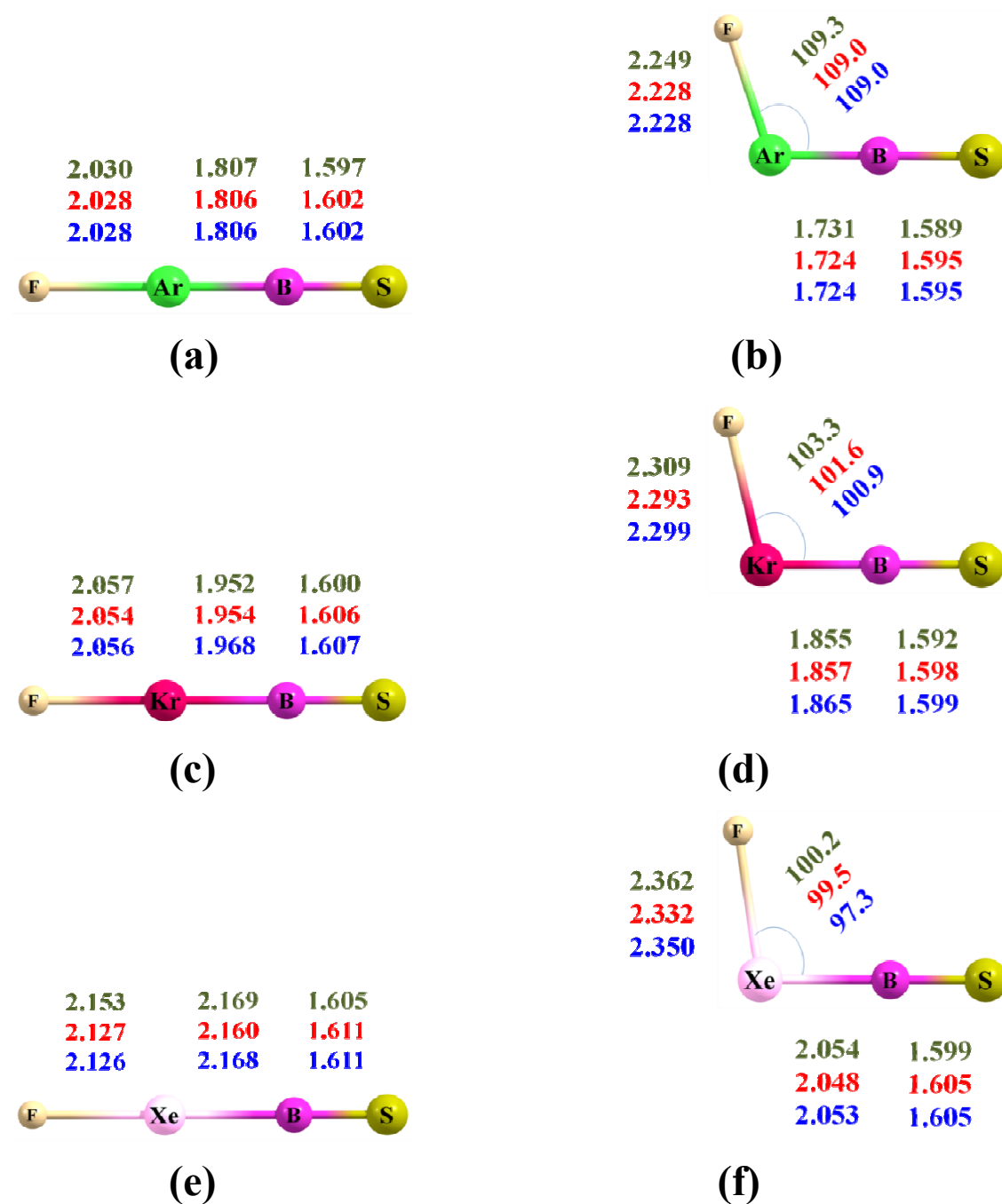


Figure 3.2. Optimized geometrical parameters in graphical format for the linear minima [(a), (c) and (e)] and planar bent transition states [(b), (d) and (f)] of FNGBS molecules (Ng = Ar, Kr, and Xe) where the bond lengths are in Å and bond angles are in degrees. The values in

green, red, and blue colors are computed at the MP2/6-311++G(2d,2p), CCSD(T)/aug-cc-pVTZ, and CCSD(T)/aug-cc-pVTZ-PP level of theory, respectively.

Table 3.1. Optimized Geometrical Parameters for the Minima Structures of HNgX' (X' = BF, CO, CS, N₂, OH₂, and OSi) Species by CCSD(T)/AVTZ Level of Theory.

Species	Bonds	He	Ne	Ar	Kr	Xe
Bare Ion	H-Ng⁺	0.776	0.992	1.282	1.416	1.607
	R_{cov(H-Ng)}^a	0.59	0.89	1.37	1.47	1.71
	R_{vdW(H-Ng)}^b	2.60	2.74	3.08	3.22	3.36
HNgBF⁺	H-Ng	0.771	... ^c	1.286	1.422	1.620
HNgCO⁺	H-Ng	0.764	... ^c	1.281	1.417	1.610
HNgCS⁺	H-Ng	0.766	0.986	1.284	1.425	1.620
HNgN₂⁺	H-Ng	0.765	... ^c	1.280	1.416	1.607
HNgOH₂⁺	H-Ng	0.754	... ^c	1.277	1.425	1.609
HNgOSi⁺	H-Ng	0.751	0.980	1.278	1.423	1.615
HNgBF⁺	Ng-B	2.240	... ^c	2.943	2.980	3.090
	R_{cov(Ng-B)}^a	1.12	1.42	1.90	2.00	2.24
	R_{vdW(Ng-B)}^b	3.31	3.45	3.67	3.93	4.07
HNgCO⁺	Ng-C	2.221	... ^c	2.911	3.068	3.124
HNgCS⁺	Ng-C	2.038	2.587	2.705	2.741	2.882
	R_{cov(Ng-C)}^a	1.04	1.34	1.82	1.92	2.16
	R_{vdW(Ng-C)}^b	3.10	3.24	3.54	3.72	3.86
HNgN₂⁺	Ng-N	2.138	... ^c	2.841	2.922	3.093
	R_{cov(Ng-N)}^a	0.99	1.29	1.77	1.87	2.11
	R_{vdW(Ng-N)}^b	3.06	3.20	3.42	3.68	3.82
HNgOH₂⁺	Ng-O	1.841	... ^c	2.523	2.583	2.714
HNgOSi⁺	Ng-O	1.747	2.282	2.419	2.456	2.555
	R_{cov(Ng-O)}^a	0.94	1.24	1.72	1.82	2.06
	R_{vdW(Ng-O)}^b	2.93	3.08	3.44	3.57	3.78

^aReference 43; ^bReference 44-46; ^cIt has not been possible to optimize the concern structures.

Figure 3.2 depicts the graphical representation of the optimized minima and transition state structure of all of the FNgBS molecules with the structural parameters obtained by MP2/6-311++G(2d,2p), CCSD(T)/aug-cc-pVTZ, and CCSD(T)/aug-cc-pVTZ-PP levels. Periodic variation of chemical properties of elements along a particular period or group in the periodic table has always been fascinating to chemists. Therefore, we have been motivated to compare the Ng-B bond lengths in the FNgBS molecules with the Ng-X (X = B, C, N) bond lengths for some noble gas inserted cationic systems, *viz.*, HNgBF⁺, HNgCO⁺,¹⁵⁷ HNgCS⁺, and HNgN₂⁺.¹⁵⁸ On going from Ar to Xe, the CCSD(T) computed Ng-B bond lengths are 2.943–3.090 Å in HNgBF⁺, the Ng-C bond lengths are 2.911–3.124 and 2.725–2.872 Å in HNgCO⁺ and HNgCS⁺, respectively, and the Ng-N bond lengths are 2.841–3.093 Å in HNgN₂⁺. Thus, the corresponding Ng-X bond lengths are found to be greater than the Ng-B bond lengths in FNgBS molecules, even though the covalent radius value of boron is the maximum among boron, carbon, and nitrogen.⁴³ It clearly indicates toward the fact that the Ng-B bond is stronger in FNgBS molecules. Here it may be noted that the Ng-C bond length is decreased considerably when O atom is replaced with S atom in HNgCO⁺ species. However, the difference in the Ng-B bond length in FNgBO and FNgBS systems is rather negligible.

In case of FXeCX molecules, the F-Xe and Xe-C bond length values are in the range 2.166–2.144 Å and 2.354–2.281 Å, for the series F-Cl-Br-I, respectively, at CCSD(T) level of calculation. In the FKrCX molecules, for the series F-Cl-Br-I, the MP2 calculated F-Kr and Kr-C bond length values are in the range 2.077–2.053 Å and 2.150–2.139 Å, respectively. Thus, both F-Ng as well as Ng-C bond lengths decrease as the electronegativity of X atom decreases. In this context, it is important to compare the F-Ng and Ng-C bond length values of FNgCN molecules with the predicted FNgCX molecules. The MP2(full)/def2-TZVPPD computed F-Ng and Ng-C bond length values are 2.041, 2.089 Å

for FXeCN and 1.934, 1.941 Å for FKrCN molecules, respectively.¹⁸³ These results indicate that the F–Ng and Ng–C bonds in FNgCX are rather weaker as compared to that in FNgCN molecules. On the other hand, the CCSD(T) computed F–Xe bond length values in FXeCF, FXeSiF,¹⁷¹ FXeGeF,¹⁶⁴ FXeSnF³¹² and FXePbF³¹² species, and the corresponding values are 2.166 Å (aug-cc-pVTZ), 2.273 Å (LJ18/6–311++G(2d,2p), 2.264 Å (aug-cc-pVTZ), 2.244 Å (def2–TZVP), and 2.259 Å (def2–TZVP) as obtained by MP2 method. It is very clear that the F–Xe bond length values are found to increase on going from C to Pb down the group, which indicate that the strongest F–Xe bond exists in FXeCF among all the tetragen series.

In the spirit of the work of Gerry and co-workers¹⁵³ on the analysis of the noble gas atom containing chemical bonds in terms of the covalent and van der Waals radii limits, denoted as R_{cov} and R_{vdW} , respectively, we have been motivated to compare the $R(\text{H–Ng})$ and $R(\text{Ng–X}')$ bond lengths with respect to the R_{cov} and the R_{vdW} . For an A–B bond these limits can be defined as $R_{\text{cov}} = r_{\text{cov}}(\text{A}) + r_{\text{cov}}(\text{B})$ and $R_{\text{vdW}} = r_{\text{vdW}}(\text{A}) + r_{\text{vdW}}(\text{B})$. Standard r_{cov} and r_{vdW} values have been taken from the literature for the calculations of R_{cov} ⁴³ and R_{vdW} .⁴⁴⁻⁴⁶ The calculated H–Ng covalent limits are found to be 0.59, 0.89, 1.37, 1.47, and 1.71 Å for H–He, H–Ne, H–Ar, H–Kr, and H–Xe, respectively, and the corresponding vdW limits are 2.60, 2.74, 3.08, 3.22, and 3.36 Å. Similarly, the calculated $R(\text{Ng–X}')$ covalent limits and the corresponding vdW limits are reported in Table 3.1. Thus it is quite evident that $R(\text{H–Ng})$ values are very close with the corresponding covalent limit, whereas the Ng–X' bond distances are in between the two limiting values for all the ions. Therefore, it is evident that a very strong interaction exists between the H and Ng atoms while relatively weak interactions are found between Ng and X' atoms in the all the predicted ions, *viz.*, HNgBF^+ , HNgCS^+ , HNgOSi^+ and HNgOH_2^+ . The formation of strong, short, and rigid H–Ng bond and weak and

large Ng–X' bond (X' = BF, CS, OH₂, and OSi) along with the bond length similarity with the HNg⁺ moiety strongly indicates that the predicted ion may exist as [HNg]⁺X'.

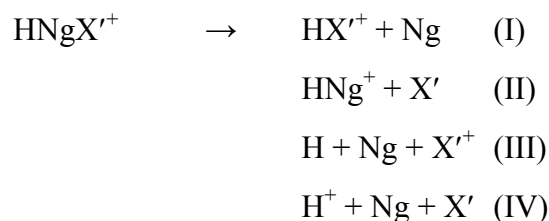
In case of neutral FNgBS molecule, the covalent limits of the F–Ng bond lengths are 1.63, 1.73, and 1.97 Å and the corresponding van der Waals limits are 3.23, 3.49, and 3.63 Å for Ng = Ar, Kr, and Xe, respectively. The covalent limits of the Ng–B bond lengths are 1.90, 2.00, and 2.24 Å for Ar–Kr–Xe, respectively, and the corresponding van der Waals limits are 3.67, 3.93, and 4.07 Å, respectively. Thus, the F–Ng bond lengths in both FNgBS and FNgBO are slightly larger than the covalent limit and deviate considerably from that of the van der Waals limit; however, it is important to note that the Ng–B bond lengths in both the series are slightly smaller than the corresponding covalent limits. It indicates that the Ng–B bond is a relatively strong chemical bond, whereas F–Ng bond is somewhat weaker than that of a covalent bond but considerably stronger than just van der Waals interaction which is in contrast with the H–Ng bond in noble gas hydrides.

Geometry of all the predicted Ng inserted neutral and ionic species transforms from linear to nonlinear bent structure from minima to the saddle point except FNgCX and HNgOH₂⁺. In case of HNgOH₂⁺ ion, the planar minima changes to non-planar bent structure in the transition state whereas both minima and transition state structures possess nonlinear bent structures. For noble gas hydride ions, there is a slight decrease in the H–Ng bond length and increase in Ng–X' bond length due to the H–Ng–X' bending mode in the transition state geometry for all the systems. The H–Ng–X' bond angles change drastically from 180⁰ to ~90–110⁰ except while going from the minima to the transition state geometry. In contrast, for the predicted FNgBS molecules, the bond lengths and bond angles are changed considerably on going from the minima state to the transition state structure. The F–Ng bond elongates by an amount of ~ 0.2 Å while the Ng–B bond contracts by an amount of ~ 0.1 Å

in the transition state. Nevertheless, the F–Ng–B angle also changes from 180° to $\sim 99\text{--}110^{\circ}$ in the transition state.

3.3.2. Thermodynamic and Kinetic Stability

In general, noble gas hydrides are meta-stable in nature. Therefore, to ascertain the stability of the predicted HNgX'^+ ($X' = \text{BF}, \text{CS}, \text{OH}_2,$ and OSi) ions, energy of the insertion complexes as well as various possible decomposition products have been calculated and reported in Table 3.2. Accurate energy diagram for the plausible 2-body and 3-body dissociation channels is considered to determine the kinetic and thermodynamic stability of the predicted insertion complex as follows.



The first and second dissociation channels correspond to the 2-body dissociation, resulting into the global and local minimum structure, respectively, on the potential energy surface. The negative energy values clearly indicate that the dissociation process is exothermic in nature and the predicted ions are thermodynamically unstable in comparison with the precursor ion and Ng atom leading to global minima products ($\text{HX}'^+ + \text{Ng}$). However, the predicted HNgX'^+ ions are thermodynamically stable corresponding to the other 2-body dissociation channel (II) ($\text{HNg}^+ + X'$) leading to local minima in the potential energy surface.

Now, it is interesting to compare the dissociation/binding energies of channel (II) of the present ions with those of the other isoelectronic systems such as HNgCO^+ and HNgN_2^+

ions. The CCSD(T) calculated dissociation energies corresponding to channel (II) are 21.2–21.1 kJ mol⁻¹ for HNgN₂⁺, 28.8–29.1 kJ mol⁻¹ for HNgCO⁺, 50.9–54.6 kJ mol⁻¹ for HNgBF⁺, 72.3–74.7 kJ mol⁻¹ for HNgOH₂⁺, 72.5–77.9 kJ mol⁻¹ for HNgCS⁺ and 109.5–122.0 kJ mol⁻¹ for HNgOSi⁺ ions along the Ar–Kr–Xe series. These energy values strongly indicate that the binding between HNg⁺ moiety and X' (X' = BF, CO, CS, N₂, OH₂ and OSi) follows the order: {[HNg⁺][N₂]} < {[HNg⁺][CO]} < {[HNg⁺][BF]} < {[HNg⁺][OH₂]} < {[HNg⁺][CS]} < {[HNg⁺][OSi]}. More endothermic behavior for channel (II) of the HNgCS⁺ ions as compared to the HNgCO⁺ species suggests that the interaction between Ng and C atoms are stronger in HNgCS⁺ ions as compared to that in the HNgCO⁺ species. The higher dissociation energy values for the HNgOSi⁺ ions as compared to the HNgCO⁺ ions with respect to channel (II) suggest that the HNg⁺ and OSi species are bound in a stronger manner in HNgOSi⁺ ions than the HNg⁺ and CO species in HNgCO⁺ ions.

The CCSD(T) calculated energies corresponding to the dissociation channel [NgHNg⁺ → NgH⁺ + Ng], are in the range 64–66 kJ mol⁻¹ along the Ar–Kr–Xe series in NgHNg⁺ cations,^{171–173} which are smaller than that of the respective energies for the HNgOH₂⁺, HNgCS⁺, and HNgOSi⁺ systems. Thus, it may be possible to prepare these metastable HNgX'⁺ ions by electron bombardment matrix isolation technique at cryogenic temperatures.

It is important to estimate the basis set super position error (BSSE) for the dissociation energies corresponding to the second dissociation channel (II), since it involves lowest dissociation energy for each of the HNgX'⁺ species. The calculated values of BSSE for the dissociation energy have been found to be in the range 0.60–0.85 kJ mol⁻¹ (with DFT) and 2.2–2.6 kJ mol⁻¹ (with MP2) for the HNgOH₂⁺ species. These values are found to be rather negligible in comparison to the computed dissociation energies of the same systems.

Table 3.2. CCSD(T)/AVTZ Calculated Energies (kJ mol⁻¹) Corresponding to Different Dissociation Channels for HNgX' (X' = BF, CO, CS, N₂, OH₂, and OSi).

Channel	Ng	HNgBF ⁺	HNgCO ^{+b}	HNgCS ⁺	HNgN ₂ ^{+c}	HNgOH ₂ ⁺	HNgOSi ⁺
HX'⁺ + Ng	He	-495.0	-406.4	-518.3	-288.4	-421.4	-475.3
	Ne	... ^a	... ^a	-530.6	... ^a	... ^a	-502.7
	Ar	-317.5	-192.3	-347.2	-98.3	-248.9	-315.3
	Kr	-239.0	-115.4	-266.9	-21.5	-170.1	-254.8
	Xe	-173.9	-52.2	-201.9	-41.4	-106.7	-183.5
HNg⁺ + X'	He	73.6	15.0	101.7	31.4	100.1	149.8
	Ne	... ^a	... ^a	62.2	... ^a	... ^a	95.1
	Ar	50.9	28.8	72.5	21.2	72.3	109.5
	Kr	53.2	29.5	76.6	21.8	74.9	118.1
	Xe	54.6	29.1	77.9	21.1	74.7	122.0
H + Ng + X'⁺	He	25.8	245.1	75.8	412.3	197.7	150.9
	Ne	... ^a	... ^a	63.5	... ^a	... ^a	123.5
	Ar	203.3	459.1	246.9	602.3	370.2	311.0
	Kr	281.9	536.1	327.2	679.1	449.0	371.4
	Xe	346.9	599.3	392.1	742.1	512.4	442.7
H⁺ + Ng + X'	He	270.1	211.5	298.2	227.9	296.5	346.2
	Ne	... ^a	... ^a	285.9	... ^a	... ^a	318.8
	Ar	447.6	425.5	469.2	417.9	468.9	506.2
	Kr	526.1	502.5	549.9	494.7	547.8	566.7
	Xe	591.1	565.7	614.5	557.6	611.2	637.9
Barrier Height	He	... ^a	22.7	13.3	2.3	2.7	7.1
Corresponds to	Ne	... ^a	... ^a	0.3	... ^a	... ^a	... ^a
Transition State	Ar	15.5	10.1	19.5	6.3	14.8	23.2
[HNgX'⁺ →	Kr	21.0	13.1	27.5	8.0	20.9	36.7
HX'⁺ + Ng]	Xe	26.7	15.0	33.9	... ^a	25.7	47.0

^aIt has not been possible to optimize the concern structures; ^bReference 157; ^cReference 158.

The endothermic nature of the 3-body dissociation channel (III) ($H + Ng + X'^+$) and the high positive energy values corresponding to another 3-body dissociation channel (IV) ($H^+ + Ng + X'$) strongly demonstrates that the predicted $HNgX'^+$ ions are more stable than the dissociated products. On going from He to Xe, the dissociation energies for the channel (IV) are 346.2–637.9 kJ mol^{-1} for $HNgOSi^+$ and 211.5–565.7 kJ mol^{-1} for $HNgCO^{+157}$ ions. These results also indicate a higher thermodynamic stability of $HNgOSi^+$ ions in comparison with the valence isoelectronic species, $HNgCO^+$.

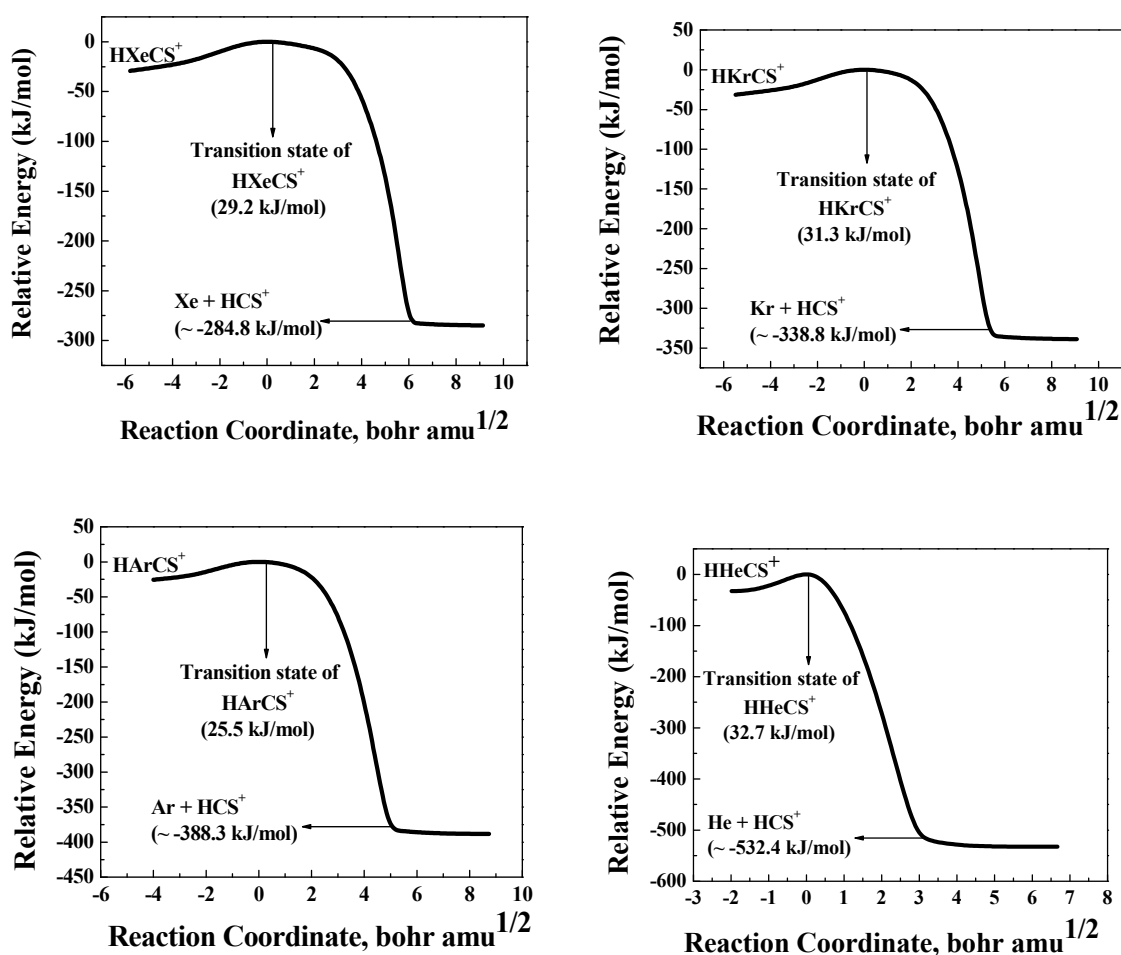


Figure 3.3. Minimum Energy Path for $[HNgCS^+ \rightarrow HCS^+ + Ng]$ Reaction ($Ng = Xe, Kr, Ar, He$)

Now, it is worthwhile to evaluate the kinetic stability of the predicted HNgX^+ ions, which are thermodynamically unstable with respect to the global minimum products ($\text{Ng} + \text{HX}^+$). The energy differences between the HNgX^+ species and the corresponding transition states, the so-called “barrier heights” have been calculated for the predicted HNgX^+ ions. We have also computed the intrinsic reaction coordinates (IRC) connecting the metastable minima and the global minima products through transition state for all the predicted ions, and the reaction pathways are depicted in Figure 3.3 for HNgCS^+ ions. The MP2 calculated zero-point energy (ZPE) corrected barrier heights are 16.1, 23.9 and 29.1 kJ mol^{-1} for the HArCS^+ , HKrCS^+ , and HXeCS^+ ions. Here it may be noted that the barrier height of the HNeCS^+ is reasonably small. This is due to the presence of p orbital leading to very less chemical reactivity of the Ne atom, which has been discussed recently by Grandinetti.¹⁶⁷ The higher barrier heights for HNgOSi^+ ions as compared to HNgCO^+ ions suggest that former ions are kinetically more stable than the latter. Because the calculated barrier heights are quite high, particularly for the Ar, Kr, and Xe containing HNgX^+ ions as shown in Table 3.2, it is clear that these kinetically stable species might be observed at cryogenic conditions, like the other noble gas containing hydrides that have been detected experimentally in recent years.

Analogous to the Ng inserted ionic species, the energetics of the neutral species are found to be similar. The negative energy values corresponding to the 2-body dissociation pathway ($\text{FBS} + \text{Ng}$) signify that the predicted FNgBS molecules are thermodynamically unstable in comparison with the global minima products. The high positive energy values for the rest of the two 2-body [$(\text{FNg} + \text{BS})$ and $(\text{F}^- + \text{NgBS}^+)$] and two 3-body [$(\text{F} + \text{Ng} + \text{BS})$ and $(\text{F}^- + \text{Ng} + \text{BS}^+)$] dissociation channels indicate the endothermic nature of these processes which illustrates that the predicted FNgBS species are thermodynamically more stable than the dissociated products. The CCSD(T) computed barrier height with respect to the $[\text{FNgBS} \rightarrow \text{Ng} + \text{FBS}]$ comes out to be 60.8, 101.6, and 132.2 kJ mol^{-1} along the

Ar–Kr–Xe series of FNgBS species, respectively, while the corresponding values for FNgBO are 76.6, 115.5, and 147.3 kJ mol⁻¹ for [FNgBO → Ng + FBO] dissociation.²⁶⁵ Therefore, it is evident that the barrier heights are almost comparable for both FNgBO and FNgBS molecules which confirms the kinetic stability of these molecules. Similar to FNgBS, all FNgCX (Ng = Kr and Xe; X = F, Cl, Br, and I) molecules are also metastable in nature. Therefore, it might be possible to prepare and characterize these predicted metastable neutral FNgBS molecules under cryogenic conditions through matrix isolation techniques.

In this context, it is important to study the singlet–triplet energy gaps (ΔE_{ST}) to ascertain the ground electronic state of the predicted FNgCX molecules since both singlet and triplet states exist in nature for carbenes and halocarbenes. The CCSD(T) calculated energy gap values are 84.5, 45.3, 39.9, and 30.0 kJ mol⁻¹ along the series F–Cl–Br–I in FXeCX species whereas the MP2 computed corresponding values are 82.3, 74.1, and 62.0 kJ mol⁻¹ for FKrCCL, FKrCBr, and FKrCI molecules. These relatively high positive energy values indicate that the singlet state is more stable than the triplet state confirming the singlet ground state geometry of the predicted FNgCX molecules and ensure that intersystem crossing between the two states would not take place. It is worthwhile to mention that the ΔE_{ST} values are more positive for FCX molecules as compared to those of the predicted FNgCX.

3.3.3. Harmonic Vibrational Frequencies

One of the most significant tests in any electronic structure calculation is their ability to reproduce the vibrational frequencies of the predicted systems. Nevertheless, it is important to note that the experimental values refer to the frequencies observed in noble gas matrix. However, the computational results are, in general, obtained using gas phase calculations within harmonic approximation. In the case of noble gas containing complexes, the vibrational frequencies obtained by the MP2 method generally resemble well with the

experimentally observed values. Moreover, for the predicted cationic noble gas insertion compounds the MP2 calculated frequency values are more closer to the corresponding CCSD(T) values. Therefore, in this section, MP2 computed vibrational frequencies are discussed unless otherwise mentioned.

The vibrational frequency values are significantly changed after the insertion of a Ng atom into the precursor ions (*viz.*, HBF^+ , HCS^+ , H_3O^+ , and HOSi^+) due to the formation of new chemical bonds within the atomic constituents in it. Thus, the predicted vibrational frequencies of HNgX^+ ions can be used to characterize these species by spectroscopic techniques. All the calculated vibrational frequency values are found to be real for the minima structures indicating that all these species are true minimum in their respective potential energy surfaces. However, the presence of only one negative frequency value corresponding to the H–Ng–X' ($\text{X}' = \text{BF}$, CS , OH_2 , and OSi) bending mode for the transition state (TS) structures confirms the saddle point nature of these TS geometries.

Among all the modes, the H–Ng stretch is associated with larger vibrational frequency value in all the predicted ions indicating covalent character of H–Ng bond. In this aspect, it would be interesting to compare the H–Ng stretching frequency values of HNgX^+ ($\text{X}' = \text{BF}$, CS , OH_2 , and OSi) ions with respect to the bare HNg^+ ions. The MP2 computed H–Ng stretching vibrational frequency values are within the range of 3240–2266 cm^{-1} for HNgBF^+ , 3399–2278 cm^{-1} for HNgCS^+ , 3609–2347 cm^{-1} for HNgOH_2^+ , and 3568–2323 cm^{-1} for HNgOSi^+ ions, along the series He–Ne–Ar–Kr–Xe, which are comparable with the H–Ng stretching vibration frequency values of bare HNg^+ ions, *i.e.*, 3259, 2930, 2652, 2574, and 2340 cm^{-1} for HHe^+ , HNe^+ , HAr^+ , HKr^+ , and HXe^+ ions, respectively. On the other hand, the B3LYP computed H–Ng stretching vibrational frequencies are 3177–2241 cm^{-1} in HNgN_2^+ and 3005–2270 cm^{-1} in HNgCO^+ along He–Ne–Ar–Kr–Xe series. The relatively

high H–Ng stretch values in HNgOH₂⁺ and HNgOSi⁺ species as compared to the other families of ions (*viz.*, HNgBF⁺, HNgCO⁺, HNgCS⁺, HNgN₂⁺) clearly indicate the presence of a strong and rigid H–Ng bond in the former ions. These results are in well agreement with the optimized structural parameters of the predicted ions.

The F–Ng stretch frequency decreases from 458 to 431 cm⁻¹ along the Ar–Kr–Xe series for FNgBS, while for FNgBO its range is 482 to 450 cm⁻¹; however, the frequency values decrease considerably in the transition state ranging from 338 to 310 cm⁻¹ for the predicted FNgBS molecules. It agrees well with the trend in increase of the F–Ng bond length values on going from minima to the transition state. The Ng–B bond stretching frequencies are 327–284 cm⁻¹ in FXeBS and 375–355 cm⁻¹ in FNgBO along the Ar–Kr–Xe series. The harmonic stretching frequency for B–O bond exceeds that of the B–S bond by almost 600 cm⁻¹ due to the larger mass of the sulfur atom. The F–Ng–B bending mode is doubly degenerate and is of special importance as it corresponds to bond dissociation, leading to the global minima products. So it has negative frequency values in the transition state for all predicted FNgBS molecules. In the minimum energy structures, the F–Ng–B bending mode has higher frequency values in FNgBO than that in FNgBS whereas the frequency values for the Ng–B–O bending mode are larger than those for the Ng–B–S mode due to the presence of heavier sulphur atom in FNgBS molecules.

Because all the predicted species are metastable in nature, it is of interest to know the various couplings operating among different vibrational modes. Therefore, the normal coordinate frequencies are partitioned into individual internal coordinates using the Boatz and Gordon approach.³⁰⁸ The slightly smaller Ng–B bond stretching frequency values in FNgBS indicates that the normal modes in FNgBS are likely to be coupled to each other in a stronger way than that in FNgBO species. Based on the above method,³⁰⁸ the computed force constant (K) values are also in accordance with the aforementioned conclusion since force constant

(K) values corresponding to the Ng–B bond in FNgBS molecules (198.4, 197.1, and 182.3 N m⁻¹ for Ar–B, Kr–B, and Xe–B bonds, respectively) are found to be stronger than the corresponding Ng–B bond in FNgBO species (172.8, 188.9, 180.6 N m⁻¹ along the Ar–Kr–Xe series). In case of noble gas hydrides, the individual coordinate analysis indicates negligible coupling in H–Ng stretching frequencies, while other stretching, bending, and torsional modes are found to be coupled with each other. The high force constant values suggest that there exists a strong and rigid bond between the H and Ng atom in HNgX⁺ ion.

3.3.4. Charge Distribution Analysis

It would be interesting to analyze the partial atomic charges to gain information about the nature of bonding that exists between the constituent atoms or fragments in the predicted species. For this purpose, we have computed partial atomic charges as obtained from the Mulliken population analysis for HNgX⁺ (X' = BF, CS, OH₂, and OSi) ions, which reveals that both the set of charges calculated using two different methods are rather similar. B3LYP calculated charge values have been considered for further discussions (Table 3.3).

The insertion of a Ng atom into the HX⁺ ions redistributes the original charges resided on individual atoms of the ions concerned. In the bare HNg⁺ ions the charges acquired by the H atoms are 0.641, 0.666, 0.405, 0.319, and 0.218 a.u. while going from He to Xe, which are almost comparable with the corresponding values in HNgX⁺ (X' = BF, CS, OH₂, and OSi) complexes. The total cumulative charges on the HNg⁺ moiety are found to be in the range of 0.773–0.949 a.u. in HNgBF⁺, 0.907–0.981 a.u. in HNgCO⁺,¹⁵⁷ 0.808–0.941 a.u. in HNgCS⁺, 0.947–0.968 a.u. in HNgN₂⁺,¹⁵⁸ 0.895–0.935 a.u. in HNgOH₂⁺, and 0.845–0.945 a.u. in HNgOSi⁺ ions, whereas unit positive charge resides on the bare HNg⁺ ions. This indicates that the maximum amount of the positive charge is concentrated on the

HNg moiety of all the predicted ions. The above mentioned data further proves that after the insertion of the noble gas atoms in the precursor (HX') ion, extensive charge redistribution has taken place due to substantial amount of charge transfer from X'⁺ moiety to HNg fragment in the HNgX'⁺ complexes. The quantitative charge separation data predict that the HNgX'⁺ ions can be best represented as [HNg⁺] X'.

Table 3.3. B3LYP Computed Mulliken Atomic Charges (a.u.) on H, Ng Atoms and HNg Fragments in the Minima of HNgX'⁺ (X' = BF, CO, CS, N₂, OH₂, and OSi) Species.

Ng	Charges	HNgBF ⁺	HNgCO ^{+b}	HNgCS ⁺	HNgN ₂ ^{+c}	HNgOH ₂ ⁺	HNgOSi ⁺
He	<i>q_H</i>	0.527	0.609	0.541	0.626	0.576	0.485
	<i>q_{Ng}</i>	0.246	0.298	0.267	0.321	0.319	0.360
	<i>q_{HNg}</i>	0.773	0.907	0.808	0.947	0.895	0.845
Ne	<i>q_H</i>	... ^a	0.631	0.563	... ^a	... ^a	0.526
	<i>q_{Ng}</i>	... ^a	0.346	0.358	... ^a	... ^a	0.419
	<i>q_{HNg}</i>	... ^a	0.977	0.921	... ^a	... ^a	0.945
Ar	<i>q_H</i>	0.342	0.392	0.348	0.414	0.367	0.268
	<i>q_{Ng}</i>	0.607	0.589	0.593	0.552	0.568	0.672
	<i>q_{HNg}</i>	0.949	0.981	0.941	0.966	0.935	0.940
Kr	<i>q_H</i>	0.231	0.280	0.229	0.289	0.245	0.155
	<i>q_{Ng}</i>	0.645	0.664	0.647	0.679	0.673	0.746
	<i>q_{HNg}</i>	0.876	0.944	0.876	0.968	0.918	0.901
Xe	<i>q_H</i>	0.158	0.202	0.160	0.205	0.174	-0.015
	<i>q_{Ng}</i>	0.764	0.750	0.727	0.761	0.754	0.932
	<i>q_{HNg}</i>	0.922	0.952	0.887	0.966	0.928	0.917

^aIt has not been possible to optimize the concern structures; ^bReference 157; ^cReference 158.

From NBO and Mulliken analysis, we can conclude that the H–Ng bond is covalent in nature while the Ng–X' bond exhibits considerable ionic character. In this context, it is very

important to point out that the order of acquiring positive charges on noble gas atoms has been found to be $\text{He} < \text{Ne} < \text{Ar} < \text{Kr} < \text{Xe}$ in all the HNgX^+ ($\text{X}' = \text{BF}, \text{CS}, \text{OH}_2, \text{and OSi}$) ions. It clearly suggests that electron transfer is maximum in the case of Xe atom, which is clearly due to more polarizable nature of xenon as compared to other noble gas atoms.

Similarly, after the insertion of the Ng atom, there has been a significant redistribution of charges on fluorine, boron, and sulphur (denoted respectively as q_{F} , q_{B} , and q_{S}) as against the same in the FBS molecule. The MP2 computed q_{F} has become more negative after molecule formation and the value change from -0.074 in FBS to -0.698 , -0.679 , and -0.607 a.u. in FArBS, FKrBS, and FXeBS species, respectively; however, there is a reasonable decrease in the positive electronic charge on the B atom, and q_{B} decreases from 0.196 to 0.113 , -0.186 and -0.194 a.u. along the Ar–Kr–Xe series in FNGBS compounds. The noble gas atom possesses partial positive charge in the FNGBS molecules, and the values are 0.450 , 0.662 , and 0.812 a.u. for FArBS, FKrBS, and FXeBS species, respectively. Now, it is worthwhile to mention that the total accumulated charges on NgBS fragment are same amount of charge reside on F atom with positive sign. It indicates that substantial charge transfer has taken place after the insertion of a noble gas atom into the neutral FBS molecule. Nevertheless, both Mulliken and NBO charges clearly indicate that the FNGBS species exists as an ionic configuration, $\text{F}^-(\text{NgBS})^+$. Similar reason holds good in case of noble gas inserted halocarbenes where these FNGBS molecules can be best described as $\text{F}^-[\text{NgCX}]^+$.

3.3.5. Analysis of Topological Properties

In addition to the charge distributions, it is also interesting to analyze the bond critical point (BCP) properties within the framework of quantum theory of Bader's AIM (atoms-in-molecule) approach,³⁰⁹ which has been quite successful in understanding the nature of a chemical bond. AIM makes a bridge between the electron charge density and the quantum

chemical concept and is highly efficient and useful for description of many chemical systems. According to the AIM model, if the atomic volumes of two atoms are overlapping with each other through interatomic surfaces then there exists a bond between them; *i.e.*, on the basis of the topology of the electron density, a bond path is considered as the line along which the electron density is the maximum with respect to a neighboring line. In space, a critical point is defined as the point where the gradient of the electron density is zero (*i.e.*, $\nabla\rho = 0$), implying the electron density is the maximum with respect to the surrounding and a (3, -1) point is referred to as the bond critical point (BCP) where two of the eigenvalues of the Hessian matrix are negative. The AIM method also allows one to locate and distinguish different types of interactions existing between the constituent atoms in a molecule.

For this purpose, we have calculated the values of electron density $[\rho]$, Laplacian of the electron density $[\nabla^2\rho]$, and the local energy density for the H–Ng and Ng–X' bonds present in the HNgX'⁺ species using the AIMPAC³⁰⁹ and Multiwfn softwares.³¹⁰ In general, a shared type of interactions resulting in a covalent bond shows $\nabla^2\rho(r_c) < 0$, while a nonshared type of interactions leading to ionic, hydrogen, and vdW bonds shows $\nabla^2\rho(r_c) > 0$ values. One of the most important quantity in the AIM analysis is to compute the local energy density, which is represented as $E_d(r) = G(r) + V(r)$, where $G(r)$ and $V(r)$ correspond to local kinetic and potential energy densities, respectively. The sign of $E_d(r_c)$ predicts whether accumulation of charge at a given point, r , is stabilizing [$E_d(r_c) < 0$] or destabilizing [$E_d(r_c) > 0$]. A negative value of $E_d(r_c)$ means that $V(r_c)$ dominates over $G(r_c)$ and the electron density accumulates in the bond region, resulting in a covalent bond.

Table 3.4. Bond Critical Point Properties [BCP Electron Density (ρ in $e a_0^{-3}$), Its Laplacian ($\nabla^2\rho$ in $e a_0^{-5}$), and the Local Energy Density (E_d in a.u.)] of HNgX'^+ (Ng = He, Ne, Ar, Kr, and Xe; $X' = \text{BF}, \text{CS}, \text{OH}_2,$ and OSi) Species Calculated Using the B3LYP Method.

Ng	BCP	HNgBF^+		HNgCS^+		HNgOH_2^+		HNgOSi^+	
		H–Ng	Ng–B	H–Ng	Ng–C	H–Ng	Ng–O	H–Ng	Ng–O
He	$\rho(\mathbf{r}_c)$	0.210	0.035	0.227	0.047	0.238	0.049	0.246	0.067
	$\nabla^2\rho(\mathbf{r}_c)$	1.562	0.062	–1.821	0.111	–2.257	0.219	–2.127	2.910
	$E_d(\mathbf{r}_c)$	–0.419	–0.001	–0.478	–0.003	–0.576	0.004	–0.552	0.000
Ne	$\rho(\mathbf{r}_c)$... ^a	... ^a	0.209	0.021	... ^a	... ^a	0.218	0.026
	$\nabla^2\rho(\mathbf{r}_c)$... ^a	... ^a	–1.698	0.080	... ^a	... ^a	–2.009	0.174
	$E_d(\mathbf{r}_c)$... ^a	... ^a	–0.467	0.002	... ^a	... ^a	–0.547	0.009
Ar	$\rho(\mathbf{r}_c)$	0.212	0.028	0.220	0.028	0.229	0.028	0.232	0.037
	$\nabla^2\rho(\mathbf{r}_c)$	–0.657	0.045	–0.711	0.078	–0.834	0.115	–0.903	0.158
	$E_d(\mathbf{r}_c)$	–0.207	0.0001	–0.220	0.001	–0.249	0.004	–0.269	0.002
Kr	$\rho(\mathbf{r}_c)$	0.242	0.024	0.194	0.029	0.247	0.028	0.200	0.041
	$\nabla^2\rho(\mathbf{r}_c)$	–1.160	0.047	–0.512	0.079	–1.097	0.111	–0.542	0.153
	$E_d(\mathbf{r}_c)$	–0.418	0.0002	–0.165	0.001	–0.414	0.004	–0.177	0.001
Xe	$\rho(\mathbf{r}_c)$	0.150	0.022	0.152	0.027	... ^b	0.026	0.162	0.040
	$\nabla^2\rho(\mathbf{r}_c)$	–0.382	0.040	–0.333	0.064	... ^b	0.088	–0.299	0.131
	$E_d(\mathbf{r}_c)$	–0.141	–0.001	–0.123	–0.001	... ^b	0.002	–0.124	–0.001

^aIt has not been possible to optimize the concerned structures. ^bDue to numerical problem, it has not been possible to obtain the BCP values for the H–Xe bond in HXeOH_2^+ .

The B3LYP computed bond critical point (BCP) parameters have been reported in Table 3.4 for H–Ng and Ng– X' bonds in all the predicted HNgX'^+ ($X' = \text{BF}, \text{CS}, \text{OH}_2,$ and OSi) complexes. All the predicted HNgX'^+ ions show high negative $\nabla^2\rho(\mathbf{r}_c)$ values at the BCPs corresponding to the H–Ng bonds, which imply that covalent character is more for these bonds. The covalent nature of the H–Ng bonds is further confirmed with the

observation of high BCP electron density values for the H–Ng bonds. In comparison to H–Ng bonds, low positive values for $\nabla^2\rho(r_c)$ as well as low $\rho(r_c)$ values are obtained for the Ng–X' bonds which clearly indicate that an ionic or van der Waals kind of weak interaction exists in between the Ng and X' in HNgX'^+ ions. The negative magnitude of the computed local energy density, $E_d(r_c)$ values for HNgX'^+ ions, emphasizes that H–Ng bonds are stable with respect to the accumulation of electron density at the bond region, leading to covalent bonding between the H and Ng atoms. The very low negative or small positive $E_d(r_c)$ values corresponding to Ng–X' bonds leads to non-covalent ionic nature in all the predicted ions. These AIM data clearly indicates that all these ions may be represented as $[\text{HNg}^+][\text{X}']$.

For both FNgBS and FNgBO molecules, a negative value of $\nabla^2\rho(r_c)$ and also a negative value of $E_d(r_c)$ for the Ng–B bond evidently indicate that this bond is associated with high covalent character; however, a positive value of $\nabla^2\rho(r_c)$ along with a negative value of $E_d(r_c)$ for the F–Ng bond implies that the nature of the bond is mainly ionic with small covalent contribution. Moreover, $\nabla^2\rho(r_c)$ is found to be negative for the B–S bond in FNgBS, while $\nabla^2\rho(r_c) > 0$ for the B–O bond in FNgBO, which indicates toward more covalent nature of the B–S bond than the B–O bond.

Apart from the calculated AIM parameters at BCP, we have also plotted the electron density (ρ) and Laplacian of the electron density ($\nabla^2\rho$) at various regions within the molecular plane in Figures 3.4 and 3.5, respectively, for FNgBO and FNgBS molecules. The electron density contour plots of the FNgBS molecules are found to be almost identical to that of the FNgBO molecules, except in the BS and BO regions. In the case of FNgBO molecules the BCP is located very close to the boron atom for the B–O bonds; however, the same is slightly away from the boron atom for the B–S bonds in FNgBS molecules.

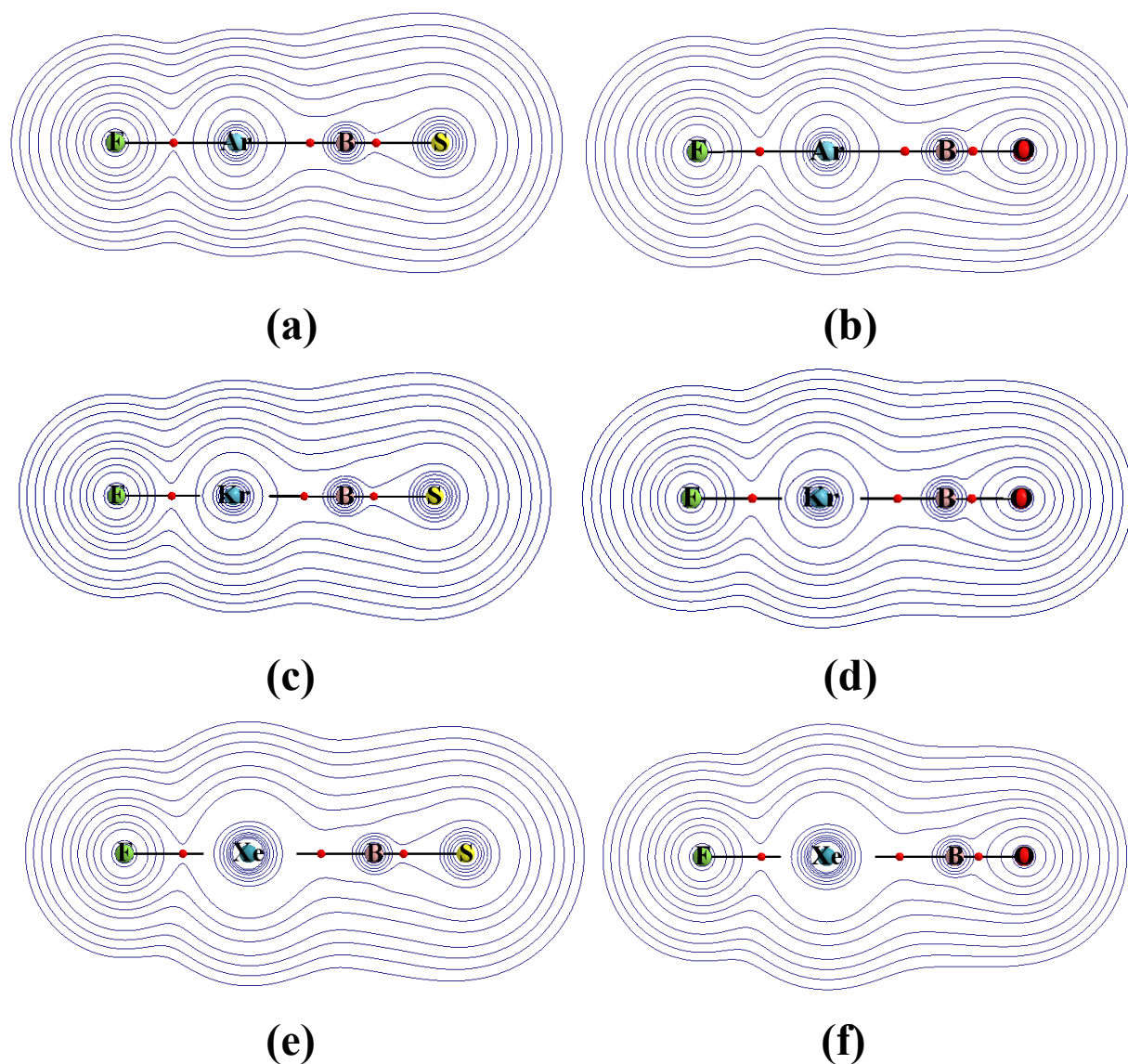


Figure 3.4. Electron density (ρ) contour plots of (a) FArBS, (b) FArBO, (c) FKrBS, (d) FKrBO, (e) FXeBS and (f) FXeBO species at the respective molecular plane calculated at the B3LYP level.

The contour lines corresponding to the $(\nabla^2\rho)$ distribution show more or less a uniform charge accumulation around the noble gas–boron–sulfur region in the FNgBS molecules; however, it is somewhat nonuniform in the case of FNgBO systems. Nevertheless, charge concentration in the Ng–B bonding region indicates that the Ng–B bond is rather covalent in nature. An in-depth analysis of Figure 3.5 reveals that the Ng–B bond becomes more

covalent in going from Ar to Xe molecule in both FNgBS and FNgBO systems. From Figure 3.5 it is also clear that the charge density is depleted around the bonding region of F–Ng bond in both FNgBS and FNgBO molecules, indicating that the F–Ng interaction is predominantly ionic in nature. Therefore, the ionic nature of F–Ng bond and the covalent character of Ng–B bond strongly suggest that these species can be represented as $F^-(NgBS)^+$.

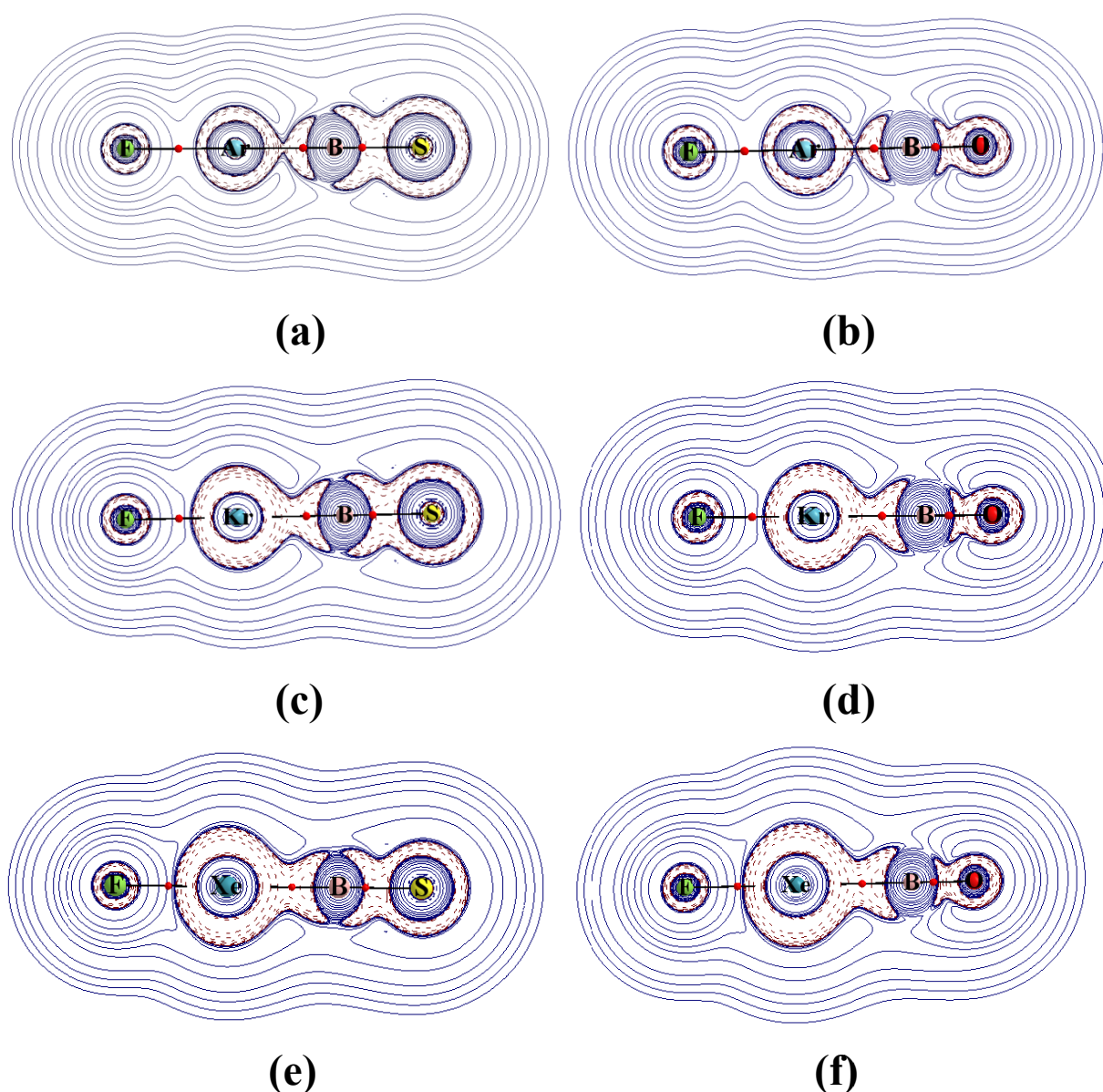


Figure 3.5. Contour plots of Laplacian of electron density ($\nabla^2\rho$) of (a) FArBS, (b) FArBO, (c) FKrBS, (d) FKrBO, (e) FXeBS and (f) FXeBO species at the respective molecular plane

calculated at the B3LYP level. The dotted lines are the regions of charge concentration and solid lines are the regions of charge depletion.

Of late, Boggs and coworkers³¹³ have performed an exhaustive study of the nature of bonding involving noble gas compounds by considering $G(r)/\rho(r)$ at the BCP as an important parameter to assess the extent of covalency in a chemical bond. Different types of covalent bonding have been assigned with respect to the following criteria at the BCP:

“type A”: $\nabla^2\rho(r_c) < 0$, $\rho(r_c) \geq 0.1$, and $E_d(r_c) < 0$

“type B”: $\rho(r_c) \geq 0.1$, and $E_d(r_c) < 0$

“type C”: $E_d(r_c) < 0$, and $G(r_c)/\rho(r_c) < 1$

“type D”: $|E_d(r_c)| < 0.005$, and $G(r_c)/\rho(r_c) < 1$

The calculated AIM results, clearly indicate that the Ng–B bond is strongly covalent in nature, which satisfies all of the requirements of “type A” covalent bond. The F–Ng bond associated with $\nabla^2\rho(r_c) > 0$, $\rho(r_c) \leq 0.1$, $E_d(r_c) < 0$, and $G(r_c)/\rho(r_c) \approx 1$ at the BCP is indicative of weak bonding interaction between the F and Ng atoms with small covalent characteristics and referred to as a “W^c type” bond.³¹³ It should be mentioned here that the B–S bonds (“type A”) in FNgBS molecules are more covalent in nature as compared to the B–O bonds (“type B”) in FNgBO. The bonding trends obtained from the AIM analysis agree very well with the calculated charge distributions.

3.4. Conclusions

In summary, we have predicted unique series of novel noble gas containing cationic species, *viz.*, HNgBF⁺, HNgCS⁺, HNgOH₂⁺, HNgOSi⁺, and neutral species, *viz.*, FNgBS, FNgCX, using various *ab initio* quantum chemical methods, *viz.*, DFT, MP2, and CCSD(T). It has been found that the predicted ions are metastable in nature, *i.e.*, they are thermodynamically

stable with respect to all possible 2-body and 3-body dissociation channels except the one which leads to the global minima products. Nevertheless, finite barrier heights for the transition states connecting the insertion complexes with the global minimum products for each of the species indicate that all these species are kinetically stable with respect to the global minimum products on their respective singlet potential energy surfaces. The IRC analysis further confirms that the predicted ions are metastable in nature and are connected to the global minima through the H–Ng–X' bending modes. The calculated bond length values, vibrational frequency results, charge distributions data, and the AIM properties clearly indicate that the H–Ng bonds in all these species are associated with considerable amount of covalency, whereas the Ng–X' bonds exhibit substantial ionic character. The calculated bond length, charge distribution, and AIM results further imply that these hydride ions can be better represented as $[\text{HNg}]^+[\text{X}']$ while the neutral FNgBS and FNgCX molecules can be represented as $\text{F}^-(\text{NgBS})^+$ and $\text{F}^-(\text{NgCX})^+$, respectively. Experimental identification of other cationic and neutral noble gas insertion compounds had been made possible through matrix isolation technique at cryogenic temperature. Therefore, all the above mentioned results clearly point towards the possibility of preparation of all these noble gas inserted compounds at cryogenic temperature and can be characterized by spectroscopic techniques.

Chapter 4. Neutral and Ionic Noble Gas Compound in the Triplet State

4.1. Introduction

In general, the insertion-type noble gas compounds have a common formula, XNgY, in which X is hydrogen or halogen or pseudo-halogen, Ng is a noble gas atom, and Y is an electronegative atom or group. These XNgY molecules are truly chemically bound species and exist as closed-shell species in a singlet electronic state. However, molecules associated with open-shell electronic configurations exhibit various interesting properties³¹⁴ for several reasons, especially for their conspicuous spectroscopic and magnetic behaviors. The very first open-shell molecular species involving an even number of valence electrons (triplet molecular state) was pointed out by Lewis and Kasha in 1944 during assignment of the lowest excited metastable state of organic molecules.³¹⁵ The first open shell noble gas insertion compound with a doublet ground electronic state, HXeO ($^2\Sigma$), was prepared in 2003 by Khriachtchev *et al.* through the UV photolysis of H₂O/Xe or N₂O/HBr/Xe solid mixtures at 7 K followed by thermal mobilization of oxygen atoms at 30 K.¹⁵² Subsequent experimental identification of another open-shell noble gas-inserted compound (HXeCC) in the doublet state was carried out by the same group.^{176a,180b} Of late, Grandinetti and co-workers successfully generated singlet F₂N–Xe⁺ ions in the gas phase by the nucleophilic displacement of HF from the protonated NF₃ by Xe, which was subsequently detected through a mass spectroscopic technique.¹⁶² They theoretically investigated and found that the singlet F₂N–Xe⁺ ion was more stable (167–251 kJ mol⁻¹) than the FN–XeF⁺ ion, while the triplet state of the latter was more stable compared to that of the corresponding singlet state by 84 kJ mol⁻¹ using CCSD(T)/def2–TZVPP level of theory. The exclusive spectroscopic

and magnetic properties³¹⁶ of these triplet state molecular species make them remarkably distinctive and worthy of investigation.

It is worthwhile to mention that the existence of NNg^+ species had been reported earlier.³¹⁷ Consequently, it is quite natural to expect that the NNg^+ ions could be stabilized in the presence of an anion such as F^- , analogous to the stabilization of ArH^+ in the presence of F^- .^{141,148} Notably, both NF and PF species are valence isoelectronic with the O_2 molecule with triplet ground state and have been investigated experimentally as well as theoretically.³¹⁸ For the first time, in a bid to predict neutral noble gas chemical compounds in their triplet electronic state, we have carried out a systematic investigation of xenon inserted FN and FP species, FNgY ($\text{Ng} = \text{Xe}$ and Kr ; $\text{Y} = \text{P}$ and N), by using quantum chemical calculations.

Of late, Grandinetti *et al.*¹⁶⁴ and Chattaraj *et al.*³¹² have studied noble gas insertion complexes with the heavier elements of the carbon group, *i.e.*, noble gas inserted Ge , Sn and Pb fluorides. In the spirit of the aforementioned work along with our own reported FNgY molecules, we have been further motivated to investigate the interaction between the noble gas and the heavier pnictides, such as arsenic, antimony and bismuth. Very recently, several solid inorganic complexes containing fluoroxenon, fluorokrypton, oxofluoroxenon, *etc.* cations have been synthesized and characterised experimentally³¹⁹ by X-ray crystallography with AsF_6^- and/or SbF_6^- as counter anions. However, to the best of our knowledge, no typical interaction has been established between the noble gas and arsenic or antimony atoms. At the same time, neutral compounds associated with Ng-As , Ng-Sb , and Ng-Bi bonding are still unexplored to the best of our knowledge. Therefore, we again propose a new series of neutral noble gas insertion compounds, FNgY ($\text{Ng} = \text{Kr}$ and Xe ; $\text{Y} = \text{As}$, Sb and Bi) with triplet ground electronic states.

The omnipresence of numerous exotic molecules in the interstellar medium and the corresponding chemical networks responsible for their production are expected to answer

some puzzling astrophysical and astronomical questions,³²⁰ *e.g.*, questions regarding the formation of stars and the origin of life.³²¹ One such molecule of extraterrestrial origin is the ketenyl radical (HCCO), which in recent years has aroused sufficient interest among researchers for them to carry out numerous kinetic,³²² spectroscopic,³²³ and theoretical^{320b,324} investigations. The HCCO radical is not only an enticing interstellar molecule, it also plays an imperative role in the combustion cycle³²⁵ of hydrocarbons, especially in the oxidation of acetylene.^{322a,326} Regarding the efficient formation mechanism of HCCO radicals, recent studies have shown that HCCO can be formed as an intermediate upon irradiation with energetic electrons and ultraviolet photons on various types of ices in dark clouds following cosmic ray impacts.³²⁷ The structure also arouses further interest and can be well described to be planar with a linear CCO backbone and a H-atom lying outside the linear axis.³²⁸ The ketenyl species not only exists as a radical, but also as a cation as well as an anion and surprisingly all the forms are equally important and are attracting immense interest as far as the interstellar medium is concerned.^{328,329} The ketenyl cationic species (HCCO⁺), which is produced from the more abundant formaldehyde molecule, plays a vital role in the extension of carbon chains³²¹ in the interstellar medium. It is noteworthy to mention that this ketenyl cation (HCCO⁺) can be generated by the selective dissociative ionization of HCCOCH₃ molecules detected through mass spectroscopic analysis, as described by Holmes.³³⁰

Although a number of noble gas hydrides in the singlet and doublet electronic states are reported in the literature, to the best of our knowledge, there is no report on noble gas hydrides with a triplet ground state. Therefore, apart from the prediction of the triplet ground electronic state neutral noble gas insertion compound, we have also investigated systematically the insertion of a noble gas atom (Ng = He, Ne, Ar, Kr, and Xe) between H and C atoms in the ketenyl cation (HCCO⁺) resulting in HN_gCCO⁺ ions through various *ab initio* quantum chemistry-based methods.

4.2. Computational Details

Details of the computational methodologies are discussed in Chapter 3 (Section 3.2) of this thesis. In addition, we have used def2-TZVPPD basis set designed by Weigend and Ahlrichs³³¹ which is represented as DEF2. Moreover, the multireference-configuration interaction (MRCI) method³³² has been used to optimize the geometries by employing MOLPRO 2012 program. For each of the systems the reference space has been generated through CASSCF calculations using a full-valence active space.

4.3. Results and Discussions

4.3.1. Optimized Structural Parameters

Interestingly, all the calculations suggest that the noble gas (Ng = Kr and Xe) inserted FY (Y = N, P, As, Sb and Bi) molecules (FNgY) show true minima on their triplet potential energy surfaces and exhibit linear structures, having $C_{\infty v}$ symmetry at the minima position and nonlinear bent planar geometry with C_s symmetry at the transition state. We have confined our discussions to the most stable triplet FNgY compounds, unless otherwise specified. Due to the close proximities of experimental results we discuss only the CCSD(T) computed results throughout the text unless otherwise mentioned.

The F–Ng bond lengths are found to be 2.018–2.177 Å in FKrY and 2.091–2.217 Å in FXeY species along the N–P–As–Sb–Bi series. On the other hand, the Ng–Y bond length values are 2.088–2.882 Å in FKrY and 2.146–2.994 Å in FXeY molecules from N to Bi. The above results reveal that the bond length order maintains periodicity along the group, *i.e.*, with increasing atomic number, the bond length also increases down the pnictogen group (N–P–As–Sb–Bi). In this context, it is very important to mention that the CCSD(T) computed F–Ng bond lengths in the HNgF molecule are 2.138 and 2.150 Å, respectively, for Kr and Xe.^{141,148} It is evident that the F–Ng bond lengths in FKrN, FKrP and FKrAs are found to be

shorter than the corresponding in FKrH molecule whereas FXeN and FXeP have shorter F–Ng bond length than that in the FXeH. Therefore, a shorter F–Ng bond indicates that a stronger interaction exists between the fluorine and the noble gas atom in these neutral FNgY species relative to that in the HNgF species. Note that the MP2-calculated Xe–N bond length values in F_2NXe^+ and $[F-Xe-N-F]^+$ ions¹⁶² are 2.467 and 2.546 Å, respectively, which are considerably larger than the corresponding MP2 value (2.146 Å) in FXeN reported here. However, the F–Xe bond is shorter in the $[F-Xe-N-F]^+$ ion¹⁶² than that in FXeN.

Table 4.1. CCSD(T) Computed F–Ng and Ng–Y Bond Length (in Å) Comparisons in ³FNgY (Ng = Kr and Xe; Y = N, P, As, Sb and Bi) with respect to the Corresponding Covalent (R_{cov})^a and van der Waals Limit (R_{vdw})^b and Bare ⁴NgY, ²NgY, ³NgY⁺ and ¹NgY⁺ species.

Bonds	FKrN	FKrP	FKrAs	FKrSb	FKrBi	FXeN	FXeP	FXeAs	FXeSb	FXeBi
F–Ng	2.018	2.088	2.119	2.152	2.177	2.088	2.149	2.165	2.190	2.217
$R_{cov}(F-Ng)$	1.73	1.73	1.73	1.73	1.73	1.97	1.97	1.97	1.97	1.97
$R_{vdw}(F-Ng)$	3.49	3.49	3.49	3.49	3.49	3.63	3.63	3.63	3.63	3.63
Ng–Y	2.088	2.443	2.597	2.788	2.882	2.146	2.577	2.698	2.903	2.994
$R_{cov}(Ng-Y)$	1.88	2.28	2.35	2.55	2.64	2.02	2.48	2.59	2.79	2.88
$R_{vdw}(Ng-Y)$	3.73	3.97	3.90	4.49	4.56	3.94	4.18	4.04	4.63	4.70
⁴[Ng–Y]	3.583	4.059	4.319	4.538	4.538	3.795	4.216	4.446	4.664	4.715
²[Ng–Y]	2.137	2.917	3.678	4.036	4.036	2.137	2.761	3.000	3.436	3.611
³[Ng–Y]⁺	1.929	2.416	2.588	2.860	2.860	2.087	2.563	2.714	2.975	3.083
¹[Ng–Y]⁺	1.881	2.409	2.588	2.867	2.867	2.013	2.544	2.705	2.976	3.090

^aReference 43; ^bReference 44-46

Next, it is very interesting to compare the bond length values of Ng–Y in these molecules with the analogous values in the bare ⁴NgY, ²NgY, ³NgY⁺ and ¹NgY⁺ species. All the calculated Ng–Y bond length values as shown in the Table 4.1 clearly suggest that the ³FNgN compounds can best be described as a hybrid of $[F + ^2[NgN]]$ and $[F^- + ^3[NgN]^+]$

species. On the other hand, the rest of $^3\text{FNgY}$ ($Y = \text{P, As, Sb and Bi}$) compounds can be considered to exist mostly as $[\text{F}^- + ^3[\text{NgY}]^+]$. Nevertheless, this kind of structural assignment based on only the bond lengths is rather speculative and more analysis has been provided in the subsequent sections dealing with the energetics and potential energy diagrams.

In analogous to the FNgY species, $C_{\infty v}$ and C_s symmetry point groups are also assigned corresponding to the linear and bent planar structures of the minima and transition state geometry of triplet HNgCCO^+ ions, respectively, on the triplet potential energy surface. In this context, it is very interesting to compare the strength of H–Ng and Ng–C bonds in HNgCO^{+157} and HNgCS^+ ions in their respective singlet electronic state configurations with the corresponding bonds in the predicted triplet HNgCCO^+ ions. This collation is also beneficial for getting an impression of the nature of bonding between the relevant bonds in HNgCCO^+ . The CCSD(T) computed H–Ng bond length values have been found to be 0.803–1.632 Å in HNgCCO^+ , 0.764–1.610 Å in HNgCO^+ and 0.766–1.620 Å in HNgCS^+ along the He–Ne–Ar–Kr–Xe series. The CCSD(T) computed H–Ng bond length values in bare HNg^+ ions have been found to be 0.776–1.607 Å on going from HHe^+ to HXe^+ . All these values indicated that the H–Ng bond length in all these ions is proximate enough to concur that the bond strength as well as the type of bonding were similar. On the other hand, the CCSD(T) calculated Ng–C bond length values are in the range of 1.945–2.809 Å in HNgCCO^+ , 2.221–3.124 Å in HNgCO^+ and 2.036–2.872 Å in HNgCS^+ along the He–Ne–Ar–Kr–Xe series. The Ng–C bond length in the HNgCCO^+ is the smallest among all the species compared here, indicating a comparatively stronger Ng–C bond in the HNgCCO^+ species. The CCSD(T) optimized Ng–C bond lengths in NgCCO^+ have been found to be 2.390, 2.501, 2.141, 2.130, and 2.201 Å along the same Ng series, which are quite a bit shorter as compared to the respective bond distances in HNgCCO^+ , except in HHeCCO^+ and HNeCCO^+ . From the above comparison, it is safe to infer that there exists a strong bonding interaction between H

and Ng atoms and a weak interaction between Ng and C atoms, which may be due to the positive charge transfer from the CCO fragment to the HNg moiety in the HNgCCO⁺ ions.

Following the works of Gerry and co-workers,¹⁵³ we have analyzed the noble gas atoms containing chemical bonds in terms of the covalent and van der Waals radii limits, denoted as R_{cov} and R_{vdW} , respectively, as defined in the Chapter 3 under ‘Section 3.3.1.’. The computed covalent limits of the F–Ng bond lengths are 1.73 and 1.97 Å,⁴³ and the corresponding van der Waals limits are 3.49 and 3.63 Å for Ng = Kr and Xe, respectively.⁴⁴ ⁴⁶ At the same time, the calculated $R(\text{Ng–Y})$ covalent limits are 1.87, 2.23, 2.35, 2.55, 2.64, 2.11, 2.47, 2.59, 2.79 and 2.88 Å for Kr–N, Kr–P, Kr–As, Kr–Sb, Kr–Bi, Xe–N, Xe–P, Xe–As, Xe–Sb, and Xe–Bi, respectively,⁴³ and the corresponding vdW limits are 3.57, 3.82, 3.90, 4.49, 4.56, 3.71, 3.96, 4.04, 4.63 and 4.70 Å.⁴⁴⁻⁴⁶ From these limiting values and the calculated bond length parameters of FNgY species, it is clearly revealed that both the F–Ng and Ng–Y bond length values are very close to the corresponding covalent limits.

On going from He to Xe, the standard covalent limits⁴³ for the H–Ng bonds are obtained to be 0.59, 0.89, 1.37, 1.47, and 1.71 Å and the corresponding van der Waals limits⁴⁴⁻⁴⁶ are 2.60, 2.74, 3.08, 3.22, and 3.36 Å, respectively. Similarly, the covalent limits⁴³ for the Ng–C bonds along the He–Ne–Ar–Kr–Xe series have been found to be 1.04, 1.34, 1.82, 1.92, and 2.16 Å and the corresponding van der Waals limits⁴⁴⁻⁴⁶ were 3.10, 3.24, 3.58, 3.72, and 3.86 Å, respectively. By comparing these data against the bond length results in HNgCCO⁺, it is observed that the H–Ng bond distances are in very close proximity to the covalent limit, indicating a strong interaction between the H and Ng atom, whereas the Ng–C bond distance in the HNgCCO⁺ ion is in between the covalent and van der Waals limit, implying that the interaction between Ng and C atoms is relatively weak. Therefore, from the detailed analysis of bond lengths, it can be concluded that the metastable HNgCCO⁺ species should exist formally as an [HNg]⁺[CCO] complex.

For all the predicted FNgY molecules, the geometry transforms from a linear to a non-linear bent structure while going from the minima state to the saddle point. Here, it is interesting to note that the F–Ng bonds are elongated by ~ 0.20 Å whereas the Ng–Y bond contracts by ~ 0.11 to 0.18 Å in the transition state structure of all the FNgY species. Nevertheless, the F–Ng–Y angle also changes from 180° to ~ 90 – 110° in the transition states of the FNgY. This trend of the increase in the F–Ng–Y bond angle from FNgN to FNgBi can be attributed to the increase in size of the pnictides while going from N to Bi.

The conversion of the metastable HNgCCO⁺ species to the global minima products (Ng + HCCO⁺) leading to a transition state geometry involves bending of the H–Ng–C angle from 180° to $\sim 100^\circ$, except for HNeCCO⁺. This conversion is accompanied with the shortening of the H–Ng bond and the elongation of Ng–C bond, again with the exception of HNeCCO⁺, where the Ng–C bond length is mitigated mildly. The remaining bond angles and the bond lengths in the transition state deviate slightly from the same in the minima state.

4.3.2. Analysis of Harmonic Vibrational Frequencies

In order to characterize a molecule experimentally, it is essential to calculate the vibrational frequencies of the predicted molecules for spectroscopic measurements. Therefore, we have performed harmonic vibrational analysis in order to distinguish the different vibrational modes with their corresponding IR frequencies for all the minima geometry, as well as the transition state structure of all the predicted FNgY molecules as well as HNgCCO⁺ ions, employing B3LYP, MP2, and CCSD(T) levels of theory.

The MP2 computed F–Ng stretch frequency values are found to be 515.1 – 355.4 cm⁻¹ in FKrY and 481.0 – 474.2 cm⁻¹ in FXeY along the N–P–As–Sb–Bi series while the corresponding Ng–Y stretch values are 400.6 – 156.9 cm⁻¹ and 437.6 – 138.4 cm⁻¹. Similarly, the calculated F–Ng–Y bend vibrations are found to be 205.3 – 94.7 in FKrY and 180.3 – 92.1

cm^{-1} in FXeY on going from N to Bi. From the abovementioned IR frequency data, it is clear that the F–Ng stretch is associated with the highest frequency value in comparison with all the normal modes found in the FNgY species. This result reveals that a strong interaction exists between the F and Ng atom, which is in good agreement with the optimized structural parameters. Furthermore, the saddle point nature of the TS structure has been confirmed by the presence of only one negative frequency value corresponding to the F–Ng–Y bending mode.

In case of triplet HNgCCO^+ ions, the MP2 computed H–Ng stretching modes possess the maximum values of vibrational frequencies in all the ions considered and are in the range of $3438\text{--}2300\text{ cm}^{-1}$ on going from He to Xe. Similarly, the vibrational frequencies of Ng–C stretching modes in all the predicted compounds are in the range of $179\text{--}137\text{ cm}^{-1}$ along the Ne–Ar–Kr–Xe series, except for He–C stretching mode, whose frequencies are 414.9 cm^{-1} . There is a gradual decrease in the harmonic frequency values of H–Ng and Ng–C stretching modes on going from HHeCCO^+ to HXeCCO^+ , which implies that the lower limit in the given ranges is the vibrational frequency of H–Xe and Xe–C stretching modes. The harmonic vibrational frequency analysis of the transition state reflects that there is an increase in vibrational frequency of H–Ng stretching mode and a decrease in the vibrational frequency of the Ng–C stretching mode, which is consistent with the analysis of the structural parameters and the energetics of HNgCCO^+ ions. The doubly-degenerate H–Ng–C bending mode in the minima state has frequency values of $481.8\text{--}406.9\text{ cm}^{-1}$ on going from HHeCCO^+ to HXeCCO^+ . This bending mode is found to possess negative frequency in the transition state, which suggests that the global minima products are obtained from the dissociation involving this mode only, which is further confirmed by the IRC calculations.

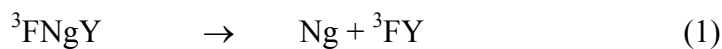
Due to the metastable nature of the predicted FNgY and HNgCCO^+ compounds, it is highly essential to determine the various couplings present among the different vibrational

modes. Therefore, the Boatz and Gordon³⁰⁸ methodology has been adopted in order to partition the normal coordinate frequencies into individual internal coordinates. Individual coordinate analysis shows that there is almost no coupling among the different vibrational modes in both the triplet state of neutral FNgY molecules and cationic HNgCCO⁺ species. The computed force constant (k) values for the F–Ng bonds are slightly higher than those of the corresponding Ng–Y bonds, indicating a slightly stronger interaction between F and Ng atoms than that between Ng and Y atoms in FNgY molecules. In case of HNgCCO⁺ ions, the previous analysis of bond parameters and energetics indicate that there exists a strong and rigid bond between H and Ng atoms and a relatively weak interaction in between Ng and C atoms. This assertion further concurs with the force constant values for these bonds. The MP2 computed force constants values for H–Ng bonds in the HNgCCO⁺ ions are 559.4–311.8 N m⁻¹ and for the Ng–C bond the values are 43.3–34.2 N m⁻¹ along the series He–Ne–Ar–Kr–Xe. The relatively high force constant for H–Ng bonds in comparison to Ng–C bonds itself articulates its strength.

4.3.3. Energetics and Stability

To analyze the stability of the predicted metastable FNgY triplet species, the energetics have been computed for all possible unimolecular dissociation channels. In this regard, we have considered six 2-body unimolecular dissociation (channels (1) to (6)) and two 3-body unimolecular dissociation (channels (7) and (8)) pathways for the FNgY molecules to determine the thermodynamic and kinetic stability of the FNgY species at the triplet state. Among all these six 2-body dissociation channels, the first one gives rise to the global minimum products and the remaining channels lead to the local minimum products on their respective potential energy surfaces. Due to the close proximity with the B3LYP and MP2

results, the CCSD(T) computed values are considered while discussing the results, unless otherwise mentioned.



Similar to many other noble gas inserted compounds, the predicted species is thermodynamically unstable with respect to the global minima products. In contrast, the FNgY species in its triplet state is thermodynamically stable relative to the other two-body dissociation channels. For the remaining 2-body dissociation pathways, the ranges of dissociation energies corresponding to channels (2)–(6) are 127 to 298, –59.2 to 68, 127 to 358, 464 to 723, and 555 to 900 kJ mol⁻¹, respectively. Very high positive energy values have been found for another 3-body dissociation channel (7), where the calculated values are 204.2–128.4 in FKrY and 310.7–201.0 kJ mol⁻¹ in FXeY molecules (Y = N to Bi). At the same time, the endothermic nature of the 3-body dissociation channel (8) exemplifies that the predicted FNgY molecules are more stable than the dissociated products (F + Ng + ⁴Y) by ~ 50–78 kJ mol⁻¹ for FXeY (Y = N to Bi). In contrast, except FKrBi, all FKrY species are unstable with respect to the same three-body dissociation. However, there may be an energy barrier when the FKrY species moves from the bound triplet state to the dissociative quintet states (channels (3) and (8)). A similar situation has been found by Khriachtchev *et al.* in the case of the HXeO radical,¹⁵² which has been observed experimentally. This radical was found to be stable with respect to (H + Xe + ¹O). However, theoretically the same radical has been

found¹⁵² to be unstable by approximately 97 kJ mol⁻¹ with respect to the dissociation into (H + Xe + ³O), although the existence of this radical was observed experimentally. Consequently, it was conjectured that the HXeO radical was formed from the reaction of (H + Xe + ¹O). Although the FKrY molecules are found to be thermodynamically unstable with respect to two dissociation channels, (3) and (8); however, the corresponding DFT results predict the FKrY molecules to be stable with respect to these dissociation channels.

Nevertheless, from the geometrical parameters it is evident that the FNgN compounds exist as a hybrid of [F + ²[NgN]] and [F⁻ + ³[NgN]⁺] species while the remaining FNgY compounds can be described mostly as [F⁻ + ³[NgY]⁺]. Although this kind of structural parameter based description is approximate, it is clear that channels (4) and (5) are more important as far as the stability of the FNgY compounds is concerned. High dissociation energy values corresponding to channels (4) and (5) indicate that the FNgY compounds are bound with respect to the dissociation into two doublet fragments (channel (4)) and the ionic dissociation (channel (5)). It is further confirmed from the calculated atoms-in-molecules (AIM) properties (discussed later).

The kinetic stability of the predicted species has been ascertained through calculating the barrier heights for the transition states connecting the metastable FNgY complexes with the global minimum products for each of the species. Intrinsic reaction coordinate (IRC) calculations have also been carried out to confirm that the transition state connects the metastable complex with the corresponding global minimum products. The CCSD(T) computed barrier heights for the transition state are found to be 166.3–59.8 for FKrY and 163.0–86.7 kJ mol⁻¹ for FXeY on going from N to Bi, which indicates that all these species are kinetically stable as far as channel (1) is concerned. The zero-point energy correction values calculated using the MP2 method are found to be ~ 1.5 to 2.2 kJ mol⁻¹ for all the

FNgY molecules. These higher positive barrier heights strongly indicate that it may be possible to prepare the metastable FNgY molecules experimentally.

Similarly, to ascertain the stability of the triplet HNgCCO⁺ species, Six unimolecular dissociation pathways (four 2-body and two 3-body dissociation channels, equation (1)–(6)) are discussed to derive the kinetic and thermodynamic stability of these species and the CCSD(T) computed energies of each dissociated species are listed in Table 4.2.

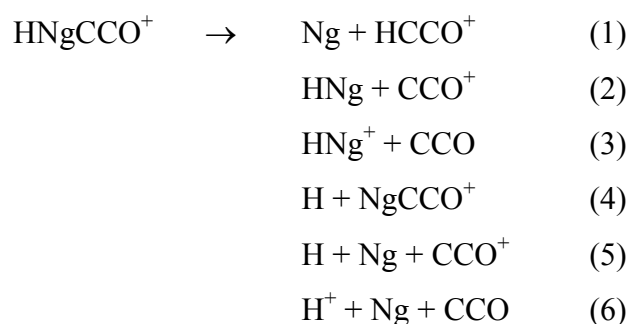


Table 4.2. Energies (in kJ mol⁻¹) of the Various Dissociated Species Relative to the ³HNgCCO⁺ (Ng = He, Ne, Ar, Kr, and Xe) Ions, Calculated at CCSD(T)/AVTZ Level.

Species	³ HHeCCO ⁺	³ HNeCCO ⁺	³ HArCCO ⁺	³ HKrCCO ⁺	³ HXeCCO ⁺
³ HNgCCO ⁺	0.0	0.0	0.0	0.0	0.0
Ng + ³ HCCO ⁺	-492.2	-504.0	-320.8	-261.3	-190.9
² HNg + ² CCO ⁺	34.8	22.8	205.7	265.2	335.5
HNg ⁺ + ³ CCO	101.5	62.4	72.6	80.2	83.3
H + ² NgCCO ⁺	30.2	35.8	155.5	165.9	166.3
H + Ng + ² CCO ⁺	34.8	23.0	206.1	265.6	336.1
H ⁺ + Ng + ³ CCO	298.0	286.1	469.3	528.8	599.3
Barrier Height^a	10.3	0.2	18.9	30.5	38.5

^aBarrier height corresponds to transition state (TS) [HNgX⁺ → HX⁺ + Ng]

Like many other noble gas-inserted metastable cationic species, HNgCCO⁺ is also a thermodynamically unstable species with respect to the global minima products, which correspond to channel (1). The CCSD(T) computed energies of the dissociated products

corresponding to channel (1) relative to HNgCCO^+ are -492.2 to -190.9 kJ mol^{-1} from He to Xe series. The negative sign indicates that the energy of the dissociated products is lower than that of HNgCCO^+ , which implies that the reaction path is exothermic and hence the current species of interest are metastable. Apart from channel (1), the rest of the pathways represent the local minima on their respective potential energy surfaces, leading to the predicted HNgCCO^+ species being thermodynamically stable. Now, it would be intriguing to compare the energetic of dissociation pathway (3) with that of the other referred systems, namely HNgCO^+ and HNgCS^+ , with respect to the dissociation into HNg^+ and residual fragments. Accordingly, the dissociation energies for pathway (3) are 72.6 – 83.3 kJ mol^{-1} for HNgCCO^+ , 28.8 – 29.1 kJ mol^{-1} for HNgCO^+ and 72.5 – 77.9 kJ mol^{-1} for HNgCS^+ species along Ar–Kr–Xe series. Just as inferred by the bond length analysis, the comparison of the dissociation energies of channel (3) also affirmed the stronger interaction between Ng and C atoms in HNgCCO^+ than in HNgCO^+ and an almost similar Ng–C bond strength in HNgCCO^+ and HNgCS^+ . The CCSD(T)-computed barrier heights are found to be 10.3, 0.2, 18.9, 30.5, and 38.5 kJ mol^{-1} for HHeCCO^+ , HNeCCO^+ , HArCCO^+ , HKrCCO^+ , and HXeCCO^+ , respectively, which implies that except for HNeCCO^+ all the other predicted compounds are kinetically stable and so they can be prepared experimentally under cryogenic conditions.

Next, it is important to compare the singlet–triplet energy gap (ΔE_{ST}) in order to determine the stability of the predicted neutral FNgY in the ground triplet state. The singlet–triplet energy gaps have been calculated by employing various methods, and the calculated values are reported in Table 4.3. In all cases, the triplet state is found to be more stable than the corresponding singlet state structure, with ΔE_{ST} values varying from 89 to 184 kJ mol^{-1} . For all the predicted FNgY molecules, significantly higher S–T energy gaps would prevent

intersystem crossing (ISC) even at a very low temperature. In case of cationic HNgCCO⁺ species, the singlet–triplet energy gap for the parent ion as well as the HNgCCO⁺ ions is reported in Table 4.4, and from these data it is clear that in all cases the triplet state is more stable than the corresponding singlet state, with sufficiently high ΔE_{ST} values in the range of 87.5–92.3 kJ mol⁻¹ for the HNgCCO⁺ species and 78.3 kJ mol⁻¹ for HCCO⁺ ion computed using CCSD(T) method.

Table 4.3. Energies of the Singlet FNgY Species Relative to the Corresponding Triplet Species (ΔE_{ST} in kJ mol⁻¹) Using B3LYP and MP2 Methods with DEF2 Basis Set and CCSD(T) Method with AVTZ Basis Set.

Methods	ΔE_{ST}									
	FKrN	FKrP	FKrAs	FKrSb	FKrBi	FXeN	FXeP	FXeAs	FXeSb	FXeBi
B3LYP	199.3	120.4	110.4	95.2	90.0	202.7	123.1	112.6	97.6	88.5
MP2	211.8	152.1	134.4	120.9	120.0	202.4	147.2	130.0	117.8	117.8
CCSD(T)	183.6	116.7	112.0	96.8	92.8	168.6	112.8	109.5	95.8	92.6

Table 4.4. Energies (in kJ mol⁻¹) of the Singlet HNgCCO⁺ (Ng = He, Ne, Ar, Kr, and Xe) Species Relative to the Corresponding Triplet Species (ΔE_{ST}), Calculated using B3LYP, MP2 Methods with DEF2 and AVTZ Basis Sets and CCSD(T) Method with AVTZ Basis Set.

Methods	ΔE_{ST}					
	HCCO ⁺	HHeCCO ⁺	HNeCCO ⁺	HArCCO ⁺	HKrCCO ⁺	HXeCCO ⁺
B3LYP/DEF2	93.8	... ^a	... ^a	102.8	102.9	102.9
B3LYP/AVTZ	93.2	... ^a	... ^a	138.8	139.4	139.2
MP2/DEF2	78.2	... ^a	... ^a	92.8	93.1	93.5
MP2/AVTZ	78.6	... ^a	... ^a	91.3	92.0	92.3
CCSD(T)/AVTZ	78.3	92.3	87.5	89.0	90.3	90.9

^aIt is not possible to optimize the singlet state geometry of HNgCCO⁺.

To check the validity of the single reference-based method, the CCSD T1 diagnostic values have been calculated for FNgY and are found to be slightly higher than the recommended value of 0.02,³³³ except FXeSb. Therefore, we have performed multireference-configuration interaction (MRCI) calculations with AVTZ basis sets. Nevertheless, for both the minima and the transition states, we have found that the ground state Hartree–Fock configuration dominates in each of the CASSCF wavefunctions, with coefficient of reference function (C_0) values greater than 0.96 for the FXeY minima and 0.84 to 0.91 for the FKrY minima, whereas this coefficient value reaches to 0.99 for all the transition state structures of the FNgY molecules. In the case of MRCI wave functions, the main contribution also comes from the reference electronic configurations for both the minima and transition state geometries, with C_0 values of about 0.95. In the case of the minima of the FNgY molecules, the coefficient of the Hartree–Fock configuration in the MRCI wavefunction varies from 0.81 to 0.86 for FKrY and 0.90 to 0.93 for FXeY molecules, whereas for the transition state structure, the coefficient is 0.94 for all the Kr and Xe containing molecules. Indeed, the calculated geometrical parameters using the MRCI method were found to agree very well with the CCSD(T) calculated values, for both the minima and the transition-state structures of all the FXeY species.

In case of HNgCCO⁺ ions, the CCSD T1 diagnostic values have been found to be 0.022, which is just above the limiting value of 0.02, except for HHeCCO⁺ (0.026). Due to the large T1 diagnostic value (0.26), we have carried out multi-reference configuration interaction (MRCI) calculations with AVTZ basis set to optimize the geometry of the HHeCCO⁺ ion. For the minima structure of the HHeCCO⁺ ion, the ground state Hartree–Fock configuration dominates the CASSCF wave function with a coefficient of reference function (C_0) greater than 0.96. In the case of the MRCI wave functions, the major contribution also has come from the reference electronic configuration, with a C_0 value of about 0.95. In this

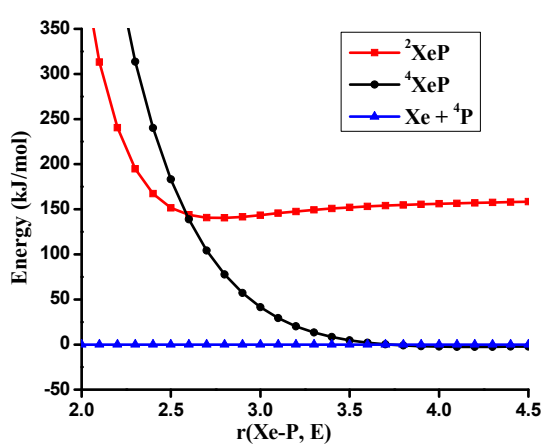
context, it is essential to mention that the results obtained by the single reference-based method (CCSD(T)) are in close proximity with the MRCI results, which is clearly revealed from the calculation of FNgY. Therefore, CCSD(T) computed results are adequate enough to describe the nature of interaction between the constituent atoms in the HNgCCO⁺ ions.

4.3.4. Analysis of Potential Energy Diagram

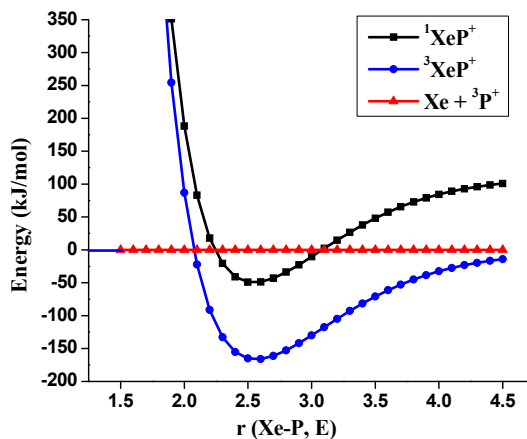
To understand the nature of bonding between the noble gas atom and the Y atom in a better way, it is essential to investigate the potential energy diagram for the various NgY species relevant to the present work. The CCSD(T) calculated potential energy diagrams of neutral XeP species are depicted in Figure 4.1a. It has been found that the quartet state is dissociative in nature; however, the doublet state is found to be bound with a very shallow potential well. We have also reported the potential energy diagrams corresponding to the XeP⁺ species in its singlet and triplet states in Figure 4.1b. Here, both the states are found to be strongly bound with respect to dissociation into atomic/ionic constituents. From these potential energy curves it is clear that an electronegative atom, which is able to attract the electron cloud from the XeP molecule, can stabilize the neutral XeP. Consequently, when an F atom is brought near the Xe atom of the XeP molecule, the resulting FXeP molecule is stabilized with a high binding energy.

The potential energy diagrams for the FXeP molecule as calculated using the CCSD(T) method are presented in Figure 4.1c for the singlet, triplet, and quintet states. The singlet and triplet states are found to be bound; however, the quintet state is dissociative in nature. Moreover, the triplet state of FXeP is stable by 78.0 kJ mol⁻¹ with respect to the 3-body dissociation channel (F + Xe + ⁴P). One significant point is that there is no crossover between the potential energy curves for the singlet and triplet states of FXeP along the Xe–P coordinate. This finding clearly suggests that these two states are isolated in the potential

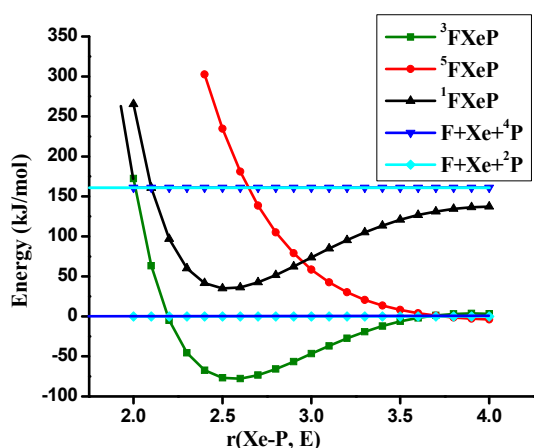
energy surface and never interact with each other up to a large Xe–P distance. Although the singlet state of FXeP is found to be bound with an equilibrium bond length value of 2.53 Å, this state crosses the repulsive quintet state at a bond length of about 2.95 Å. Subsequently, the energy of the quintet state becomes lower than that of the singlet state. However, the energy difference between the equilibrium position and the singlet–quintet crossing point is approximately 69 kJ mol⁻¹, which acts as a barrier to prevent the singlet state from dissociating into the quintet state. This situation is analogous to the metastable singlet state of the FNgO⁻ anion¹⁵⁴ with respect to the corresponding repulsive triplet state.



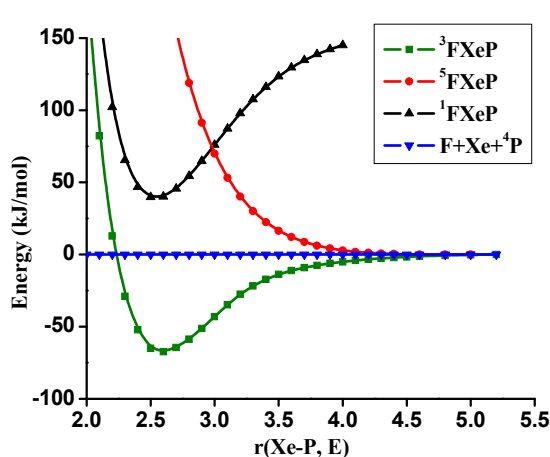
(a)



(b)



(c)



(d)

Figure 4.1. Potential-energy profile at CCSD(T)/aug-cc-pVTZ level for (a) XeP, (b) XeP⁺ and (c) FXeP, and (d) FXeP potential-energy profile at MRCI/aug-cc-pVTZ level. The energies of singlet, triplet and quintet states of FXeP are relative to (²F + Xe + ⁴P) and (F + Xe + ²P) with F–Xe distance fixed at 2.149 Å.

For the purpose of comparison we have also calculated the potential energy diagrams for the FXeP molecule using the MRCI method for all three electronic states (Figure 4.1d). The natures of the curves are found to be similar to those obtained using CCSD(T) and MRCI-based methods. The MRCI calculated triplet state of FXeP is also found to be more stable than the singlet state by 106 kJ mol⁻¹. Once again, the singlet state, associated with an equilibrium bond length of 2.55 Å, crosses the repulsive potential energy curve corresponding to the quintet state at a distance of about 2.98 Å, and the corresponding singlet–quintet crossing energy barrier is approximately 75 kJ mol⁻¹. Due to the presence of this energy barrier it may also be possible to observe the high-energy singlet state experimentally.

4.3.5. Charge and Spin Distribution Analysis

To elucidate the nature of the bonding that exists between the constituent atoms or fragments in a molecule, it is essential to know the electronic charge density distributions in the molecule. The B3LYP calculated Mulliken charges of the constituent atoms in the FN_gY molecules have been considered for the purpose of this discussion unless otherwise stated. The atomic charges on F (q_F) in the bare ³FN, ³FP, ³FAs, ³FSb and ³FBi species are -0.003, -0.250, -0.358, -0.478 and -0.525 a.u., respectively, whereas the corresponding atomic charges on N (q_N), P (q_P), As (q_{As}), Sb (q_{Sb}) and Bi (q_{Bi}) are found to be 0.003, 0.250, 0.358, 0.478 and 0.525 a.u. in the respective bare ³FY molecules. Nevertheless, it is clear from the

reported results that significant charge redistribution has taken place on the fluorine and pnictide atoms (denoted respectively as q_F and q_Y) in the 3FY molecule after the insertion of the noble gas atom. The partial atomic charges on F (q_F) changes to -0.530 , -0.580 , -0.645 , -0.672 , -0.677 a.u. in FKrY and -0.500 , -0.540 , -0.631 , -0.650 -0.663 a.u. in FXeY (Y = N to Bi). Simultaneously, the partial charge q_N changes from 0.003 to -0.187 and -0.196 a.u., q_P changes from 0.250 to 0.077 and -0.030 a.u., q_{As} changes from 0.358 to 0.166 and 0.052 a.u., q_{Sb} changes from 0.478 to 0.277 and 0.133 a.u., and q_{Bi} changes from 0.525 to 0.324 and 0.193 a.u. for FKrY and FXeY, respectively (Y = N to Bi). The partial atomic charge possessed by the Ng atom has been found to be 0.716 – 0.353 a.u. in FKrY and 0.696 – 0.470 a.u. in FXeY. It is also worthwhile to mention that the total accumulated charges on the NgyY fragments are found to be 0.529 – 0.677 a.u. in FKrY and 0.500 – 0.663 a.u. in FXeY, whereas the same amounts of negative charge reside on the fluorine atoms in the respective FNgyY molecules. Both the Mulliken and NBO analyses show that N and P atoms bear negative charges while As, Sb and Bi atoms hold positive charges in FNgyY molecule, since electronegativity decreases along the series N–P–As–Sb–Bi. Nevertheless, the predicted FNgyY molecule can be best represented as $[F^- + {}^3[NgyY]^+]$ according to the results obtained using NBO and Mulliken spin population analysis, which is also in good agreement with the structural parameters and energetic of the predicted FNgyY molecules.

It would be interesting to compare the partial atomic charges in the parent $HCCO^+$ ion with those in the predicted $HNgyCCO^+$ ions. The partial atomic charges in the parent $HCCO^+$ ion are $q_H = 0.597$ a.u., $q_C = -0.089$ a.u., $q_C = 0.496$ a.u., and $q_O = -0.005$ a.u., respectively. For the $HHeCCO^+$, $HNeCCO^+$, $HArCCO^+$, $HKrCCO^+$, and $HXeCCO^+$ ions, the partial atomic charges acquired by H are 0.527 , 0.595 , 0.266 , 0.146 , and 0.331 a.u., respectively, and similarly the charges acquired by the C attached with Ng are -0.073 , -0.310 , -0.154 , -0.121 ,

and -0.246 a.u.. In HNgCCO^+ ions, the atomic charges on the Ng atoms are 0.575 , 0.652 , 0.617 , 0.734 and 0.948 a.u. along the He–Ne–Ar–Kr–Xe series, respectively, which clearly reveal that the partial charges on the noble gas atoms are highly positive, especially for the heavier noble gases, which is due to the higher polarizability. It has been found that the cumulative charges on HNg^+ fragments in HNgCCO^+ ions are 0.789 , 0.949 , 0.857 , 0.880 , and 0.973 a.u. along the He–Ne–Ar–Kr–Xe series. These results are very close to the unit positive charge on the bare HNg^+ ions, which indicates that, upon insertion of a noble gas atom in the HCCO^+ ion, extensive charge redistribution takes place from the CCO^+ fragment to the HNg^+ moiety. The analysis of the Mulliken atomic charges as well as NBO charges strongly suggests a reasonable ionic character between Ng and C and strong covalent bonding between H and Ng so as to convincingly predict that the metastable species should exist primarily as $[\text{HNg}]^+[\text{CCO}]$.

4.3.6. Atoms-in-molecule (AIM) Analysis

Detail description of BCP (bond critical point) parameters, *viz.*, like the electron density $[\rho]$, Laplacian of the electron density $[\nabla^2\rho]$, and the local energy density $[E_d]$ has been discussed in detail in this chapter ‘Section 3.3.5’. Here, we will discuss only the MP2 computed BCP parameters unless otherwise mentioned. The predicted FNgY molecules show high positive $\nabla^2\rho(r_c)$ values at the BCPs corresponding to the F–Ng bond, indicating the existence of ionic character. In contrast to the F–Ng bond, the Ng–Y bond shows low positive values for $\nabla^2\rho(r_c)$ at their respective BCPs, except the Xe–N and Xe–As bonds, for which the $\nabla^2\rho(r_c)$ value are -0.040 and $-0.017 e a_0^{-5}$, respectively. This indicates that the Xe–N and Xe–As bonds in FXeN and FXeAs species, respectively, are associated with higher degree of covalency among all the Ng–Y bonds considered here. Nevertheless, the BCP electron

density ($\rho(r_c)$) values are found to be reasonably high and lie in the ranges of 0.08–0.11 and 0.05–0.14 $e a_0^{-3}$ for the F–Ng and Ng–Y bonds, respectively. In the present study, the $E_d(r_c)$ values for both the F–Ng and Ng–Y bonds are found to be negative. From the computed AIM results, it is clear that the covalency gradually increases along the N–P–As–Sb–Bi series for both the F–Ng and Ng–Y bonds which can be attributed as the increase in polarizability down the group with increase in size of the pnictides. In general, all the calculated AIM properties at the BCPs are in good agreement with the trends obtained from the optimized geometrical parameters and energetics, as well as the charge distribution analysis discussed above.

Table 4.5. Bond Critical Point Properties [BCP Electron Density (ρ in $e a_0^{-3}$), It's Laplacian ($\nabla^2\rho$ in $e a_0^{-5}$), the Local Electron Density (E_d in a.u.) and the Ratio of Local Kinetic Energy Density and Electron Density (G/ρ in a.u.)] of ${}^3\text{HNgCCO}^+$ (Ng = He, Ne, Ar, Kr, and Xe) Ions, Calculated using the MP2 Method with AVTZ Basis Set.

Species	H–Ng				Ng–C			
	$\rho(r_c)$	$\nabla^2\rho(r_c)$	$E_d(r_c)$	$G(r_c)/\rho(r_c)$	$\rho(r_c)$	$\nabla^2\rho(r_c)$	$E_d(r_c)$	$G(r_c)/\rho(r_c)$
${}^3\text{HHeCCO}^+$	0.244	–3.039	–0.770	0.049	0.037	0.116	–0.001	0.807
${}^3\text{HNeCCO}^+$	0.223	–2.900	–0.767	0.188	0.017	0.084	0.004	1.013
${}^3\text{HArCCO}^+$	0.237	–1.120	–0.325	0.189	0.025	0.081	0.001	0.790
${}^3\text{HKrCCO}^+$	0.207	–0.630	–0.202	0.213	0.029	0.080	–0.001	0.717
${}^3\text{HXeCCO}^+$	0.168	–0.337	–0.139	0.327	0.030	0.071	–0.002	0.656

For HNgCCO^+ ions, the MP2 calculated BCP parameters have been reported in Table 4.5. using MP2 method with AVTZ basis set by employing the AIMPAC³⁰⁹ program. The negative value of $\nabla^2\rho(r_c)$ and a high value of $\rho(r_c)$ signifies that the H–Ng bond is associated with covalent bonding in all HNgCCO^+ ions. Similarly, low electron density [$\rho(r_c) < 0.1$] values and positive values of $\nabla^2\rho(r_c)$ at BCP for a chemical bond are associated with an

unshared type of interaction. These criteria are fulfilled by Ng–C bond in the HNgCCO^+ species, and so the Ng–C interaction can be considered as a weak chemical bond. From the Table 4.5, it is quite evident that the negative $E_d(r_c)$ values signify the existence of a strong covalent bond between H and Ng atoms, whereas the type of interaction pertaining to Ng and C atoms can be primarily classified as an ion–dipole interaction due to very low negative or positive $E_d(r_c)$ values.

Following Boggs and co-workers,³¹³ an in-depth analysis of the nature of chemical bonds involving noble gas compounds have been carried out as discussed in ‘Section 3.3.5’. Here, the calculated AIM results clearly indicate that both the F–Ng and Ng–Y bonds (Ng = Kr and Xe; Y = N, P, As, Sb and Bi) have covalent character, with “type C” covalent bonding except the Xe–N bond in FXeN which possesses ‘type A’ covalent bonding. On the other hand, the $G(r_c)/\rho(r_c)$ values corresponding to the Ng–Y bonds are smaller (< 0.54) compared to those of the F–Ng bonds (> 0.73), which indicates that the Ng–Y bonds possess a higher degree of covalency than the F–Ng bonds. From the above discussions, it is obvious that the bonding nature as obtained from the AIM analysis agrees very well with the charge distribution results.

In case of HNgCCO^+ ions, the H–Ng bonds belong to “type A” category while the Ng–C bonds are associated with “type D” covalent bonding in nature, except in the HNeCCO^+ ion, where $G(r_c)/\rho(r_c) > 1$ and $E_d(r_c) > 0$, which clearly indicates that the Ne–C bond is of a “ W^n type”, involving a weak molecular interaction with a non-covalent character. Thus, it can be inferred that a negligible covalent character exists between Ng and C atoms in HNgCCO^+ ions and hence the AIM approach also affirms the existence of the predicted species as $[\text{HNg}]^+[\text{CCO}]$.

4.4. Concluding Remarks

For the first time neutral noble gas insertion molecules with pnictides of the formula FNgY (Ng = Kr, Xe; Y = N, P, As, Sb and Bi) and noble gas hydrides HNgCCO⁺ (Ng = He to Xe), have been predicted theoretically to be stable, and the triplet state is found to be the most stable state with high triplet–singlet energy gap. The structural parameters, energetics, charge distribution, harmonic vibrational frequencies and AIM properties have been calculated by employing MP2, DFT, and CCSD(T) based techniques using different types of basis sets. In addition, a multireference configuration interaction (MRCI) based approach has been adopted to optimize the structures of the FNgY and HNgCCO⁺ species. Both the predicted neutral FNgY and cationic HNgCCO⁺ species are found to be energetically stable with respect to all plausible 2- and 3-body dissociation channels, except for the two-body channel leading to the global minimum product (Ng + FY) and (Ng + HCCO⁺), respectively. The calculated barrier heights are found to be quite high to prevent the dissociation of both the metastable species into the global minima products, which confirms that all the predicted FNgY and HNgCCO⁺ species are kinetically stable. All the calculated results clearly indicate that the FNgY compounds can best be described as [F⁻ + ³[NgY]⁺]. It is very important to emphasize that all the computed parameters clearly suggest that it may be possible to prepare the FNgY compounds under cryogenic conditions in a glow discharge containing FY and Ng through a matrix isolation technique. At the same time, the detailed analysis of the various aspects of this enticing HNgCCO⁺ triplet species indicates that they should exist primarily as [HNg]⁺[CCO] and can be observed by suitable experimental technique(s) under cryogenic conditions.

Chapter 5. Investigation of ‘Super-Strong’ Noble Metal–Noble Gas Bonding

5.1. Introduction

Recent experimental investigation reveals that single gold atom can exhibit chemistry analogous to the hydrogen atom in SiAu_n clusters.³³⁴ The unusual chemistry of gold is mostly due to the strong relativistic effects,³³⁵ which stabilize the valence $6s$ orbital and destabilize the $5d$ orbitals of gold resulting into decrease in size of former as compared to that of the latter. The behavior of gold as hydrogen is also supported by the similar electronegativity of gold and hydrogen atom. In the recent past, it has been verified that gold atom behaves like a hydrogen atom in the hydrogen-bonded complex of AuOH with water.³³⁶ Earlier our group have explored the feasibility study of noble gas inserted compounds, MNgF and MNgOH ($\text{M} = \text{Cu}, \text{Ag}, \text{and Au}$; $\text{Ng} = \text{Ar}, \text{Kr}, \text{and Xe}$) using *ab initio* quantum chemical calculations.¹⁵⁵

As mentioned, noble gas–noble metal bonding has been investigated extensively over the years; however, the nature of this kind of bonding has been controversial as pointed out very recently by Fielicke and co-workers.³³⁷ In fact, they proposed trimeric coinage metal cluster as a prototype system to unravel the nature of Ar–M bonding ($\text{M} = \text{Ag}$ and Au) and showed that the total Ar binding energy in $\text{Au}_3^+ \cdot \text{Ar}_3$ is considerably higher than that in $\text{Ag}_3^+ \cdot \text{Ar}_3$ (cf. 81.1 vs 43.4 kJ mol^{-1}). Moreover, through far IR multiple-photon dissociation spectroscopy it has been demonstrated that Ar atoms in the $\text{Ag}_3^+ \cdot \text{Ar}_3$ complex act merely as messengers while the same participate in conventional Ar–Au chemical bonding in the $\text{Au}_3^+ \cdot \text{Ar}_3$ complex and thereby modify the IR spectra significantly. Also, the Ar–M bond energy in ArAg_3^+ complex (15.4 kJ mol^{-1}) is found to increase with the replacement of Ag with Au atom and finally reaches 29.9 kJ mol^{-1} in the ArAu_3^+ complex. The study of this

kind of bonding is very important in elucidating the structure of a metal cluster, because the electronic structure and the IR spectra of metal cluster are highly dependent on the nature and strength of noble gas–noble metal interaction.³³⁸ Apart from the experimental investigations on the interaction of a noble gas atom with coinage metal atom trimer cations, very recently, theoretical studies involving a similar kind of complexes have been reported in the literature.³³⁹

In this context, one question comes whether it is possible to further increase the noble gas–noble metal bonding interaction exceptionally as compared to that in the ArAu_3^{+337} system. To answer this question quantitatively, we have considered various noble gas atoms (Ng = Ar, Kr, and Xe) and hydrogen-doped gold trimers, which is motivated by the gold–hydrogen analogy as proposed by Li *et al.*,³⁴⁰ and subsequently investigated by others for various systems.^{341,135} Here it may be noted that both hydrogen-doped small size gold/silver clusters and H_2 adsorbed gold clusters have been shown to behave as a better catalyst in the oxidation of carbon monoxide;³⁴² however, the catalytic activity remains almost unchanged when the Au_{20} cluster is doped with hydrogen atom.³⁴³ Therefore, it is further interesting to investigate the change in the nature and strength of Ng–Au bonding in NgAu_3^+ through successive replacement of Au atom(s) with H atom(s), resulting in NgAu_2H^+ and NgAuH_2^+ species. In this connection, it is worthwhile to mention that the hydrogen-doped noble metal clusters have been investigated experimentally as well as theoretically.³⁴⁴

5.2. Computational Details

Most of the computational methodologies are same as mentioned before in ‘Section 3.2’ and ‘Section 4.2’. Instead of B3LYP, we have used density functional theory (DFT) with the dispersion-corrected ω separated form of Becke’s 1997 hybrid functional with short-range HF exchange (ω B97X-D) functional.²⁵¹ Here additionally we have carried out the energy

decomposition analysis (EDA) of the predicted systems. In the frozen core approximations up to $3d$ and $4d$ orbitals for silver and gold, respectively, and $2p$ orbital for both copper and argon atoms, electrons are kept in the core for the ADF calculations, and the corresponding Slater type orbital TZ2P³⁴⁵ basis sets have been used. Zeroth-order regular approximation (ZORA) has been used to take into account the scalar relativistic effects. To obtain the interaction energies between the two fragments (Ng and $M_{3-k}H_k^+$) in the $NgM_{3-k}H_k^+$ complexes, energy decomposition analysis (EDA)³⁴⁶ of the total interaction energy has been performed with ADF 2013³⁴⁷ software using PBE-D3 (Perdew–Burke–Ernzerhof with dispersion correction) functional. The total interaction energy, ΔE_{int} can be decomposed into four components, *viz.*,

$$\Delta E_{\text{int}} = \Delta E_{\text{elec}} + \Delta E_{\text{Pauli}} + \Delta E_{\text{orb}} + \Delta E_{\text{dis}} \quad (5.1)$$

where ΔE_{elec} and ΔE_{Pauli} represent the electrostatic interaction energy and the Pauli repulsive energy, respectively, between the fragments. ΔE_{orb} is the stabilizing orbital interaction term, which includes polarization term and covalency factor due to the overlap between the noble gas and noble metal orbitals. The term ΔE_{dis} denotes the dispersion energy.

5.3. Results and Discussions

5.3.1. Structural Analysis of Hydrogen Doped $NgAu_3^+$ Ions

The precursor ions, *viz.*, Au_3^+ , Au_2H^+ , and AuH_2^+ exhibit a nonlinear planar structure for the minima. Now the interaction of the Ng atom with these ions leads to the formation of strongly bonded $NgAu_3^+$, $NgAu_2H^+$, and $NgAuH_2^+$ complexes, as depicted in Figure 5.1 which shows the variation of Ng–Au bond lengths in these complexes. The decrease in the Ar–Au bond length value from 2.605 Å in $ArAu_3^+$ to 2.518 Å in $ArAu_2H^+$ and 2.429 Å in $ArAuH_2^+$, respectively, as obtained by CCSD(T) indicates that the Ng–Au interaction is increased considerably in $ArAuH_2^+$ species. It implies that the Ng–Au bond strength is

enhanced drastically with the doping of two hydrogen atoms in a pure Au trimer cation. In this context it is important to note that the CCSD(T) computed Ng–Au bond length values in NgAu^+ are generally larger (2.537, 2.553, and 2.617 Å in ArAu^+ , KrAu^+ , and XeAu^+ , respectively) than that in the NgAuH_2^+ complexes, which indicate that the Ng–Au bond strength is greater in the latter complexes.

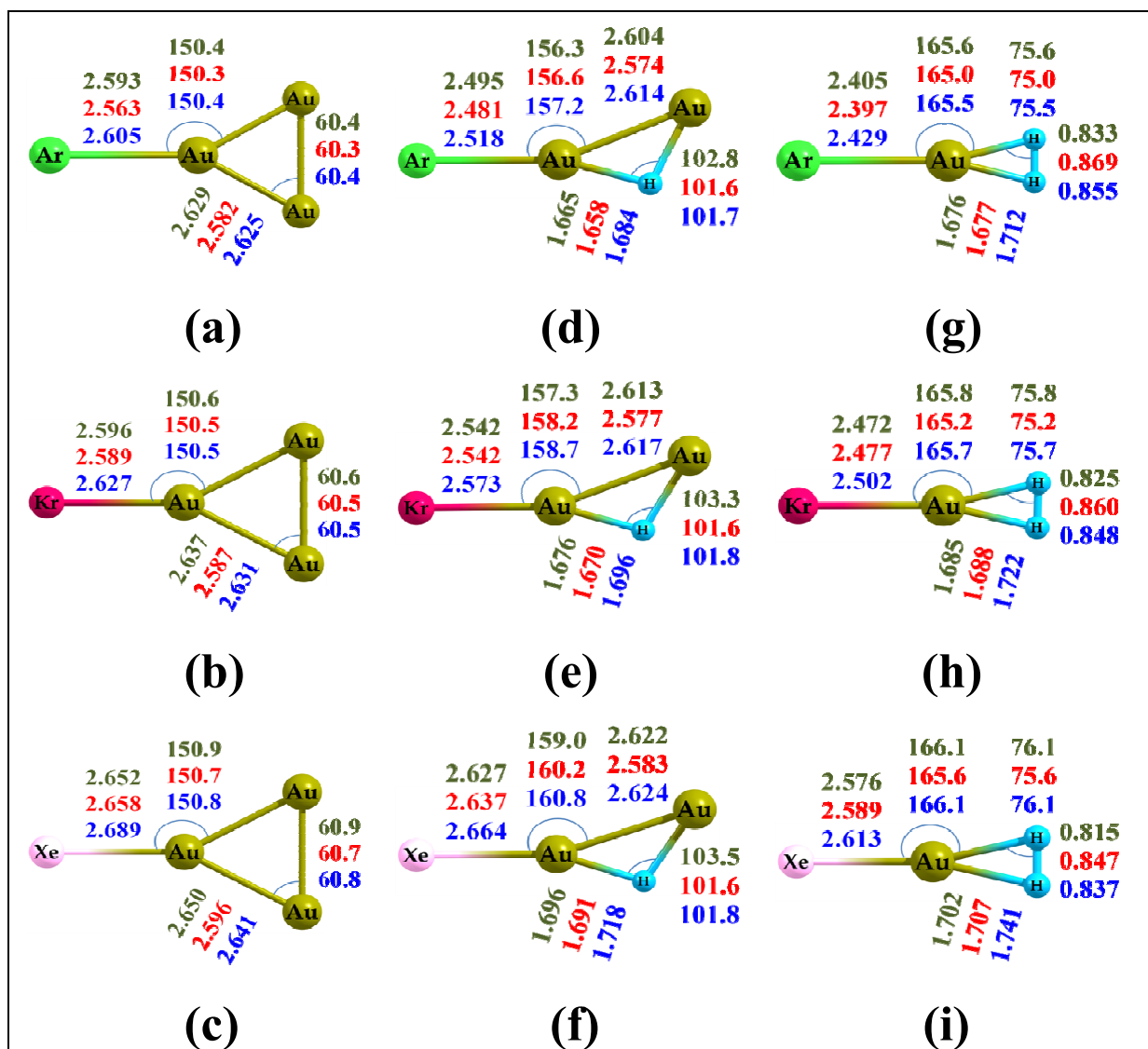


Figure 5.1. Optimized geometrical parameters of planer NgAu_3^+ (a, b, c), NgAu_2H^+ (d, e, f) and NgAuH_2^+ (g, h, i) (Ng = Ar, Kr, Xe) where the bond lengths are in angstroms and bond

angles are in degrees. The values in green, red, and blue are computed at the ω B97X–D/DEF2, MP2/DEF2, and CCSD(T)/AVTZ levels of theory, respectively.

Table 5.1. CCSD(T) Computed Bond Dissociation Energy (BE in kJ mol^{-1}) and MP2 Calculated Stretching Frequency (ν in cm^{-1}) and Force Constant (k in N m^{-1}) Values for Ng–Au Bond in NgAu_3^+ , NgAu_2H^+ and NgAuH_2^+ Species.

Ions	BE (Ng–Au)			$\nu(\text{Ng–Au})$			$k(\text{Ng–Au})$		
	Ar	Kr	Xe	Ar	Kr	Xe	Ar	Kr	Xe
NgAu_3^+	31.9	50.7	81.2	120.5	116.7	114.1	39.4	60.3	81.0
NgAu_2H^+	47.5	69.3	102.4	142.2	126.3	116.4	63.4	81.1	95.6
NgAuH_2^+	72.0	100.7	142.0	223.2	183.0	166.2	97.8	115.2	125.3

In the spirit of Gerry and co-workers,¹⁵³ we have analyzed the Ng–Au bond length with respect to the covalent limit (R_{cov}) and van der Waals limit (R_{vdW}) as discussed in ‘Section 3.3.1’. The R_{cov} values obtained from the recently reported literature⁴³ are 2.20, 2.41, and 2.55 Å for Ar–Au, Kr–Au and Xe–Au bond, respectively, and the corresponding R_{vdW} ⁴⁴⁻⁴⁶ values are 4.15, 4.57, and 4.38 Å. It is quite evident from the above data that the Ng–Au bond length values in $\text{NgAu}_{3-k}\text{H}_k^+$ ($k = 0-2$) are in close proximity with the covalent limits. In fact, a slightly higher value of the Ng–Au bond distance in the $\text{NgAu}_{3-k}\text{H}_k^+$ species implies that both covalent and induction and dispersion interactions are likely to coexist in the Ng–Au bonding.

5.3.2. Energetics and Stability

The endothermicity of the two-body dissociation channel ($\text{NgAu}_{3-k}\text{H}_k^+ \rightarrow \text{Ng} + \text{Au}_{3-k}\text{H}_k^+$) illustrates that the predicted species are more stable than the dissociated products as revealed from the zero-point energy (ZPE) and basis set superposition error (BSSE)-corrected Ng–Au

bond dissociation energy values reported in Table 5.1. The Ng–Au binding energy in NgAuF and NgAu⁺ have been calculated to be 46.0, 44.1 kJ mol⁻¹ in Ar, 64.4, 73.5 kJ mol⁻¹ in Kr, and 92.4, 121.6 kJ mol⁻¹ in Xe containing complexes, respectively, at the same level. All these results clearly indicate that the Ng–Au bonding strength not only is greatly enhanced with the hydrogen doping in pure Au trimers but also is found to be greater than that in the NgAuF and NgAu⁺ species. As far as binding energy is concerned, the Ng–Au bonding interaction has been found to be increased by 2.26 times for Ar, 1.99 times for Kr, and 1.75 times for Xe complexes in going from NgAu₃⁺ to NgAuH₂⁺ complex as predicted by the CCSD(T) method. Therefore, it is quite obvious that the enhancement in the Ng–Au bond strength is more pronounced in the case of Ar containing H-doped Au trimers in comparison with the corresponding Kr and Xe complexes. From all these results it is evident that the H doping in pure noble metal trimers increases the noble gas–noble metal bonding significantly.

5.3.3. Change in Vibrational Frequencies on Hydrogen Doping in NgAu₃⁺ Ions

Subsequently, we have calculated the Ng–Au stretching vibrational frequency along with the force constant values with all levels of theory and Table 5.1 lists the MP2/DEF2 computed values due to its close proximity with the experimental results. For the present Ng–Au systems, the MP2/DEF2 computed Ng–Au stretching vibrational frequency value changes from 142.1 to 223.2 cm⁻¹ in Ar, 108.1 to 183.0 cm⁻¹ in Kr, and 101.9 to 166.2 cm⁻¹ in Xe containing complexes on going from NgAu₃⁺ to NgAuH₂⁺ species, respectively, and the corresponding force constant values are changed from 39.4 to 97.8 N m⁻¹ in Ar, 60.3 to 115.2 N m⁻¹ in Kr, and 81.0 to 125.3 N m⁻¹ in Xe containing complexes (Table 5.1). Both the Ng–Au stretching frequency and force constant values strongly reveals that the Ng–Au bonding strength is greatly enhanced with the hydrogen doping in pure Au trimers which is found to be concurrence with the optimized structures and energetics.

5.3.4. Molecular Orbitals and HOMO–LUMO Energies

The relevant molecular orbitals depicting the Ar–Au bonding represented in Figure 5.2 reveal that the π orbitals from both Ar and Au are involved in the bonding. Moreover, the nature of the Ar–Au interaction in ArAu_3^+ , ArAu_2H^+ and ArAuH_2^+ ions is found to be almost the same, at least qualitatively. Nevertheless, the Ar–Au bonding orbitals for the ArAuH_2^+ ion is found to be associated with the lowest eigenvalue.

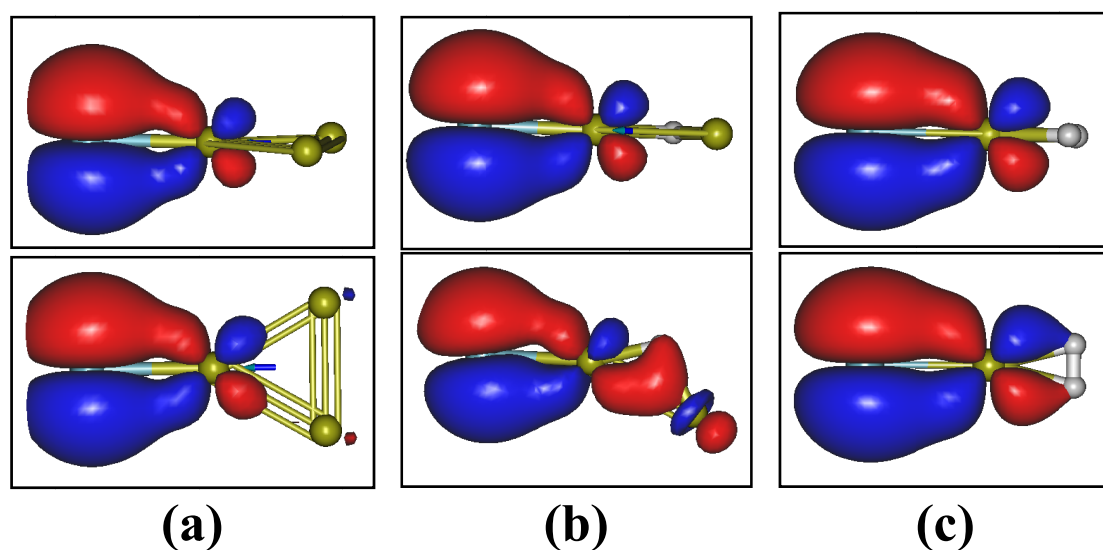


Figure 5.2. Degenerate molecular orbitals depicting the Ar–Au bonding in (a) ArAu_3^+ , Orbital energy = -18.86 eV; (b) ArAu_2H^+ , Orbital energy = -19.65 eV; and (c) ArAuH_2^+ , Orbital energy = -20.90 eV.

In view of significant differences in various bonding parameters as discussed above, it is interesting to analyze the enhancement of the Ng–Au binding energy in terms of the HOMO (highest occupied molecular orbital) and LUMO (lowest unoccupied molecular orbital) energy of the precursor species and their complexes. The Ar–Au bond energy has been shown to correlate very well with the LUMO energy of the precursor ion (Figure 5.3). The $\omega\text{B97X-D/DEF2}$ computed LUMO energy for Au_3^+ , Au_2H^+ , and AuH_2^+ species have

been found to be -6.66 , -7.27 , and -8.12 eV, respectively, whereas the HOMO energy for Ar, Kr, and Xe are -13.93 , -12.71 , and -11.34 eV, respectively. Thus, through successive replacement of Au atom(s) by the H atom(s) in pure Au trimer, the LUMO of the $\text{Au}_{3-k}\text{H}_k^+$ species has been stabilized more and more, resulting in decreases in the energy gap between the HOMO of Ng and LUMO of AuH_2^+ , which leads to the formation of the most stable Ng–Au bond in NgAuH_2^+ complexes, among all the complexes considered here. This is one of the factors for the enhancement of Ng–Au bonding interaction on doping with a hydrogen atom in the pure Au trimer. The HOMO–LUMO energy gaps of 7.88 , 8.92 , and 11.11 eV in Ar, 7.86 , 8.97 , and 11.23 eV in Kr, 7.81 , 9.00 , and 11.20 eV in Xe containing complexes in the NgAu_3^+ , NgAu_2H^+ , and NgAuH_2^+ species, respectively, are also found to be higher as compared to that for the respective precursor, Au_3^+ , Au_2H^+ , and AuH_2^+ . Moreover, this increase of the HOMO–LUMO gap is the maximum for the AuH_2^+ ion, in agreement with the highest stability of the NgAuH_2^+ complex.

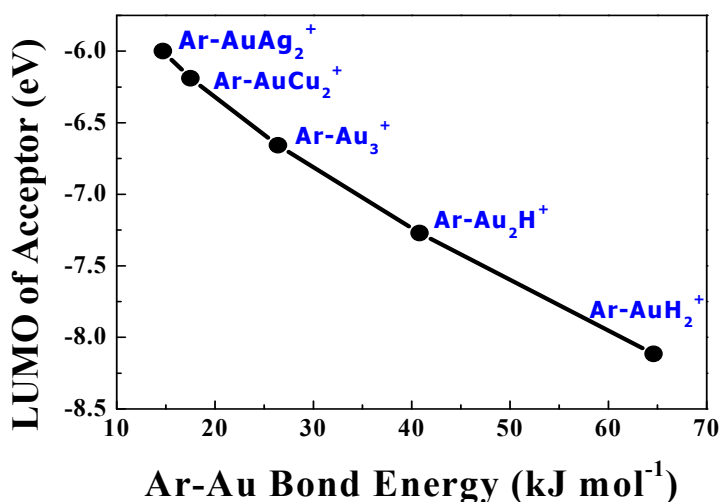


Figure 5.3. Plot of the Ar–Au bond energy vs the LUMO energy, calculated using $\omega\text{B97X–D/DEF2}$ Method (Correlation Coefficient corresponding to linear least square fit, $R^2 = 0.988$).

In this context, it may be noted that Ar–Au⁺ bonding is not as strong as the Ar–AuH₂⁺ interaction, although the LUMO of Au⁺ (–9.73 eV) is more stabilized. It is due to the limited scope of charge reorganization in Ar–Au⁺ ion as compared to that in the Ar–AuH₂⁺ ion. As a result, the HOMO–LUMO gap of the Au⁺ ion (9.12 eV) remains almost the same as in the Ar–Au⁺ ion (9.02 eV). Here it may be noted that the performance of ω B97X-D functional in predicting the HOMO–LUMO gap is very good³⁴⁸ as compared to that of the other density functionals.³⁴⁹

5.3.5. Charge Distribution Analysis

The MP2 computed NBO charges of the constituent atoms in Au₃⁺, Au₂H⁺, AuH₂⁺, NgAu₃⁺, NgAu₂H⁺, and NgAuH₂⁺ (Ng = Ar, Kr, and Xe) species are reported in Table 5.2.

Table 5.2. MP2/AVTZ Calculated Values of the NBO Charges in Au₃⁺, Au₂H⁺, AuH₂⁺, NgAu₃⁺, NgAu₂H⁺, and NgAuH₂⁺ (Ng = Ar, Kr, and Xe) Species.

Species	Atoms	Cation	Ar	Kr	Xe
Au ₃ ⁺ /	Ng	...	0.076	0.123	0.202
NgAu ₃ ⁺	Au1 ^a	0.333	0.291	0.264	0.215
	Au2	0.333	0.317	0.306	0.291
	Au3	0.333	0.317	0.306	0.291
Au ₂ H ⁺ /	Ng	...	0.107	0.174	0.259
NgAu ₂ H ⁺	Au1 ^a	0.627	0.513	0.445	0.376
	Au2	0.627	0.619	0.603	0.580
	H	-0.254	-0.240	-0.222	-0.215
AuH ₂ ⁺ /	Ng	...	0.145	0.219	0.315
NgAuH ₂ ⁺	Au ^a	0.925	0.716	0.634	0.545
	H1	0.037	0.070	0.073	0.070
	H2	0.037	0.070	0.073	0.070

^aCharge corresponding to the Au atom bonded with the Ng atom is represented in boldface.

The calculated NBO charges (Table 5.2) reveal that the positive charge on the metal atom is increased considerably in going from the Au_3^+ ($q_{\text{Au}} = 0.333$ a.u.) to AuH_2^+ ($q_{\text{Au}} = 0.925$ a.u.) ion, which enhances the electron density transfer from the HOMO of the Ng atom to the LUMO of the AuH_2^+ species, leading to the formation of a stronger Ng–Au bond. Moreover, the NBO charge on the Au atom in $\text{Au}_{3-k}\text{H}_k^+$ is decreased on complexation with Ng and the extent of decrease is the maximum in the AuH_2^+ ion (from 0.925 to 0.716, 0.634, 0.545 a.u. in ArAuH_2^+ , KrAuH_2^+ , and XeAuH_2^+ , respectively) among all the Au containing trimers because of the lowest LUMO energy of the AuH_2^+ ion. Consequently, charge transfer from the Ng atom to the trimer cation is also found to be the maximum in the case of the Ng– AuH_2^+ complex. It implies that charge reorganization in AuH_2^+ is the maximum after complexation, indicating an increase in the charge-induced dipole interaction in the series $\text{Ng–Au}_3^+ < \text{Ng–Au}_2\text{H}^+ < \text{Ng–AuH}_2^+$.

5.3.6. Analysis of Topological Properties of Hydrogen Doped NgAu_3^+ Ions

Detail description on Bader's quantum theory of atoms-in-molecules (QTAIM),³⁰⁹ has been discussed in 'Section 3.3.5'. In $\text{NgAu}_{3-k}\text{H}_k^+$ ($k = 0-2$) complexes, the BCP parameters at the Ng–Au bond strongly indicate that the bonding between Ng and Au atoms are of “ W^c type” covalent bonding as defined by Boggs and co-workers³¹³ which is already discussed in detail in 'Section 3.3.5'. Therefore, we can emphasize that the bonding between the Ng and Au atoms bears a partial covalent character, which is also evident from the Ng–Au bond length values that are even smaller than the covalent limit as discussed in the structural part. Moreover, the variation of all these computed above mentioned BCP parameters clearly indicate that the Ng–Au bonding in NgAuH_2^+ complexes possesses the highest degree of covalency.

Table 5.3. Various Topological Properties [Local Electron Energy Density (E_d in a.u.), the Electron Density (ρ in $e a_0^{-3}$), and Ratio of Local Electron Energy Density and Electron Density ($-E_d/\rho$ in au)] at the Local Energy Density Critical Points [(3, +1) HCP] for the Ng–Au Bond in NgAu_3^+ , NgAu_2H^+ , and NgAuH_2^+ (Ng = Ar, Kr, and Xe) Species As Obtained by Using the ωB97XD and MP2 Methods with the DEF2 Basis Set.

Species	E_d		ρ		$-E_d/\rho$	
	ωB97XD	MP2	ωB97XD	MP2	ωB97XD	MP2
ArAu₃⁺	−0.004	−0.004	0.046	0.047	0.090	0.085
ArAu₂H⁺	−0.009	−0.008	0.057	0.057	0.152	0.140
ArAuH₂⁺	−0.016	−0.015	0.071	0.070	0.224	0.214
KrAu₃⁺	−0.009	−0.009	0.058	0.057	0.155	0.158
KrAu₂H⁺	−0.013	−0.012	0.065	0.063	0.200	0.190
KrAuH₂⁺	−0.019	−0.018	0.077	0.074	0.247	0.243
XeAu₃⁺	−0.016	−0.014	0.065	0.064	0.239	0.219
XeAu₂H⁺	−0.018	−0.016	0.071	0.067	0.254	0.239
XeAuH₂⁺	−0.024	−0.022	0.079	0.076	0.304	0.289

Very recently, Grandinetti and coworkers³⁵⁰ reported that this energy density based topological analysis is highly successful in predicting the nature of bonding that exists in a large number of noble gas containing compounds. For this purpose, we have computed the critical points corresponding to the local energy density (denoted as HCP) and the $\omega\text{B97X-D}$ and MP2 calculated values of $\rho(r)$ and $E_d(r)/\rho(r)$ for the Ng–Au bond at the corresponding HCPs for the $\text{NgAu}_{3-k}\text{H}_k^+$ ($k = 0-2$) complexes are reported in Table 5.3. The bond degree (BD),^{350,351} which is defined as the negative value of $E_d(r)/\rho(r)$ at HCP, is an important index for characterizing the nature of a chemical bond. For Ng–Au bond, the MP2 computed BD values are positive, and the values are increased monotonically from 0.085, 0.158, 0.219 a.u. in NgAu_3^+ to 0.140, 0.190, 0.239 a.u. and 0.214, 0.243, 0.289 a.u. in NgAu_2H^+ and NgAuH_2^+

along Ar–Kr–Xe series, respectively, evidently indicating an increasing trend in the Ng–Au covalent bonding in NgAu_3^+ with the successive replacement of Au atom(s) by the H atom(s).

An increase in both covalent characteristics and charge induced dipole interaction through successive replacement of Au atom with H atom in Ng–Au_3^+ complex is further supported by the calculated values of various energy components (Table 5.4), which reveal that there has been an increase of both electrostatic and orbital components in going from NgAu_3^+ to NgAuH_2^+ species. It is also very important to note that the extent of increase in orbital component is significantly higher, particularly for the Ar– Au_3^+ complex.

Table 5.4. Calculated Values (kJ mol^{-1}) of Energy Decomposition Analysis for NgAu_3^+ , NgAu_2H^+ , and NgAuH_2^+ (Ng = Ar, Kr, and Xe) Species as Obtained Using PBE-D3 Method with TZ2P Basis Set by Employing ADF Packages and Taking MP2 Optimized Geometry.

Complexes	Pauli Repulsion Energy	Electrostatic Energy	Orbital Interaction Energy	Dispersion Energy	Total Bonding Energy
ArAu₃⁺	112.33	–67.31	–77.88	–2.16	–35.02
ArAu₂H⁺	132.91	–77.56	–102.11	–1.49	–48.25
ArAuH₂⁺	144.14	–85.47	–142.82	–0.83	–84.99
KrAu₃⁺	169.73	–109.27	–114.45	–2.86	–56.84
KrAu₂H⁺	177.37	–111.67	–136.69	–1.92	–72.92
KrAuH₂⁺	179.63	–115.21	–180.49	–1.05	–117.12
XeAu₃⁺	242.26	–165.37	–162.74	–3.77	–89.62
XeAu₂H⁺	233.96	–156.88	–182.44	–2.44	–107.80
XeAuH₂⁺	224.74	–154.33	–229.03	–1.27	–159.89

5.3.7. Comparative Accounts of $\text{NgAu}_{3-k}\text{H}_k^+$ with $\text{NgAg}_{3-k}\text{H}_k^+$ and $\text{NgCu}_{3-k}\text{H}_k^+$ Ions

The optimized Ng–M bond lengths, the bond dissociation energy, and the Ng–M stretching frequency and the corresponding force constant values for $\text{NgM}_{3-k}\text{H}_k^+$ (M = Cu and Ag; k = 0–2) complexes show that similar trends have been observed in the case of Ag and Cu complexes as observed by Au complexes. All the HOMO–LUMO energy values and the NBO charges of the concerned $\text{M}_{3-k}\text{H}_k^+$ and $\text{NgM}_{3-k}\text{H}_k^+$ complexes strongly indicate that the decrease in the energy gap between the HOMO of Ng and LUMO of MH_2^+ and considerable increase of positive charge on the metal atom in MH_2^+ ion enhance the electron density transfer from HOMO of Ng atom to the LUMO of MH_2^+ species leading to the formation of stronger Ng–M bonding in the case of all $\text{NgM}_{3-k}\text{H}_k^+$ complexes. Moreover, the BCP and HCP parameters for all the $\text{NgM}_{3-k}\text{H}_k^+$ complexes clearly indicate that the Ng–Ag and Ng–Cu bonds are associated with a higher degree of covalency in NgAgH_2^+ and NgCuH_2^+ complexes as is observed in the case of NgAuH_2^+ complexes. Various energy components for all the NgMH_2^+ complexes clearly reveal that the electrostatic and orbital components of bonding energy play a key role for the formation of a strong Ng–M bond in NgMH_2^+ complexes. It is worthwhile to mention that the $\text{NgAg}_{3-k}\text{H}_k^+$ and $\text{NgCu}_{3-k}\text{H}_k^+$ complexes follow similar trends in chemical properties while going from pure metal trimers to hydrogen doped metal trimers as is observed in the case of $\text{NgAu}_{3-k}\text{H}_k^+$ complexes. However, all these effects are more pronounced in $\text{NgAu}_{3-k}\text{H}_k^+$ complexes due to the presence of strong relativistic effects in gold.³³⁵

5.4. Conclusion

In a nutshell, the unprecedented strengthening of the Ng–Au bonding has been observed with successive replacement of Au atom by the H atom in pure Au trimers. The concept of gold–hydrogen analogy makes it possible to evolve this pronounced effect of hydrogen

doping in Au trimers leading to the strongest Ng–Au bond in NgAuH₂⁺ species, as revealed from the calculated values of Ng–Au bond length, bond energy, vibrational frequency and force constant. Similar trends have been found in the case of Ng–Ag and Ng–Cu complexes. The enhancement of Ng–M bonding interaction in Ng–MH₂⁺ (Ng = Ar, Kr, and Xe; M = Cu, Ag, and Au) as compared to that in Ng–M₃⁺ can be attributed to considerable increase in the Ng–M covalency as revealed from the electron density based topological properties and energy decomposition analysis. Calculated values of HOMO and LUMO energies, and partial atomic charges further indicate that an enhancement in the charge–induced dipole interaction is also responsible for the surprisingly high Ng–M bonding interaction in Ng–MH₂⁺ species. All the theoretical results reported in the present work and earlier experimental existence of AgH₂⁺,^{344b} Au_xH₂⁺,^{338b} and Ng–MX (Ng = Ar, Kr, Xe; M = Cu, Ag, Au; X = F, C)^{132,133,153} species along with very recent experimental identification of Ar complexes of mixed noble metal clusters, Ar_kAu_nAg_m⁺ (n + m = 3; k = 0–3) by Fielicke and co-workers³³⁷ strongly suggest that the predicted Ng–MH₂⁺ species would be observed experimentally.

Chapter 6. Electronic Structure and Stability of Noble Gas Encapsulated Endohedral Zintl Ions

6.1. Introduction

It is well-known that the Zintl ions of groups 14 and 15 are incredible chemical systems with unexpected stoichiometries, and intriguing structures, which make them unique for potential applications.³⁵² Among them, lead and tin clusters, plumbaspherene (Pb_{12}^{2-}) and stannaspherene (Sn_{12}^{2-}) are of considerable interest because of their hollow and spherical nature, high stability, and large diameter. It was discovered that Pb_{12}^{2-353} and Sn_{12}^{2-354} form a highly stable icosahedral cage cluster bonded by four delocalized radial π bonds and nine delocalized on-sphere σ bonds from $6p$, $6s$ and $5p$, $5s$ orbitals, respectively. Moreover, Sn_{12}^{2-} and Pb_{12}^{2-} cage diameters are 6.1 and 6.3 Å, respectively, which are slightly smaller than that of C_{60} (7.1 Å). This large interior volume of Sn_{12}^{2-} and Pb_{12}^{2-} cages accounts for the existence of many endohedral clusters analogous to that of fullerenes. Thus, the spherically symmetric 26-electron systems, plumbaspherene and stannaspherene, can be considered as inorganic analogues of fullerenes. In fact, Sn_{12}^{2-} and Pb_{12}^{2-} cage-based several endohedral clusters,^{355,356} encapsulating different atoms/ions, have been investigated experimentally as well as theoretically. Apart from the endohedral Sn_{12}^{2-} and Pb_{12}^{2-} clusters, in recent years, metal atom/ion encapsulated silicon and germanium clusters have also attracted considerable attention.^{357,358}

Discovery of the Zintl ions, Pb_{12}^{2-} and Sn_{12}^{2-} , motivated the scientists to investigate the atom encapsulation within these cages. Through experiments as well as theoretical calculations, it has been demonstrated that Pb_{12}^{2-355} and Sn_{12}^{2-356} can trap not only alkali, alkaline earth, and rare-earth atoms, but also more interesting transition metals. A highly

stable 32-electron system of $\text{Pu}@{\text{Pb}}_{12}$ and other actinide encapsulated Pb_{12}^{2-355} clusters have also been investigated. In contrast to $\text{M}@{\text{Au}}_{12}$ and encapsulated Ge and Si clusters where dopants are critical in stabilizing cage structures,³⁵⁷ $\text{M}@{\text{Pb}}_{12}$ and $\text{M}@{\text{Sn}}_{12}$ derive stability from the intrinsic stability of parent clusters, Pb_{12}^{2-} and Sn_{12}^{2-} , due to their greater aromaticity as compared to Ge_{12}^{2-} .³⁵⁸ Zintl-like ions composed of only transition metal atoms such as $[\text{Ni}@{\text{Au}}_6]^{2-}$ and $[\text{Ti}@{\text{Au}}_{12}]^{2-}$ have also been proposed recently³⁵⁹ on the basis of the 18-electron rule. All of these aspects have motivated us to explore the stability of noble gas encapsulated Pb_{12}^{2-} and Sn_{12}^{2-} clusters.

Despite the highly inert nature of noble gas atoms, in recent years, noble gas containing various chemical compounds has been observed. Thus, the reactive nature of noble gas atoms has prompted us to predict new Ng-compounds. Moreover, not only the noble gas encapsulated fullerenes but also several new species involving noble gas atoms have been reported from time to time in the past decade. For instance, noble gas filled group 14 clathrates³⁶⁰ ($\text{Ng}_n[\text{M}_{136}]$, Ng = Ar, Kr, Xe and M = Si, Ge, Sn, n = 8, 24) have been reported to be stable. Noble gas compounds with main group elements under high pressure (ArLi_n , XeLi_n , Ng-Mg, Na_2He , Na_2HeO , etc.)^{247,248,361} show peculiar chemistry where noble gas atom has been found to be anionic in nature, which is highly counterintuitive. The noble gas atom has been found to become more reactive and acquire a high negative charge under high pressure condition.^{247,248,361} Apart from fundamental interests on the structure and bonding of noble gas compounds, in recent years, trapping of noble gas atom into various novel materials has attracted considerable attention from applications point of view.^{234,236,362} It may be noted here that the host anions (Pb_{12}^{2-} and Sn_{12}^{2-}) possess the highest symmetry, I_h point group (analogous to buckminsterfullerene, C_{60}). All of these aspects made us curious to know whether noble gas atom can be trapped into Pb_{12}^{2-} and Sn_{12}^{2-} cages, resulting in endohedrally encapsulated Zintl ions.

We have attempted to explore whether noble gas atoms with high positive electron affinity values can be encapsulated within a doubly negatively charged cluster. Therefore, the optimized structures, energetics, and stability of noble gas encapsulated Pb_{12}^{2-} and Sn_{12}^{2-} clusters have been investigated through electronic structure calculations as well as *ab initio* molecular dynamics simulations.³⁶³ Molecular dynamics simulation studies have been carried out at different temperatures such as 298, 500 K, etc., to infer the dependence of temperature on the interaction pattern between the concerned atoms and the stability of the clusters over the course of time. Moreover, Ng@KPb_{12}^- , Ng@KSn_{12}^- , $\text{Ng@K}_2\text{Pb}_{12}$, and $\text{Ng@K}_2\text{Sn}_{12}$ systems have also been investigated to see the effect of counterion(s) on the structure and stability of these noble gas encapsulated clusters.

6.2. Computational Details

In this study, all of the theoretical computations including electronic structure optimizations and *ab initio* molecular dynamics simulations have been performed using TURBOMOLE-6.6 package,³⁶⁴ and a hybrid density functional, B3LYP (defined in ‘Section 3.2’),²⁵⁰ has been used to describe the exchange and correlation interactions. We have employed def-TZVP basis sets for lighter atoms in our endohedral cluster such as He, Ne, Ar, Kr, and H, whereas the ECP along with def-TZVP basis set has been utilized for heavier elements like Pb, Sn, and Xe during the calculations.³⁰⁴ This combination of basis set is denoted as DEF. Initial geometries have been optimized at B3LYP/DEF level of theory and this results have been discussed throughout the text unless otherwise mentioned. The harmonic vibrational frequencies have been calculated with the same level of theory, and all real frequency values confirm the minima state of the clusters studied here on their respective potential energy surfaces (PES). Furthermore, natural population analysis (NPA) has been employed to calculate the charges on noble gas and cage atoms. The thermodynamic stability of the noble

gas encapsulated clusters has been determined on the basis of their binding energy values. It has been calculated according to the equation:

$$BE = - [E(\text{Ng}@Pb_{12}^{2-}/\text{Ng}@Sn_{12}^{2-}) - E(\text{Ng}) - E(Pb_{12}^{2-}/Sn_{12}^{2-})] \quad (6.1)$$

Thus, negative value of binding energy calculated using equation 6.1 represents that the noble gas encapsulated Pb_{12}^{2-} and Sn_{12}^{2-} clusters are thermodynamically unstable, while its positive value shows their thermodynamically stable behaviour.

Now it is important to include the dispersion correction term for accurate calculation of the structural parameters and binding energy in the Ng encapsulated Zintl ions. Therefore, we have used Grimme's approach for inclusion of this term (DFT-D3),³⁶⁵ which has been highly successful³⁶⁶ for the description of weakly interacting chemical systems. Later, to check the effect of basis set size on the structural and energetic parameters of $\text{Ng}@Pb_{12}^{2-}$ and $\text{Ng}@Sn_{12}^{2-}$ clusters, we have used aug-cc-pVTZ basis sets for noble gas atoms, while for Pb and Sn we have used the aug-cc-pVTZ-PP basis set (denoted as AVTZ). For all the clusters, the calculated structural and energetic parameters are found to be almost the same for both of these basis sets with and without the incorporation of dispersion correction.

To determine the dynamics of the noble gas encapsulated molecular cage clusters of our study, *ab initio* molecular dynamics simulation has been performed on the basis of Born-Oppenheimer molecular dynamics (BOMD) as implemented in TURBOMOLE³⁶⁴ with B3LYP/DEF optimized geometries as the starting point. Default random velocity generator in TURBOMOLE has been utilized to generate initial mass-weighted Cartesian velocities on the basis of Boltzmann velocity distribution at a particular temperature. Temperature has been maintained at specific values of 100, 298, 500, and 700 K for finite temperature simulations of clusters using a Nosé-Hoover thermostat for a total simulation time of 5000 fs with a time step of 1 fs.

6.3. Results and Discussions

6.3.1. Electronic Structure Analysis

The clusters of our study, Ng@Pb_{12}^{2-} and Ng@Sn_{12}^{2-} , exhibit an icosahedral (I_h) structure similar to that of their parent clusters, while $\text{He}_2\text{@Pb}_{12}^{2-}$, $\text{H}_2\text{@Pb}_{12}^{2-}$, and $\text{H}_2\text{@Sn}_{12}^{2-}$ exhibit D_{5d} symmetric structure at their respective minima. The pictorial representations for bare Pb_{12}^{2-} , Ng encapsulated plumbaspherene, Ng@Pb_{12}^{2-} , and Ng_2 encapsulated plumbaspherene, $\text{Ng}_2\text{@Pb}_{12}^{2-}$ are shown in Figure 6.1. The optimized structural parameters are reported in Table 6.1 and 6.2. Encapsulation of xenon atom in these clusters is not theoretically possible because their cavity size is not too large to trap the large size atom like xenon. Except $\text{He}_2\text{@Pb}_{12}^{2-}$, the optimized geometries obtained after the encapsulation of other noble gas dimers in plumbaspherene are found to be unstable because they exhibit imaginary frequencies. On the other hand, $\text{He}_2\text{@Sn}_{12}^{2-}$ system is found to be unstable at the same computational level. This suggests a greater stability of encapsulated plumbaspherene clusters as compared to those of stannaspherene. This observation may be attributed to the greater cavity size and larger HOMO–LUMO gap in Pb_{12}^{2-} as compared to that in the Sn_{12}^{2-} .

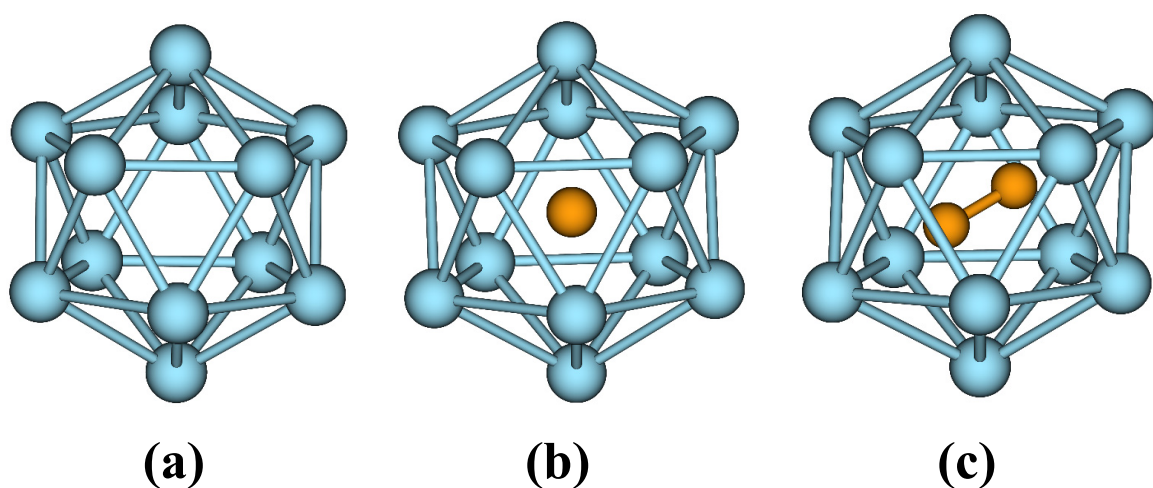


Figure 6.1. Optimized structures of (a) plumbaspherene (Pb_{12}^{2-}), (b) noble gas encapsulated Pb_{12}^{2-} , Ng@Pb_{12}^{2-} , and (c) noble gas dimer encapsulated Pb_{12}^{2-} , $\text{Ng}_2\text{@Pb}_{12}^{2-}$ as obtained by B3LYP/DEF levels of theory.

Table 6.1. Optimized Ng–Pb/Ng–Sn Distances ($R_{(\text{Ng-Pb/Ng-Sn})}$, in Å)^a, Shortest Pb–Pb/Sn–Sn Distances ($R_{(\text{Pb-Pb/Sn-Sn})}$, in Å), Dissociation Energies (BE, in kJ mol⁻¹), HOMO–LUMO Gap (ΔE_{Gap} , in eV) and NPA Charge at Noble Gas Atom (q_{Ng} in a.u.) of Ng@Pb₁₂²⁻ and Ng@Sn₁₂²⁻ (Ng = He, Ne, Ar, and Kr) Clusters Calculated at B3LYP/DEF Level.

Cluster	Sym.	$R_{(\text{Ng-Pb/Ng-Sn})}^b$	$R_{(\text{Pb-Pb/Sn-Sn})}^b$	BE	ΔE_{Gap}	q_{Ng}
Pb ₁₂ ²⁻ ^a	I _h	3.151 (3.158)	3.314 (3.321)	...	3.047	...
He@Pb ₁₂ ²⁻	I _h	3.172 (3.175)	3.335 (3.339)	-63.6	3.081	-0.028
Ne@Pb ₁₂ ²⁻	I _h	3.209 (3.204)	3.375 (3.369)	-144.8	2.825	-0.024
Ar@Pb ₁₂ ²⁻	I _h	3.321 (3.327)	3.492 (3.498)	-449.6	2.288	-0.021
Kr@Pb ₁₂ ²⁻	I _h	3.382 (3.395)	3.556 (3.570)	-616.2	1.974	-0.024
Sn ₁₂ ²⁻ ^a	I _h	3.030 (3.043)	3.186 (3.199)	...	2.720	...
He@Sn ₁₂ ²⁻	I _h	3.056 (3.069)	3.213 (3.227)	-81.6	2.720	-0.027
Ne@Sn ₁₂ ²⁻	I _h	3.098 (3.102)	3.258 (3.262)	-180.4	2.617	-0.024
Ar@Sn ₁₂ ²⁻	I _h	3.216 (3.254)	3.382 (3.421)	-529.1	2.073	-0.020
Kr@Sn ₁₂ ²⁻	I _h	3.277 (3.310)	3.446 (3.480)	-710.8	1.763	-0.022

^aIn the case of Pb₁₂²⁻ and Sn₁₂²⁻, $R_{(\text{Ng-Pb/Ng-Sn})}$ refers to the distance from the centre to the cage atoms. ^bDispersion corrected values are given in parenthesis.

In case of bare Pb₁₂²⁻ and Sn₁₂²⁻ clusters, the cage diameters are computed to be 6.303 and 6.061 Å, respectively, while the cage size is increased to some extent after noble gas encapsulation. It shows that the cages get slightly distorted while accommodating the noble gas atoms. The computed results reveal that the cage diameter increases in the range of 6.344–6.764 Å for Ng@Pb₁₂²⁻ and 6.111–6.555 Å for Ng@Sn₁₂²⁻ as we go from He to Kr. The distortion has been found to be the largest in case of He₂@Pb₁₂²⁻ with a cage diameter of 6.808 Å (*i.e.*, maximum Pb–Pb distance). The distance between the inserted noble gas atom and the cage atom is also found to increase from He to Kr in both of the clusters. The Ng–Pb distances are found to be 3.172, 3.209, 3.321, and 3.382 Å for He, Ne, Ar, and Kr, respectively. It is worth mentioning here that the Pu–Pb distance was reported to be 3.33 Å

by Pyykkö and co-workers for the Pu@Pb₁₂ cluster.³⁵⁵ We have also evaluated the distance between the dopant at the center and the cage atoms by encapsulating a dummy atom inside Pb₁₂²⁻ and Sn₁₂²⁻ clusters. As expected, the calculated distances of 3.151 and 3.030 Å for bare Pb₁₂²⁻ and Sn₁₂²⁻ clusters, respectively, are found to be lower than the Ng–Pb and Ng–Sn distance values of noble gas encapsulated clusters.

Table 6.2. Calculated Values of He–He/H–H Distances ($R_{(\text{He–He/H–H})}$, in Å), Shortest Pb–Pb/Sn–Sn Distances ($R_{(\text{Pb–Pb/Sn–Sn})}$, in Å), Dissociation Energies (BE, in kJ mol⁻¹), HOMO–LUMO Gap (ΔE_{Gap} , in eV) and NPA Charge at Encapsulated Atoms ($q_{\text{He}}/q_{\text{H}}$ in a.u.) of He₂@Pb₁₂²⁻, H₂@Pb₁₂²⁻ and H₂@Sn₁₂²⁻ Clusters as Performed at B3LYP/DEF Level.

Cluster	Symmetry	$R_{(\text{He–He/H–H})}$	$R_{(\text{Pb–Pb/Sn–Sn})}$	BE	ΔE_{Gap}	$q_{\text{He}}/q_{\text{H}}$
He ₂ @Pb ₁₂ ²⁻	D _{5d}	1.561	3.347	-265.4	2.422	-0.022
H ₂ @Pb ₁₂ ²⁻	D _{5d}	0.738	3.339	-98.0	3.079	-0.057
H ₂ @Sn ₁₂ ²⁻	D _{5d}	0.739	3.216	-116.8	2.702	-0.062

A remarkable observation is that the He–He bond length in the [He₂@Pb₁₂]²⁻ cluster is considerably shorter than that in the free He–He dimer as reported in previous papers of Ng₂ encapsulated clusters.^{193,194,215} Here, the He–He bond distance in [He₂@Pb₁₂]²⁻ is observed to be 1.561 Å, while that in free helium dimer is 3.852 Å. On the other hand, the H–H bond distances in H₂@Pb₁₂²⁻ and H₂@Sn₁₂²⁻ are found to be 0.738 and 0.739 Å, respectively, as compared to the bond length of 0.744 Å in free H₂ molecule. It indicates that helium atoms come closer to each other on confinement into the Zintl ion cages than that of the hydrogen atoms. Furthermore, the distortion in cage diameter is found to be higher in He₂@Pb₁₂²⁻ than that in H₂@Pb₁₂²⁻, as expected. These results revealed that the stability of encapsulated clusters is strongly dependent on the size of the entrapped atom.

In this context, it is of interest to compare the H–H and He–He bond lengths in the Zintl ion cages with the corresponding covalent (R_{cov}) and van der Waals (R_{vdW}) limits, defined in ‘Section 3.3.1’, following the approach of Gerry and co-workers.¹⁵³ The covalent⁴³ and van der Waals⁴⁴⁻⁴⁶ limits of the H–H bond are 0.64 and 2.40 Å, respectively, while the corresponding He–He bond length values are 0.92 and 2.86 Å considering the single bond radii of the H and He atoms. On comparison with the calculated values, it is found that the H–H bond length (0.738 Å in $\text{H}_2@\text{Pb}_{12}^{2-}$ and 0.739 Å in $\text{H}_2@\text{Sn}_{12}^{2-}$) is very close to the covalent limit, whereas the He–He bond length (1.561 Å in $\text{He}_2@\text{Pb}_{12}^{2-}$) is between the covalent and van der Waals limit. Nevertheless, the H–H bond length in H_2 encapsulated Zintl ion cages is even slightly smaller than that in free H_2 molecule (0.744 Å), indicating a strong covalent bonding between the H atoms inside the cages. On the other hand, although the He–He bond lengths in $\text{He}_2@\text{Pb}_{12}^{2-}$ is very small as compared to the free helium dimer (3.852 Å), the nature of He–He bonding inside the cages is in between the covalent and van der Waals interactions.

6.3.2. Harmonic Vibrational Frequencies

To characterize the noble gas and H_2 encapsulated Zintl ion clusters further, a harmonic vibrational frequency analysis is performed for all the clusters. The vibrational frequencies have been calculated for bare clusters, $\text{Ng}@\text{Pb}_{12}^{2-}$, $\text{H}_2@\text{Pb}_{12}^{2-}$, $\text{H}_2@\text{Sn}_{12}^{2-}$, and $\text{He}_2@\text{Pb}_{12}^{2-}$ clusters by employing B3LYP/DEF method. The H–H stretching vibrational frequencies have been found to be 4380.5 and 4323.9 cm^{-1} for $\text{H}_2@\text{Pb}_{12}^{2-}$ and $\text{H}_2@\text{Sn}_{12}^{2-}$, respectively, while the corresponding value in free H_2 molecule is slightly higher (4417.1 cm^{-1}). On the contrary, the He–He stretching vibrational frequency is 1026.9 cm^{-1} for $\text{He}_2@\text{Pb}_{12}^{2-}$, whereas the corresponding value in free helium dimer is extremely small (31.5 cm^{-1}). This trend provides a clear signature of strong interaction playing between the two He atoms

inside the plumbaspherene cage as compared to that of the free helium dimer. In this circumstance, it is worthwhile to mention that the frequency values correlate well with the optimized structural parameters. Here, it is interesting to compare the experimentally observed red-shift in the IR frequency of the H₂ molecule encapsulated inside a C₆₀ cluster. Our calculated red-shift for the H₂@Sn₁₂²⁻ cluster (93.2 cm⁻¹) is very close to the corresponding experimentally observed shift of 98.8 cm⁻¹ for the H₂@C₆₀ system.²²²

6.3.3. Energetics and Stabilities of Ng@Zintl Ions

The stability of the molecular cage clusters can be inferred from their binding energies and the HOMO–LUMO energy gaps calculated by using B3LYP/DEF level of theory (Table 6.1 and 6.2). The negative values of binding energy indicate that the process of encapsulation of noble gas atoms in Pb₁₂²⁻ and Sn₁₂²⁻ clusters is thermodynamically unfavorable. However, these noble gas inserted negatively charged clusters are kinetically stable, can be prepared, which is more elaborately dealt with in the molecular dynamics section in this Chapter. The binding energies corresponding to equation (6.1) for Ng@Pb₁₂²⁻ and Ng@Sn₁₂²⁻ clusters are from -63.6 to -616.2 kJ mol⁻¹ and from -81.6 to -710.8 kJ mol⁻¹, respectively, from He to Kr. These values suggest that the destabilization caused by noble gas encapsulation in Pb₁₂²⁻ and Sn₁₂²⁻ clusters increases with an increase in the size of the noble gas atom. It may be due to the less space available inside the Pb₁₂²⁻ and Sn₁₂²⁻ cages for the encapsulation of a larger atom like Kr. As reported in the literature on the noble gas encapsulation, it is imperative to suggest that destabilization originates from distortion in the cages as well as repulsion between electrons of the dopant and the cage atoms, both of which increase with increase in the size of the encapsulated atom. This trend of decrease in dissociation energies of Ng@Pb₁₂²⁻ and Ng@Sn₁₂²⁻ has been observed to comply well with the increase in the bond lengths of cage atoms (Pb/Sn) along the series He–Ne–Ar–Kr.

The computed values of the HOMO–LUMO gap are 3.081–1.974 eV for Ng@Pb₁₂²⁻ and 2.720–1.763 eV for Ng@Sn₁₂²⁻ along the series He–Ne–Ar–Kr, while the corresponding values for bare Pb₁₂²⁻ and Sn₁₂²⁻ clusters are 3.047 and 2.720 eV, respectively. It has also been found that the HOMO–LUMO gap in He@Pb₁₂²⁻ is slightly higher than that in the bare Pb₁₂²⁻ cluster. It is noteworthy to mention that the calculated values of the HOMO–LUMO gap of Ng encapsulated clusters further support our hypothesis that the stability of Ng@Pb₁₂²⁻ and Ng@Sn₁₂²⁻ clusters is found to reduce with an increase in the size of the noble gas atom. The larger binding energies and higher HOMO–LUMO gap values of Ng@Pb₁₂²⁻ as compared to those of Ng@Sn₁₂²⁻ indicate that noble gas entrapped Pb₁₂²⁻ clusters are more stable than the corresponding Sn₁₂²⁻ clusters.

The He₂@Pb₁₂²⁻ cluster also maintains a quite high HOMO–LUMO gap (2.422 eV), and the dissociation energy with respect to two He atoms and bare Pb₁₂²⁻ cluster is computed to be –265.4 kJ mol⁻¹, while the corresponding value for H₂@Pb₁₂²⁻ is found to be –98.0 kJ mol⁻¹, with a HOMO–LUMO gap of 3.079 eV. It indicates that encapsulation of helium dimer in Pb₁₂²⁻ cluster results in a less stable product as compared to that of hydrogen dimer in Pb₁₂²⁻. Likewise, lower binding energy and HOMO–LUMO gap values of H₂@Sn₁₂²⁻ in comparison with H₂@Pb₁₂²⁻ further reveal the greater stability of H₂ encapsulated plumbaspherene than the corresponding stannaspherene.

6.3.4. Molecular Orbital Ordering of Ng@Zintl Ions

The molecular orbital energy diagrams for Pb₁₂²⁻, Ng@Pb₁₂²⁻ and Sn₁₂²⁻, Ng@Sn₁₂²⁻ are represented in Figure 6.2. The symmetry of the HOMO and LUMO for bare plumbaspherene has been found to be t_{1u} and g_g, respectively. On the other hand, for the bare stannaspherene, the HOMO and LUMO are of h_g and g_g symmetry, respectively, although the energy difference between the t_{1u} and h_g orbitals is negligibly small. Similar to the Pb₁₂²⁻ cluster, the

HOMO and LUMO in all of the Ng@Pb_{12}^{2-} systems are found to be the t_{1u} and g_g . However, for the Ng@Sn_{12}^{2-} systems, the HOMO–LUMO ordering does not remain the same. Similar to the bare Sn_{12}^{2-} system, the h_g MO is found to be the HOMO in the He@Sn_{12}^{2-} cluster; on the other hand, the t_{1u} MO is found to be the HOMO for the other Ng@Sn_{12}^{2-} systems. As mentioned, the t_{1u} and h_g MOs are almost degenerate in the cases of Pb_{12}^{2-} and He@Pb_{12}^{2-} systems, and the energy gap between these two MOs is found to increase gradually on going from He to Kr because the h_g MO is stabilized more in going from He to Kr. The energy of the HOMO is almost the same for all of the Ng@Pb_{12}^{2-} systems including the bare Pb_{12}^{2-} cluster. Similar to the h_g MO, the LUMO (g_g) is found to be stabilized in going from He to Kr. As a result, the HOMO–LUMO gap is decreased in going from He@Pb_{12}^{2-} to Kr@Pb_{12}^{2-} cluster. Similar trends are found in the case of Ng@Sn_{12}^{2-} systems. Nevertheless, it is to be emphasized here that the HOMO and LUMO states may vary from one cluster to another depending on the encapsulated species into the respective Pb_{12}^{2-} and Sn_{12}^{2-} cages.

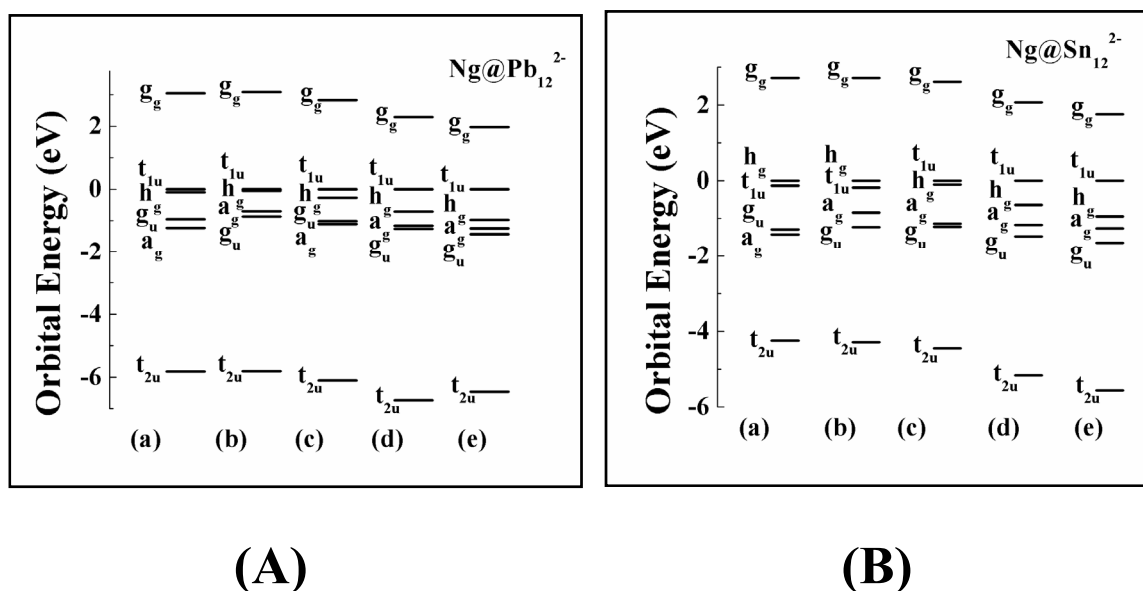
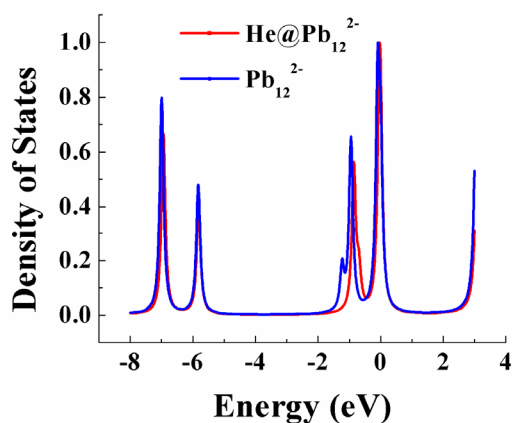
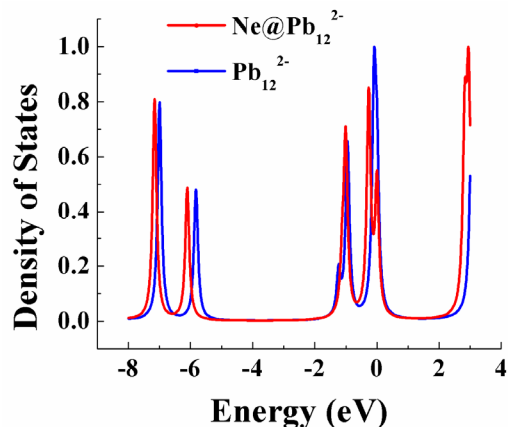


Figure 6.2. (A) Orbital energies of (a) Pb_{12}^{2-} , (b) He@Pb_{12}^{2-} , (c) Ne@Pb_{12}^{2-} , (d) Ar@Pb_{12}^{2-} , and (e) Kr@Pb_{12}^{2-} ; (B) Orbital energies of (a) Sn_{12}^{2-} , (b) He@Sn_{12}^{2-} , (c) Ne@Sn_{12}^{2-} , (d) Ar@Sn_{12}^{2-} , and (e) Kr@Sn_{12}^{2-} .

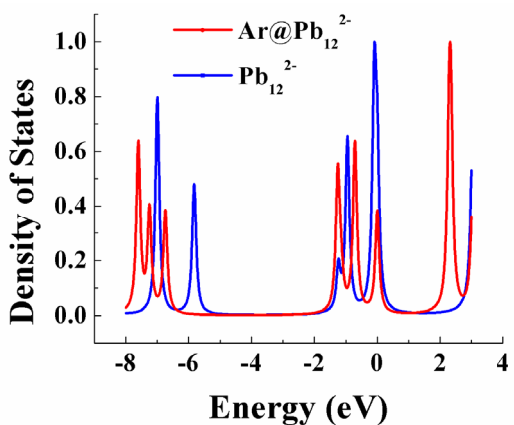
6.3.5. Density of States of Ng@Zintl Ions



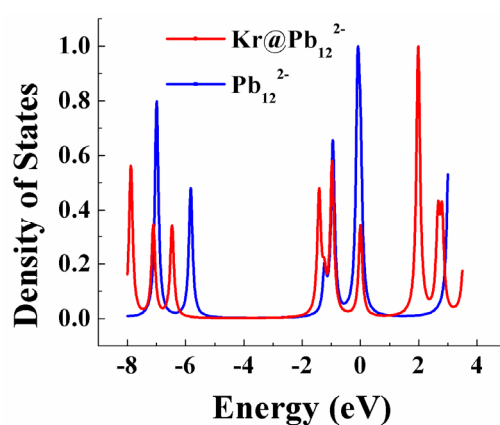
(a)



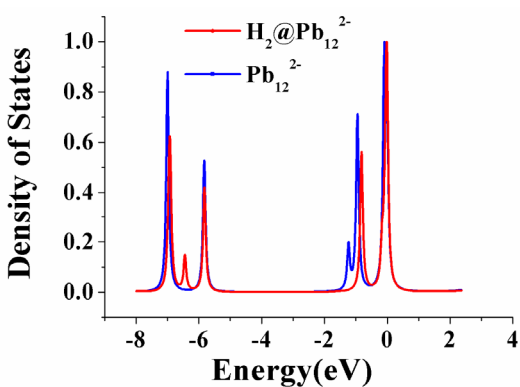
(b)



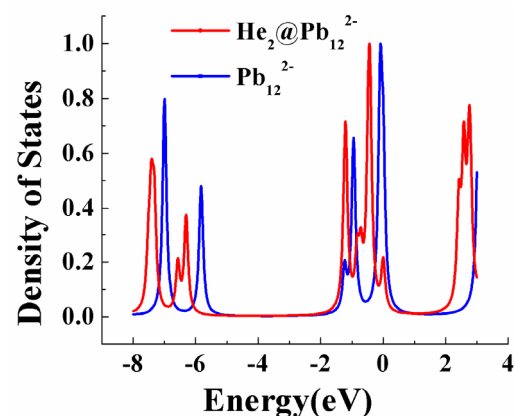
(c)



(d)



(e)



(f)

Figure 6.3. The variation of density of states (DOS) as a function of orbital energies of noble gas encapsulated Pb clusters for (a) He@Pb₁₂²⁻, (b) Ne@Pb₁₂²⁻, (c) Ar@Pb₁₂²⁻, (d) Kr@Pb₁₂²⁻, (e) H₂@Pb₁₂²⁻, and (f) He₂@Pb₁₂²⁻.

The density of states (DOS) have been studied for bare Pb_{12}^{2-} and Sn_{12}^{2-} cages and their noble gas and hydrogen molecule entrapped clusters. It has been observed that the natures of DOS plots are quite similar for both the Pb_{12}^{2-} and Sn_{12}^{2-} cages. Therefore, for simplicity we have plotted the DOS for Pb_{12}^{2-} related clusters and depicted in Figure 6.3. A profound band structure is observed around 0.00 eV (relative energy of HOMO) in both Pb_{12}^{2-} and Sn_{12}^{2-} corresponding to their valence orbitals $6p$ and $5p$, respectively. Similar band structure is observed in all of the noble gas encapsulated clusters excluding some differences. The DOS plot of He@Pb_{12}^{2-} and He@Sn_{12}^{2-} is found to be almost same as that of their parent Pb_{12}^{2-} and Sn_{12}^{2-} clusters, respectively, whereas for the neon inserted ones the DOS is shifted slightly deeper in energy although the peak positions almost remain the same. In case of Ar@Pb_{12}^{2-} , Ar@Sn_{12}^{2-} , Kr@Pb_{12}^{2-} , and Kr@Sn_{12}^{2-} , more energy levels are seen to be profound as compared to its lower analogues, and DOS is shifted deeper in energy. It is observed that the larger is the atomic radius of the encapsulated atom, the extent of shift is more for the occupied levels. Similar to the He@Pb_{12}^{2-} system, the DOS plot for the $\text{H}_2\text{@Pb}_{12}^{2-}$ system remains almost the same as in the bare Pb_{12}^{2-} cluster. Moreover, the density of states plot of $\text{He}_2\text{@Pb}_{12}^{2-}$ is found to be similar to that of Ar@Pb_{12}^{2-} in terms of the number of occupied energy levels near HOMO as well as the shift in the energy levels. All of the DOS results clearly indicate that the extent of increase of cage size coincides with the increase in the size of the encapsulated atom/molecule, which in turn modifies energies of different MOs. These results also indicate that the interaction between the cage atoms and Ng atoms becomes stronger as the size of the Ng atom increases.

6.3.6. Natural Population Analysis (NPA) of Ng@Zintl Ions

Charge distribution in the charged clusters is found to be quite different from that of neutral ones. In contrary to the previous studies on noble gas encapsulation in neutral and positively

charged clusters, here the encapsulated noble gas atom develops a slightly negative charge. This implies that the negative (-2) charge of the bare cluster is being shared by the Ng atoms via electron transfer from the cage atoms to the Ng atoms. The computed net NPA charges on encapsulated noble gas atoms have been reported in Table 6.1 and 6.2. The charges acquired by the Ng atoms are found to be -0.028 , -0.024 , -0.021 , and -0.024 a.u. for He, Ne, Ar, and Kr, respectively, in Ng@Pb_{12}^{2-} , while the corresponding values are -0.027 , -0.024 , -0.020 , and -0.022 a.u. in Ng@Sn_{12}^{2-} along the series He–Ne–Ar–Kr. These values clearly reveal that the noble gas atom acquires a small negative charge irrespective of the nature of the Ng atom or the cage atoms. This finding is in contrast to the earlier studied neutral charged Ng@cage . Electron transfer from Pb/Sn atom to the Ng atom decreases from He–Ar except for Kr as expected from their increasing positive electron affinity values. It is observed that Ng atoms inserted into Pb_{12}^{2-} clusters develop a slightly more negative charge than those in Ng@Sn_{12}^{2-} , although the cage diameter of Sn_{12}^{2-} is less as compared to that of Pb_{12}^{2-} and the fact that atoms in a smaller cavity are supposed to interact more strongly. The observed result may be due to the more electropositive nature of Pb in comparison with Sn. The computed NPA values further support our previous conclusion that the noble gas encapsulated Pb_{12}^{2-} clusters are more stable than the corresponding Sn_{12}^{2-} ones.

In this context, we have also analyzed the charge distribution on $\text{H}_2@\text{Pb}_{12}^{2-}$, $\text{H}_2@\text{Sn}_{12}^{2-}$ and $\text{He}_2@\text{Pb}_{12}^{2-}$ clusters. The calculated NPA charge on each He atom in $\text{He}_2@\text{Pb}_{12}^{2-}$ is -0.022 a.u., whereas that on each H atom in $\text{H}_2@\text{Pb}_{12}^{2-}$ is found to be -0.057 a.u.. The individual NPA charges and shared electron density values suggest more electron transfer from Pb to H atoms than to He atoms in $\text{He}_2@\text{Pb}_{12}^{2-}$, which in turn reflects strong interaction and more stable nature of $\text{H}_2@\text{Pb}_{12}^{2-}$ as compared to $\text{He}_2@\text{Pb}_{12}^{2-}$. As expected from the smaller cavity size of Sn_{12}^{2-} clusters, the H atoms in $\text{H}_2@\text{Sn}_{12}^{2-}$ gain more negative charge than that in $\text{H}_2@\text{Pb}_{12}^{2-}$, indicating stronger interaction between H and Sn atoms in

$\text{H}_2@\text{Sn}_{12}^{2-}$ than the corresponding atoms in $\text{H}_2@\text{Pb}_{12}^{2-}$. The shared electron density values of 1.213 a.u. for H–H in $\text{H}_2@\text{Pb}_{12}^{2-}$ and 1.113 a.u. for H–H in $\text{H}_2@\text{Sn}_{12}^{2-}$ suggest a strong covalent kind of interaction between the two hydrogen atoms in these clusters. However, feeble negative charges developed on the Ng atoms imply a weak van der Waals interaction between the encapsulated noble gas atom and the cage atoms. Therefore, here, we have established the fact that noble gas on confinement in electron-rich species can gain electrons despite their positive electron affinity values. Very recently, it has been shown that the noble gas atom can acquire negative charge in various Ng compounds with main group elements under high pressure (ArLi_n , XeLi_n , Ng–Mg, Na_2He , and Na_2HeO , etc.)^{247,248,361} Therefore, the effect of high pressure is somewhat similar to the confinement effect in the present work as far as charge distribution is concerned.

6.3.7. *Ab Initio* Molecular Dynamics Simulation of Ng@Zintl Ions

To determine the kinetic stability and dynamical behavior of the aforementioned clusters, *ab initio* molecular dynamics simulation has been carried out at 298 and 500 K, and their trajectories have been analyzed for 5 ps. The average Pb–Pb/Sn–Sn and Ng–Pb/Ng–Sn distances have been computed for a better analysis of these simulations. In this context, it is important to mention that the variation of total energies of $\text{Ng}@\text{Sn}_{12}^{2-}$ clusters are similar as observed in case of $\text{Ng}@\text{Pb}_{12}^{2-}$ systems. The variations in average bond distances are presented in Figure 6.4 for Ng–Pb bond and Figure 6.5 for Pb–Pb bond of the $\text{Ng}@\text{Pb}_{12}^{2-}$ cluster, while the similar behaviour have been observed in case of Sn–Sn and Ng–Sn bond distances for the $\text{Ng}@\text{Sn}_{12}^{2-}$ clusters. The variation in these parameters with respect to time gives an idea about the distortion caused by the interaction between the encapsulated atoms and the cage as well as the forces that play inside the cage. The interplay between the internal force stabilizing the system and centrifugal force inflating the cage determines the stability of

encapsulated clusters. It is observed that total energies and average Pb–Pb/Sn–Sn and Ng–Pb/Ng–Sn distances oscillate around a mean value depending on the temperature that is maintained during the simulation. These oscillations are assumed to have resulted from the increase in nuclear kinetic energies as the noble gas atom approaches the wall of the cage, which causes distortion in the $\text{Pb}_{12}^{2-}/\text{Sn}_{12}^{2-}$ cluster producing higher energy structures. It is evident from the plots that the fluctuations and the average values of bond distances increase with rise in temperature.

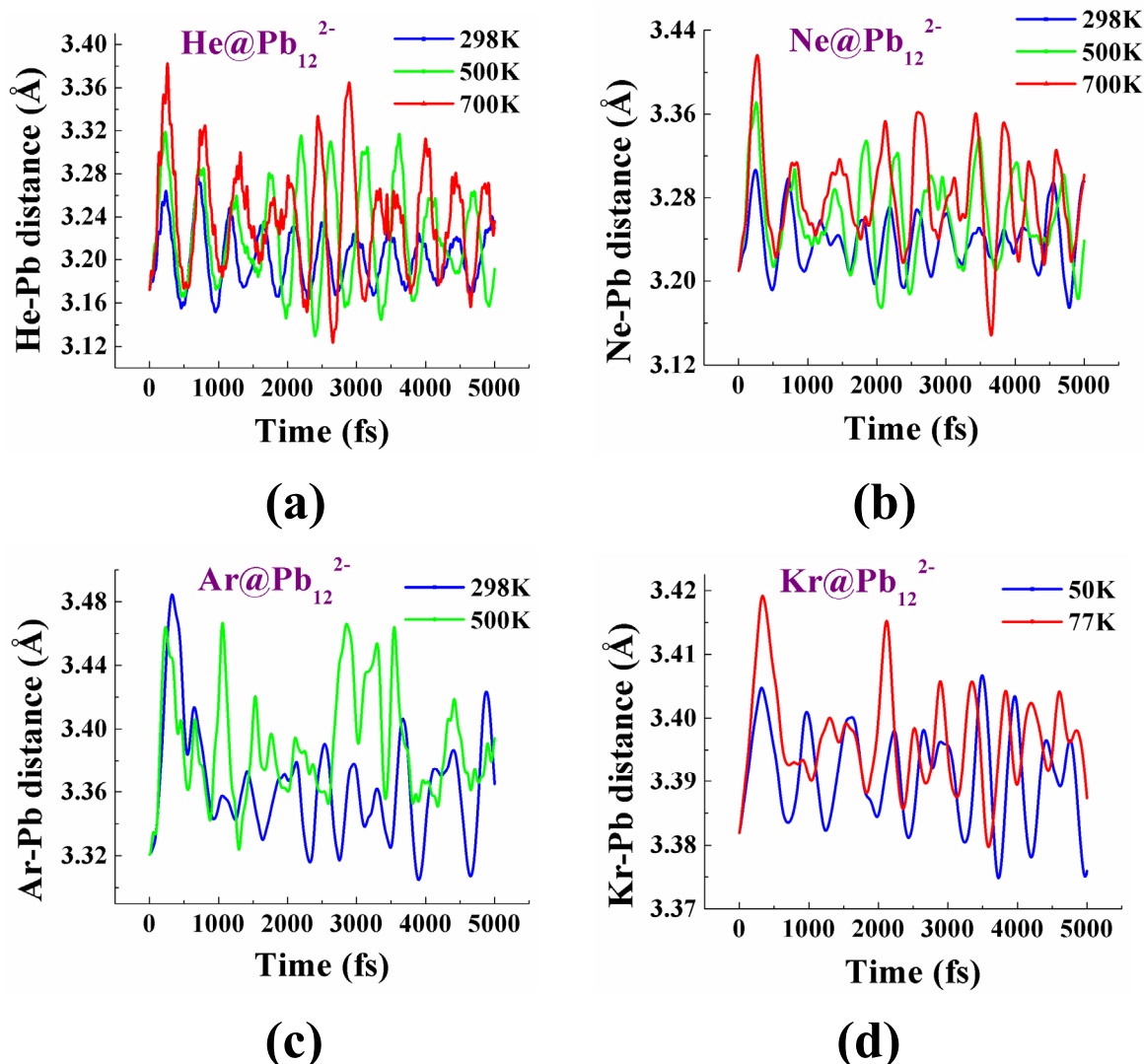


Figure 6.4. The variation in Ng–Pb distances of noble gas encapsulated Pb clusters for (a) He@Pb_{12}^{2-} , (b) Ne@Pb_{12}^{2-} , (c) Ar@Pb_{12}^{2-} , and (d) Kr@Pb_{12}^{2-} with respect to time at different temperatures during the course of molecular dynamics simulations.

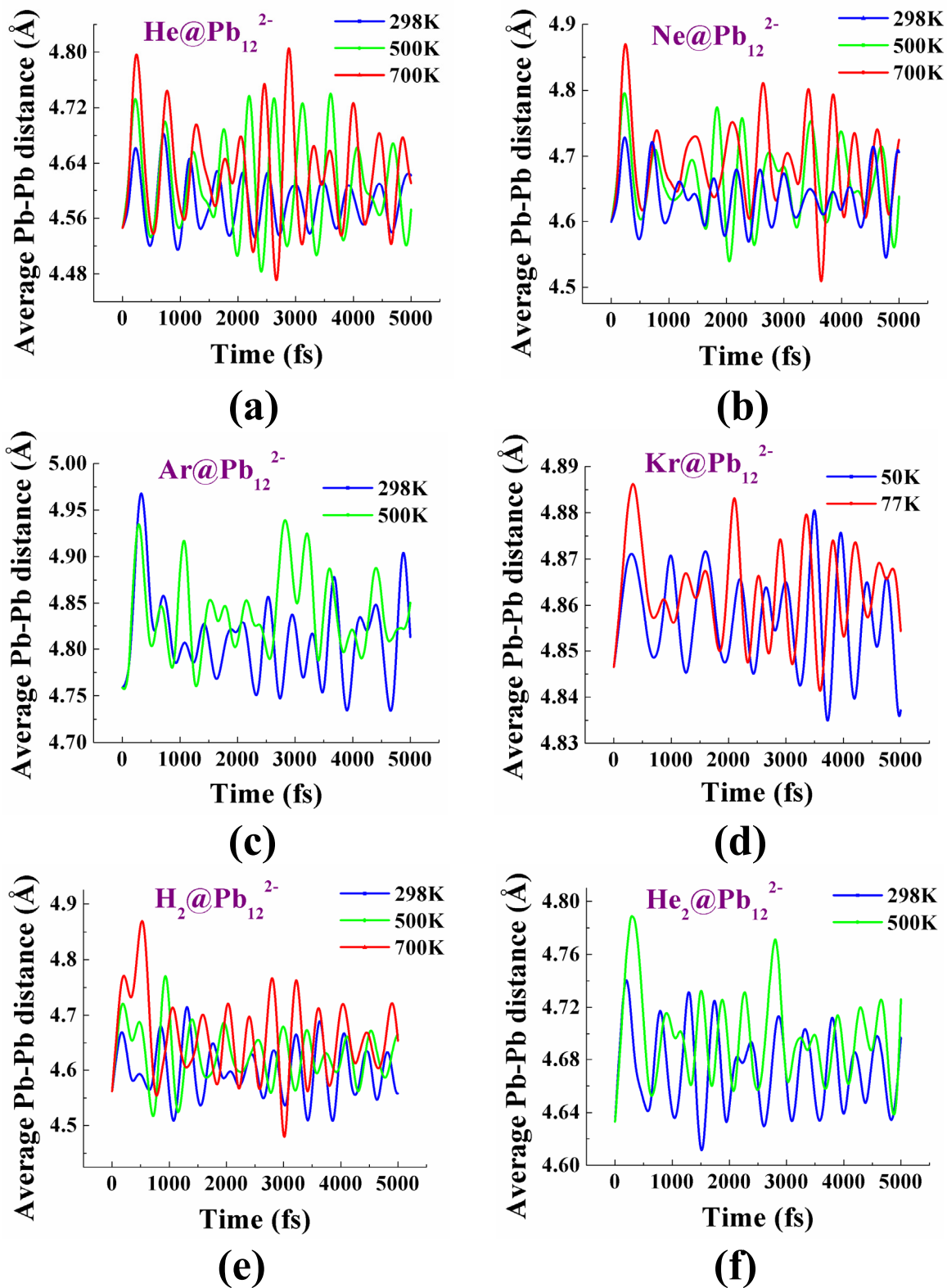


Figure 6.5. The variation in average Pb–Pb distances of noble gas encapsulated Pb clusters for (a) He@Pb_{12}^{2-} , (b) Ne@Pb_{12}^{2-} , (c) Ar@Pb_{12}^{2-} , (d) Kr@Pb_{12}^{2-} , (e) $\text{H}_2\text{@Pb}_{12}^{2-}$, (f)

$\text{He}_2@\text{Pb}_{12}^{2-}$, and bare Pb cluster (g) Pb_{12}^{2-} with respect to time at different temperatures during the course of molecular dynamics simulation.

For a better understanding of the temperature dependence on the stability of the cage clusters, we have performed MD simulations at higher temperature (700 K) as well as lower temperatures (50, 77, 100, and 150 K). Throughout the simulation, He and Ne atoms and H_2 remain within the cavity of the cages concerned, and the structural integrity of the cages is retained, except for the loss of symmetry, even at a temperature as high as 700 K. This reveals the high stability of these encapsulated clusters. However, fluctuations in the average Ng–Pb/Ng–Sn and Pb–Pb/Sn–Sn distances are found to be larger for He encapsulated clusters as compared to other Ng entrapped ones as shown in Figures 6.4 and 6.5. It is due to the smaller mass of the helium atom and the larger space available inside the cage for this atom resulting in its higher degree of movement. $\text{Ar}@\text{Pb}_{12}^{2-}$, $\text{Ar}@\text{Sn}_{12}^{2-}$, $\text{Kr}@\text{Pb}_{12}^{2-}$, and $\text{Kr}@\text{Sn}_{12}^{2-}$ clusters are found to be less stable. It is observed that the $\text{Ar}@\text{Pb}_{12}^{2-}$ cluster fragments at a high temperature of 700 K as the argon atom emerges out of the cage. However, the $\text{Ar}@\text{Sn}_{12}^{2-}$ cluster fragments in the course of MD simulation at 298 and 500 K and is stable only at lower temperatures like 150 and 100 K. The Kr encapsulated clusters are found to be even less stable. Krypton atom is observed to emerge out of the Sn_{12}^{2-} cage through a “window” mechanism as reported in fullerenes,¹⁸⁹ even at 20 K, indicating its very low stability, whereas the $\text{Kr}@\text{Pb}_{12}^{2-}$ cluster retains its structure at 77 K. It is also interesting to note that the Ng atoms come out of the distorted cage in a shorter time during simulation at higher temperatures. Here, on analyzing the simulation of $\text{Kr}@\text{Pb}_{12}^{2-}$ at 100 K, it is observed that one of the triangular faces of the cage gets distorted as Kr approaches that part of the wall of the cage. These results demonstrate that the stable clusters exist at least kinetically even if they are thermodynamically unstable. The simulation results have been observed to be

in good agreement with the geometrical parameters and energetics data. This further confirms the better stability of Ng@Pb_{12}^{2-} over Ng@Sn_{12}^{2-} clusters. In addition to the Ng atom encapsulated clusters, we have also performed simulations for the $\text{He}_2@\text{Pb}_{12}^{2-}$ and $\text{H}_2@\text{Pb}_{12}^{2-}$ clusters. The $\text{He}_2@\text{Pb}_{12}^{2-}$ cluster has been observed to retain its structure at temperatures as high as 500 K, whereas at 700 K both He atoms remain enclosed within the cage.

It is clear that the oscillations in this parameter are present for dimer encapsulated clusters also and the amplitude of vibration of H–H/He–He and X–Pb/X–Sn (where X = H/He) distances is enhanced with rise in temperature. No abrupt change in average He–He distance has been observed with respect to time. It indicates that He–He dimer inside Pb_{12}^{2-} undergoes only the usual processes of stretching and compression. From this, we can infer the existence of some sort of bonding between the two He atoms inside the cage. Therefore, we can conclude from these results that the formation and kinetic stability of the aforementioned Ng encapsulated clusters primarily depend on the size of the encapsulated moiety.

6.3.8. Electron Density Analysis of Ng@Zintl Ions

Following Bader's quantum theory of atoms-in-molecules (QTAIM)³⁰⁹ as discussed in 'Section 3.3.5', we have carried out the electron density analysis to get a better understanding of the nature of the interaction between the noble gas atom and the cage atoms as well as between the two trapped gas atoms of the noble gas and hydrogen molecule encapsulated plumbaspherene and stannaspherene cage clusters. At the bond critical point (BCP), the negative and positive values of $\nabla^2\rho(r_c)$ are related to the concentration and depletion of electron density, respectively. In general, a high value of $\rho(r_c)$ and a negative value of $\nabla^2\rho(r_c)$ at the BCP emphasize the covalent interaction, whereas a low value of $\rho(r_c)$ and positive values of $\nabla^2\rho(r_c)$ represent a "closed-shell type bonding". In the present cases, all of the

bonds are associated with a low value of $\rho(r_c)$ and a positive value of $\nabla^2\rho(r_c)$, indicating the closed-shell type bonding, except the H–H bond in both $\text{H}_2@\text{Pb}_{12}^{2-}$ and $\text{H}_2@\text{Sn}_{12}^{2-}$ clusters, which is covalent in nature.

From the results, it has been found that the Pb–Pb and Sn–Sn bonds are a combination of “type C” and “type D” bonds in all of the presently studied clusters, while the Ng–Pb and Ng–Sn bonds are considered as “type D” bond in case of all Ng encapsulated Zintl ion clusters. Therefore, it is evident that the Pb–Pb and Sn–Sn bonds are associated with a comparatively higher degree of covalency as compared to that of the corresponding Ng–Pb and Ng–Sn bonds. In case of H_2 trapped Pb_{12}^{2-} and Sn_{12}^{2-} cage clusters, the corresponding H–Pb and H–Sn bonds are found to be “type D” covalent bonds, while the H–H bond is of “type A” covalent bond in both the $\text{H}_2@\text{Pb}_{12}^{2-}$ and the $\text{H}_2@\text{Sn}_{12}^{2-}$. On the contrary, in case of the $\text{He}_2@\text{Pb}_{12}^{2-}$ cluster, the He–Pb bond can be attributed to a “type D” covalent bond, whereas the He–He bond can be assigned to be a “Wⁿ” type bond, which is due to weak interactions with some noncovalent properties. Here, it may be noted that Ng–Sn and Ng–Pb bonds are noncovalent bond of “type C” with the positive value of $\nabla^2\rho(r_c)$ in FNgSnF_3 , FNgPbF_3 , FNgSnF , and FNgPbF systems as reported by Chattaraj and co-workers³¹² recently, while in our systems, Ng–Sn and Ng–Pb bonds are a comparatively weaker noncovalent bond of “type D” with a positive value of $\nabla^2\rho(r_c)$.

6.3.9. Effect of Counterion on the Structure and Properties of $\text{Ng}@\text{Pb}_{12}^{2-}$ and $\text{Ng}@\text{Sn}_{12}^{2-}$ Clusters

Experimentally, it may be difficult to investigate the doubly negative charged $\text{Ng}@\text{Pb}_{12}^{2-}$ and $\text{Ng}@\text{Sn}_{12}^{2-}$ clusters because of an increase in the electron–electron repulsion. Therefore, we have used alkali metal cation as the counterion for balancing the excess electrons and investigated the structure and properties of anionic $\text{Ng}@\text{MPb}_{12}^-$ and $\text{Ng}@\text{MSn}_{12}^-$ and neutral

Ng@M₂Pb₁₂ and Ng@M₂Sn₁₂ clusters (M = Li and K). The structures of these systems are depicted in Figure 6.6. It has been found that the I_h structure of LiPb₁₂⁻ and LiSn₁₂⁻ anions, where Li occupies the center of the icosahedron, is the most stable. On the other hand, in the KPb₁₂⁻ and KSn₁₂⁻ anions, the K⁺ ion at the exohedral position with C_{3v} symmetry is the most stable, where the K⁺ ion is placed on the triangular face of the icosahedron. Here, it may be noted that the KPb₁₂⁻ and KSn₁₂⁻ species that have been investigated experimentally^{353,354} correspond to the C_{3v} structure, as reported earlier^{353,354} and as also obtained by us. Similarly, in the case of Li₂Pb₁₂ and Li₂Sn₁₂ clusters, the most stable structure corresponds to the one with one Li⁺ ion occupying the center of the icosahedron cage. In contrast, both K⁺ ions are found to occupy the exohedral position in the most stable structure of K₂Pb₁₂ and K₂Sn₁₂ clusters, where two K⁺ ions are placed at each of the opposite triangular face of the icosahedron resulting in D_{3d} symmetry.

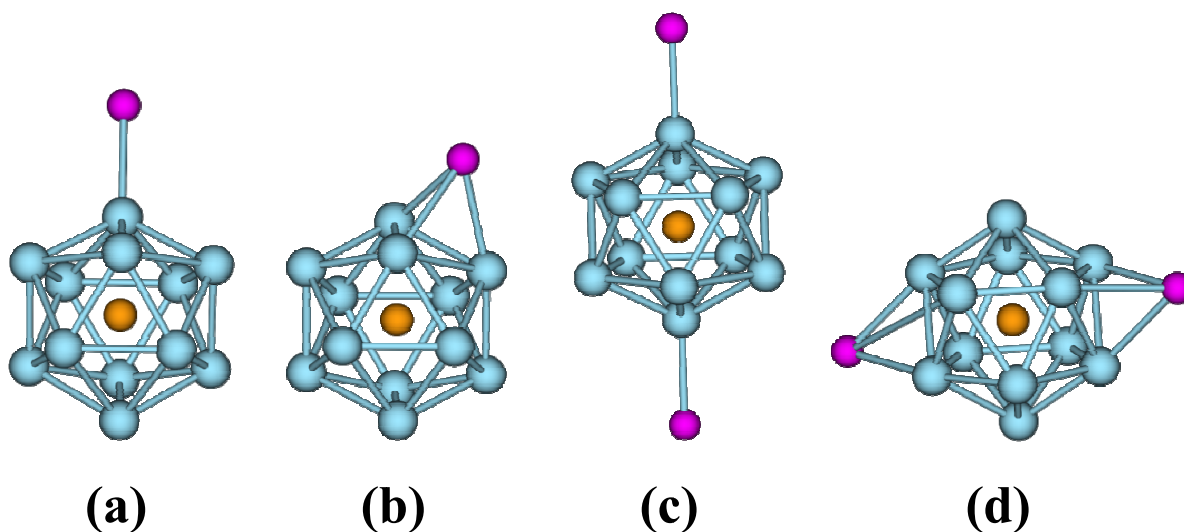


Figure 6.6. Optimized structures of (a) C_{5v} Ng@KPb₁₂⁻, (b) C_{3v} Ng@KPb₁₂⁻, (c) D_{5d} Ng@K₂Pb₁₂ and (d) D_{3d} Ng@K₂Pb₁₂ as obtained by B3LYP/DEF levels of theory.

At this point, it may be noted that the higher energy C_{5v} and D_{5d} structures (Figure 6.6) are associated with imaginary frequency. Therefore, it is clearly evident that endohedral encapsulation of an Ng atom is not possible within the LiPb₁₂⁻, LiSn₁₂⁻, Li₂Pb₁₂, and Li₂Sn₁₂

cages. Accordingly, we have investigated the Ng encapsulated structures of KPb_{12}^- , KSn_{12}^- , K_2Pb_{12} , and K_2Sn_{12} clusters by calculating the optimized structures, binding energies, HOMO-LUMO gaps, vibrational frequencies, charges, etc. The addition of K^+ ion(s) does not lead to any significant change in the Pb–Pb or Sn–Sn bond length. However, slightly smaller HOMO–LUMO gaps have been found after the addition of K^+ ion(s) in the Ng@Pb_{12}^{2-} and Ng@Sn_{12}^{2-} clusters. Charge on the K atom in these clusters is found to be in the range of 0.80–0.87 a.u. and 0.91–0.94 a.u. for the monopotassium and dipotassium clusters, respectively, indicating that all of these clusters can best be described as $[\text{K}^+\text{Ng@M}_{12}^{2-}]$ and $[2\text{K}^+\text{Ng@M}_{12}^{2-}]$. It is important to note that the calculated binding energy values are found to be positive, which indicates that the K^+ ion(s) stabilized noble gas encapsulated Zintl clusters are thermodynamically stable. It is in contrast to the Ng encapsulated bare Zintl ions.

6.3.10. Energy Decomposition Analysis

Energy decomposition analysis (EDA) is a very powerful method for analyzing the intermolecular interaction in any system using either Hartree–Fock method or density functional theory. To know the nature of interaction between the Ng atom and the host cluster ($\text{Pb}_{12}^{2-}/\text{Sn}_{12}^{2-}$) in Ng@Pb_{12}^{2-} and Ng@Sn_{12}^{2-} systems, we have performed energy decomposition analysis as implemented in GAMESS³⁰¹ by Su and Li³⁶⁷ using the B3LYP/DEF level of theory including dispersion interaction. For EDA calculations, clusters have been considered to dissociate into two fragments, Ng atom and $\text{Pb}_{12}^{2-}/\text{Sn}_{12}^{2-}$ cluster, and the interaction energy is decomposed into electrostatic, exchange, repulsion, polarization, and dispersion terms. Thus, decomposition energy can be expressed as $\Delta E = \Delta E_{\text{ele}} + \Delta E_{\text{ex}} + \Delta E_{\text{rep}} + \Delta E_{\text{pol}} + \Delta E_{\text{disp}}$. The energy terms ΔE_{ele} , ΔE_{ex} , ΔE_{pol} , and ΔE_{disp} are all attractive in nature, while the ΔE_{rep} term is repulsive in nature. The percentage contribution of the attractive energy term, ΔE_{ele} , to the total attractive interaction has been found to be 21.5, 35.5, 37.1,

37.4, 21.8, and 22.9 for the Ng@Pb₁₂²⁻ systems (Ng = He, Ne, Ar, Kr), and the He₂@Pb₁₂²⁻ and H₂@Pb₁₂²⁻ systems, respectively, while the same has been found to be 23.4, 38.5, 40.4, 40.3, and 22.6 for the corresponding Sn₁₂²⁻ systems.

However, in all of these systems, the percentage of the exchange term is higher and is in the range of 41.4–45.0 and 41.9–42.7 for Pb₁₂²⁻ and Sn₁₂²⁻ systems, respectively. Very small percentage contribution has been found for the polarization (7.3–22.3 for Pb₁₂²⁻ and 8.7–25.1 for Sn₁₂²⁻) and dispersion terms (8.0–19.2 for Pb₁₂²⁻ and 6.3–14.3 for Sn₁₂²⁻). Among all terms, the repulsive term has been found to be most dominating term that makes the overall interaction energy repulsive in nature. Thus, the larger repulsion between the noble gas atom and the cluster leads to thermodynamically unstable noble gas atom encapsulated Zintl ions. Furthermore, all energy terms are found to increase with the size of noble gas atom. However, we have found a tremendous increase in the repulsive term (ΔE_{rep}) as compared to increase in attractive energy terms (ΔE_{ele} , ΔE_{ex} , ΔE_{pol} , and ΔE_{disp} taken together). Consequently, large size Ng atom encapsulated systems are found to be more unstable.

Subsequently, we have done the energy decomposition analysis for the Ng@KPb₁₂⁻, Ng@KSn₁₂⁻, Ng@K₂Pb₁₂, and Ng@K₂Sn₁₂ systems. For the EDA calculation, chosen fragments are Ng atom, K⁺ ion, and Pb₁₂²⁻ or Sn₁₂²⁻ cluster. In Ng@KPb₁₂⁻ and Ng@KSn₁₂⁻ clusters, the ΔE_{ele} term has a percentage contribution of 67.5, 63.8, 59 and 64.9, 61.8, 51.1, respectively, in the total attractive interaction energy of the systems along the series, He–Ne–Ar. Unlike Ng@Pb₁₂²⁻ and Ng@Sn₁₂²⁻ systems, in Ng@K₂Pb₁₂ and Ng@K₂Sn₁₂ systems the contribution from the ΔE_{ele} term has been found to be tremendously higher with percentage contributions of 76.5, 73.2, and 64.8 in Ng@K₂Pb₁₂ systems, and 74.9, 71.5, and 63.0 in Ng@K₂Sn₁₂ systems along the He–Ne–Ar series. Besides, a repulsive term (ΔE_{rep}) is found to be smaller as compared to the attractive term (ΔE_{ele}), in Ng@KPb₁₂⁻, Ng@KSn₁₂⁻,

Ng@K₂Pb₁₂, and Ng@K₂Sn₁₂ systems. In all of the systems, the ΔE_{ele} is the most negative, and therefore makes the overall energy of the system attractive in nature. However, with increase in the size of the noble gas atom, we have found a significant decrease in percent contribution from ΔE_{ele} terms, which in turn reduces the attractive interaction between the large size noble gas atom and the Zintl ions. Therefore, large size noble gas encapsulated Zintl ion clusters are found to be less stable as compared to the small size noble gas atom encapsulated Zintl ion clusters.

Moreover, to know the nature of chemical bonding between Ng–Pb/Ng–Sn, Pb–Pb/Sn–Sn, and K–Pb/K–Sn, we have also calculated the bond critical point properties for the Ng@KPb₁₂[–], Ng@KSn₁₂[–], Ng@K₂Pb₁₂, and Ng@K₂Sn₁₂ systems. In the Ng@KPb₁₂[–] and Ng@KSn₁₂[–] systems, Pb–Pb/Sn–Sn bonding is of “type C” and “type D” covalent bond, while Ng–Pb/Ng–Sn chemical bonding is of “type D”, analogous to the same in the Ng@Pb₁₂^{2–} and Ng@Sn₁₂^{2–} systems. Also, the K–Pb/K–Sn bonding is of “type D”. Similar bonding trends are found in the Ng@K₂Pb₁₂ and Ng@K₂Sn₁₂ clusters.

6.3.11. Energy Barrier Calculation

Energy barrier provides an important aspect regarding the kinetic stability of clusters. We have calculated energy barrier for the He-encapsulated clusters, He@Pb₁₂^{2–}, He@Sn₁₂^{2–}, He@KPb₁₂[–], He@KSn₁₂[–], He@K₂Pb₁₂, and He@K₂Sn₁₂, by moving the He atom from its equilibrium position to outside the cage through the triangular face of the C_{3v} and D_{3d} structures for the mono- and di-potassium cases, respectively. Naturally, when the He atom is located at the surface, the energy of the system attains its maximum value, and the difference between this energy and the energy corresponding to the He atom encapsulated equilibrium geometry can be considered as the approximate energy barrier. The calculated values of energy barrier are 592.7, 580.2, 563.0, 584.4, 591.5, and 628.7 kJ mol^{–1} for He@Pb₁₂^{2–},

He@Sn₁₂²⁻, He@KPb₁₂⁻, He@KSn₁₂⁻, He@K₂Pb₁₂, and He@K₂Sn₁₂ clusters, respectively. Thus, all of the He-encapsulated clusters are found to be kinetically stable because of the very high energy barrier. Therefore, once the He-encapsulated clusters are formed, they cannot dissociate into its fragments due to the very high energy barrier. The barrier height will be even larger for other Ng-encapsulated clusters because of the larger size of the Ng atom.

6.4. Concluding Remarks

In summary, we have predicted the theoretical existence and kinetic stability of noble gas encapsulated plumbaspherene and stannaspherene cage clusters, Ng@Pb₁₂²⁻ and Ng@Sn₁₂²⁻, through systematic calculations of the electronic structure optimization and *ab initio* molecular dynamics simulation. Similar to the bare Pb₁₂²⁻ and Sn₁₂²⁻ clusters, the Ng encapsulated analogues are also found to maintain comparable HOMO–LUMO energy gap values, revealing their electronic stability. Structural parameters, calculated at the B3LYP/AVTZ level and dispersion corrected B3LYP/DEF level, are found to be in good agreement with the B3LYP/DEF level calculated parameters. Moreover, we have also predicted the structural parameters corresponding to the counterion containing Ng@KPb₁₂⁻, Ng@KSn₁₂⁻, Ng@K₂Pb₁₂, and Ng@K₂Sn₁₂ systems, which are found to be very similar to the Ng@Pb₁₂²⁻ and Ng@Sn₁₂²⁻ systems and are bonded by weak noncovalent type of interaction similar to Ng@Pb₁₂²⁻ and Ng@Sn₁₂²⁻ systems. The possible existence of He₂@Pb₁₂²⁻ has also been established through the DFT and *ab initio* MD simulation-based techniques. The basic concept that noble gas atoms with highly positive electron affinity values cannot gain electrons is not obeyed here because Ng atoms in the present systems develop a small negative charge via electron transfer from Pb/Sn atoms to the Ng atom. The computed values of structural parameters, energetics, and natural population analysis suggest the existence of a weak van der Waals interaction between the Ng and the cage atoms. *Ab*

initio molecular dynamics simulation shows that He, Ne, and H₂ encapsulated Pb₁₂²⁻ and Sn₁₂²⁻ clusters remain intact up to 5000 fs even at temperatures as high as 700 K. However, Kr@Sn₁₂²⁻ cluster is found to fragment at 20 K itself, while Kr@Pb₁₂²⁻, Ar@Pb₁₂²⁻, Ar@Sn₁₂²⁻, and He₂@Pb₁₂²⁻ are found to retain their structural integrity at 77, 500, 150, and 500 K, respectively. The fact that encapsulated atoms with larger atomic radii distort the cage to a greater extent has been established through geometrical parameters and simulation data. EDA has revealed that in all of the Ng encapsulated clusters, the repulsive term is more predominant as compared to the attractive terms, except in Ng@KPb₁₂⁻, Ng@KSn₁₂⁻, Ng@K₂Pb₁₂, and Ng@K₂Sn₁₂ systems. Furthermore, a very high energy barrier has been observed for He@Pb₁₂²⁻, He@Sn₁₂²⁻, He@KPb₁₂⁻, He@KSn₁₂⁻, He@K₂Pb₁₂, and He@K₂Sn₁₂ systems. All of these findings indicate that, although the Ng encapsulated dianionic cage clusters are thermodynamically unstable with respect to dissociation into noble gas atoms, they are kinetically stable. Nevertheless, Ng@KPb₁₂⁻, Ng@KSn₁₂⁻, Ng@K₂Pb₁₂, and Ng@K₂Sn₁₂ systems are found to be kinetically as well as thermodynamically stable. The insertion of noble gas atoms into C₆₀ fullerenes and the synthesis of He@C₂₀H₂₀ have already been reported.^{208,210} Experimental observations^{353,354} of KPb₁₂⁻ and KSn₁₂⁻ and very recent experimental preparations^{247b} of noble gas compounds with main group elements under high pressure along with recent theoretical investigations^{360,361} suggest that it might be possible to identify the alkali metal cation stabilized endohedral noble gas encapsulated Zintl ions experimentally. Our present work will encourage further studies toward the possible realization of Ng@Pb₁₂²⁻ and Ng@Sn₁₂²⁻ clusters experimentally, analogous to noble gas atom encapsulated fullerenes and related systems.

Chapter 7. Summary and Outlook

In this concluding chapter, we summarize all the works discussed throughout the thesis as well as possible future perspectives of the work that can be inferred from our previous discussions. In this thesis we have made an attempt to understand the electronic structure, properties and reactivity of different kinds of noble gas containing chemical compounds. The study of chemical bonding and reactivity is of immense interest due to its enormous importance in diverse areas of chemical and physical science. In fact, in recent times, the computational chemistry has been proven to be a rationally versatile tool in obtaining meaningful insights into the functioning of various chemical systems and processes. Therefore, the theoretical modeling approach can only provide a better way to predict new novel noble gas containing chemical systems. It is worthwhile to mention that the first principle based *ab initio* quantum chemical calculations have been widely used to explore various properties of several solid, liquid and gaseous materials over the past few decades. In this context, *ab initio* density functional theory (DFT) and post-Hartree-Fock based electronic structure calculations have been established to be highly successful in predicting many ground state electronic properties of a large number of chemical systems. Although, accurate estimation of the bonding energies and measure of reactivity in small molecules can in principle be obtained through *ab initio* quantum mechanical calculations, understanding this prediction in terms of simple chemical concepts is an equally important and interesting topic of investigation. The work presented in this thesis has been carried out by density functional theory (DFT) as well as post-Hartree-Fock based methods which provide alternative appealing frameworks for the quantum mechanical study of electronic structure and properties. In the present thesis we have made an attempt to provide clear theoretical insights into the nature of interaction between the noble gas atom and the constituent atoms of the

concerned molecular system of interest by using *ab initio* density functional theory, perturbation theory and coupled cluster theory based methods.

Chapter 1 outlines history of discovery of noble gas elements and its compounds with distinctive physical and chemical properties. This introductory chapter also highlights the enormous importance of noble gas containing chemical compounds, *viz.*, noble gas insertion compounds, super strong van der Waals complexes and noble gas encapsulated clusters in the field of astronomical science, environmental science, basic fundamental science and potential application in medicinal biology and nuclear waste management. It emphasizes the prerequisite knowledge of chemical intuition and understanding of nature of interaction between the constituent elements in order to choose the chemical system which can form conventional chemical bond with the noble gas atom. This concept is also essential for the formation of exceptionally strong noble gas-noble metal bond and noble gas encapsulated molecular cage clusters. Moreover, we have also provided some commonly used experimental techniques to prepare and characterize these noble gas compounds.

It is well established that theoretical modeling is an essential tool for better understanding on the complexation or encapsulation behavior of any molecular system or cluster towards Ng atom(s). Chapter 2 describes the significance of computational methods which can only provide some of the most valuable information that experiments cannot. It includes a brief outline of the computational methodologies which have been used to investigate the noble gas containing chemical systems. This chapter also highlights the essential description of quantum mechanics, including DFT followed by some post-Hartree–Fock-based correlated methods employed for our calculations.

In Chapter 3, we have proposed the possibility of existence of few novel class of fascinating compounds obtained through the insertion of a noble gas atom into the molecules of interstellar origin. The new class of noble gas containing cationic and neutral species, *viz.*,

HNgOH_2^+ , HNgBF^+ , XNgCO^+ , HNgCS^+ , HNgOSi^+ , FNgBS , and FNgCX (Ng = Noble Gas, X = Halides) have been investigated by various *ab initio* quantum chemical techniques. DFT, MP2, and CCSD(T) based techniques have been used to explore the structure, energetics, charge distribution, and harmonic vibrational frequencies of these compounds in their respective singlet potential energy surfaces. All the predicted species are found to be thermodynamically stable with respect to all possible 2-body and 3-body dissociation channels, except the dissociation path leading to the respective global minimum products. Nevertheless, all these compounds are found to be kinetically stable with finite barrier heights corresponding to their transition states, which are connected to their respective global minima products. The atoms-in-molecules (AIM) analysis strongly reveals that there exists conventional chemical bonding with the noble gas atom in all the predicted compounds. Successful experimental identification of our earlier predicted Ng insertion compound (HXeOBr) by Khriachtchev *et al.*¹⁶¹ indicates that it may be possible to identify all the predicted singlet metastable noble gas insertion compounds through suitable experimental technique(s).

For the first time, in a bid to predict neutral noble gas chemical compounds in their triplet electronic state, a systematic investigation of noble gas inserted pnictides, FNgY (Ng = Kr and Xe; Y = N, P, As, Sb and Bi) species have been discussed in Chapter 4. Density functional theory and various post-Hartree-Fock-based correlated methods, including the multireference configuration interaction technique have been employed to elucidate the structure, energetics, charge distribution, and harmonic vibrational frequencies. Further extending the prediction of noble gas chemical compounds in the triplet state, we have explored a new series of noble gas hydrides in the triplet ground electronic state for the first time by employing similar methods. All the predicted species are found to be thermodynamically stable with respect to all possible 2-body and 3-body dissociation

channels except the global minima products. Nevertheless, high barrier height values corresponding to the transition state, connecting the metastable species to their respective global minima products, ensures the kinetic stability of those species. Experimental detection of open-shell noble gas insertion compounds like ${}^2\text{HXeO}$ and ${}^2\text{HXeCC}$ by Khriachtchev and co-workers^{r152,176a,180b} clearly indicates that it may also be possible to prepare and characterize the predicted triplet metastable noble gas insertion compounds through suitable experimental technique(s) under cryogenic environment.

The unprecedented enhancement of noble gas–noble metal bonding strength in NgM_3^+ (Ng = Ar, Kr, and Xe; M = Cu, Ag, and Au) ions through hydrogen doping have been explored by employing various *ab initio* based techniques. Chapter 5 provides an in-depth theoretical insight into the nature of interaction between the noble metal and noble gas atom which is of immense interest since both the elements are extremely reluctant to form any chemical bonds to other element in the periodic table. Detail optimized structural parameters, energetics, vibrational frequency, charge distribution values have been reported using DFT, MP2, and CCSD(T) based methods with different basis sets. It has been found that among all the predicted $\text{NgM}_{3-k}\text{H}_k^+$ complexes ($k = 0-2$), the strongest Ng–M bonding has been observed in NgMH_2^+ complex, particularly, in case of ArAuH_2^+ complex. The concept of gold–hydrogen analogy makes it possible to evolve this pronounced effect of hydrogen doping in Au-trimers leading to the strongest Ng–Au bond in NgAuH_2^+ species. Very recent successful experimental identification of Ar-complexes of mixed noble metal clusters, $\text{Ar}_k\text{Au}_n\text{Ag}_m^+$ ($n + m = 3$; $k = 0-3$) by Fielicke and co-workers³³⁷ clearly indicate that it is possible to experimentally realize the predicted species, NgMH_2^+ with suitable technique(s).

Chapter 6 deals with the selective encapsulation of noble gas atom inside the inorganic fullerene clusters. The theoretical existence and thermodynamic stability of noble gas encapsulated endohedral Zintl ions, $\text{Ng}@M_{12}^{2-}$ (Ng = He, Ne, Ar, and Kr; M = Sn and

Pb), have been investigated through density functional theory while the kinetic stability of the clusters have been studied through *ab initio* molecular dynamics simulation. Detail optimized structural parameters, binding energies, vibrational frequencies, and charge distribution values are reported by employing DFT based methods for noble gas encapsulated plumbaspherene, [Ng@Pb₁₂²⁻] and stannaspherene, [Ng@Sn₁₂²⁻] cage clusters. It has been found that the Ng@M₁₂²⁻ clusters are kinetically stable and thermodynamically unstable whereas the K⁺ salt of Ng@M₁₂²⁻ clusters are found to be both kinetically as well as thermodynamically stable. Therefore, our results would incite further studies into the experimental methods through which these molecular carriers for noble gas atoms can be produced.

To conclude, we can emphasize that the preparation and characterization of novel unique noble gas containing chemical systems by suitable experimental techniques will be most fascinating as well as highly challenging task to the experimentalists. At the same time, considering the importance of these type of noble gas containing chemical compounds in diverse fields, high level theoretical calculations are also exceedingly demanding to explore the feasibility of occurrence of these species in the universe. Moreover, the endohedral encapsulation of noble gas atom in inorganic analogues of fullerene is also a new concept and till now limited theory or lab scale identification has been pursued. Therefore, working in this area is also very challenging and it is a potential area of research for both the theoreticians and experimentalists. In a nutshell, being the follower of Prof. Neils Bartlett towards exploring the possibility of existence of noble gas compounds, we have contributed to the science by predicting new chemical systems involving noble gas atom which certainly alter the fundamental perception of ‘unreactive’ nature of ‘inert’ noble gas elements.

References:

1. (a) H. Cavendish, *Philos. Trans. Roy. Soc. (London)*, 1785, 106; (b) H. Cavendish, *Philos. Trans. Roy. Soc. (London)*, 1786, 241; (c) H. Cavendish, *Philos. Trans. Roy. Soc. (London)*, 1790, 101.
2. (a) L. Rayleigh, *Nature*, 1892, **46**, 512; (b) L. Rayleigh, *Proc. Roy. Soc. (London)*, 1893, **53**, 134.
3. (a) L. Rayleigh, W. Ramsay, *B. A. Rep.*, 1894, 614; (b) L. Rayleigh, *Roy. Soc. Proc. (London)*, 1894, **55**, 340; (c) L. Rayleigh, *Roy. Inst. Proc. (London)*, 1895, **14**, 524.
4. W. Crookes, *Philos. Trans. Roy. Soc. (London) A*, 1895, **186**, 243.
5. L. Rayleigh, W. Ramsay, *Roy. Soc. Proc. (London)*, 1894-1895, **57**, 265.
6. W. F. Hillebrand, *J. Am. Chem. Soc.*, 1895, **17**, 718.
7. W. Crookes, *Nature*, 1895, **52**, 428.
8. J. N. Lockyer, *Roy. Soc. Proc. (London)*, 1895, **58**, 67.
9. (a) W. Ramsay, *Roy. Soc. Proc. (London)*, 1895, **58**, 65; (b) W. Ramsay, *Nature*, 1895, **52**, 224; (c) W. Ramsay, *Nature*, 1895, **52**, 544.
10. (a) W. Ramsay, J. N. Collie and M. W. Travers, *J. Chem. Soc., Trans.*, 1895, **67**, 684; (b) W. Ramsay, *Science*, 1897, **6**, 493; (g) W. Ramsay and M. W. Travers, *Roy. Soc. Proc. (London)*, 1898, **62**, 225.
11. W. Ramsay and M. W. Travers, *Roy. Soc. Proc. (London)*, 1898, **63**, 405.
12. W. Ramsay and M. W. Travers, *Roy. Soc. Proc. (London)*, 1898, **63**, 437.
13. (a) W. Ramsay and M. W. Travers, *Nature*, 1898, **58**, 545; (b) W. Ramsay, *Roy. Soc. Proc. (London)*, 1899, **64**, 181; (c) W. Ramsay and M. W. Travers, *Roy. Soc. Proc. (London)*, 1899, **64**, 183.
14. F. E. Dorn, *Abh. Natur. J. Ges. Halle.*, 1901, **23**, 1.
15. (a) E. Rutherford and F. Soddy, *Philos. Mag.*, 1902, **4**, 370; (b) E. Rutherford and F. Soddy, *Philos. Mag.*, 1902, **4**, 569.
16. F. W. Aston, G. P. Baxter, B. Brauner, A. Debiere, A. Leduc, T. W. Richards, F. Soddy and G. Urbain, *J. Am. Chem. Soc.*, 1923, **45**, 867.
17. W. Ramsay and J. N. Collie, *Roy. Soc. Proc. (London)*, 1904, **73**, 470.
18. (a) R. W. Gray and W. Ramsay, *J. Chem. Soc., Trans.*, 1909, **95**, 1073; (b) R. W. Gray and W. Ramsay, *J. Chem. Soc., Trans.*, 1910, **97**, 185; (c) R. W. Gray and W. Ramsay, *Roy. Soc. Proc. (London)*, 1911, **84**, 536.

19. J. E. Cederblom, “The Nobel Prize in Physics 1904 Presentation Speech”
<https://www.nobelprize.org/prizes/physics/1904/ceremony-speech/>
20. J. E. Cederblom, “The Nobel Prize in Chemistry 1904 Presentation Speech”
<https://www.nobelprize.org/prizes/chemistry/1904/ceremony-speech/>
21. (a) D. Porcelli, C. J. Ballentine and R. Wieler, *Rev. Mineral. Geochem.*, 2002, **47**, 1;
 (b) D. Porcelli and C. J. Ballentine, *Rev. Mineral. Geochem.*, 2002, **47**, 411.
22. P. Sarda, T. Staudacher and C. J. Allègre, *Earth Planet. Sci. Lett.*, 1985, **72**, 357.
23. (a) J. Dymond and L. Hogan, *Earth Planet. Sci. Lett.*, 1973, **20**, 131; (b) H. Craig and J. Lupton, *Earth Planet. Sci. Lett.*, 1976, **31**, 369; (c) M. Ozima and G. Igarashi, *Earth Planet. Sci. Lett.*, 2000, **176**, 219.
24. (a) M. Honda, I. McDougall, D. B. Patterson, A. Doulgeris and D. A. Clague, *Nature*, 1991, **349**, 149; (b) R. Salvaterra, M. Della Valle, S. Campana, G. Chincarini, S. Covino, P. D’Avanzo, A. Fernández-Soto, C. Guidorzi, F. Mannucci, R. Margutti, *et al.*, *Nature*, 2009, **461**, 1258.
25. C. J. Ballentine, P. E. van Keken, D. Porcelli and E. H. Hauri, *Phil. Trans. Roy. Soc. (London) A*, 2002, **360**, 2611.
26. C. J. Ballentine and P. G. Burnard, *Rev. Mineral. Geochem.*, 2002, **47**, 481.
27. (a) M. Ozima, K. Seki, N. Terada, Y. N. Miura, F. A. Podosek and H. Shinagawa, *Nature*, 2005, **436**, 655; (b) M. Ozima, R. Wieler, B. Marty and F. A. Podosek, *Geochim. Cosmochim. Acta*, 1998, **62**, 301; (c) F. A. Podosek, M. Honda and M. Ozima, *Geochim. Cosmochim. Acta*, 1980, **44**, 1875.
28. (a) P. Burnard, D. Graham and G. Turner, *Science*, 1997, **276**, 568; (b) G. Holland and C. J. Ballentine, *Nature*, 2006, **441**, 186; (c) M. Moreira, J. Kunz and C. Allègre, *Science*, 1998, **279**, 1178.
29. M. Ozima and F. A. Podosek, *J. Geophys. Res.*, 1999, **104**, 25493.
30. I. Tolstikhin, B. E. Lehmann, H. H. Loosli and A. Gautschi, *Geochim. Cosmochim. Acta*, 1996, **60**, 1497.
31. (a) E. Mazor, *Geochim. Cosmochim. Acta*, 1972, **36**, 1321; (b) E. Mazor, M. Molcho, *J. Hydrol.*, 1972, **15**, 37; (c) E. Mazor and A. Bosch, *Appl. Geochem.*, 1987, **2**, 621.
32. J. Matsuda and K. Nagao, *Geochem. J.*, 1986, **20**, 71.
33. (a) C. J. Ballentine, R. K. O’Nions and M. L. Coleman, *Geochim. Cosmochim. Acta*, 1996, **60**, 831; (b) D. L. Pinti and B. Marty, *Geochim. Cosmochim. Acta*, 1995, **59**, 3389.

34. J. –C. Fontes, J. N. Andrews, W. M. Edmunds, A. Guerre and Y. Travi, *Water Resour. Res.*, 1991, **27**, 199.
35. N. C. Sturchio, X. Du, R. Purtschert, B. E. Lehmann, M. Sultan, L. J. Patterson, Z. – T. Lu, P. Müller, T. Bigler, K. Bailey, *et al.*, *Geophys. Res. Lett.*, 2004, **31**, L05503.
36. N. F. Mott, *Biogr. Mem. Fell. Roy. Soc.*, 1955, **1**, 174.
37. F. Grandinetti, *Noble Gas Chemistry: Structure, Bonding, and Gas-Phase Chemistry*, ed., Wiley-VCH, Weinheim, Germany, 2018.
38. N. N. Greenwood and A. Earnshaw, *Chemistry of the Elements* (2nd ed.), Oxford : Butterworth-Heinemann, UK, 1997.
39. A. Kramida, Y. Ralchenko and J. Reader, the NIST ASD Team. 2015, NIST Atomic Spectra Database (v. 5.3), online, URL: <http://physics.nist.gov/asd>
40. (a) L. C. Allen, *J. Am. Chem. Soc.*, 1989, **111**, 9003; (b) J. Furtado, F. D. Proft and P. Geerlings, *J. Phys. Chem. A*, 2015, **119**, 1339.
41. D. R. Lide, 1993-1994 *CRC Handbook of Chemistry and Physics* (74th ed.), Boca Raton, FL, Chemical Rubber Company, p. 9.
42. (a) J. C. Wheeler, *J. Chem. Educ.*, 1997, **74**, 123; (b) J. Kalcher and A. F. Sax, *Chem. Rev.*, 1994, **94**, 2291.
43. (a) P. Pyykkö, *J. Phys. Chem. A*, 2015, **119**, 2326; (b) P. Pyykkö, M. Atsumi, *Chem. –Eur. J.*, 2009, **15**, 12770; (c) B. Cordero, V. Gómez, A. E. Platero-Prats, M. Revés, J. Echeverría, E. Cremades, F. Barragán and S. Alvarez, *Dalton Trans.*, 2008, 2832.
44. A. Bondi, *J. Phys. Chem.*, 1964, **68**, 441.
45. P. Pyykkö, *Chem. Rev.*, 1997, **97**, 597.
46. (a) J. Vogt and S. Alvarez, *Inorg. Chem.*, 2014, **53**, 9260; (b) S. Alvarez, *Dalton Trans.*, 2013, **42**, 8617.
47. M. Rahm, R. Hoffmann and N. W. Ashcroft, *Chem. –Eur. J.*, 2016, **22**, 14625.
48. J. Wilks, *The Properties of Liquid and Solid Helium*, Oxford : Clarendon Press, UK, 1967, 703.
49. W. Kossel, *Ann. Phys. (Leipzig)*, 1916, **49**, 229.
50. G. N. Lewis, *J. Am. Chem. Soc.*, 1916, **38**, 762.
51. M. Ozima and F. A. Podosek, *Noble Gas Geochemistry*, Cambridge University Press, UK, 2002.
52. Bobrow Test Preparation Services, Cliffs A P Chemistry, 2007, 15.
53. C. J. Zhang, X. T. Zhou and L. Yang, *IEEE Trans. Magn.*, 1992, **28**, 957.

54. G. Horhoianu, D. V. Ionescu and G. Olteanu, *Ann. Nucl. Energy*, 1999, **26**, 1437.
55. I. R. Dunkin, *Chem. Soc. Rev.*, 1980, **9**, 1.
56. H. H. Loosli and H. Oeschger, *Earth Planet. Sci. Lett.*, 1969, **7**, 67.
57. F. A. Podosek and M. Ozima, *The Xenon Age of the Earth in Origin of the Earth and Moon*, eds. R. M. Canup and K. Righter, The University of Arizona Press, USA, 2000.
58. R. D. Sanders, D. Ma and M. Maze, *Brit. Med. Bull.*, 2005, **71**, 115.
59. (a) H. Hiyagon, M. Ozima, B. Marty, S. Zashu and H. Sakai, *Geochim. Cosmochim. Acta*, 1992, **56**, 1301; (b) M. Honda, I. McDougall, D. B. Patteson, A. Doulgeris and D. A. Clague, *Geochim. Cosmochim. Acta*, 1993, **57**, 859.
60. T. D. Swindle, A. H. Treiman, D. J. Lindstrom, M. K. Burkland, B. A. Cohen, J. A. Grier, B. Li and E. K. Olson, *Meteorit. Planet. Sci.*, 2000, **35**, 107.
61. D. Basting, G. Marowsky, *Excimer Laser Technology*, Springer-Verlag, Berlin Heidelberg, Germany, 2005.
62. R. Edward, *Science*, 1901, **13**, 268.
63. L. Pauling, *J. Am. Chem. Soc.*, 1933, **55**, 1895.
64. N. Bartlett, *Proc. Chem. Soc.*, 1962, **112**, 218.
65. W. Grochala, *Chem. Soc. Rev.*, 2007, **36**, 1632.
66. C. L. Chernick, H. H. Claassen, P. R. Fields, H. H. Hyman, J. G. Malm, W. M. Manning, M. S. Matheson, L. A. Quarterman, F. Schreiner, H. H. Selig, *et al.*, *Science*, 1962, **138**, 136.
67. (a) S. M. Williamson and C. W. Koch, *Science*, 1963, **139**, 1046; (b) S. R. Gunn and S. M. Williamson, *Science*, 1963, **140**, 177; (c) R. Hoppe, W. Dähne, H. Mattauch and K. Rödder, *Angew. Chem. Int. Ed.*, 1962, **1**, 599.
68. J. G. Malm, H. Selig, J. Jortner and S. A. Rice, *Chem. Rev.*, 1965, **65**, 199.
69. (a) J. J. Turner and G. C. Pimentel, *Science*, 1963, **180**, 974; (b) R. D. Burbank, W. E. Falconer and W. A. Sunder, *Science*, 1972, **178**, 1285.
70. A. V. Grosse, A. D. Kirshenbaum, A. G. Streng and L. V. Streng, *Science*, 1963, **139**, 1047.
71. J. Slivuik, B. Volavsek, J. Marsel, V. Vrscaj, A. Smalc, B. Frlec and Z. Zemljic, *Croat. Chem. Acta*, 1963, **35**, 81.
72. W. F. Howard and L. Andrews, *J. Amer. Chem. Soc.*, 1974, **96**, 7864.
73. D. R. MacKenzie and R. H. Wiswall, Jr., *Inorg. Chem.*, 1963, **2**, 1064.

74. D. R. MacKenzie, *Science*, 1963, **141**, 1171.
75. D. R. MacKenzie and J. Fajer, *Inorg. Chem.*, 1966, **5**, 699.
76. L. Y. Nelson and G. C. Pimentel, *Inorg. Chem.*, 1967, **6**, 1758.
77. N. Bartlett and F. O. Sladky, *Comprehensive Inorganic Chemistry*, Pergamon: Oxford, 1973; vol. 1, ch. 6.
78. (a) P. S. Bagus, B. Liu, D. H. Liskow and H. F. Schaefer III, *J. Am. Chem. Soc.*, 1975, **97**, 7216; (b) S. Huzinaga, M. Klobukowski and Y. Sakai, *J. Phys. Chem.*, 1984, **88**, 4880; (c) H. Bürger, S. Ma, J. Breidung, W. Thiel, *J. Chem. Phys.*, 1996, **104**, 4945.
79. H. Bürger, R. Kuna, S. Ma, J. Breidung and W. Thiel, *J. Chem. Phys.*, 1994, **101**, 1.
80. R. M. Gavin and L. S. Bartell, *J. Chem. Phys.*, 1968, **48**, 2460.
81. L. S. Bartell, R. M. Gavin, H. B. Thompson and C. L. Chernick, *J. Chem. Phys.*, 1965, **43**, 2547.
82. M. –S. Liao and Q. –E. Zhang, *J. Phys. Chem. A*, 1998, **102**, 10647.
83. H. Selig, *Science*, 1964, **144**, 537.
84. B. Žemva, A. Jesih, D. H. Templeton, A. Zalkin, A. K. Cheetham, N. Bartlett, *J. Am. Chem. Soc.*, 1987, **109**, 7420.
85. N. Bartlett, B. G. DeBoer, F. J. Hollander, F. O. Sladky, D. H. Templeton, A. Zalkin, *Inorg. Chem.*, 1974, **13**, 780.
86. F. O. Sladky, P. A. Bulliner, N. Bartlett, B. G. DeBoer and A. Zalkin, *Chem. Commun. (London)*, 1968, 1048.
87. V. M. McRae, R. D. Peacock and D. R. Russell, *J. Chem. Soc. D*, 1969, 62.
88. S. Seidel and K. Seppelt, *Angew. Chem. Int. Ed. Engl.*, 2001, **40**, 4225.
89. D. E. McKee, A. Zalkin and N. Bartlett, *Inorg. Chem.*, 1973, **12**, 1713.
90. R. J. Gillespie and G. J. Schrobilgen, *Inorg. Chem.*, 1976, **15**, 22.
91. W. Grochala, L. Khriachtchev, M. Räsänen, *Noble–Gas Chemistry*. In *Physics and Chemistry at Low Temperatures*; ed. L. Khriachtchev, CRC Press, Boca Raton, FL, 2011; ch. 13, p. 419.
92. H. St. A. Elliott, J. F. Lehmann, H. P. A. Mercier, H. D. B. Jenkins and G. J. Schrobilgen, *Inorg. Chem.*, 2010, **49**, 8504.
93. (a) J. B. Nielsen, S. A. Kinkead, P. G. Eller, *Inorg. Chem.*, 1990, **29**, 3622; (b) K. O. Christe and W. W. Wilson, *Inorg. Chem.*, 1988, **27**, 1296.
94. K. O. Christe and W. W. Wilson, *Inorg. Chem.*, 1988, **27**, 3763.

95. C. L. Chemick, H. H. Claassen, J. G. Malm and P. L. Plurien, *Noble Gas Compounds*, ed. H. H. Hyman, University of Chicago Press: Chicago, IL, and London, 1963; p. 287.
96. H. Selig, H. H. Claassen, C. L. Chernick, J. G. Malm and J. L. Huston, *Science*, 1964, **143**, 1322.
97. E. H. Appelman and J. G. Malm, *J. Am. Chem. Soc.*, 1964, **86**, 2141.
98. M. Gawrilow, H. Beckers, S. Riedel and L. Cheng, *J. Phys. Chem. A*, 2018, **122**, 119.
99. (a) D. E. McKee, C. J. Adams and N. Bartlett, *Inorg. Chem.*, 1973, **12**, 1722; (b) R. J. Gillespie, B. Landa and G. J. Schrobilgen, *Inorg. Chem.* 1976, **15**, 1256.
100. R. D. LeBlond, D. D. DesMarteau, *J. Chem. Soc., Chem. Commun.*, 1974, 555.
101. J. F. Sawyer, G. J. Schrobilgen and S. J. Sutherland, *J. Chem. Soc., Chem. Commun.*, 1982, 210.
102. (a) G. A. Schumacher and G. J. Schrobilgen, *Inorg. Chem.*, 1983, **22**, 2178; (b) A. A. Emara and G. J. Schrobilgen, *J. Chem. Soc., Chem. Commun.*, 1987, 1644; (c) G. J. Schrobilgen, *J. Chem. Soc., Chem. Commun.*, 1988, 1506.
103. Y. L. Yagupolskii, W. Tyrra, R. Gnann, N. Maggiorosa and D. Naumann, *J. Fluorine Chem.*, 2002, **113**, 143.
104. G. L. Smith, H. P. A. Mercier and G. J. Schrobilgen, *Inorg. Chem.*, 2007, **46**, 1369.
105. (a) G. J. Schrobilgen, *J. Chem. Soc., Chem. Commun.*, 1988, 863; (b) J. C. P. Sanders and G. J. Schrobilgen, *J. Chem. Soc., Chem. Commun.*, 1989, 1576.
106. D. Naumann and W. Tyrra, *J. Chem. Soc., Chem. Commun.*, 1989, 47.
107. H. J. Frohn and S. Jakobs, *J. Chem. Soc., Chem. Commun.*, 1989, 625.
108. (a) H. J. Frohn and V. V. Bardin, *Organometallics*, 2001, **20**, 4750; (b) H. Butler, D. Naumann and W. Tyrra, *Eur. J. Solid State Inorg. Chem.*, 1992, **29**, 739; (c) D. Naumann, H. Butler, R. Gnann and W. Tyrra, *Inorg. Chem.*, 1993, **32**, 861.
109. (a) N. Maggiorosa, D. Naumann and W. Tyrra, *Angew. Chem., Int. Ed.*, 2000, **39**, 4588; (b) H. J. Frohn and M. Theissen, *Angew. Chem., Int. Ed.*, 2000, **39**, 4591.
110. H. J. Frohn, N. LeBlond, K. Lutar and B. Žemva, *Angew. Chem., Int. Ed.*, 2000, **39**, 391.
111. H. J. Frohn, T. Schroer and G. Henkel, *Angew. Chem., Int. Ed.*, 1999, **38**, 2554.
112. M. B. Simpson, M. Poliakoff, J. J. Turner, W. B. Maier and J. G. J. McLaughlin, *J. Chem. Soc., Chem. Commun.*, 1983, 1355.
113. J. R. Wells and E. Weitz, *J. Am. Chem. Soc.*, 1992, **114**, 2783.

114. X. Z. Sun, M. W. George, S. G. Kazarian, S. M. Nikiforov and M. Poliakoff, *J. Am. Chem. Soc.*, 1996, **118**, 10525.
115. C. A. Thompson and L. Andrews, *J. Am. Chem. Soc.*, 1994, **116**, 423.
116. G. Frenking, W. Koch, J. Gauss and D. Cremer, *J. Am. Chem. Soc.*, 1988, **110**, 8007.
117. (a) P. Pyykkö and Y. -F. Zhao, *J. Phys. Chem.*, 1990, **94**, 7753; (b) P. Pyykkö, *Chem. Phys. Lett.*, 1989, **162**, 349; (c) P. Pyykkö and Y. -F. Zhao, *Mol. Phys.*, 1990, **70**, 701.
118. S. Borocci, N. Bronzolino and F. Grandinetti, *Chem. Phys. Lett.*, 2004, **384**, 25.
119. Q. Wang and X. Wang, *J. Phys. Chem. A*, 2013, **117**, 1508.
120. (a) Q. Zhang, M. Chen, M. Zhou, D. M. Andrada and G. Frenking, *J. Phys. Chem. A*, 2015, **119**, 2543; (b) R. Saha, S. Pan, G. Merino and P. K. Chattaraj, *J. Phys. Chem. A*, 2015, **119**, 6746.
121. Q. Zhang, W. -L. Li, L. Zhao, M. Chen, M. Zhou, J. Li and G. Frenking, *Chem. – Eur. J.*, 2017, **23**, 2035.
122. W. Yu, X. Liu, B. Xu, X. Xing and X. Wang, *J. Phys. Chem. A*, 2016, **120**, 8590.
123. (a) J. Li, B. E. Bursten, B. Liang and L. Andrews, *Science*, 2002, **295**, 2242; (b) L. A. Mück, A. Y. Timoshkin, M. V. Hopffgarten and G. Frenking, *J. Am. Chem. Soc.*, 2009, **131**, 3942; (c) I. Infante, L. Andrews, X. Wang and L. Gagliardi, *Chem. –Eur. J.*, 2010, **16**, 12804.
124. (a) L. Andrews, B. Liang, J. Li and B. E. Bursten, *Angew. Chem. Int. Ed. Engl.*, 2000, **39**, 4565; (b) J. Li, B. E. Bursten, B. Liang and L. Andrews, *Science*, 2002, **295**, 5563; (c) B. Liang, L. Andrews, J. Li and B. E. Bursten, *J. Am. Chem. Soc.*, 2002, **124**, 9016; (d) L. Andrews, B. Liang, J. Li and B. E. Bursten, *J. Am. Chem. Soc.*, 2003, **125**, 3126.
125. D. Schröder, H. Schwarz, J. Hrušák and P. Pyykkö, *Inorg. Chem.*, 1998, **37**, 624.
126. P. Pyykkö, *J. Am. Chem. Soc.*, 1995, **117**, 2067.
127. J. P. Read and A. D. Buckingham, *J. Am. Chem. Soc.*, 1997, **119**, 9010.
128. S. Seidel and K. Seppelt, *Science*, 2000, **290**, 117.
129. (a) R. G. Raptis, H. H. Murray, R. J. Staples, L. C. Porter and J. P. Fackler Jr., *Inorg. Chem.*, 1993, **32**, 5576; (b) E. J. Fernández, M. C. Gimeno, P. G. Jones, A. Laguna, M. Laguna and J.M. López de Luzuriaga, *J. Chem. Soc., Dalton Trans.*, 1992, 3365; (c) X. -Y. Li and X. Cao, *Phys. Rev. A*, 2008, **77**, 022508.
130. K. Seppelt, *ZAnorg. Allg. Chem.*, 2003, **629**, 2427.

131. (a) R. Cipollini and F. Grandinetti, *J. Chem. Soc., Chem. Commun.*, 1995, 773; (b) P. Antoniotti, E. Bottizzo, L. Operti, R. Rabezzana, S. Borocci and F. Grandinetti, *J. Phys. Chem. Lett.*, 2010, **1**, 2006.
132. C. J. Evans, A. Lesarri and M. C. L. Gerry, *J. Am. Chem. Soc.*, 2000, **122**, 6100.
133. (a) C. J. Evans and M. C. L. Gerry, *J. Chem. Phys.*, 2000, **112**, 1321; (b) C. J. Evans and M. C. L. Gerry, *J. Chem. Phys.*, 2000, **112**, 9363; (c) C. J. Evans, D. S. Rubinoff and M. C. L. Gerry, *Phys. Chem. Chem. Phys.*, 2000, **2**, 3943; (d) J. M. Michaud and M. C. L. Gerry, *J. Am. Chem. Soc.*, 2006, **128**, 7613 and references therein; (e) D. Kurzydowski and W. Grochala, *Z. Anorg. Allg. Chem.*, 2008, **634**, 1082; (f) L. Belpassi, I. Infante, F. Tarantelli and L. Visscher, *J. Am. Chem. Soc.*, 2008, **130**, 1048.
134. C. J. Evans, T. G. Wright and A. M. Gardner, *J. Phys. Chem. A*, 2010, **114**, 4446.
135. (a) X. Wang, L. Andrews, K. Willmann, F. Brosi and S. Riedel, *Angew. Chem., Int. Ed.*, 2012, **51**, 10628; (b) X. Wang, L. Andrews, F. Brosi, S. Riedel, *Chem. –Eur. J.*, 2013, **19**, 1397.
136. (a) S. Pan, A. Gupta, R. Saha, G. Merino and P. K. Chattaraj, *J. Comput. Chem.*, 2015, **36**, 2168; (b) D. Chakraborty and P. K. Chattaraj, *J. Phys. Chem. A*, 2015, **119**, 3064.
137. (a) R. Hagiwara, F. Hollander, C. Maines, N. Bartlett, *Eur. J. Solid State Inorg. Chem.*, 1991, **28**, 855; (b) K. Matsumoto, R. Hagiwara and Y. Ito, *Solid State Sci.*, 2002, **4**, 1465.
138. (a) M. Tramšek, P. Benkič and B. Žemva, *Solid State Sci.*, 2002, **4**, 9; (b) G. Tavčar, P. Benkič and B. Žemva, *Inorg. Chem.*, 2004, **43**, 1452; (c) G. Tavčar, M. Tramšek, T. Bunič, P. Benkič and B. Žemva, *J. Fluorine Chem.*, 2004, **125**, 1579.
139. (a) M. Tramšek, E. Lork, R. Mews and B. Žemva, *J. Solid State Chem.*, 2001, **162**, 243; (b) K. Lutar, H. Borrmann, Z. Mazej, M. Tramšek, P. Benkič and B. Žemva, *J. Fluorine Chem.*, 2000, **101**, 155; (c) M. Tramšek, P. Benkič, A. Turičnik, G. Tavčar and B. Žemva, *J. Fluorine Chem.*, 2002, **114**, 143.
140. (a) A. Turičnik, P. Benkič and B. Žemva, *Inorg. Chem.*, 2002, **41**, 5521; (b) P. Benkič, M. Tramšek and B. Žemva, *Solid State Sci.*, 2002, **4**, 1425; (c) M. Tramšek, P. Benkič and B. Žemva, *Angew. Chem. Int. Ed.*, 2004, **43**, 3456.
141. (a) L. Khriachtchev, M. Pettersson, N. Runeberg, J. Lundell and M. Räsänen, *Nature (London)*, 2000, **406**, 874; (b) L. Khriachtchev, M. Pettersson, A. Lignell and M. Räsänen, *J. Am. Chem. Soc.*, 2001, **123**, 8610.

142. R. B. Gerber, *Annu. Rev. Phys. Chem.*, 2004, **55**, 55.
143. M. Pettersson, L. Khriachtchev, J. Lundell and M. Räsänen in *Inorganic Chemistry in Focus II*, eds. G. Meyer, D. Naumann and L. Wesemann, Wiley-VCH, Weinheim, 2005, p. 15.
144. L. Khriachtchev, M. Räsänen and R. B. Gerber, *Acc. Chem. Res.*, 2009, **42**, 183.
145. M. Pettersson, J. Lundell, L. Khriachtchev, E. Isoniemi and M. Räsänen, *J. Am. Chem. Soc.*, 1998, **120**, 7979.
146. M. Pettersson, L. Khriachtchev, J. Lundell and M. Räsänen, *J. Am. Chem. Soc.*, 1999, **121**, 11904.
147. J. Lundell, G. M. Chaban and R. B. Gerber, *Chem. Phys. Lett.*, 2000, **331**, 308.
148. N. Runeberg, M. Pettersson, L. Khriachtchev, J. Lundell and M. Räsänen, *J. Chem. Phys.*, 2001, **114**, 836.
149. K. O. Christe, *Angew. Chem. Int. Ed.*, 2001, **40**, 1419.
150. A. V. Nemukhin, B. L. Grigorenko, L. Khriachtchev, H. Tanskanen, M. Pettersson and M. Räsänen, *J. Am. Chem. Soc.*, 2002, **124**, 10706.
151. A. Cohen, J. Lundell and R. B. Gerber, *J. Chem. Phys.*, 2003, **119**, 6415.
152. L. Khriachtchev, M. Pettersson, J. Lundell, H. Tanskanen, T. Kiviniemi, N. Runeberg and M. Räsänen, *J. Am. Chem. Soc.*, 2003, **125**, 1454.
153. (a) S. A. Cooke and M. C. L. Gerry, *J. Am. Chem. Soc.*, 2004, **126**, 17000; (b) J. M. Michaud, S. A. Cooke and M. C. L. Gerry, *Inorg. Chem.*, 2004, **43**, 3871.
154. T. –H. Li, C. –H. Mou, H. –R. Chen and W. –P. Hu, *J. Am. Chem. Soc.*, 2005, **127**, 9241.
155. (a) T. K. Ghanty, *J. Chem. Phys.*, 2005, **123**, 074323. (b) T. K. Ghanty, *J. Chem. Phys.*, 2006, **124**, 124304.
156. T. Jayasekharan and T. K. Ghanty, *J. Chem. Phys.*, 2006, **124**, 164309.
157. T. Jayasekharan and T. K. Ghanty, *J. Chem. Phys.*, 2008, **129**, 184302.
158. T. Jayasekharan and T. K. Ghanty, *J. Chem. Phys.*, 2012, **136**, 164312.
159. A. Lignell, L. Khriachtchev, J. Lundell, H. Tanskanen and M. Räsänen, *J. Chem. Phys.*, 2006, **125**, 184514.
160. L. Khriachtchev, K. Isokoski, A. Cohen, M. Räsänen and R. B. Gerber, *J. Am. Chem. Soc.*, 2008, **130**, 6114.
161. L. Khriachtchev, S. Tapio, A. V. Domanskaya, M. Räsänen, K. Isokoski and J. Lundell, *J. Chem. Phys.*, 2011, **134**, 124307.

162. L. Operti, R. Rabezzana, F. Turco, S. Borocci, M. Giordani and F. Grandinetti, *Chem. –Eur. J.*, 2011, **17**, 10682.
163. S. Pan, D. Moreno, J. Cabellos, J. Romero, A. Reyes, G. Merino and P. K. Chattaraj, *J. Phys. Chem. A*, 2014, **118**, 487.
164. S. Borocci, M. Giordani and F. Grandinetti, *J. Phys. Chem. A*, 2014, **118**, 3326.
165. J. Kalinowski, R. B. Gerber, M. Räsänen, A. Lignell and L. Khriachtchev, *J. Chem. Phys.*, 2014, **140**, 094303.
166. M. J. Barlow, B. M. Swinyard, P. J. Owen, J. Cernicharo, H. L. Gomez, R. J. Ivison, O. Krause, T. L. Lim, M. Matsuura, S. Miller, G. Olofsson and E. T. Polehampton, *Science*, 2013, **342**, 1343.
167. F. Grandinetti, *Nat. Chem.*, 2013, **5**, 438.
168. L. Chen, P. S. Reiss, S. Y. Chong, D. Holden, K. E. Jelfs, T. Hasell, M. A. Little, A. Kewley, M. E. Briggs, A. Stephenson, *et al.*, *Nat. Mater.*, 2014, **13**, 954.
169. T. R. Hogness and E. G. Lunn, *Phys. Rev.*, 1925, **26**, 44.
170. (a) M. Tsuge, S. Berski, R. Stachowski, M. Räsänen, Z. Latajka and L. Khriachtchev, *J. Phys. Chem. A*, 2012, **116**, 4510; (b) R. B. Gerber, E. Tsivion, L. Khriachtchev and M. Räsänen, *Chem. Phys. Lett.*, 2012, **545**, 1.
171. (a) J. Lundell, *J. Mol. Struct.*, 1995, **355**, 291; (b) J. Lundell, J. Panek and Z. Latajka, *Chem. Phys. Lett.*, 2001, **348**, 147.
172. T. D. Fridgena and J. M. Parnis, *J. Chem. Phys.*, 1998, **109**, 2155.
173. (a) T. D. Fridgena and J. M. Parnis, *J. Chem. Phys.*, 1998, **109**, 2162; (b) M. Beyer, A. Lammers, E. V. Savchenko, G. Niedner-Schatteburg and V. E. Bondybey, *Phys. Chem. Chem. Phys.*, 1999, **1**, 2213; (c) J. Lundell, M. Pettersson and M. Räsänen, *Phys. Chem. Chem. Phys.*, 1999, **1**, 4151.
174. M. Pettersson, J. Lundell, L. Khriachtchev and M. Räsänen, *J. Chem. Phys.*, 1998, **109**, 618.
175. (a) H. J. Frohn and V. V. Bardin, *Chem. Commun.*, 1999, 919; (b) H. J. Frohn and V. V. Bardin, *Chem. Commun.*, 2003, 2352; (c) H. J. Frohn and V. V. Bardin, *Eur. J. Inorg. Chem.*, 2006, 3948.
176. (a) L. Khriachtchev, H. Tanskanen, J. Lundell, M. Pettersson, H. Kiljunen and M. Räsänen, *J. Am. Chem. Soc.*, 2003, **125**, 4696; (b) V. I. Feldman, F. F. Sukhov, A. Y. Orlov and I. V. Tyulpina, *J. Am. Chem. Soc.*, 2003, **125**, 4698; (c) E. Tsiviona and R. B. Gerber, *Phys. Chem. Chem. Phys.*, 2011, **13**, 19601.

177. L. Khriachtchev, A. Domanskaya, J. Lundell, A. Akimov, M. Räsänen and E. Misochko, *J. Phys. Chem. A*, 2010, **114**, 4181.
178. L. Khriachtchev, A. Lignell, H. Tanskanen, J. Lundell, H. Kiljunen and M. Räsänen, *J. Phys. Chem. A*, 2006, **110**, 11876.
179. H. Tanskanen, L. Khriachtchev, J. Lundell, H. Kiljunen and M. Räsänen, *J. Am. Chem. Soc.*, 2003, **125**, 16361.
180. (a) L. Khriachtchev, H. Tanskanen, A. Cohen, R. B. Gerber, J. Lundell, M. Pettersson, H. Kiljunen and M. Räsänen, *J. Am. Chem. Soc.*, 2003, **125**, 6876; (b) H. Tanskanen, L. Khriachtchev, J. Lundell and M. Räsänen, *J. Chem. Phys.*, 2004, **121**, 8291; (c) K. Willmann, T. Vent-Schmidt, M. Räsänen, S. Riedel and L. Khriachtchev, *RSC Adv.*, 2015, **5**, 35783.
181. C. Zhu, M. Räsänen and L. Khriachtchev, *J. Chem. Phys.*, 2015, **143**, 244319.
182. T. Arppe, L. Khriachtchev, A. Lignell, A. V. Domanskaya and M. Räsänen, *Inorg. Chem.*, 2012, **51**, 4398.
183. C. Zhu, M. Räsänen and L. Khriachtchev, *J. Chem. Phys.*, 2015, **143**, 074306.
184. (a) M. Attinà, F. Cacace, A. Cartoni and M. Rosi, *J. Phys. Chem. A*, 2000, **104**, 7574. (b) M. Attinà, F. Cacace, A. Cartoni and M. Rosi, *J. Mass Spectrom.*, 2001, **36**, 392.
185. T. Jayasekharan and T. K. Ghanty, *J. Chem. Phys.*, 2006, **125**, 234106.
186. (a) T. Jayasekharan and T. K. Ghanty, *J. Chem. Phys.*, 2007, **127**, 114314; (b) T. Jayasekharan and T. K. Ghanty, *J. Chem. Phys.*, 2008, **128**, 144314.
187. (a) W. Grochala, *Phys. Chem. Chem. Phys.*, 2012, **14**, 14860; (b) P. Szarek and W. Grochala, *J. Phys. Chem. A*, 2015, **119**, 2483.
188. Y. –L. Liu, Y. –H. Chang, T. –H. Li, H. –R. Chen and W. –P. Hu, *Chem. Phys. Lett.* 2007, **439**, 14.
189. M. Saunders, H. A. Jiménez-Vázquez, R. J. Cross, R. J. Poreda, *Science*, 1993, **259**, 1428.
190. M. S. Syamala, R. J. Cross and M. Saunders, *J. Am. Chem. Soc.*, 2002, **124**, 6216.
191. R. J. Cross, A. Khong and M. Saunders, *J. Org. Chem.*, 2003, **68**, 8281.
192. A. Khong, H. A. Jiménez-Vázquez, M. Saundres, R. J. Cross, J. Laskin, T. Peres, C. Lifshitz, R. Strongin and A. B. Smith, *J. Am. Chem. Soc.*, 1998, **120**, 6380.
193. M. Khatua, S. Pan and P. K. Chattaraj, *J. Chem. Phys.*, 2014, **140**, 164306.
194. M. Khatua, S. Pan and P. K. Chattaraj, *Chem. Phys. Lett.*, 2014, **610–611**, 351.

195. S. Mondal and P. K. Chattaraj, *Phys. Chem. Chem. Phys.*, 2014, **16**, 17943.
196. A. Krapp and G. Frenking, *Chem. –Eur. J.*, 2007, **13**, 8256.
197. E. Cerpa, A. Krapp, R. Flores-Moreno, K. J. Donald and G. Merino, *Chem. –Eur. J.*, 2009, **15**, 1985.
198. S. Pan, S. Mandal and P. K. Chattaraj, *J. Phys. Chem. B*, 2015, **119**, 10962.
199. T. Ohtsuki, K. Ohno, K. Shiga, Y. Kawazoe, Y. Maruyama and K. Masumoto, *Phys. Rev. Lett.*, 1998, **81**, 967.
200. V. V. Albert, J. R. Sabin and F. E. Harris, *Int. J. Quantum Chem.*, 2007, **107**, 3061.
201. P. Ravinder and V. Subramanian, *J. Phys. Chem. A*, 2011, **115**, 11723.
202. M. Bühl, S. Patchkovskii and W. Thiel, *Chem. Phys. Lett.*, 1997, **275**, 14.
203. T. Peres, B. P. Cao, W. D. Cui, A. Khong, R. J. Cross, M. Saunders and C. Lifshitz, *Int. J. Mass Spectrom.*, 2001, **210–211**, 241.
204. J. Laskin, T. Peres, C. Lifshitz, M. Saunders, R. J. Cross and A. Khong, *Chem. Phys. Lett.*, 1998, **285**, 7.
205. T. Sternfeld, R. E. Hoffman, M. Saunders, R. J. Cross, M. S. Syamala and M. Rabinovitz, *J. Am. Chem. Soc.*, 2002, **124**, 8786.
206. D. Manna, T. K. Ghanty, *J. Phys. Chem. C*, 2012, **116**, 25630.
207. T. Weiske, D. K. Bohme and H. Schwartz, *J. Phys. Chem.*, 1991, **95**, 8451.
208. M. Saunders, H. A. Jiménez-Vázquez, R. J. Cross, S. Mroczkowski, M. L. Gross, D. E. Giblin and R. J. Poreda, *J. Am. Chem. Soc.*, 1994, **116**, 2193.
209. L. Becker, R. J. Poreda and J. L. Bada, *Science*, 1996, **271**, 249.
210. R. J. Cross, M. Saunders and H. Prinzbach, *Org. Lett.*, 1999, **1**, 1479.
211. H. A. Jiménez-Vázquez, J. Tamariz and R. J. Cross, *J. Phys. Chem. A*, 2001, **105**, 1315.
212. W. Zou, Y. Liu, W. Liu, T. Wang and J. E. Boggs, *J. Phys. Chem. A*, 2010, **114**, 646.
213. R. B. Darzynkiewicz and G. E. Scuseria, *J. Phys. Chem. A*, 1997, **101**, 7141.
214. D. Moran, H. L. Woodcock, Z. F. Chen, H. F. Schaefer and P. V. R. Schleyer, *J. Am. Chem. Soc.*, 2003, **125**, 11442.
215. D. Chakraborty and P. K. Chattaraj, *Chem. Phys. Lett.*, 2015, **621**, 29.
216. D. Chakraborty, S. Pan and P. K. Chattaraj, *Theor. Chem. Acc.*, 2016, **135**, 119.
217. K. E. Whitener Jr., R. J. Cross, M. Saunders, S. Iwamatsu, S. Murata, N. Mizorogi and S. Nagase, *J. Am. Chem. Soc.*, 2009, **131**, 6338.

218. K. E. Whitener Jr., M. Frunzi, S. Iwamatsu, S. Murata, R. J. Cross and M. Saunders, *J. Am. Chem. Soc.*, 2008, **130**, 13996.
219. C. M. Stanisky, R. J. Cross and M. Saunders, *J. Am. Chem. Soc.*, 2009, **131**, 3392.
220. A. Krachmalnicoff, R. Bounds, S. Mamone, S. Alom, M. Concistrè, B. Meier, K. Kouřil, M. E. Light, M. R. Johnson, S. Rols, *et al.*, *Nat. Chem.*, 2016, **8**, 953.
221. M. Ge, U. Nagel, D. Hübner, T. Rößler, S. Mamone, M. H. Levitt, M. Carravetta, Y. Murata, K. Komatsu, X. Lei and N. J. Turro, *J. Chem. Phys.*, 2011, **135**, 114511.
222. M. Ge, U. Nagel, D. Hübner, T. Rößler, S. Mamone, M. H. Levitt, M. Carravetta, Y. Murata, K. Komatsu, J. Y. -C. Chen and N. J. Turro, *J. Chem. Phys.*, 2011, **134**, 054507.
223. S. Mamone, M. Ge, D. Hübner, U. Nagel, A. Danquigny, F. Cuda, M. C. Grossel, Y. Murata, K. Komatsu, M. H. Levitt, T. Rößler and M. Carravetta, *J. Chem. Phys.*, 2009, **130**, 081103.
224. A. J. Horsewill, K. S. Panesar, S. Rols, M. R. Johnson, Y. Murata, K. Komatsu, S. Mamone, A. Danquigny, F. Cuda, S. Maltsev, M. C. Grossel, M. Carravetta and M. H. Levitt, *Phys. Rev. Lett.*, 2009, **102**, 013001.
225. M. Straka, J. Vaara, *J. Phys. Chem. A*, 2006, **110**, 12338.
226. B. Arash and Q. Wang, *Sci. Rep.*, 2013, **3**, 1782.
227. M. Foroutan and A. T. Nasrabadi, *Chem. Phys. Lett.*, 2010, **497**, 213.
228. M. Foroutan and A. T. Nasrabadi, *Phys. E*, 2011, **43**, 851.
229. P. Pyykkö, C. Wang, M. Straka and J. A. Vaara, *Phys. Chem. Chem. Phys.*, 2007, **9**, 2954.
230. C. Wang, M. Straka and P. Pyykkö, *Phys. Chem. Chem. Phys.*, 2010, **12**, 6187.
231. X. Chen, A. M. Plonka, D. Banerjee, R. Krishna, H. T. Schaefer, S. Ghose, P. K. Thallapally and J. B. Parise, *J. Am. Chem. Soc.*, 2015, **137**, 7007.
232. J. Liu, P. K. Thallapally and D. Strachan, *Langmuir*, 2012, **28**, 11584.
233. P. K. Thallapally, J. W. Grateb and R. K. Motkuria, *Chem. Commun.*, 2012, **48**, 347.
234. D. Banerjee, C. M. Simon, A. M. Plonka, R. K. Motkuri, J. Liu, X. Chen, B. Smit, J. B. Parise, M. Haranczyk and P. K. Thallapally, *Nat. Commun.*, 2016, **7**, 11831.
235. C. A. Fernandez, J. Liu, P. K. Thallapally and D. M. Strachan, *J. Am. Chem. Soc.*, 2012, **134**, 9046.
236. T. Vazhappilly, T. K. Ghanty and B. N. Jagatap, *J. Phys. Chem. C*, 2016, **120**, 10968.

237. J. Liu, D. M. Strachana and P. K. Thallapally, *Chem. Commun.*, 2014, **50**, 466.
238. T. Vazhappilly, T. K. Ghanty and B. N. Jagatap, *J. Nucl. Mater.*, 2017, **490**, 174.
239. V. K. de Souza, J. D. Stevenson, S. P. Niblett, J. D. Farrell and D. J. Wales, *J. Chem. Phys.*, 2017, **146**, 124103.
240. T. Drews and K. Seppelt, *Angew. Chem., Int. Ed.*, 1997, **36**, 273.
241. S. Seidel, K. Seppelt, C. van Wüllen and X. Y. Sun, *Angew. Chem., Int. Ed.*, 2007, **46**, 6717.
242. J. A. Gascón, R. W. Hall, C. Ludewigt and H. Haberland, *J. Chem. Phys.*, 2002, **117**, 8391.
243. R. N. Keeler, M. van Thiel and B. J. Alder, *Physica*, 1965, **31**, 1437.
244. K. Syassen and W. B. Holzapfel, *Phys. Rev. B*, 1978, **18**, 5826.
245. (a) D. A. Nelson Jr. and A. L. Ruoff, *Phys. Rev. Lett.*, 1979, **42**, 383; (b) K. A. Goettel, J. H. Eggert, I. F. Silvera and W. C. Moss, *Phys. Rev. Lett.*, 1989, **62**, 665; (c) R. Reichlin, K. E. Brister, A. K. McMahan, M. Ross, S. Martin, Y. K. Vohra and A. L. Ruoff, *Phys. Rev. Lett.*, 1989, **62**, 669.
246. (a) A. Karpov, J. Nuss, U. Wedig and M. Jansen, *Angew. Chem., Int. Ed.*, 2003, **42**, 4818; (b) M. I. Erements, K. Shimizu, T. C. Kobayashi and K. Amaya, *Science*, 1998, **281**, 1333; (c) T. A. Grzybowski and A. L. Ruoff, *Phys. Rev. Lett.*, 1984, **53**, 489.
247. (a) L. Zhu, H. Liu, C. J. Pickard, G. Zou and Y. Ma, *Nat. Chem.*, 2014, **6**, 644; (b) M. –S. Miao, X. –L. Wang, J. Brgoch, F. Spera, M. G. Jackson, G. Kresse and H. –Q. Lin, *J. Am. Chem. Soc.*, 2015, **137**, 14122.
248. X. Dong, A. R. Oganov, A. F. Goncharov, E. Stavrou, S. Lobanov, G. Saleh, G. –R. Qian, Q. Zhu, C. Gatti, V. L. Deringer, *et al.*, *Nat. Chem.*, 2017, **9**, 440.
249. (a) P. Hohenberg and W. Kohn, *Phys. Rev.*, 1964, **136**, B864; (b) W. Kohn and L. J. Sham, *Phys. Rev.*, 1965, **140**, A1133.
250. (a) A. D. Becke, *J. Chem. Phys.* 1993, **98**, 1372; (b) C. Lee, W. Yang and R. G. Parr, *Phys. Rev. B: Condens. Matter Mater. Phys.*, 1988, **37**, 785.
251. (a) J. –D. Chai and M. Head-Gordon, *J. Chem. Phys.*, 2008, **128**, 084106; (b) J. –D. Chai and M. Head-Gordon, *Phys. Chem. Chem. Phys.*, 2008, **10**, 6615.
252. M. Born and R. Oppenheimer, *Ann. Phys. (Leipzig)*, 1927, **84**, 457.
253. (a) I. Levine, *Quantum Chemistry*, Prentice Hall of India Pvt. Ltd., 2001; (b) A. Szabo and N. S. Ostlund, *Modern Quantum Chemistry: Introduction to Advanced Electronic Structure Theory* McGraw-Hill, INC. New York, **1989**.

254. V. Fock, *Z. Phys.*, 1930, **61**, 126.
255. R. G. Parr and W. Yang, *Density Functional Theory of Atoms and Molecules*, Oxford University Press, New York, USA, 1989.
256. M. J. Frisch, M. Head-Gordon and J. A. Pople, *Chem. Phys. Lett.*, 1990, **166**, 275.
257. C. Hampel, K. Peterson and H. –J. Werner, *Chem. Phys. Lett.*, 1992, **190**, 1.
258. (a) L. H. Thomas, *Proc. Camb. Phil. Soc.*, 1927, **23**, 542; (b) E. Fermi, *Rend. Accad. Naz. Linc*, 1927, **6**, 602; (c) E. Fermi, *Z. Phys.*, 1928, **48**, 73.
259. (a) S. H. Vosko, L. Wilk and M. Nusair, *Can. J. Phys.*, 1980, **58**, 1200; (b) J. P. Perdew and Y. Wang, *Phys. Rev. B*, 1992, **46**, 12947; (c) A. D. Becke, *Phys. Rev. A*, 1988, **38**, 3098; (d) A. D. Becke, *J. Chem. Phys.*, 1993, **98**, 1372; (e) J. P. Perdew, *Phys. Rev. B*, 1986, **33**, 8822; (f) A. D. Becke, *J. Chem. Phys.*, 1993, **98**, 5648; (g) C. Lee, W. Yang and R. G. Parr, *Phys. Rev. B*, 1988, **37**, 785; (h) J. P. Perdew, K. Burke and M. Ernzerhof, *Phys. Rev. Lett.*, 1996, **77**, 3865.
260. J. C. Slater, *Phys. Rev.*, 1930, **36**, 57.
261. P. M. W. Gill, *Adv. Quantum Chem.*, 1994, **25**, 141.
262. (a) K. R. Asmis, N. L. Pivonka, G. Santambrogio, M. Brummer, C. Kaposta, D. M. Neumark and L. Woste, *Science*, 2003, **299**, 1375; (b) J. M. Headrick, E. G. Diken, R. S. Walters, N. I. Hammer, R. A. Christie, J. Cui, E. M. Myshakin, M. A. Duncan, M. A. Johnson and K. D. Jordon, *Science*, 2005, **308**, 1765; (c) D. Marx, M. E. Tuckerman, J. Hutter and M. Parrinello, *Nature (London)*, 1999, **397**, 601;
263. K. Mizuse and A. Fujii, *Phys. Chem. Chem. Phys.*, 2011, **13**, 7129.
264. S. G. Lias, J. E. Bartmess, J. F. Liebman, J. L. Holmes, R. D. Levin and W. G. Mallard, *J. Phys. Chem. Ref. Data*, 1988, **17**(Suppl 1), 1.
265. T. Y. Lin, J. B. Hsu and W. –P. Hu, *Chem. Phys. Lett.*, 2005, **402**, 514.
266. P. Antoniotti, S. Borocci, N. Bronzolino, P. Cecchi and F. Grandinetti, *J. Phys. Chem. A*, 2007, **111**, 10145.
267. S. –G. He, F. X. Sunahori and D. J. Clouthier, *J. Am. Chem. Soc.*, 2005, **127**, 10814.
268. (a) K. Kawaguchi and E. Hirota, *Chem. Phys. Lett.*, 1986, **123**, 1; (b) N. T. Hunt, Z. Liu and P. B. Davies, *Mol. Phys.*, 1999, **97**, 205.
269. (a) D. Buhl and L. E. Snyder, *Nature (London)*, 1970, **228**, 267; (b) J. Warnatz, In *Combustion Chemistry*, ed., W.C. Gardiner Jr., Springer-Verlag: Berlin, Germany, 1984; p 197; (c) W. Klemperer, *Nature*, 1970, **227**, 1230.

270. (a) B. E. Turner, *Astrophys. J. Lett.*, 1974, **193**, L83; (b) S. Green, J. A. Montgomery Jr. and P. Thaddeus, *Astrophys. J. Lett.*, 1974, **193**, L89; (c) P. Thaddeus and B. E. Turner, *Astrophys. J. Lett.*, 1975, **201**, L25.
271. P. Thaddeus, M. Guélin and R. A. Linke, *Astrophys. J.*, 1981, **246**, L41.
272. C. S. Gudeman, N. N. Haese, N. D. Piltch and R. C. Woods, *Astrophys. J.*, 1981, **246**, L47.
273. M. Bogey, C. Demuynck, J. L. Destombes and B. Lemoine, *J. Mol. Spectrosc.*, 1984, **107**, 417.
274. P. Botsch-wina and P. Sebald, *J. Mol. Spectrosc.*, 1985, **110**, 1.
275. (a) P. D. Davies and W. J. Rothwell, *J. Chem. Phys.*, 1985, **83**, 1496; (b) N. H. Rosenbaum, J. C. Owrutsky, L. M. Tack and R. J. Saykally, *J. Chem. Phys.*, 1985, **83**, 4845.
276. (a) S. A. Nizkorodov, J. P. Maier and E. J. Bieske, *J. Chem. Phys.*, 1995, **103**, 1297; (b) S. A. Nizkorodov, O. Dopfer, M. Meuwly, J. P. Maier and E. J. Bieske, *J. Chem. Phys.*, 1996, **105**, 1770; (c) S. A. Nizkorodov, O. Dopfer, T. Ruchti, M. Meuwly, J. P. Maier and E. J. Bieske, *J. Phys. Chem.*, 1995, **99**, 17118.
277. (a) P. Botschwina, M. Oswald, *J. Mol. Spectrosc.*, 1992, **155**, 360; (b) J. Sauer, *Chem. Rev.*, 1989, **89**, 199.
278. J. R. Flores, *J. Phys. Chem.*, 1992, **96**, 4414.
279. (a) B. E. Turner, *Astrophys. J.*, 1991, **376**, 573; (b) Y. T. Qi, F. Pauzat and G. Berthier, *Astron. Astrophys.*, 1984, **135**, L1.
280. (a) H. E. Warner, A. Fox, T. Amano and D. K. Bohme, *J. Chem. Phys.*, 1989, **91**, 5310; (b) N. Moazzen-Ahmadi, A. R. W. McKellar, H. E. Warner and T. Amano, *J. Chem. Phys.*, 1989, **91**, 5313.
281. (a) R. Srinivas, D. Suelzle, W. Koch, C. H. DePuy and H. Schwarz, *J. Am. Chem. Soc.*, 1991, **113**, 5970; (b) J. L. Turner and A. Dalgarno, *Astrophys. J.*, 1977, **213**, 386.
282. (a) A. Fox and D. K. Bohme, *Chem. Phys. Lett.*, 1991, **187**, 541; (b) A. Nowek and J. Leszczynski, *J. Phys. Chem.*, 1996, **100**, 7361; (c) Y. Yamaguchi, H. F. Schaefer III, *J. Chem. Phys.*, 1995, **102**, 5327.
283. (a) D. J. Lucas, L. A. Curtiss and J. A. Pople, *J. Chem. Phys.*, 1993, **99**, 6697; (b) M. J. Powell, B. C. Easton and O. F. Hill, *Appl. Phys. Lett.*, 1981, **38**, 794; (c) H. U. Lee and J. P. DeNeufville, *Chem. Phys. Lett.*, 1983, **99**, 394.

284. (a) V. V. Azatyan, V. A. Kalkanov and A. A. Shavard, *React. Kinet. Catal. Lett.*, 1980, **15**, 367; (b) J. Sauer, *J. Phys. Chem.*, 1987, **91**, 2315.
285. (a) P. J. O'Malley and J. Dwyer, *J. Chem. Soc., Chem. Commun.*, 1987, 72; (b) P. Ugliengo, V. R. Saunders and E. Garrone, *J. Phys. Chem.*, 1989, **93**, 5210; (c) A. Tachibana, Y. Kurosaki, H. Fueno, T. Sera and T. Yamabe, *J. Phys. Chem.*, 1992, **96**, 3029.
286. (a) D. W. Fahey, F. C. Fehsenfeld, E. E. Ferguson and L. A. Viehland, *J. Chem. Phys.*, 1981, **75**, 669; (b) M. J. Kushner, *J. Appl. Phys.*, 1988, **63**, 2532.
287. (a) R. V. Olkhov, S. A. Nizkorodov and O. Dopfer, *Chem. Phys.*, 1998, **239**, 393; (b) R. V. Olkhov and O. Dopfer, *Chem. Phys. Lett.*, 1999, **314**, 215.
288. S. Pan, D. Moreno, G. Merino and P. K. Chattaraj, *Chem. Phys. Chem.*, 2014, **15**, 3554.
289. S. Pan, R. Saha and P. K. Chattaraj, *Int. J. Mol. Sci.*, 2015, **16**, 6402.
290. Cunje, A.; Baranov, V. I.; Ling, Y.; Hopkinson, A. C.; Bohme, D. K., *J. Phys. Chem. A*, 2001, **105**, 11073.
291. J. -L. Chen, C. -Y. Yang, H. -J. Lin and W. -P. Hu, *Phys. Chem. Chem. Phys.*, 2013, **15**, 9701.
292. (a) J. S. Francisco, *J. Chem. Phys.*, 2006, **124**, 114303; (b) C. Puzzarini, *Phys. Chem. Chem. Phys.*, 2004, **6**, 344; (c) L. Bizzocchi and C. D. Esposti, *J. Chem. Phys.*, 2001, **115**, 7041.
293. (a) W. T. Borden, *Diradicals*, Wiley-Interscience, Inc., New York, 1982; (b) P. S. Skell, *Tetrahedron*, 1985, **41**, 1427; (c) R. S. Mulliken, *Phys. Rev.*, 1932, **41**, 751.
294. J. F. Harrison, *Acc. Chem. Res.*, 1974, **7**, 378.
295. B. Chen, A. Y. Rogachev, D. A. Hrovat, R. Hoffmann and W. T. Borden, *J. Am. Chem. Soc.*, 2013, **135**, 13954.
296. (a) E. T. Seidl and H. F. Schaefer III, *J. Chem. Phys.*, 1992, **96**, 4449; (b) D. L. S. Brahms and W. P. Dailey, *Chem. Rev.*, 1996, **96**, 1585; (c) A. P. Scott, M. S. Platz and L. Radom, *J. Am. Chem. Soc.*, 2001, **123**, 6069.
297. (a) G. Maier and J. Endres, *Chem. -Eur. J.*, 1999, **5**, 1590; (b) N. Bru and J. Vilarrasa, *Chem. Lett.*, 1980, **9**, 1489.
298. (a) B. J. Finlayson-Pitts and J. N. Pitts, *Atmospheric Chemistry: Fundamentals and Experimental Techniques*, Wiley, New York, 1986; (b) W. T. Miller and C. S. Y. Kim, *J. Am. Chem. Soc.*, 1959, **81**, 5008.

299. (a) Y. L. Yung, J. P. Pinto, R. J. Watson and S. P. Sander, *J. Atmos. Sci.*, 1980, **37**, 339; (b) M. J. Molina, L. T. Molina and C. E. Kolb, *Annu. Rev. Phys. Chem.*, 1996, **47**, 327; (c) R. P. Wayne, *Chemistry of Atmospheres*, 3rd ed., Oxford University Press, New York, 2000.
300. (a) S. Gronert, J. R. Keeffe and R. A. More O'Ferrall, *J. Am. Chem. Soc.*, 2011, **133**, 3381; (b) P. Rivero, C. A. Jiménez-Hoyos and G. E. Scuseria, *J. Phys. Chem. A*, 2013, **117**, 8073; (c) E. Sun, H. Lv, D. Shi, C. Wei, H. Xu and B. Yan, *J. Phys. Chem. A*, 2014, **118**, 2447.
301. M. W. Schmidt, K. K. Baldridge, J. A. Boatz, S. T. Elbert, M. S. Gordon, J. H. Jensen, S. Koseki, N. Matsunaga, K. A. Nguyen, S. Su, *et al.* *J. Comput. Chem.*, 1993, **14**, 1347.
302. H. -J. Werner, P. J. Knowles, G. Knizia, F. R. Manby, M. Schütz, P. Celani, T. Korona, R. Lindh, A. Mitrushenkov, G. Rauhut, *et al.* MOLPRO, version 2012.1, a Package of *ab initio* Programs, 2012; see <http://www.molpro.net>.
303. A. Nicklass, M. Dolg, H. Stoll and H. Preuss, *J. Chem. Phys.*, 1995, **102**, 8942.
304. (a) K. A. Peterson, *J. Chem. Phys.*, 2003, **119**, 11099; (b) K. A. Peterson, D. Figgen, E. Goll, H. Stoll and M. Dolg, *J. Chem. Phys.*, 2003, **119**, 11113.
305. (a) R. A. Kendall, T. H. Dunning Jr. and R. J. Harrison, *J. Chem. Phys.*, 1992, **96**, 6796; (b) D. E. Woon and T. H. Dunning Jr., *J. Chem. Phys.*, 1993, **98**, 1358.
306. K. K. Baldridge, M. S. Gordon, R. Steckler and D. G. Truhlar, *J. Phys. Chem.*, 1989, **93**, 5107.
307. C. Gonzalez and H. B. Schlegel, *J. Phys. Chem.*, 1990, **94**, 5523.
308. A. Boatz and M. S. Gordon, *J. Phys. Chem.*, 1989, **93**, 1819.
309. (a) R. F. W. Bader, *Atoms in Molecules—A Quantum Theory*, Oxford University Press: Oxford, U.K., 1990; (b) F. W. Biegler-könig, R. F. W. Bader and T. H. Tang, *J. Comput. Chem.*, 1982, **3**, 317; (c) R. F. W. Bader, *Chem. Rev.*, 1991, **91**, 893.
310. T. Lu and F. Chen, *J. Comput. Chem.*, 2012, **33**, 580.
311. J. Panek, Z. Latajka and J. Lundell, *Phys. Chem. Chem. Phys.*, 2002, **4**, 2504.
312. S. Pan, A. Gupta, S. Mandal, D. Moreno, G. Merino and P. K. Chattaraj, *Phys. Chem. Chem. Phys.*, 2015, **17**, 972.
313. W. Zou, D. Nori-Shargh and J. Boggs, *J. Phys. Chem. A*, 2013, **117**, 207.
314. F. Lang, K. Winkler, C. Strauss, R. Grimm and J. H. Denschlag, *Phys. Rev. Lett.*, 2008, **101**, 133005.

315. G. N. Lewis and M. Kasha, *J. Am. Chem. Soc.*, 1944, **66**, 2100.
316. F. Lang, K. Winkler, C. Strauss, R. Grimm and J. H. Denschlag, *Phys. Rev. Lett.*, 2008, **101**, 133005.
317. G. Frenking and D. Cremer, in *Structure and Bonding 73 (Noble Gas and High Temperature Chemistry)* (Eds.: M. J. Clarke, J. B. Goodenough, J. A. Ibers, C. K. Jørgensen, D. M. P. Mingos, J. B. Neilands, G. A. Palmer, D. Reinen, P. J. Sadler, R. Weiss and R. J. P. Williams) Springer-Verlag, Berlin, Heidelberg, 1990 pp. 17.
318. (a) A. E. Douglas and W. E. Jones, *Can. J. Phys.*, 1966, **44**, 2251; (b) R. Colin, J. Devillers and F. Prevot, *J. Mol. Spectrosc.*, 1972, **44**, 230.
319. (a) G. L. Smith, H. P. A. Mercier and G. J. Schröbilgen, *J. Am. Chem. Soc.*, 2009, **131**, 7272; (b) D. S. Brock, J. J. Casalis de Pury, H. P. A. Mercier, G. J. Schröbilgen and B. Silvi, *J. Am. Chem. Soc.*, 2010, **132**, 3533; (c) D. S. Brock, H. P. A. Mercier and G. J. Schröbilgen, *J. Am. Chem. Soc.*, 2013, **135**, 5089.
320. (a) D. L. Cooper, *Astrophys. J.*, 1983, **265**, 808; (b) B. E. Turner and T. J. Sears, *Astrophys. J.*, 1989, **340**, 900.
321. D. Rehder, *Chemistry in Space: From Interstellar Matter to the Origin of Life*, Wiley-VCH, Weinheim, 2010.
322. (a) J. Peeters, I. Langhans, W. Boullart, M. T. Nguyen and K. J. Devriendt, *J. Phys. Chem.*, 1994, **98**, 11988; (b) J. Peeters, W. Boullart and K. J. Devriendt, *J. Phys. Chem.*, 1995, **99**, 3583; (c) S. A. Carl, Q. Sun and J. Peeters, *J. Chem. Phys.*, 2001, **114**, 10332.
323. (a) Y. Ohshima and Y. Endo, *J. Mol. Spectrosc.*, 1993, **159**, 458; (b) D. H. Mordaunt, D. L. Osborn, H. Choi, R. T. Bise and D. M. Neumark, *J. Chem. Phys.*, 1996, **105**, 6078; (c) L. R. Brock, B. Mischler and E. A. Rohlfing, *J. Chem. Phys.*, 1999, **110**, 6773.
324. (a) C. H. Hu, H. F. Schaefer, Z. L. Hou and K. D. Bayes, *J. Am. Chem. Soc.*, 1993, **115**, 6904; (b) B. Schaefer, M. Peric and B. Engels, *J. Chem. Phys.*, 1999, **110**, 7802; (c) B. Schaefer-Bung, B. Engels, T. R. Taylor, D. M. Neumark, P. Botschwina and M. Peric, *J. Chem. Phys.*, 2001, **115**, 1777.
325. J. Warnatz, in *Combustion Chemistry*, ed. W. C. Gardiner, Springer, Berlin, 1984, p. 288.
326. J. V. Michale and A. F. Wagner, *J. Phys. Chem.*, 1990, **94**, 2453.

327. (a) R. L. Hudson and M. J. Loeffler, *Astrophys. J.*, 2013, **773**, 109; (b) S. Maity, R. I. Kaiser and B. M. Jones, *Astrophys. J.*, 2014, **789**, 36.
328. M. Agúndez, J. Cernicharo and M. Guélin, *Astron. Astrophys.*, 2015, **577**, L5.
329. T. T. Tidwell, *Ketenes*, John Wiley and Sons, Inc., New York, 1995; T. T. Tidwell, *Ketenes II*, John Wiley and Sons, Inc., Hoboken, New Jersey, 2006.
330. J. L. Holmes, C. Aubry and P. M. Mayer, *Assigning Structures to Ions in Mass Spectrometry*, CRC Press, Boca Raton, FL, 2007.
331. F. Weigend and R. Ahlrichs, *Phys. Chem. Chem. Phys.*, 2005, **7**, 3297.
332. (a) H. –J. Werner and P. J. Knowles, *J. Chem. Phys.*, 1988, **89**, 5803; (b) P. J. Knowles and H. –J. Werner, *Chem. Phys. Lett.*, 1988, **145**, 514.
333. T. J. Lee and P. R. Taylor, *Int. J. Quantum Chem.*, 1989, **36**, 199.
334. B. Kiran, X. Li, H. –I. Zhai, L. –F. Cui and L. –S. Wang, *Angew. Chem., Int. Ed.*, 2004, **43**, 2125.
335. P. Pyykkö, *Angew. Chem., Int. Ed.*, 2004, **43**, 4412.
336. A. Avramopoulos, M. G. Papadopoulos and A. J. Sadlej, *Chem. Phys. Lett.*, 2003, **370**, 765.
337. (a) A. Shayeghi, R. L. Johnston, D. M. Rayner, R. Schäfer and A. Fielicke, *Angew. Chem., Int. Ed.*, 2015, **54**, 10675; (b) A. Shayeghi, R. Schäfer, D. M. Rayner, R. L. Johnston and A. Fielicke, *J. Chem. Phys.*, 2015, **143**, 024310.
338. (a) P. Gruene, D. M. Rayner, B. Redlich, A. F. van der Meer, J. T. Lyon, G. Meijer and A. Fielicke, *Science*, 2008, **321**, 674; (b) L. M. Ghiringhelli, P. Gruene, J. T. Lyon, D. M. Rayner, G. Meijer, A. Fielicke and M. Scheffler, *New J. Phys.*, 2013, **15**, 083003 and references therein.
339. S. Pan, R. Saha, S. Mandal and P. K. Chattaraj, *Phys. Chem. Chem. Phys.*, 2016, **18**, 11661.
340. X. Li, B. Kiran and L. –S. Wang, *J. Phys. Chem. A*, 2005, **109**, 4366.
341. T. K. Ghanty, *J. Chem. Phys.*, 2005, **123**, 241101.
342. (a) S. Buckart, G. Ganteför, Y. D. Kim and P. Jena, *J. Am. Chem. Soc.*, 2003, **125**, 14205; (b) S. M. Lang, T. M. Bernhardt, R. N. Barnett, B. Yoon and U. Landman, *J. Am. Chem. Soc.*, 2009, **131**, 8939; (c) N. K. Jena, K. R. S. Chandrakumar and S. K. Ghosh, *J. Phys. Chem. Lett.*, 2011, **2**, 1476.
343. K. Mondal, S. Agrawal, D. Manna, A. Banerjee and T. K. Ghanty, *J. Phys. Chem. C*, 2016, **120**, 18588.

344. (a) H. –J. Zhai, B. Kiran and L. –S. Wang, *J. Chem. Phys.*, 2004, **121**, 8231; (b) G. N. Khairallah and R. A. J. O’Hair, *Dalton Trans.*, 2005, 2702; (c) H. –T. Liu, Y. –L. Wang, X. –G. Xiong, P. D. Dau, Z. A. Piazza, D. –L. Huang, C. –Q. Xu, J. Li and L. –S. Wang, *Chem. Sci.*, 2012, **3**, 3286; (d) H. Xie, X. Xing, Z. Liu, R. Cong, Z. Qin, X. Wu, Z. Tang and H. Fan, *Phys. Chem. Chem. Phys.*, 2012, **14**, 11666; (e) K. Vetter, S. Proch, G. F. Ganteför, S. Behera and P. Jena, *Phys. Chem. Chem. Phys.*, 2013, **15**, 21007.
345. E. van Lenthe and E. J. Baerends, *J. Comput. Chem.*, 2003, **24**, 1142.
346. (a) T. Ziegler and A. Rauk, *Theor. Chim. Acta*, 1977, **46**, 1; (b) F. M. Bickelhaupt and E. J. Baerends, In *Reviews on Computational Chemistry*; eds. K. B. Lipkowitz and D. B. Boyd, Wiley-VCH: New York, 2000, Vol. 15, pp 1–86.
347. (a) G. te Velde, F. M. Bickelhaupt, S. J. A. van Gisbergen, C. Fonseca-Guerra, E. J. Baerends, J. G. Snijders and T. Ziegler, *J. Comput. Chem.*, 2001, **22**, 931; (b) E. J. Baerends, ADF 2013.01, SCM, Theoretical Chemistry, Vrije Universiteit: Amsterdam, The Netherlands, 2013.
348. C. –W. Tsai, Y. –C. Su, G. –D. Li and J. –D. Chai, *Phys. Chem. Chem. Phys.*, 2013, **15**, 8352.
349. G. Zhang and C. B. Musgrave, *J. Phys. Chem. A*, 2007, **111**, 1554.
350. S. Borocci, M. Giordani and F. Grandinetti, *J. Phys. Chem. A*, 2015, **119**, 6528.
351. E. Espinosa, E. Alkorta, J. Elguero and E. Molins, *J. Chem. Phys.*, 2002, **117**, 5529.
352. S. Scharfe, F. Kraus, S. Stegmaier, A. Schier and T. F. Fässler, *Angew. Chem., Int. Ed.*, 2011, **50**, 3630.
353. L. –F. Cui, X. Huang, L. –M. Wang, J. Li and L. –S. Wang, *J. Phys. Chem. A*, 2006, **110**, 10169.
354. L. –F. Cui, X. Huang, L. –M. Wang, D. Y. Zubarev, A. I. Boldyrev, J. Li and L. –S. Wang, *J. Am. Chem. Soc.*, 2006, **128**, 8390.
355. (a) J. –P. Dognon, C. Clavaguera and P. Pyykkö, *Angew. Chem., Int. Ed.*, 2007, **46**, 1427; (b) Dognon, J. –P.; C. Clavaguéra, P. Pyykkö, *C. R. Chim.*, 2010, **13**, 884;
356. (a) L. –F. Cui, X. Huang, L. –M. Wang, J. Li and L. –S. Wang, *Angew. Chem.*, 2007, **119**, 756; (b) J. –Q. Wang, S. Stegmaier, B. Wahl and T. F. Fässler, *Chem. – Eur. J.*, 2010, **16**, 1793; (c) U. Rohrmann and R. Schäfer, *J. Phys. Chem. C*, 2015, **119**, 10958.

357. (a) V. Kumar, A. K. Singh and Y. Kawazoe, *Nano Lett.*, 2004, **4**, 677; (b) K. Koyasu, M. Akutsu, M. Mitsui and A. Nakajima, *J. Am. Chem. Soc.*, 2005, **127**, 4998; (c) G. Espinoza-Quintero, J. C. A. Duckworth, W. K. Myers, J. E. McGrady and J. M. Goicoechea, *J. Am. Chem. Soc.*, 2014, **136**, 1210.
358. (a) N. Shao, S. Bulusu and X. C. Zeng, *J. Chem. Phys.*, 2008, **128**, 154326; (b) A. C. Castro, E. Osorio, J. O. C. Jiménez-Halla, E. Matito, W. Tiznado and G. Merino, *J. Chem. Theory Comput.*, 2010, **6**, 2701; (c) T. B. Tai and M. T. Nguyen, *J. Chem. Theory Comput.*, 2011, **7**, 1119.
359. J. Zhou, S. Giri and P. Jena, *Phys. Chem. Chem. Phys.*, 2014, **16**, 20241.
360. A. J. Karttunen and T. F. Fässler, *Chem. –Eur. J.*, 2014, **20**, 6693.
361. (a) X. Li, A. Hermann, F. Peng, J. Lv, Y. Wang, H. Wang and Y. Ma, *Sci. Rep.*, 2015, **5**, 16675; (b) Z. Liu, J. Botana, M. Miao and D. Yan, *Europhys. Lett.*, 2017, **117**, 26002.
362. (a) S. K. Ghose, Y. Li, A. Yakovenko, E. Dooryhee, L. Ehm, L. E. Ecker, A.–C. Dippel, G. J. Halder, D. M. Strachan and P. K. Thallapally, *J. Phys. Chem. Lett.*, 2015, **6**, 1790; (b) D. Banerjee, A. J. Cairns, J. Liu, R. K. Motkuri, S. K. Nune, C. A. Fernandez, R. Krishna, D. M. Strachan and P. K. Thallapally, *Acc. Chem. Res.*, 2015, **48**, 211.
363. D. Marx and J. Hutler, *Ab Initio Molecular Dynamics: Theory and Implementation*. In *Modern Methods and Algorithms of Quantum Chemistry*, ed., J., Grotendorst, John von Neumann Institute for Computing (NIC); Germany, 2000, Vol. 3, pp 329–446.
364. TURBOMOLE is a program package developed by the Quantum Chemistry Group at the University of Karlsruhe, Germany: R. Ahlrichs, M. Bär, M. Häser, H. Horn and C. Kölmel, *Chem. Phys. Lett.*, 1988, **162**, 165.
365. S. Grimme, J. Antony, S. Ehrlich and H. Krieg, *J. Chem. Phys.*, 2010, **132**, 154104.
366. (a) S. Grimme, A. Hansen, J. G. Brandenburg, C. Bannwarth, *Chem. Rev.*, 2016, **116**, 5105; (b) J. R. Reimers, M. J. Ford, S. M. Marcuccio, J. Ulstrup and N. S. Hush, *Nat. Rev. Chem.*, 2017, **1**, 0017.
367. P. Su and H. Li, *J. Chem. Phys.*, 2009, **131**, 014102.